A NOVEL TOOL FOR PREDICTING THE TENSILE STRAIN CAPACITY OF WELDED ONSHORE VINTAGE PIPELINES

by

Sylvester Ikechukwu Agbo

A thesis submitted in partial fulfillment of the requirements for the degree of

Doctor of Philosophy

in

Structural Engineering

Department of Civil and Environmental Engineering
University of Alberta

ABSTRACT

Pipelines can be exposed to a wide variety of loads, depending on the environments and the area of application. These loads especially the displacement-controlled types may impose large longitudinal plastic strain on pipelines, which could constitute a significant threat to the structural integrity of the thin-walled cylindrical shell structure. The fracture and failure mechanism of the ductile shell structure is inherently influenced by a variety of parameters that may exhibit direct linear and nonlinear relationships with the resultant stresses and the consequent straining of the structure, under these complex loading conditions. Traditional stress-based design methods may become uneconomical in the design of pipelines subjected to large plastic strain. In view of the extensive use of such pipelines in remote areas where oil and gas resources are currently being extracted, reliable calibration of the tensile strain capacity (TSC) plays a critical role in strain-based design (SBD) methodology. This study focused on the development of a novel predictive tool capable of characterizing the TSC of lower grade vintage pipelines, specifically of X42 steel grade, which is currently in service, in their numbers across North America, by investigating the parameters that significantly affect the TSC response of such pipelines under load. Firstly, eight full-scale pressurized four-point bending tests were conducted on X42, NPS 22 vintage pipes with 12.7 mm wall thickness to investigate the effect of internal pressure and flaw size on the TSC. The pipes were subjected to internal pressure levels equivalent to 80% and 30% of the specified minimum yield strengths (SMYS) and different girth weld flaw sizes machined at the girth weld centerline.

Secondly, the extended finite element method (XFEM) in the ABAQUS CAE was used to simulate the four-point bending tests to demonstrate the capability of the XFEM in simulating full-scale ductile fracture response of pipelines subjected to biaxial loading, and the numerical results were

validated against the full-scale test results. Moreover, a nonlinear parametric study investigating the effects of pipe and defect geometries, as well as loading conditions on the pipe TSC was conducted using the XFEM technique to fully understand the influence of these parameters on the TSC. The trends of TSCs obtained for the various combinations and interactions of the parameters considered were examined to derive an appropriate individual variable function representing each parameter combination. Nonlinear regression analysis was then employed to develop a nonlinear semi-empirical model (tool) for predicting the TSC of welded X42 vintage pipe.

The TSCs predicted using the new tool (*TSCvin.*) was compared with those evaluated using the full-scale-test-validated XFEM models. Excellent goodness-of-fit with the TSCs obtained from the validated XFEM simulations was obtained for the developed predictive tool.

Finally, I conducted a statistical analysis to ensure the model is unbiased and can predict conservative TSCs by running a probabilistic error analysis to quantify the error and use the result to modify the predictive model. The modified predictive model is useful in practical applications because it provides a quantifiable degree of conservatism to the predicted TSCs.

The modified TSC model was applied to some hypothetical X42 pipeline cases to demonstrate the applicability and accuracy of the new tool, which confirmed the efficiency of the model by replicating the trend obtained from both the experimental tests and the XFEM numerical simulations

PREFACE

All the research work presented for this thesis forms part of a research collaboration between the University of Alberta, Enbridge Liquid Pipelines Ltd., TransCanada Pipelines Ltd., and ExxonMobil Upstream Research, Houston, TX, USA, with Professor Samer Adeeb being the lead collaborator at the University of Alberta, Nader Yoosef-Ghodsi, Da-Ming Duan and Justin Crapps being responsible for facilitation and acquisition of research funding at Enbridge, TransCanada Pipelines and ExxonMobil respectively.

The two introductory chapters in this thesis, i.e., Chapter 1 (Introduction), and Chapter 2 (Literature Review) are all my original work and include appropriate citations of references as required. The subsequent chapters (Chapter 3 – Chapter 6) are derived from either conference proceedings, journal publications, or research articles intended for publication in selected journals. Chapter 3 is derived from a paper presented in a conference proceeding: Agbo, Sylvester, Lin, Meng, Ahmed, Arman, Cheng, J.J. Roger, and Adeeb, Samer, Prediction of Burst Load in Pressurized Pipelines using Extended Finite Element Method (XFEM) in: The 6th International Conference of Engineering Mechanics and Materials, CSCE, May 31 - June 3, Vancouver, B.C., Canada, 2017. Chapter 4 is derived from a research article published in the Elsevier International Journal of Pressure Vessels and Piping: Agbo, S., Lin, M., Ameli, I., Imanpour, A., Duan, D., Cheng, J. J. R, Adeeb, S., Experimental Evaluation of the Effect of Internal Pressure and Flaw Size on the Tensile Strain Capacity of Welded X42 Vintage Pipelines, International Journal of Pressure Vessels and Piping (2019), 10.1016/j.ijpvp.2019.04.010.

Chapter 5 is derived from the published conference proceeding: Agbo, S., Lin, M., Ameli, I., Imanpour, A., Duan, D., Cheng, J. J., Adeeb, S., Evaluation of the Effect of Internal Pressure and Flaw Size on the Tensile Strain Capacity of X42 Vintage Pipeline using Damage Plasticity Model in the Extended Finite Element Method (XFEM), Proceedings of the ASME 2019 Pressure Vessels & Piping Conference, July 14 - 19, 2019, San Antonio, Texas, USA PVP2019-94005, doi:https://doi.org/10.1115/PVP2019-94005

Chapter 6 is derived from a research article submitted for publication in the ASME Journal of Pressure Vessel Technology PVT-19-1216, (under review). I was the lead investigator for all the

research conducted herein and, therefore, responsible for concept formation, data collection and analysis, and manuscript composition. Being the corresponding author, S. Adeeb and A. Imanpour were involved in concept improvement and manuscript editing. All other authors, including both S. Adeeb and A. Imanpour, provided extensive and resourceful technical input for methodology formulation and result validation.

S. I. Agbo

Dedicated with love

to

my beautiful and amazing family

ACKNOWLEDGMENTS

First and foremost, I will like to give thanks to the Almighty God, the creator of heaven and earth, the giver of life and Jesus Christ, my redeemer. Thank you, Lord. It is only by Your favour, grace, and enablement that I achieved this feat, may all the glory and honour be unto Your Name.

My deepest gratitude goes to my supervisors, Prof. Samer Adeeb and Dr. Ali Imanpour, for their inestimable support, motivation, mentorship, and ever continuous availability to guide my steps throughout this academic journey. I am extremely grateful to you, Sirs, for your unalloyed support, which has encouraged me all these years always to strive to exceed expectations. You never viewed very challenging tasks from the problematic perspective; rather, you saw through the lens of solution, owing to your perpetual indomitable disposition. Thank you for your excellent mentorship in my academic, professional and career endeavours. And thank you for always being so kind, patient and understanding.

My sincere appreciation also goes to every member of my examination committee, Prof. J. J. Roger Cheng, Dr. Ali Imanpour, Dr. Yong Li, and Dr. Ahmed Hammad for their intelligent direction, and for graciously encouraging me towards producing a better version of this research work. I am also grateful to my external examiner, Dr. Sam Nakhla, for his investment of time and effort into making this research endeavour a success.

Further thanks go to all my professors in the Structures group, Prof. Robert Driver, Dr. Carlos Cruz-Noguez, Dr. Y. H. Chui, Dr. Mustafa Gul, Dr. Douglas Tomlinson, Dr. Yuxiang Chen and Dr. Vivek Bindiganavile, whose masterly tutelage and invaluable academic insight have immensely contributed to my current academic achievements and, undoubtedly, to my future career accomplishments.

My sincere acknowledgment also goes to all my professors outside the Structures group, Prof. Ben Jar, Prof. John A. Nychka, Prof. Patricio Mendez and Prof. Weixing Chen, whose tutelage contributed to my current academic achievements and to a large extent my career.

Many thanks also go to the wonderful and cooperative technicians at the I. F. Morrison Structural Engineering Laboratory, Greg Miller and Cameron West, for their constructive technical and safety guidance, which enabled me to successfully conduct series of large scale experimental tests programs, which formed a major part of my research.

I want to appreciate the foreign Ph.D. sponsorship funding I received from my home country Nigeria, through the Tertiary Education Trust Fund (TETFund), this was indeed the stepping stone.

The research will not have been possible without funding facilitated by my supervisor, Prof. Samer Adeeb, in collaboration with the industrial partners Enbridge Pipelines Inc., TransCanada Pipelines Ltd., and ExxonMobil Upstream Research, I am overly appreciative. Also, for the funds provided by the Faculty of Graduate Studies and Research (University of Alberta Doctoral Recruitment Scholarship), MITACS Accelerate, and Enbridge Pipelines Edmonton, provided an internship position for me, where I acquired first-hand industrial experience, I am very grateful.

What will the world be without good friends and fond memories? My heartfelt thanks go to all my friends at the University of Alberta: Onyekachi Ndubuaku, Chike Okoloekwe, Meng Lin, Janine Woo, Jonelle Baptiste, Diana Abdulhameed, Allan Okodi, Ronald Ekyalimpa, Odin Guzman Sanchez, Jesus Salazar, Palizi Mehrdad, Saher Attia, Nahid Elyasi, Pablo Cano, Vahab Esmaeili, Eziolu Ilozumba, Aboifazl Ashrafi, Eshagh Derakhshan Houreh, Kairs Wong, Yueying Li, Remi Avione, Nguyet Duong, Edrien John Blancas, Fatemeh Fallahi Arezodar, Maliheh Ghaneei, Bernado Garcia, Jeffrey Hung, Victoria Buffam, Riley Quintin, Danny Romero, Leichuan Tan, Shaghayegh Abtahi, Xinfang Zhang, Prempeh Owusu, Iman Ameli and Xiaoben Liu. I am grateful for all the happy conversations, joyful moments, academic collaborations and supports we shared.

I also like to express my sincere appreciation to my parents, Mr. Frederick E. Agbo (although no longer with us, continues to inspire by his exemplary legacy and dedication to education) and Mrs. Mary Agbo. The candle of knowledge you gave to me is still burning and lighting my path to destiny. I will forever be grateful to both of you for your endless love and care.

I am utterly thankful from the bottom of my heart to my siblings; Pharm. & Dr. Frederick I. Agbo, Engr. Dr. Kenneth C. Agbo, Dr. Anthony C. Agbo, Bar. Emmanuel C. Agbo, Miss. Fidelia C. Agbo, Mrs. Blessing N. Onyishi, and Mr. Christian U. Agbo, for their prayers, encouragement, and emotional support, I am very grateful.

Last but not the least, to my loving wife, Ogechi, the joy and happiness you have given me every day of this endeavour cannot be expressed with words. Your patient and understanding encouraged me the most. To my lovely children, Angel, Emmanuel, and Kenechukwu, your presence and tender cares took away all my worries; you are indeed our bundle of joy, thank you for the patience and understanding why Daddy is not always at home with you. God bless you all.

TABLE OF CONTENTS

LIST OF FIGURES

LIST OF TABLES

LIST OF SYMBOLS AND ABBREVIATIONS

a	Crack depth
$2C$	Crack length
°	Degrees
D	Outer diameter of the pipe
E	Young's modulus (Modulus of elasticity)
E'	E, under plane stress condition
G	Shear Modulus (Modulus of rigidity)
G_C	Fracture Energy
J	J-integral
J_{Ic}	Plane strain fracture toughness
Jel	Elastic
K	Stress intensity factor
Kc	Plane stress fracture toughness characterized
KI	Mode I
KIc	Plane strain fracture toughness characterized
KII	Mode II
$KIII$	Mode III
M_{axpe}	Maximum principal strain
P_i	Internal pressure
r	Inner radius of
t	Thickness of pipe wall
γ	Shear strain
δ	Crack-tip opening displacement (CTOD)
δIc	Plane strain fracture toughness characterized by CTOD
$\varepsilon tcrit$	Longitudinal tensile strain capacity
εe	Elastic strain
εh	Hoop strain
εL	Longitudinal strain
η	Ratio of defect
λ	Ratio of yield strength to tensile strength (λ=Y/T)
ξ	Ratio of defect length
σeng	Engineering stress
$\sigma true$	TRUE Stress
σh	Hoop stress
σL	Longitudinal stress
σY	Effective yield
τ	Shear stress
σ	Standard deviation
μ	Mean
ν	Poisson's ratio
API	American Petroleum Institute

ASD	Allowable stress design
ASME	American Society of Mechanical Engineers
BM	Base metal
CDF	Cumulative distribution function
CE	Carbon equivalent
CMOD	Crack mouth opening displacement
CSA	Canadian Standard Association
CSCE	Canadian Society of Civil Engineers
CTOD	Crack-tip opening displacement
CVN	Charpy V-notch
CWP	Curved wide plate
DIC	Digital image correlation
ECA	Engineering critical assessment
EM	ExxonMobil
FEA	Finite element analysis
FM	Fracture mechanics
FMDA	Fracture mechanics design approach
GTN	Gurson-Tvergaard and Needleman
HAZ	Heat-affected zone
IPC	International Pipeline Conferences
ISO	Organization for Standardization
MTS	Material testing systems
MWP	Medium wide plate
NDT	Non-destructive testing
NPS	Nominal pipe size
PRCI	Pipeline research council international
PSL	Product specification levels
PVP	Pressure vessels and pipping
PVT	Pressure vessels technology
SBD	Strain-based design
SBECA	Strain-based engineering critical assessment
SENT	Single edge notch tension
SMYS	Specified minimum yield strength
TAPS	Trans-Alaska Pipeline System
TDA	Traditional design approach
TSC	Tensile strain capacity
TSC_{vin}	Tensile strain capacity for X42 vintage pipes
UEL	Uniform elongation
UYS	Upper yield strength
WCL	Weld center line
WM	Weld metal

1. INTRODUCTION

Oil and natural gas have been important energy resources for over a century. As the global energy demand continues to grow, energy industries have pushed all the limits through increasing exploration and extraction activities of energy resources, even in remote regions of the world, especially in the arctic and sub-arctic regions of North America. Canada has abundant energy resources, the primary productions are crude oil and natural gas, which consisted of about 43% and 33% respectively of the total domestic energy production in 2014, as shown in Figure 1-1[1]. Such large oil and natural gas reserves are often located far from major markets; the products recovered from these reserves must, therefore, be transported through long distances to ports, refineries, and distribution hubs. The development of oil and natural gas resources is highly dependent on the economics and technical feasibility of transporting the recovered resources to the marketplace. For example, steel pipelines consist of about 86% of the total energy pipelines in the province of Alberta [2]. Improving long-distance transportation economics is a critical factor in determining whether oil and natural gas recovery from remote reserves are cost-effective with an acceptable return on investment [3]. Thus, pipelines are generally recognized as the safest and most economical method for transporting oil and natural gas over long distances.

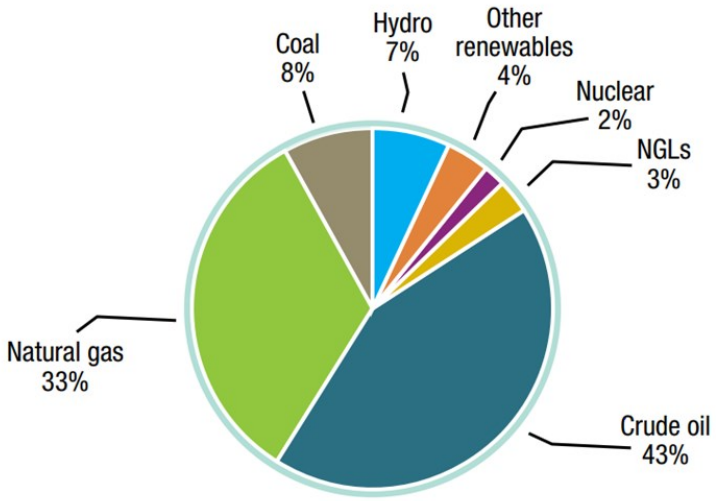

Figure 1-1 Canadian primary energy production in 2014 (Natural Resources Canada, Energy Fact Book 2016)

There are more than 840,000 kilometres (km) of energy pipelines in Canada (Natural Resources Canada, 2016). Steel pipelines are typically used offshore and onshore as a safe and economical means of transporting fluids such as; water, oil, gases, and sewage. In order to efficiently transport

such energy fluids from the source to target locations, many pipeline networks are installed such that they traverse a wide variety of soil types, geological conditions, and regions of varying seismicity (Figure 1-2) [4]. As a result, such pipelines may be exposed to geohazards, which pose a significant risk to their integrity, especially in mountainous areas containing landslides, areas with differential permafrost, areas that are seismically active, or areas where the ground is prone to subsidence [5]. Transmission pipelines that traverse these regions may experience large longitudinal strains and plastic circumferential elongation as the pipeline experiences alignment changes [6]. Buried steel pipelines, especially those used to transport crude oil and other hydrocarbons from natural reservoirs at significantly high internal pressures and temperatures, are subjected to more complex loading conditions by these hazards. These induced loads, such as internal pressure changes caused by the fluid action, axial forces induced by thermal effects, tensile stresses developed in the hoop direction, and bending caused by differential soil movement, can adversely affect the structural capacity and leak-tight integrity of the transmission pipeline. Thermal loads due to the heat of the hydrocarbons flowing through the pipeline induce axial extension, which is restrained by the pipe-soil frictional forces along the length of the buried pipeline resulting in a more complicated loading condition [7]. Trans-Alaska Pipeline System (TAPS), shown in Figure 1-2, was constructed in the arctic region of Alaska in the 1970s. [4]. A pipeline is a non-redundant long structure constructed by joining different pipe segments using girth weld, meaning that there is no alternate load-carrying path to compensate for the failure [8].

Figure 1-2 The Trans –Alaska oil pipeline stretching over 1000 miles [4].

1.1 Pipeline girth weld

During the construction of oil and gas transportation pipelines, different pipe segments are welded together on-site in the case of onshore pipelines. In contrast, for offshore pipelines, welded pipe segments are wound onto a spool and transported to the site for installation. The circumferential girth welds connecting the pipe segments might contain defects related to the welding process and hence constitute a potential weakest link in the pipeline. Different defect types can be identified, for example, cracks, lack of fusion and undercut etc. [9]. In addition, to the occurrence of defects in (or adjacent to) the weld metal (WM), the welding process potentially involves other detrimental effects such as misalignment weld, e between the connected pipe sections and the heat-affected zone (HAZ), which potentially deteriorates the material properties of the base metal (BM) adjacent to the WM. A typical girth weld containing defects is schematically shown in Figure 1-3 [9].

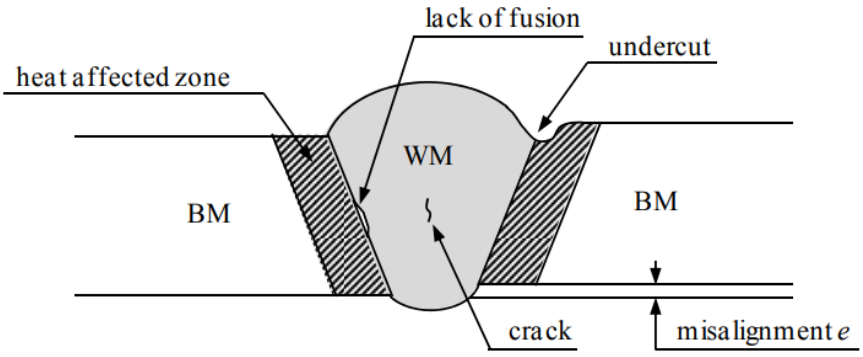

Figure 1-3 Schematic representation of a typical girth weld containing defects [9].

1.2 Defect assessment procedure

To assess the criticality of girth weld defects, two major levels of assessment are available; the first assessment level is typically based on a screening of defect dimensions against workmanship criteria. Such criteria require limited input parameters (e.g. only defect type and length, 2*C*) and, for individual defects, tend to allow defects no longer than 50 mm [10-12]. The defect depth (*a)* is, in this case, of minor importance and thus not required. Despite the simplistic nature of this method, it potentially leads to overly conservative assessments. As the cost of a weld repair can be estimated as high as ten times the cost of a normal weld [13], minimizing repair welding without sacrificing safety became important. As a result, a higher-level approach consisting of an engineering critical assessment (ECA) is often advised. This assessment method aims at allowing larger defects, based on more detailed material characterization and taking into account the exact pipe and defect dimensions and loading conditions. Within an ECA, detailed defect sizing such as defect length and defect depth become a primary variable. Consequently, this approach implies extra costs, originating from, e.g. the material testing and non-destructive evaluation. It is believed that this cost can be compensated for by the lower weld repair rate if larger defects become acceptable [14].

1.3 Stress versus strain-based design approach

When assessing the severity of weld defects, the loading condition to which the pipeline is subjected during construction and operation is of major importance. Traditionally, the allowable stress design (ASD) approach has been considered for onshore applications, where the service stress originates from the internal pressure (*Pi*). This method is primarily focused on the pressure containment by limiting the hoop stress to a certain percentage of the specified minimum yield strength (SMYS) of the pipe material (e.g. 72% or 80%) [15] Eq. (1-1). The hoop stress, σ_{hoop} is calculated as follows:

$$\sigma_{hoop} = Pi\frac{(D)}{2t} \qquad (1-1)$$

where *D* represents the pipe outer diameter and *t*, the wall thickness of the pipe.

ASD based pipeline codes lack the precise methodologies required for the design and assessment of pipelines that may experience high longitudinal local strains in service.

As a result of the increasing extraction of energy resources from the remote fields exposed to harsh geo-environment and the detrimental interactions between the pipelines and this environment, the pipelines in service sometimes experience an upward surge in plastic strain [5, 16-19]. Although both tensile and compressive strain should be considered, this study is solely focused on the tensile deformations. Considering a traditional ASD methodology, undesirable effects are controlled through a design (safety) margin with respect to the characteristic strength of the material, resulting in the allowable stress. The characteristic strength (SMYS) is usually taken as the stress at 0.5% strain. Therefore, the strain corresponding to the service load is reduced below the elastic limit (i.e. smaller than 0.5% - Figure 1-4 a) [3, 20]. As a result, a substantially different defect assessment approach is required to design for pipelines deformed beyond the elastic limit (large plastic strain); therefore, the strain-based design (SBD) approach becomes more suitable. However, the SBD approach is a complementary tool to the traditional stress-based design methodology [21-23].

Within the SBD methodology, the maximum allowed service load is expressed in terms of tensile or compressive strain (strain capacity) instead of tensile or compressive stress (SMYS).

Accordingly, applying a design margin leads to a design strain (target strain demand), that can exceed the elastic limit (Figure 1-4).

Two major limit states considered in the SBD method are tensile rupture and compressive buckling. The tensile rupture is an ultimate limit state which is related to the breach of the pressure containment boundary. The compressive buckling could be either a service limit state or an ultimate limit state [24]. To design for these limit states, it is necessary to quantify the magnitude of strain demands and strain capacity. The strain demand is the strain imposed on the pipeline by its operational and environmental conditions, while the strain capacity is the limit of the tolerable strain level beyond which a failure condition is reached. The design condition requires that the strain capacity be greater than the strain demand by an appropriate safety margin. A comparison of the ASD and SBD methods is shown in Figure 1-4 a & b.

The tensile strain capacity (TSC) of a pipeline is typically controlled by the ability of girth welds containing defects to resist fracture when subjected to tensile stresses and strain imposed due to operational and environmental loads. In the SBD approach, the pipeline design loads and capacities are quantified in terms of longitudinal strain and the pipelines are designed to sustain a prescribed level of strain without rupture [25-26].

The majority of onshore pipelines are buried in different cold regions with harsh environments where plastic strains may be imposed in the longitudinal direction due to the geo-environmental hazards.

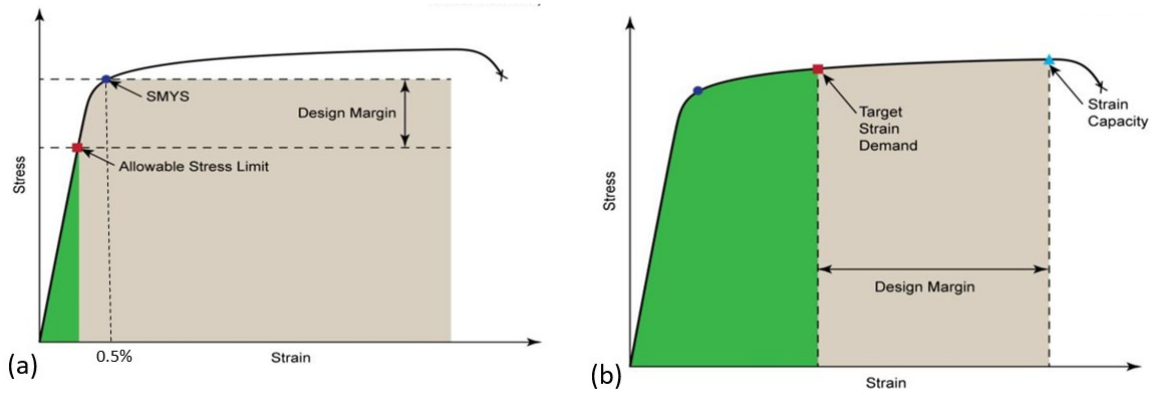

Figure 1-4 Comparison of two major pipeline design methods showing the design margin obtainable in each case (a) ASD and (b) SBD [3]

A typical pipeline buried in discontinuous permafrost region, experiencing frost heave and differential thaw settlement as a result of the external interactive displacements with respect to the pipe axis, leading to localized stresses and strains (Figure 1-5) [27]. To assess the structural integrity and safety of pipelines against large plastic strains, it is necessary first to determine the strain demand applied to the pipeline as well as strain capacity. The strain capacity is defined as the strain value to cause the violation of leak-tight integrity (ultimate limit state) of a pipeline at rupture [24]. The full-scale testing can be used to evaluate the ultimate limit state of the pipe when tensile rupture occurs. In offshore pipelines, the highest deformations occur in the process of pipeline installation by reeling where the girth welded segments of a pipeline are wound onto a spool and therefore experiences high bending strains, as shown in Figure 1-6 [28].

When assessing pipeline defects, a more conservative approach is; assuming all defects to be surface-breaking (Figure 1-7), since surface-breaking defects are generally more critical than the embedded defects [9]. For that reason, in the case of embedded defects, their depth is converted to an equivalent surface breaking defect depth. It is thereby assumed that buried defects are less severe compared to their surface breaking equivalent [10, 21-23].

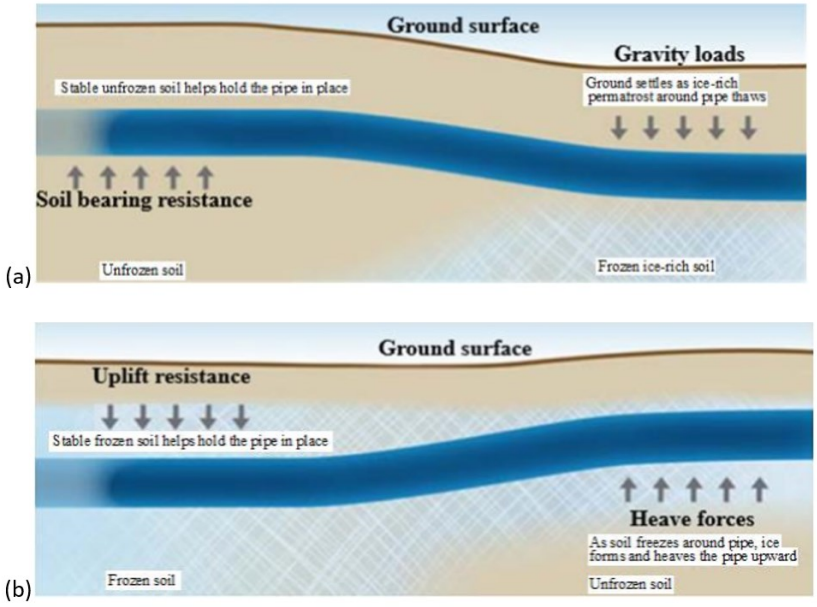

Figure 1-5 Bending deformations of pipeline buried in permafrost due to (a)Thaw settlement (b) Frost heave [27]

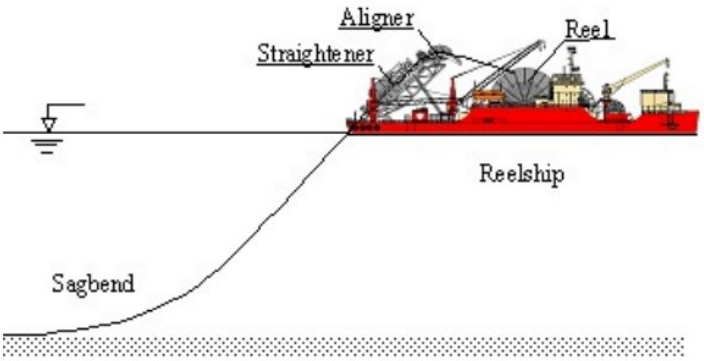

Figure 1-6 Pipeline bending during the reeling process in an offshore installation. [28]

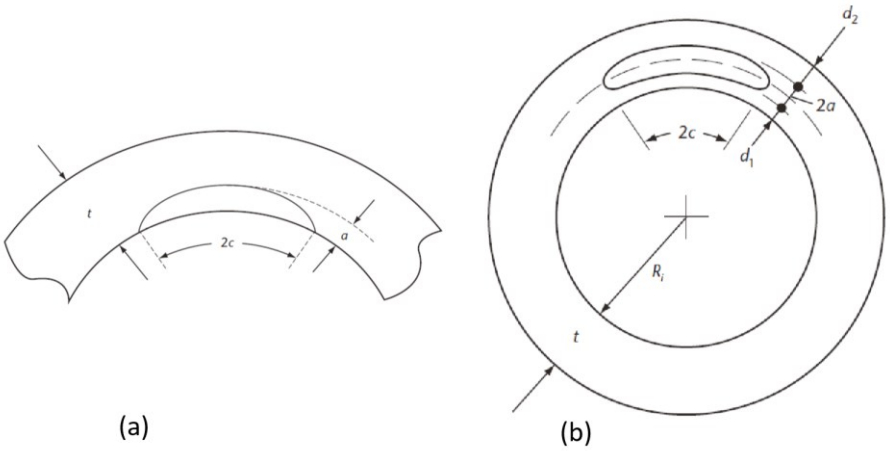

Figure 1-7 Schematic classification of weld defects according to CSA Z662.11 (a) surface breaking and (b) embedded defects [10]

Within the framework of this study, the focus is on how to accurately determine the tensile strain capacity of a girth welded vintage pipe specimen with a given initial flaw size, internal pressure level, and pipe geometry. Full-scale testing and numerical approach are the intended method for estimating the tensile strain capacity of the welded X42 vintage steel pipeline. This is based on the failure assessment approach and will be extended to the development of a semi-empirical equation for a simplified TSC prediction.

1.4 Problem statement

The majority of studies (e.g. 29-32) conducted on pipeline structures in recent years were essentially focused on the evaluation of the compressive strain capacity when buckling occurs, which mostly represents a serviceability limit state. Such research studies do not capture the effect of girth weld defect. A summary of the past research work is given first to identify the lack of research in the area of vintage pipes made of steel grade X42, which will lead to the need for this research project.

On the other hand, major studies performed on the TSC of pipelines neglected the effect of the pipe internal pressure level. The tensile strain equations specified by the Canadian Standards Association (CSA) Z662 Annex C [33] were validated against curved wide plate (CWP) test data based on extensive research by Wang et al. [34-38] and tests performed at the University of Waterloo and the Welding Institute of Canada, published by Glover and coworkers [39–41]. These tests did not consider the effect of internal pressure.

Ostby et al. [42] conducted series of full-scale tests that investigated the effects of internal pressure on TSC of pipes, and their results showed that the internal pressure significantly reduces the TSC of the pipe from a level of 3.5–4% to a level of 1.5–2%. They equally observed that the unpressurized specimens failed due to local buckling at the compression side. In contrast, the pressurized specimens failed due to fracture at the flawed locations on the tension side.

Similarly, Igi et al. [43] conducted a series of full-scale pressurized tests and unpressurized CWP tests on X80 pipes, for the prediction of the TSC in the presence of surface defects. The surface defects were machined into the HAZ of the girth weld. The effect of internal pressure was investigated by comparing the results of the full-scale pressurized test to the results of the CWP test. It was observed that the TSC decreased by approximately 50% due to the internal pressure.

Mathias et al. [9] adopted a research methodology that is based on experimental and numerical methods to measure the ductile crack extension using single edge notch tension (SENT) and medium wide plate (MWP) tests. They investigated the crack-tip constraints of both specimens and the influence of internal pressure on the TSC by relating the TSC of pressurized pipes to CWP

specimens. They observed that the constraint in SENT specimens is higher compared to MWP specimens; this suggested that a defect assessment based on SENT tests is potentially more conservative compared to an assessment based on wide plate test results. The study also led to the formulation of an analytical pressure correction function that allows assessing the TSC of pressurized pipes from CWP test data.

Abdulhameed et al. [44], recently conducted a series of pressurized full-scale tests on X52 vintage pipeline to characterize the TSC. The test results showed that the level of internal pressure could reduce the TSC by 50% or more depending on the flaw size. The tests did not capture the influence of biaxial loading due to a combination of bending moment and internal pressure as well as the effect of flaw location at the weld centerline (WCL) or HAZ, which are potentially prone to defects, instead the flaws were located in the BM.

Pipelines buried in permafrost and sites prone to soil movement are typically subjected to displacement-controlled loading, which often leads to the bending of the pipe, as illustrated in Figure 1-5. Most of the researches mentioned above was conducted on pipelines with steel grades of X65 and above except the work by Abdulhameed et al. [44] conducted on X52 vintage pipes. In addition to the experimental studies, some analytical equations proposed by ExxonMobil (EM) [45, 46] and Pipeline Research Council International (PRCI) [24] were available in the literature for the prediction of TSC of pipes of grade X65 to X80 with a specific set of geometric and material parameters. However, the analytical equations mentioned above are yet to be incorporated into the pipeline design codes for TSC prediction. The TSC equation prescribed by the CSA Z662 standard - Annex C [33] was later removed in the recent edition of the standard. The published TSC equation in 33 did not cover vintage pipelines of grades X56 and below and, as mentioned earlier, did not consider the effect of internal pressure. However, it is recommended not to use these equations in case of pipes with steel grade X42 [24, 45-46].

Predictive models developed by EM [45, 46] and PRCI [24] respectively did not equally capture low strength vintage pipes as the models were calibrated for high toughness (CTOD ranging from 1.8-1.9) pipe materials ranging from X65 to X80. However, predictive models, whether based on analytical equations or finite element modelling, must be validated against experimental data produced in tests that should reproduce the event under consideration as realistically as possible. This condition justifies the use of full-scale testing on pipe section long enough to reproduce the

conditions of interest with limiting border effects as the preferred approach for measuring the tensile strain capacity of pipelines.

There is a lack of data and methods to predict the tensile strain capacity of girth welded vintage pipes made of steel grade X42. This perceived potential research gap requires urgent attention; thus, a predictive model for evaluating the TSC of girth welded vintage steel pipes of X42 grade is needed.

1.5 Significance of the study:

The results of this project will be applicable to the design, integrity assessment and maintenance of vintage pipelines that are buried in large numbers under Canadian soil and can be extended to other pipeline communities abroad through which crude oil is currently being transported. Most of the new pipeline projects utilize X65, and higher grades for construction, the exact material behaviour of these grades has been validated using detailed experimental and finite element modelling programs. There is still an extensive network of vintage pipelines of grades X42, X46, X52, X56, etc. that required exhaustive experimental tests to understand their material and structural behaviour [47]. The results of this project will be published in the International Pipeline Conferences (IPC) and will be presented to the pipeline community for consideration in future code enhancements. It will help the energy industries to efficiently and safely manage to operate their vintage pipelines of grades X42 by providing information that can enhance the design, maintenance, safety, and pipeline integrity and reliability management. The results of this study will have a great economic impact on the whole pipeline communities in Canada, North America, as well as on global energy development.

1.6 Objectives and scope

The main objective of this research is to evaluate the TSC of welded X42 vintage pipelines and to develop a novel tool for predicting the TSC of such pipelines.

Specific objectives are summarized as follows:

1. Performing an extensive literature review on existing studies carried out on the TSC of pipelines in general and specifically on the welded vintage pipeline to identify the limitations that exist.
2. Evaluating the TSC of welded X42 pipes by conducting an expanded full-scale experimental test program.
3. Comparing the experimental results with existing TSC predictive models in the literature to verify their applicability to X42 vintage pipes.
4. Developing an extended finite element method (XFEM) of numerical models to replicate the full-scale four-point bending tests while validating the models against the full-scale test results.
5. Conducting extensive parametric analyses using the validated XFEM models to examine the effects of influential parameters on the TSC of X42 vintage pipelines.
6. Based on the parameterization approach presented, develope a model capable of predicting reliable TSCs of welded X42 vintage pipes.

1.7 Research methodology

This Ph.D. work was accomplished in five steps using the experimental and numerical simulation methods as described below:

1. Eight full-scale experimental tests were designed and conducted on some welded X42 Enbridge's vintage pipes to study the effect of flaw size and internal pressure on the TSC.
2. The experimental results were compared with the TSCs predicted using the existing predictive models to verify the applicability of the models to X42 vintage pipes.
3. XFEM numerical models were developed to simulate the eight full-scale tests by calibrating the damage parameters for characterizing the X42 material and validating the models against the full-scale test results.
4. The validated XFEM models were employed in an expanded numerical program by conducting nonlinear parametric analysis investigating the influence of the essential

parameters on the TSC of X42 vintage pipelines subjected to internal pressure and bending using the general-purpose finite element analysis (FEA) software package (ABAQUS CAE) [48]. The main parameters considered in the parametric evaluation are the flaw size, i.e., flaw length and flaw depth, the internal pressure, and geometric properties (diameter-to-thickness ratio, *D/t*). An average longitudinal tensile strain extracted from 1 *OD* gauge length prior to the moment the crack penetrated through the pipe wall is used in defining the TSC of the pipe models [46]. The proposed test matrix includes four variations of the flaw depth, four variations of the flaw length, four variations of the pressure factor and two variations of the *D/t*. The parametric analyses were conducted such that every possible combination of the three major constituent parameters is investigated while the effect of *D/t,* which is reported in the literature [46] not to have a major effect on the TSC, is only partially combined. Consequently, a total of 128 XFEM runs were performed in this study.

5. Finally, advanced nonlinear multiple regression techniques using powerful software program Wolfram Mathematica [49], is used to derive a nonlinear expression suitable for predicting the TSC of X42 pipes under the investigated conditions. Statistical analysis is conducted to ensure the model is unbiased and predicts conservative TSCs by modifying the model using probabilistic error analysis [46,50].

1.8 Organization of thesis

The thesis is broken into seven chapters: starting with Chapter 1 – introduction, problem statement, significant of study, objectives, and scope, research methodology, and organization of thesis; and ending with Chapter 7 − summary, scientific contributions, conclusions, and recommendation for future research.

Chapter 2 summarizes the findings obtained from the pieces of literature on issues such as the behaviour of welded pipes subjected to tensile loads — the specification and grades of pipes, evolution of pipe grades, weldability of steel pipes, tensile strain capacity of welded pipelines, fracture, FEA and XFEM.

Chapters 3 to 6 correspond to different peer-reviewed publications that are separately focused on various aspects of this research objective. The chapters are arranged chronologically with respect to the date of publication of the different papers, and a sequential arrangement aimed at following a systematic progression of the specific objectives of the research is adopted.

It is important to mention that; because this thesis is paper-based, similar or identical information such as research background, literature review, assumptions, model calibration, and validation data/methods, references, etc. might be repeated in different chapters.

Chapter 3 describes the numerical modelling of 2 full-scale test programs previously conducted in our research group on pressurized X52 vintage pipes subjected to eccentric tensile force using the XFEM approach. The XFEM numerical results were validated against the full-scale test results. This model was a useful guide in the design of components and test setup for the proposed pressurized full-scale four-point bending test program on X42 vintage pipes. This chapter is derived from a published conference proceeding, the 2017 Canadian Society of Civil Engineers (CSCE) 6th International Conference on Engineering Mechanics and Materials.

In line with the second specific objective, Chapter 4 utilized the recommended approach of characterizing the structural capacity of pipelines by conducting a series of full-scale tests on welded X42 vintage pipes. In this chapter, eight full-scale pressurized four-point bending experimental pipe tests were designed, conducted and analyzed to investigate the effect of internal pressure and flaw size on the TSC. The XFEM numerical technique developed in chapter 3 was instrumental in the design of the setup and the capacity of components used in the four-point pipe bending tests. The tests were conducted on nominal pipe size (NPS) 22 inches (558.8 mm) diameter X42 grade welded vintage pipes with D/t of 44 to examine the effect of the influential parameters on the TSC. Biaxial strain gauges and digital image correlation (DIC) system were major instrumentations used for measuring strain. The results were used to examine the crack growth rate by estimating the crack-mouth opening displacement (CMOD) at failure and the effects of internal pressure and flaw size on the TSC. The TSC obtained from the tests were compared with those predicted using available TSC predictive models proposed by EM and PRCI. The contents of this chapter are obtained from a paper published in the International Journal of Pressure Vessels and Piping. Extra data and information obtained from the experimental program are presented in the Appendix.

In Chapter 5, all the eight full-scale tests conducted in Chapter 4 were numerically simulated. Chapter five follows the same procedure as Chapter three except that the XFEM pipe models were developed for X42 vintage steel pipes subjected to internal pressure and four-point bending, thus only 3D deformable solid elements were used. Also, one of the damage parameters (Maximum principal strain, *Maxpe*) for simulating the ductile fracture behaviour of X42 vintage pipes was different from that used in Chapter 3. Investigation showed that a combination of maximum principal strain, *Maxpe,* and fracture energy, G_C is more suitable damage parameters for simulating the nonlinear ductile fracture behaviour of X42 vintage pipes subjected to full-scale four-point bending. These parameters were calibrated using a full-scale local fracture response and a global tensile strain response. The XFEM numerical results were validated against the eight full-scale test results. The effect of internal pressure, flaw depth, and flaw length on the TSC were investigated. This chapter is derived from a published conference proceeding, the America Society of Mechanical Engineers (ASME) 2019 Pressure Vessels and Piping (PVP) Conference.

Chapter six extends the methodology presented in Chapter five for conducting a parametric study to investigate the TSC of welded X42 vintage pipe by varying robustly the influential parameters affecting the TSC. The effect of internal pressure variations, as well as other essential parameters, on the TSC of the numerical XFEM pipe models under bending, is investigated, followed by a nonlinear regression analysis to fit the TSC predictive model, derived based on the results of the parametric XFEM analyses. This chapter is based on a research paper submitted to the ASME Journal of Pressure Vessel Technology (PVT).

Chapter seven provides a general summary and conclusions of the undertakings of this research program, notable scientific contributions, assumptions and limitations of the model, as well as highlights of recommended areas for further research work.

1.9 References

[1] Natural Resources Canada (NRCan) Energy fact book 2016-2017

[2] Alberta Energy Regulator (2013, August). Report 2013-B: Pipeline Performance in Alberta, 1990-2012. Retrieved from: http://www.aer.ca/documents/reports/R2013-B.pdf

[3] Lower, M., 2014. (Strain based) Oak Ridge National Laboratory. ORNL/TM-2014/106 Design Methodology of Large Diameter grade X80 Line pipe, Spring field VA, USA.

[4]Wikipedia.org/wiki/Trans-Alaska_Pipeline_System#/media/File:Trans-Alaska_Pipeline_System_Luca_Galuzzi_2005.

[5] Lee, J.P. and Bohinsky, J.A. (1996). Design of buried pipeline subjected to large fault movement. In Proceedings of the 11th World Conference on Earthquake Engineering, Acapulco, Mexico (pp. 23-28).

[6] W. Ramberg and W. R. Osgood, "Description of stress-strain curves by three parameters," Technical Note No. 902, National Advisory Committee for Aeronautics, Washington DC., 1943.

[7] Fyrileiv, O. and Collberg, L., (2005). Influence of pressure in pipeline design: effective axial force. In ASME 2005 24th International Conference on Offshore Mechanics and Arctic Engineering (pp. 629-636). American Society of Mechanical Engineers.

[8] Nobahar, A., Kenny, S., Phillips, R., 2007, "Buried Pipelines Subject to Subgouge Deformations," International Journal of Geomechanics 7, pp. 206-216.

[9] Verstraete, M., De Waele, W., Hertelé, S. and Denys, R., 2014, "Experimental-Numerical Evaluation of Ductile Tearing Resistance and Tensile Strain Capacity of Biaxially Loaded Pipelines," (Ph.D. Dissertation). Department of Mechanical Construction and Production, Faculty of Engineering and Architecture, Ghent University, Belgium.

[10] Canadian Standards Association, 2011, Z662 - 11: Oil and Gas Pipeline Systems.

[11] 2010, API 1104: Welding of Pipelines and Related Facilities.

[12] Knauf, G., and Hopkins, P., 1996, "The EPRG Guidelines on the Assessment of Defects in Transmission Pipeline Girth Welds," 3R International, 35, pp. 620-624.

[13] Ahmed, H., Abbas, M. I., and Shahen, M. A. K., 2013, "Girth Weld Fitness after Multiple SMAW Repairs," Pipeline and Gas Journal, 240, pp. 1-4.

[14] Lee, K. Y., 2008, "Reducing Pipeline Construction Costs with Girth Weld ECA," Pipeline and Gas Journal, 235, pp. 16-17.

[15] McLamb, M., Hopkins, P., Marley, M., and Nessim, M., 2002, "A Justification for Designing and Operating Pipelines up to Stresses of 80% SMYS", International Pipeline Conference, Calgary, Alberta, Canada, paper n° IPC02-27007.

[16] DNV, Major New Oil Discovery in the Barents Sea, via www.dnv.com accessed on 02-02-2012.

[17] Lillig, D. B., 2008, "The First (2007) ISOPE Strain Based Design Symposium - a Review", International Offshore and Polar Engineering Conference, Vancouver, Canada, pp. 1-12.

[18] Lillig, D. B., Newbury, B. D., and Altstadt, S. A., 2009, "The Second (2008) ISOPE Strain-based Design Symposium - a Review", International Offshore and Polar Engineering Conference, Osaka, Japan, pp. 1-10.

[19] Arslan, H., Hamilton, J., Lele, S., Minnaar, K., Albrecht, B., Cook, M. F., and Wong, P., 2010, "Strain Demand Estimation for Pipelines in Challenging Arctic and Seismically Active Regions," International Pipeline Conference, Calgary, Alberta, Canada, paper number IPC2010-31505.

[20] Vitali, L., Torselletti, E., Marchesani, F., and Bruschi, R., 1996, "Use (and Abuse) of Strain Based Criteria in Offshore Pipeline Technology," Advances in Subsea Pipeline Engineering and Technology, Aberdeen, UK, paper number ASPECT96-135.

[21] Wang, Y. Y., Liu, M., Horsley, D., and Zhou, J., 2006, "A Quantitative Approach to Tensile Strain Capacity of Pipelines," International Pipeline Conference, Calgary, Alberta, Canada, paper no IPC2006-10474.

[22] Wang, Y. Y., Cheng, W., and Horsley, D., 2004, "Tensile Strain Limits of Buried Defects in Pipeline Girth Welds," International Pipeline Conference, Calgary, Alberta, Canada, paper no IPC04-0524.

[23] Olso, E., Berg, E., Holthe, K., Nyhus, B., Skallerud, B., Thaulow, C., and Ostby, E., 2008, "Effect of Embedded Defects in Pipelines Subjected to Plastic Strains During Operation," International Offshore and Polar Engineering Conference, Vancouver, Canada, pp. 143-148.

[24] Yong-Yi W, Ming L, and Yaxin S., 2011, "Second Generation Models for Strain-Based Design." PRCI.

[25] Verma, N., Fairchild, D. P., Noecker, F. F., Macia, M. L., and Nissley, N. E., 2014, "Advanced Strain-Based Design Pipeline Welding Technologies," ASME Paper No. IPC2014-33079.

[26] Kibey, S., Wang, X., Minnaar, K., Macia, M. L., Fairchild, D. P., Kan, W. C., Ford, S. J., and Newbury, B., 2010, "Tensile Strain Capacity Equations for Strain-Based Design of Welded Pipelines," ASME Paper No. IPC2010-31661.

[27] National Energy Board, (2014) Mackenzie Gas Project

[28] Nyhus, B., Østby, E., Zhang, Z., Olsø, E., Røstadsand, P A., Eikrem, P A., (2009). "Large Scale Tests of Strain Capacity of pipe Sections with Circumferential Defects Subjected to Installation-induced Plastic Strain History." Proceedings of the ASME 28th International Conference on Ocean, Offshore and Arctic Engineering OMAE2009 May 31 - June 5, 2009, Honolulu, Hawaii.

[29] Sen M., Cheng J. J. R., Zhou, J. (2011): "Behaviour of Cold Bend Pipes under Bending Loads," Journal of Structural Engineering, Volume 137, Issue 5, DOI:10.1061/(ASCE)ST.1943541X.0000219.

[30] Sen M. (2006); "Behaviour of Cold Bend Pipes Under Combined Loads" Ph.D. dissertation, University of Alberta

[31] Ahmed, A. U. (2010). Failure criteria for tearing of telescoping wrinkles (Ph.D. Dissertation). Structural Engineering, University of Alberta, Edmonton, AB, Canada.

[32] Ndubuaku, O. (2019). A new material characterization approach for evaluating the deformational capacity of onshore pipelines (Ph.D. Dissertation). Structural Engineering, University of Alberta, Edmonton, AB, Canada.
[33] CSA Z662-11. Oil and gas pipeline systems. Sixth Edition; Update No 1; January 2012.

[34] Wang Y.Y., Cheng W. (2004)," Guidelines on Tensile Strain Limits. Gas Research Institute Report 04/0030", Des Plaines, IL.

[35] Wang Y.Y., Cheng W., Horsley D. (2004)," Tensile Strain Limits of Buried Defects in Pipeline Girth Welds," Proceedings of IPC2004, International Pipeline Conference, IPC2004524

[36] Wang Y.Y., Cheng W., Horsley D. (2004), "Tensile Strain Limits of Girth Welds with Surface-Breaking Defects Part I – An Analytical Framework," Proceedings of the 4th International Conference on Pipeline Technology, 235-249.

[37] Wang Y.Y., Cheng W., Horsley D. (2004), "Tensile Strain Limits of Girth Welds with Surface-Breaking Defects Part II – Experimental Correlation and Validation," Proceedings of the 4th International Conference on Pipeline Technology, 251-266.

[38] Wang Y.Y., Rudland D., Denys R., Horsley D. (2002), "A Preliminary Strain Based Design Criterion for Pipeline Girth Welds," Proceedings of 4th International Pipeline Conference, Calgary, IPC2002-27169.

[39] Pick, R. J., Glover, A. G., and Coote, R. I., 1980, "Full-Scale Testing of Large Diameter Pipelines," Proceedings of the Pipeline Energy Plant Piping Conference, The Welding Institute of Canada, Calgary, Alberta, Canada, pp. 357–366.

[40] Glover, A. G., Coote, R. I., and Pick, R. J., 1981, "Engineering Critical Assessment of Pipeline Girth Welds," Conference on Fitness for Purpose Validation of Welded Construction, The Welding Institute, London.

[41] Glover, A. G., and Coote, R. I., 1984, "Full-Scale Fracture Tests of Pipeline Girth Welds," Circumferential Cracks in Pressure Vessels and Piping, Vol. II, PVP Vol. 95, G. M. Wilkowski, ed., American Society of Mechanical Engineers, New York, pp. 107–121.

[42] Østby, E., and Hellesvik, A., 2007, "Fracture Control–Offshore Pipelines JIP Results From Large Scale Testing of the Effect of Biaxial Loading On the Strain Capacity of Pipes with Defects,"

17th International Offshore and Polar Engineering Conference (ISOPE), Lisbon, Portugal, Jul. 1–6, Vol. 4, Paper No. ISOPE-I-07-516.

[43] Igi, S., Sakimoto, T., and Endo, S., 2011, "Effect of Internal Pressure on Tensile Strain Capacity of X80 Pipeline," Proc. Eng., 10, pp. 1451–1456.

[44] Abdulhameed, D., Cakiroglu, C., Lin, M., Cheng, R., Nychka, J., Sen, M., and Adeeb, S., 2016, "The effect of internal pressure on the tensile strain capacity of X52 pipelines with circumferential Abaqus," Journal of Pressure Vessel Technology, 138(6).

[45] Fairchild, D. P., Kibey, S. A., Tang, H., Krishnan, V. R., Wang, X., Macia, M. L., and Cheng, W., 2012, "Continued Advancements Regarding Capacity Prediction of Strain-Based Pipelines," ASME Paper No. IPC 2012-90471.

[46] Tang, H., Fairchild, D. P., Noecker, F. F., Panico, M., Crapps, J., and Cheng, W., 2014, "Strain Capacity Prediction of Strain-based Pipelines," ASME Paper No. IPC2014- 33749.

[47] Kiefner, J. F., and Trench, C. J., (2001) Oil Pipeline Characteristics and Risk Factor; Illustrations from the Decade of Construction" Kiefner & Associates Inc. and Allegro Energy Group for American Petroleum Institute Pipeline Committee.

[48] ABAQUS CAE 6.14-2 / Documentation.

[49] Wolfram Research Inc., Mathematica, Version 11.3, Champaign, IL, 2018.

[50] Fairchild, D. P., Crapps, J. M., Cheng, W., Tang, H., and Shafrova, S., 2014, "Full-scale Pipe Strain Test Quality and Safety Factor determination for Strain-based Engineering critical Assessment," ASME Paper No. IPC2016- 64191.

2. LITERATURE REVIEW

2.1 Introduction

The objectives of this review are to cite literature that will help to build-up knowledge regarding previous research carried out on a strain-based approach to the evaluation of the TSC of welded energy pipelines subjected to various loading conditions, and hence, to provide some necessary information to guide this research program. Emphasis has been given to better understand the procedure involved in the development of the predictive model for estimating the TSC of welded energy pipelines necessary for their strain-based engineering critical assessment (SBECA). This review will cover a brief discussion on several topics, including pipeline specifications and grades, weld defect classification and the Canadian oil and gas pipeline systems specification (CSA Z662.11) [1], fracture, and additional details of the full-scale testing program adopted in this research.

2.2 Specification and grades of pipes

Pipeline systems are standardized in many pipe specifications or standards, such as American Petroleum Institute (API) Spec. 5L (2012) [2]. The API specification 5L adheres to the International Organization for Standardization (ISO) 3183 [3] and identifies two basic product specification levels (PSL), which are PSL 1 and PSL 2. They represent different levels of standard technical requirements for seamless or welded steel pipes [4].

For intermediate pipe grades, the steel grades are named in these two major formats:

(1) For PSL 1, the letter L followed by the specified minimum yield strength in MPa and, for PSL 2 pipe, the letter describing the delivery condition is added as a suffix; R, N, Q or M, representing As-Rolled, Normalized, Quenched and Heat treatment of weld area only respectively [2].

(2) For PSL 1, the letter X followed by a two or three-digit numbers equal to the specified minimum yield strength in 1000 psi rounded down to the nearest integer and, for PSL 2 pipe, the letter describing the delivery condition as described in format (1) is added as a suffix [2].

It is important to note that, today, the second format, using the letter X, is popularly used in pipeline specification and is equally adopted in this research.

PSL 1 is a standard quality for line pipes, while PSL 2 contains additional quality for chemical composition, mechanical properties, and testing requirements. Pipe grades covered by API Spec 5L include A25, A, B, and X-grades such as; X42, X46, X52, X56, X60, X65 and X70 for PSL 1 pipes, and X-grade from X42 to X70, including X80, X90, X100 and X120 for PSL 2 pipes. Illustrating the naming formats explained above, using the pipe grade, which forms the research object of this thesis, for PSL 1, we have L290 and X42 using formats 1 and 2, respectively. For an As-rolled PSL 2 pipe, we have L290R and X42R using formats 1 and 2, respectively [2, 4].

2.3 Evolution pipe grades

Until the early 1960s, vintage pipelines (pipeline steels with relatively low yield strengths, manufactured using old materials and construction techniques) were used for pipeline construction [5]. Types X42, X46, X52 and X56 pipelines with yield strengths of 42,000 psi, 52,000 psi, and 56,000 psi, respectively, were used almost exclusively [2]. In the 1970s, normal strength pipes, X60, X65, and X70 began to gain acceptance but were not widely used because of limitations in the welding technology [5]. The use of thermomechanical treatment of steel to improve pipe mechanical properties and welding technology made these grades more popular and paved the way for modern pipes with higher grades. Modern pipes with a higher strength but lower ductility such as X80, X100, and X120 were manufactured but were not fully in use due to inadequate load response history. Pipelines constructed with relatively low-strength, high-ductility vintage steel have historically proven to safely accommodate large strains generated by the applied loads, especial through differential ground movement. These steel pipelines are capable of deforming plastically and maintaining their structural capacity and leak-tight integrity [6, 7].

2.4 Weldability of steel pipes

Weldability expresses the ease by which a material can be welded (Drive, 2013) [8]. Good weldability ensures the adequate strength and toughness of the weld and HAZ. As presented in the SteelConstruction. info [9], welding is an important process used in fabricating steel pipes; the most common method is the use of arc welding. An electric arc is used to generate intense heat to melt the BM at the joint, and separate consumable filler material (electrode), is usually added in the fusion. Upon cooling and solidification, a metallurgical bond - WM is created. If the filler matches the chemical composition of the BM, the WM is described as "matching" WM, which has similar mechanical properties to the BM, particularly in strength; if the filler matches the chemical composition of a metal with lower/higher material properties than the BM, then the WM is described as "undermatching/overmatching" WM, respectively [9]. The region in the BM close to the WM is referred to as the HAZ, which has not been melted, but the heat from welding has alternated its mechanical properties. Butt welds (groove welds) and fillet welds are the major types of welds, shown in Figure 2-1. A typical weld can be referred to as weld with full penetration or partial penetration depending on the level of penetration adopted in the welding technique. The full penetration weld typically has equal strength as the BM, while the partial penetration has less strength because of the associated smaller cross-sectional area compared to the BM. A fillet weld is easier to manufacture but is less effective to restore the strength than a butt weld.

Virtually all steels are weldable, but there is significant variation in both the quality and cost of welds. Low carbon steels usually exhibit better weldability than high carbon steels. This is because of the higher possibility that high carbon steel cracks in the WM or HAZ during the cooling process after welding. A preheated or post-heated treatment is necessary for high carbon steel to create quality joints [8]. Overall, the weldability increases with a decrease in the carbon content or more accurately as the carbon equivalent (CE) decreases Eq. 2-1. The international expression of the CE for a typical pipe with a minimum of 0.12% carbon composition, is provided by [2] as:

$$\mathrm{CE} = \mathrm{C} + \frac{M_n}{6} + \frac{C_r + M_o + V}{5} + \frac{N_i + C_u}{15} \qquad (2-1)$$

where: carbon (C), manganese (Mn), chromium (Cr), molybdenum (Mo), vanadium (V), nickel (Ni), copper (Cu).

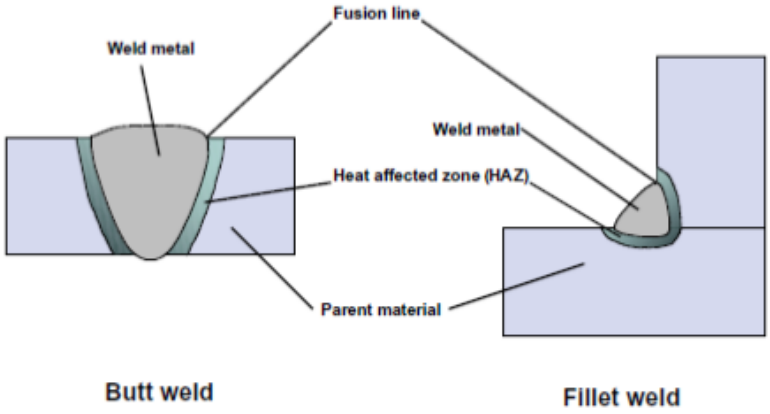

Figure 2-1 Butt weld and fillet weld [9]

2.5 Tensile strain capacity of welded pipelines

The majority of studies (e.g. [10-13]) conducted on pipeline structures in recent years were essentially focused on the evaluation of the compressive strain capacity when buckling occurs, which represents a serviceability limit state. Such research studies do not capture the effect of girth weld defects and, consequently, TSC.

To the author's knowledge, there has been no previous research before the commencement of this research that discussed the prediction of the TSC of welded vintage pipes, and particularly X42 welded vintage pipes. For this reason, a review of some research conducted on the TSC of straight welded pipes is presented.

It is important to mention that a good number of studies conducted on the TSC of pipelines neglected the effect of the internal pipe pressure.

2.5.1 Research by Wang, et al. (2002, 2004) [14-17]

Wang et al. (2002) [14] developed a methodology for establishing the preliminary SBD criteria for girth welds using the concept of CTOD. The CTOD was expressed in terms of applied strain in other to establish an accurate strain design criterion. The critical strain was defined as the longitudinal strain value at the point where the CTOD in the full-scale tests or finite element models reaches the CTOD toughness of the material. The location of the critical strain was chosen to be remote from the girth weld. Therefore, this strain value is also called the remote strain.

Wang, et al. (2004) [15-17] conducted a considerable experimental program and numerical simulation of full pipe behaviour of girth welds containing buried defects in the pipe wall and surface-breaking defects subjected to high longitudinal strains. Part I of the surface-breaking defect investigation was conducted using an analytical framework. Part II of the surface-breaking defect investigation was conducted by experimental correlation and validation. Pipe grades ranging from X65 to X80 of NPS 30 straight pipes with wall thickness ranging from 6.35 mm to 19.05 mm containing both surface-breaking and buried defects of various sizes were examined. The crack driving force methodology, in conjunction with a constraint-sensitive fracture mechanics approach, was applied to examine the factors affecting the strain limits of the girth welds.

They compared the strain limits between buried and surface-breaking defects. They concluded that surface-breaking defects are more detrimental to the tolerance of high longitudinal strains than buried defects of the same size.

This finding confirmed the assumption that surface braking defects are more critical than buried defects of the same size and thus formed the basis of its usage throughout this research in the characterization of TSC of X42 vintage pipes.

2.5.2 Research by Ostby et al. (2007) [18]

Østby et al. [18] carried out considerable full-scale experimental pipe test programs that included six (pressurized and unpressurized) NPS 12 X65 steel grade straight pipe specimens subjected to four-point bending. In the test program, a crack with 100 mm circumferential length was placed at the location of the pipe where the wall thickness was smallest. The crack depth to pipe wall thickness ratio was kept constant in all tests. Two of the experiments were carried out without

internal pressure, and in the remaining tests, two different levels of internal pressure were tested corresponding to 25% SMYS and 60% SMYS. The strain measurements were made using strain gauges located 0.5 *D*, 1 *D*, and 2 *D* away from the center of the pipe. The CMOD of the flaw was measured using clip gauges with an attack point 0.2 mm below the external pipe surface. CTOD and crack growth (Δa), was measured using silicone replica of the flaws which, were made at different stages of the experiments. It was observed that the internal pressure significantly reduces the TSC of the pipe from a level of 3.5 – 4 % to a level of 1.5 – 2%. Furthermore, it was confirmed that the unpressurized specimens failed due to local buckling on the compression side. In contrast, the pressurized specimens failed due to fracture at the flawed locations on the tension side.

Ostby et al. (2008) [19] also conducted extensive experimental and numerical work on the behaviour of straight X65 steel grade pipes with a diameter to thickness ratio of 22. The specimens were surface cracked pipes subjected to four-point bending with and without internal pressure to investigate the TSC. The numerical simulation of the ductile tearing failure mode was conducted using the GTN model in Abaqus finite element method. The numerical results were validated against full-scale test results. They conducted a parametric study of the surfaced cracked pipe subjected to tension investigating the effects of internal pressure and flaw size on TSC of the pipes. Similar results as obtained from the full-scale experiments were observed; the internal pressure significantly influenced the TSC, and the increase in crack depth increased the CTOD. They equally observed that the unpressurized specimens failed due to local buckling on the compression side. In contrast, the pressurized specimens failed due to fracture at the flawed locations on the tension side.

2.5.3 Research by Igi et al. (2011) [20]

Similarly, Igi et al. (2011)[20] conducted a series of pressurized full-scale tests and unpressurized CWP and SENT tests in addition to robust FEA simulation program on NPS 20, X80 welded pipes, with a wall thickness of 14.3 mm for the prediction of the TSC in the presence of surface defects. The surface defects were machined into the HAZ of the girth weld. The effect of internal pressure was investigated by comparing the results of the full-scale pressurized test to the results of the

CWP test. They observed that the TSC decreases by approximately 50% due to the internal pressure and that the TSC of pressurized pipes can be predicted by using the R-curve from SENT tests and the crack driving curve from FEA.

2.5.4 Research by Mathias et al. (2013) [21]

Mathias et al. (2013) adopted a mixed experimental-numerical research methodology to; measure the ductile crack extension using SENT tests, MWP tests and investigated the influence of internal pressure on the TSC by relating the TSC of pressurized full pipe specimens to CWP specimens.

They observed that the constraint in SENT specimens is higher compared to MWP specimens, this suggested that a defect assessment based on SENT tests is potentially more conservative compared to an assessment based on wide plate test results.

The study also led to the formulation of an analytical pressure correction function that allows assessing the TSC of pressurized pipes from CWP test data.

2.5.5 Research by Abdulhameed et al. (2016) [22]

Abdulhameed et al. (2016) [22], conducted eight full-scale pipe tests program to characterize the TSC of straight pipes at the University of Alberta. The eight specimens tested in the experimental program were X52 vintage NPS 12 pipes with a wall thickness of 6.91 mm. The initial outer surface breaking flaw was machined on the pipe metal close to the HAZ of the specimens. During testing, the internal pressure for the specimens caused hoop stresses ranging from 30% to 80% SMYS, and an eccentric tensile force was applied to the pressurized pipes.

They concluded that the level of internal pressure could reduce the TSC by 50% or more depending on the flaw size. On the other hand, the CMOD was not affected by the level of internal pressure and was a function of the flaw dimensions.

CSA Z662 [1] and PRCI [23] equations show a highly conservative result when compared with the test results, while ExxonMobil's generalized equation [24] was slightly conservative compared to the test results.

It is important to mention that; current pipeline design codes do not provide prediction methods for the determination of TSC of girth welded pipelines subjected to large plastic strain in the presence of internal pressure [22].

2.5.6 Research by Research by ExxonMobil Upstream Company

2.5.6.1 Fairchild et al. (2012) [24] of the EM Upstream Company undertook a comprehensive experimental and numerical program to characterize the TSC of welded pipelines after their previous research publications [25-29], the authors have described methods for strain capacity prediction through FEA or simplified equations, strain capacity can be predicted based on input parameters such as pipe geometry, internal pressure, material properties, girth weld defect size, and high-low misalignment. These models (equations) were validated against a database of about 50 full-scale pipe strain tests that included a broad range of geometries and pipe grades (8" – 42", 13 mm – 25 mm, X60 – X80). A pressure factor (P_f) was incorporated into the models, (Eq. 2-2), the pressure factor allows the calculation of strain capacity as a function of pressure that results in hoop stresses from zero to 80% SMYS.

The simplified equation is considered a level two SBECA procedure. It was shown that the strain capacity depends on flaw size, weld misalignment, weld metal strength overmatch, pipe geometry, material properties, yield to tensile ratio (Y/T), uniform elongation (UEL), toughness, and internal pressure.

$$\varepsilon_c = \mathrm{P_f}.\left[\beta_1 \ln\left[\frac{\mathrm{aC}}{(t-a)^2}\right] + \beta_2\right] \qquad (2-2)$$

where ε_c is the tensile strain capacity, a is the flaw depth, C is half of the flaw length, P_f is the pressure factor, and t is the pipe wall thickness. $\beta_1$and β_2 are functions of flaw length, misalignment, overmatch, pipe material properties and R-curve.

2.5.6.2 Tang et al. (2014) [30] of the EM Upstream Company, continued the strain-based TSC research by extending the experimental and numerical program, by leveraging damage mechanics modelling to develop TSC predictive models capable of evaluating the TSC of welded pipelines ranging from X60 to X100. Their research included full-scale testing, the development of a finite element model using the GTN model, and the development of design equations to predict the TSC of welded straight pipes. A finite element model was also developed to simulate the experimental behaviour.

A parametric study using the finite element model was completed on additional pipe geometries and loading conditions. Based on this study, design equations were developed that could predict the TSC of welded pipelines.

Another generalized equation (Eq. 2-3) was proposed by EM to cover a wider range of variables. The generalized equation was considered level three of the SBECA technique, which resulted in a more complex, yet accurate equation. The equation was validated against 93 full-scale test (FST) data. This equation is used to evaluate the TSC at a pressure level of 80% SMYS; then, a correction factor is used to evaluate the TSC at the actual applied internal pressure [30].

$$\mathrm{TSC}_{0.8} = \frac{\left[\Phi\left(\frac{\mathrm{K}}{\sigma}, \lambda, \frac{\mathrm{e}}{t}\right).\frac{\delta}{t} + C7\right].\left(C1\frac{D}{t} + C2\right)}{C6 + C8\left(\frac{\frac{a}{t}}{1-\frac{a}{t}}\right)^{C3}.\tanh\left(\mathrm{C}\,4\left(\frac{2\mathrm{C}}{t}\right)^{C5}\right)} \qquad (2-3)$$

where C_1 to C_8 are part of the coefficients (C_1 to C_{44}) ranging from -29.99 to 41.77, Φ is a material property parameter, K is a strength coefficient, N is the strain hardening coefficient, σ_Y is the true yield strength, λ is the weld strength overmatch, e is the weld misalignment, δ is the weld toughness parameter (CTOD), a is the flaw depth, t is the wall thickness, and $2C$ is the flaw length.

2.5.7 Research by PRCI/CRES

Wang et al. (2011) [23] of the PRCI/Center for Reliable Energy Systems (CRES), used a multidisciplinary approach involving fundamental fracture mechanics, small-scale material characterization and full-scale pipe tests to develop TSC predictive models for welded pipelines ranging from X56 to X100. This study involved fundamental fracture mechanics, small-scale material characterization tests, and full-scale tests of pipes. As a result of this study, Eq. 2-4 was developed to define the tensile design models provided for the strain-based design of pipelines.

$$\mathrm{TSC}_P = \mathrm{A}\frac{f(\delta_A)}{1+f\ (\delta_A)} \qquad (2-4)$$

where $f(\delta_A)= (C\delta_A)^{B{\delta_A}^D}$ and A, B, C, and D represent functions of flaw size, pipe material, weld mismatch, toughness and pipe dimensions, as presented in the PRCI report [23]. The proposed equation evaluates the TSC for pipes with pressure factor equal to 0.72 and wall thickness 15.9 mm. Furthermore, two correction factors were presented to account for the different internal pressure levels and pipe wall thicknesses. FEA was conducted, and the resulting driving force curves were used to develop a thickness correlation function using a curve-fitting procedure. The effect of internal pressure was investigated and found that as the internal pressure increases, the higher driving force is obtained; accordingly, a pressure factor correction was introduced.

2.6 Fracture

The term fracture describes the local detachment of material cohesion in a solid body. Fracture is an ultimate limit state of materials, which can be described by the separation of a structural body in response to the applied stress [31]. The general process of a fracture can be described by the crack formation followed by crack propagation [31, 32]. The sequence of formation of a cup-and-cone fracture in a typical ductile steel specimen, such as an X42 vintage pipe specimen in response to uniaxial tensile stress is shown in Figure 2-2. When a ductile steel specimen is subjected to tensile load, it elongates to some extent, followed by the formation of necking; consequently, small microvoids are generated in the interior of the specimen as a result of the triaxial tensile stresses due to geometrical changes. The microvoids then begin to coalesce (combine) to form internal crack. The crack grows gradually outwards perpendicular to the tensile stress into larger cracks

and later propagates rapidly to the edge of the specimen at 45° to the tensile stress. In the final stage, shear lips were formed by shear stress; these shear lips around the periphery of the neck constitute the cup-shaped and the cone-shaped final fracture surfaces [33, 34].

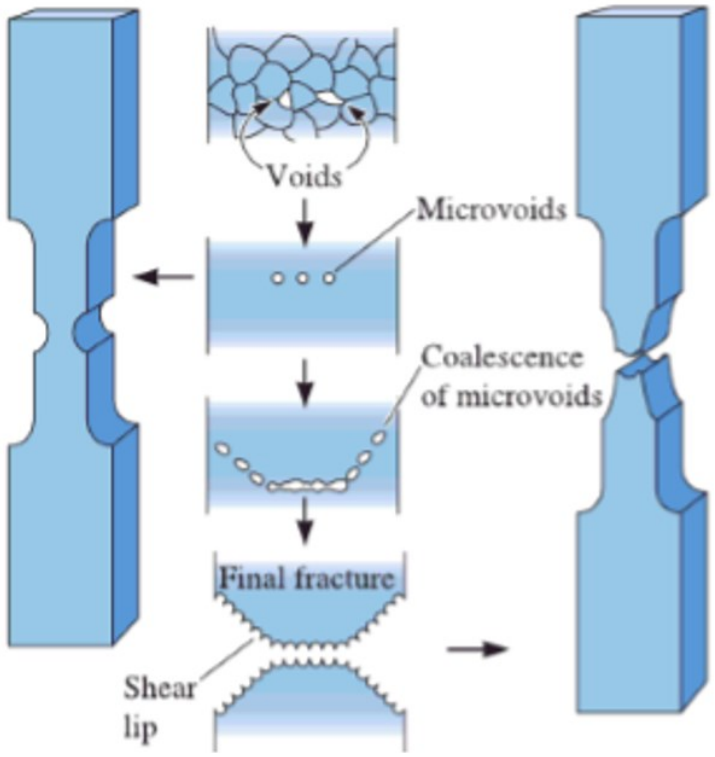

Figure 2-2 The sequence of formation of tensile fracture from a ductile steel specimen [33]

2.6.1 Fracture mechanics

Fracture mechanics (FM) is the specific field which deals with fracture and failure processes in engineering materials and constructions. In FM, it is assumed that every component and every real material inevitably possesses flaws or other defects [35].

For this reason, the existence of such defects is explicitly assumed in FM and modelled as cracks of depth size, *a* and length *2C*. Also, in FM, the behaviour of cracks in bodies is described from a

macroscopic point of view in the context of continuum mechanics [35]. Such a discrete crack is surrounded by defect-free material, which is described by the established material laws of a continuum, as shown in Figure 2-3.

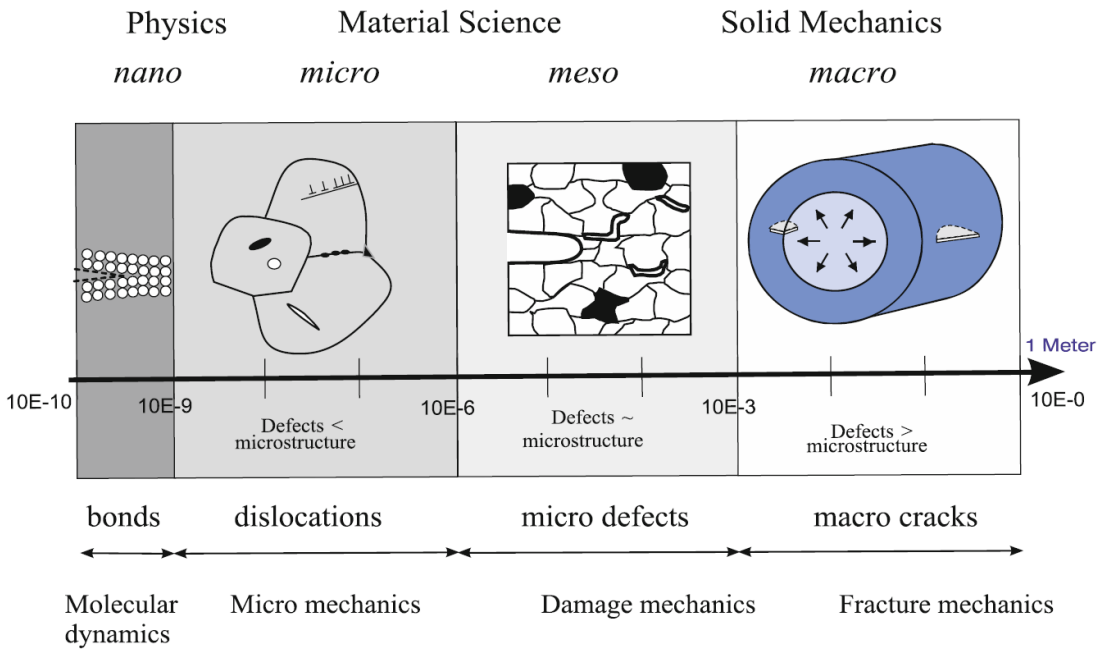

Figure 2-3 Fracture processes at different scales and levels [35]

The traditional design approach (TDA) and fracture mechanics design approach (FMDA) for the design of structures and selection of materials were identified in the past and described by many researchers, such as [36, 37]. The TDA is a design approach that focuses on the strength of materials. The yield and tensile strength of the material are usually measured in a tension test to obtain the material resistance to applied tensile stress. On the other hand, the FMDA added the crack size as a new parameter and measured the fracture toughness of a material rather than its tensile strength properties. The fracture toughness measures the ability of a material to resist crack formation and propagation. It can be directly measured using a fracture toughness test to obtain a toughness parameter (G, K, J, $CTOD$ or δ) or measured indirectly using a CVN impact test to estimate the energy required to fracture a notched specimen [4].

Prefabricating a crack or notch to produce the stress concentration and extreme condition in the vicinity of crack-tip to measure the fracture toughness of a material is very important [31].

However, the underlying principle of the FM approach is to characterize the stress and strain field in the vicinity of the crack tip by a single toughness parameter, such as the stress-intensity factor (K). The crack begins to grow when the stresses adjacent to the crack tip reaches the material fracture toughness, [36]. A subscript is used to denote the fracture mode in the stress-intensity factor, K.

The stress intensity factors for the three basic fracture modes, due to the loading applied to the crack plane are Mode I (denoted by K_I), Mode II (denoted by K_{II}), and Mode III, (denoted by K_{III}). The stress-intensity factor (K) is a function of the applied stress, the size of the crack and the constraint effect of the specimen geometry, which can be generally expressed by Anderson, 2005 [36]; Czicho, Saito and Smith, 2006 [37] as Eq. 2-5.

$$K_{(I,II,III)} = \beta\sigma\sqrt{\pi a} \qquad (2\text{-}5)$$

where $K_{(I,\,II,\,III)}$ is the stress intensity factor related to each mode of loading ($MPa\sqrt{m}$), σ is the applied remote stress (MPa), a is the crack depth (m), and β is a factor that depends on the geometry of the specimen and the mode of loading.

The fracture modes expressed as a result of the load applied to the crack surfaces are shown in Figure 2-4:

Mode I (Opening mode): The crack opens perpendicular to the crack plane. In this case, the tensile stress is applied normal to the plane of the crack.

Mode II (In-plane shear mode): This is the condition in which shear stress is parallel to the plane of the crack and perpendicular to the crack front. The crack faces are displaced on their plane, normal to the crack front, which correlates to a transversal shearing load.

Mode III (Out-of-plane tearing mode): The crack faces are displaced on their plane, parallel to the crack front, which is related to the anti-plane longitudinal shearing load [35].

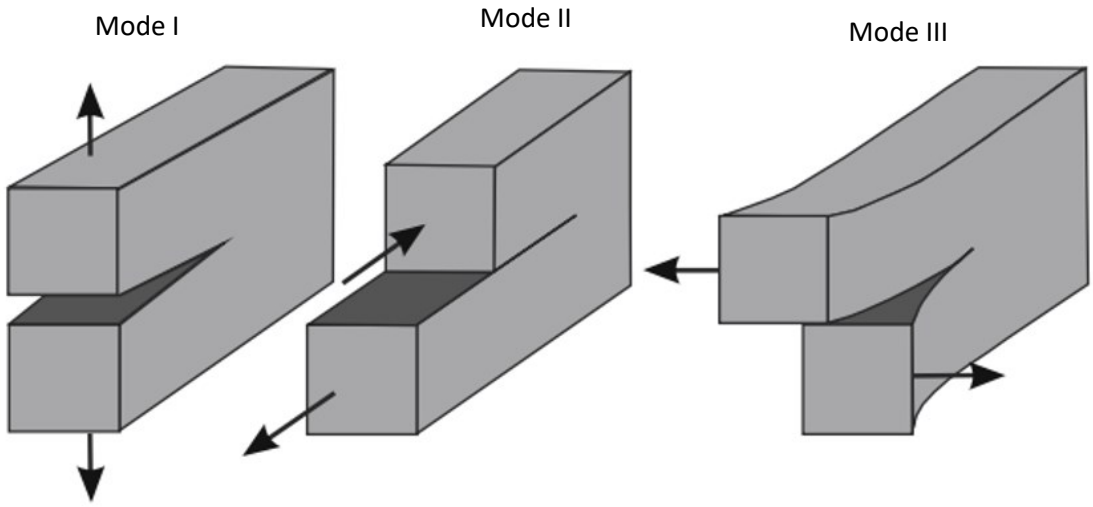

Figure 2-4 The three crack opening modes [36]

For Mode I case, the remote stress field perpendicular to the crack plane and the displacement of the crack plane as a result of the applied remote stress can be evaluated using the Eq. 2-6 and Eq. 2-7;

For Mode I load case, the singular stress fields components are given as:

$$\sigma_y = \frac{K_I}{\sqrt{2\pi r}} \cos\left(\frac{\theta}{2}\right)\left[1 - \sin\left(\frac{\theta}{2}\right)\sin\left(\frac{3\theta}{2}\right)\right] \qquad (2-6)$$

The nonzero displacement components for Mode I load scenario are given as:

$$u_y = \frac{K_I}{2\mu}\sqrt{\frac{r}{2\pi}}\sin\left(\frac{\theta}{2}\right)\left[\kappa + 1 - 2\cos^2\left(\frac{\theta}{2}\right)\right] \qquad (2-7)$$

where μ is the shear modulus, ν is the Poisson's ratio, $\kappa = 3 - 4\nu$, (plane strain) and $\kappa = (3-\nu)/(1+\nu)(plane\ stress)$

2.6.2 Linear elastic fracture mechanics and elastic-plastic fracture mechanics

FM is divided into two major categories; linear elastic FM and elastic-plastic FM, but the theory for the first category is the basis of the two categories [35-37]. Linear elastic FM theory is valid for isotropic and linear elastic materials. That is, it applies to materials with the crack tip dominated by linear elastic deformation or with small scale plastic deformation (small scale yielding, Figure 2-5a). A sharp crack with limited plasticity formed at the crack tip, which propagates rapidly (brittle fracture), characterizes the linear elastic FM.

The elastic-plastic FM theory is valid for both the nonlinear elastic materials and elastic-plastic materials without considering unloading. It applies to materials whose crack tip is dominated with a large volume of plastic deformation, which leads to the blunting of the crack tip (large scale yielding). An initially sharp crack blunts with plastic deformation, resulting in a finite displacement (δ) at the crack tip (Figure 2-5 b).

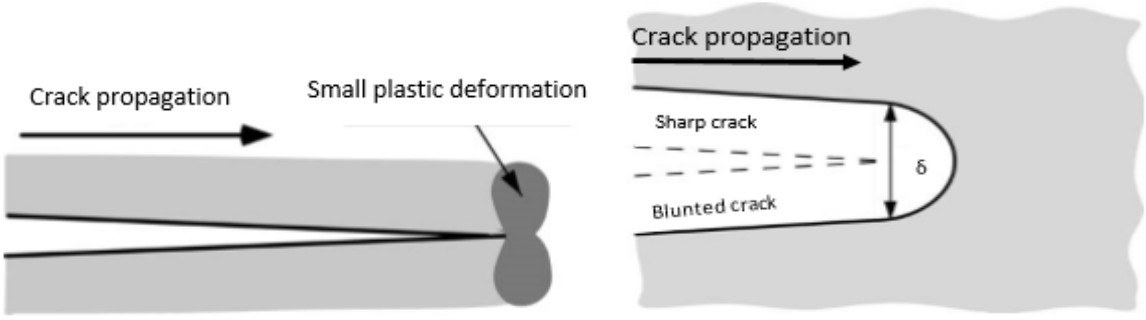

(a) Sharp crack with small plasticity at crack tip (b) Crack blunts by δ at the crack tip

Figure 2-5 Linear elastic fracture mechanics and elastic-plastic fracture mechanics (Anderson, 2005 pp. 34 and pp. 104) [36]

The loading paths are identical, but the unloading paths are different, as depicted in Figure 2-6. The unloading of the nonlinear elastic material follows the original loading path while the unloading of the elastic-plastic steel materials follows the path that is parallel to the linear loading path with a slope equal to Young's modulus [36].

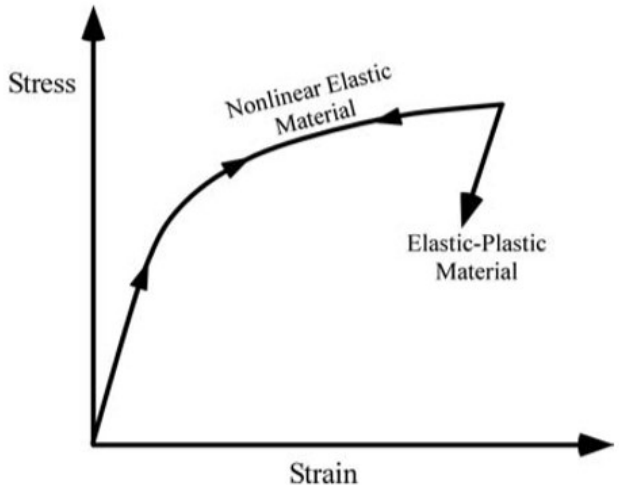

Figure 2-6 Schematic comparison of the loading and unloading of nonlinear elastic and elastic-plastic materials [36]

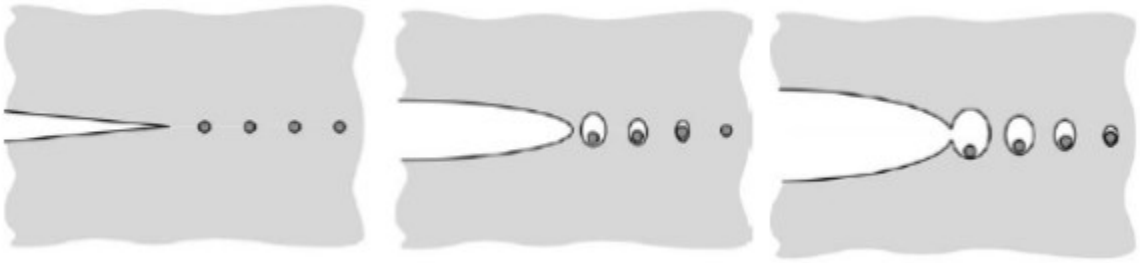

Figure 2-7 Ductile crack growth process (From Anderson, 2005, pp.232) [36]

The crack-tip opening displacement and the development of ductile crack growth in the elastic-plastic FM process are shown in Figure 2-7 [36]. As the cracked specimen is loaded, the microvoids initiate and then develop to voids. As the initial sharp crack blunts with a large scale of plasticity at the crack tip, voids continue to grow and eventually coalesce with the main crack. Due to the ductile crack growth, the specimen is torn slowly and stably [4, 36].

2.6.3 Fracture Toughness

In materials science, fracture toughness is a property which describes the ability of a material to resist fracture. The fracture toughness of a material say, for instance, steel can be characterized by conducting a fracture toughness test, to obtain a fracture toughness parameter such as the stress-intensity factor (K), the energy release rate (G), the J-integral (J), and the crack-tip opening displacement ($CTOD$) or δ. They can be measured by a single point value of fracture toughness under the plane strain conditions, such as K_{Ic}, G_{Ic}, J_{Ic} and δ_{Ic}, or an entire resistance curve (R-curve) where a parameter (K, G, J, δ) is plotted against the crack extension [36]. The fracture toughness is determined at the point close to the crack initiation (point of instability). It is usually characterized by plain strain fracture toughness K-factor (K_{Ic}) or by the energy release rate (G_{Ic}). The material resistance beyond the crack initiation is small, and thus the measurement is not required (Zhu & Joyce, 2012). The energy release rate (G) is an indication of the energy required to cause crack propagation, and it is related to the stress-intensity factor (K_I) based on crack tip constraints, given below in Eq. 2-8 [36].

$$G = \frac{{K_I}^2}{E'} \qquad (2-8)$$

where $\mathrm{E}' = \mathrm{E}$ under plane stress condition, and $\mathrm{E}' = \frac{E}{(1-\nu)^2}$ under plane strain condition

In the elastic-plastic FM, fracture toughness is determined by plotting an entire resistance curve (R-curve), such as the J-integral resistance curve (J – R curve) or CTOD resistance curve (δ – R curve), this explains the slow and stable crack tearing process. The J_{Ic} or δ_{Ic} is often traced from the R-curve at the onset of ductile crack growth, which is shown at a point on the curve whose slope changes dramatically, based on the requirement of a single point value of fracture toughness in many methods and applications [36 – 38]. The terms J_{Ic} or δ_{Ic}, indicates elastic-plastic initiation toughness, which are still measured under plane strain conditions. J-integral is a measure of the energy required to grow the crack and can be mathematically expressed as a line or surface integral that encloses the crack tip from one crack surface to the other [39].

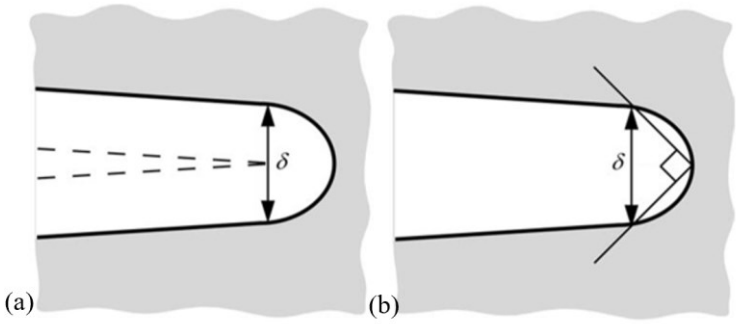

Figure 2-8 The definition of CTOD (a) displacement at the original crack tip and (b) displacement at the intersection of a 90 ° vertex with the crack flanks [36]

The $CTOD$ or δ is the displacement at the original crack tip (Figure 2-8) [36]. It should be noted that the elastic components of the fracture toughness can be determined in linear elastic FM, for example, the elastic component of J-integral, J_{el} is equal to the elastic energy release rate and is related to the stress-intensity factor for linear elastic Mode I loading shown in Eq. 2-9 [36].

$$J_{el} = \frac{{K_I}^2}{E'} \qquad (2-9)$$

The relationship between the J-integral and the crack tip opening displacement is given based on a constraint factor (m) and effective yield strength (σ_Y) Eq. 2-10. API 579-1/ASME FFS1 (2007) [40] takes 1.4 as an approximate value of m in the absence of detailed information. The effective yield strength is the average of the static yield strength and ultimate tensile strength, which is the flow strength.

$$J = m \cdot \sigma_Y \cdot \delta \qquad (2\text{-}10)$$

2.7 Finite element analysis

Formulation of the displacement function used in the finite element method:

The one-dimensional axial bar with two quadratic elements, having nodal coordinates x_1, x_2, and x_3 such that $x_1 < x_2 < x_3$, while N_i are the interpolation functions that have a value of 1 unit at the nodes and decrease linearly to zero at the neighbouring nodes (Figure 2-9) [41].

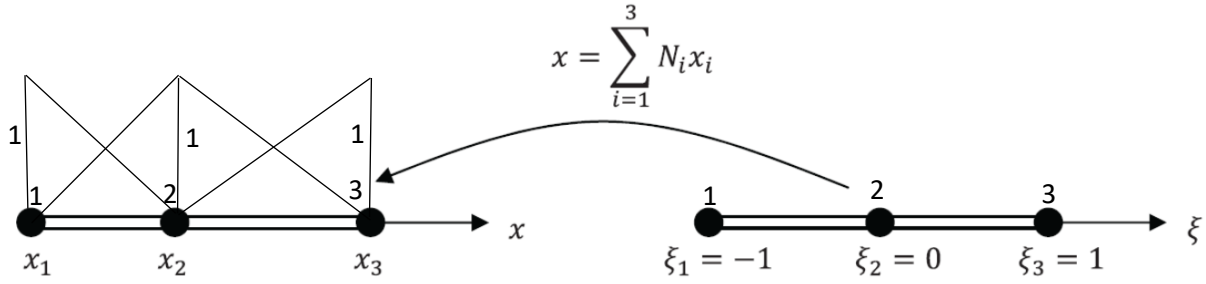

Figure 2-9 One dimensional quadratic isoparametric mapping [41]

A mapping between the general coordinate system x and the coordinate system ξ is defined (Figure 2-9) using the same shape functions that define the displacement in the coordinate system ξ as follows Eq. 2-11 [41]

$$x = N_1 x_1 + N_2 x_2 + N_3 x_3 \qquad (2-11)$$

The shape functions have the forms shown in Eq. 2-12 to Eq. 2-14:

$$N_1 = \frac{\xi(1-\xi)}{2} \qquad (2-12)$$

$$N_2 = (1+\xi)(1-\xi) \qquad (2-13)$$

$$N_3 = \frac{\xi(1+\xi)}{2} \qquad (2-14)$$

The gradient of the mapping is given in Eq. 2-15 as:

$$\frac{dx}{d\xi} = \sum_{i=1}^{3} \frac{dN_i}{d\xi} x_i \qquad (2-15)$$

If $u_1, u_2\ and, u_3$ are horizontal displacement of the nodes 1, 2 and 3, the horizontal displacement function is defined by Eq. 2-16 and Eq. 2-17 in the ξ coordinate system as:

$$u = N_1 u_1 + N_2 u_2 + N_3 u_3 \qquad (2\text{-}16)$$

$$u = \sum_{1}^{3} N_i u_i \qquad (2-17)$$

2.8 The extended finite element method (XFEM)

The XFEM is capable of simulating discontinuities such as crack due to major modifications in the displacement function of the traditional finite element method. Figure 2-10 is a one-dimensional axial bar with three linear elements, used to illustrate how a special function (Heaviside enrichment function) is used in the approximation field of the extended finite element to enable the XFEM to simulate a strong discontinuity such as crack. Linear shape functions employed for each element are shown in Eq. 2-18 to Eq. 2-20 as:

$N_1(\xi) = (1 - \xi)$ (2-18)

$N_2(\xi) = \xi$ (2-19)

$N_3(\xi) = (1+\xi)$ (2-20)

While the middle element is assumed to have a strong discontinuity, such as a crack, at an arbitrary location *C* between nodes 2 and 3 with φ(xc) = 0, as shown in Figure 2-10 [42]. To enrich the nodal points 2 and 3, the Heaviside sign function H(x) is employed, in which H(φ(x2)) = − 1 for the left side of the crack and H(φ(x3)) = + 1, for the right side of the crack, as shown in Figure 2-10. In this figure, the enriched Heaviside shape functions, that is, $N_j(x)$ H(x), is represented for nodal points 2 and 3. Obviously, the value of displacement u(x) at enriched nodes 2 and 3 is Eq. 2-21: [42]

$$u(x) = \sum_{i=1}^{n} N_i(x) u_i + \sum_{j=1}^{m} N_j(x)\, H(x) a_j \qquad (2-21)$$

Since the value of the displacement at an enriched node is not necessarily zero, the enriched displacement field can be corrected to Eq. 2-22

$$u(x) = \sum_{i=1}^{n} N_i(x)u_i + \sum_{j=1}^{m} N_j(x)\ (H(x) - H(x_j))a_j \qquad (2-22)$$

where $N_j(x)\ H(x)$ is the term representing the Heaviside enrichment function, while the jump in the displacement field across the strong discontinuity is represented by $N_j(x)\ (H(x) - H(x_j))$, which takes place at the discontinuity (crack) interface, u_i is the displacement at the non enriched nodes and u_i.

In such discontinuous cases, the kinematics of the strong discontinuity can be defined based on the Heaviside function. The Heaviside function is one of the most popular functions used to model the crack discontinuity in the XFEM formulation. The Heaviside function is defined as Eq. 2-22 [42]:

$$H(x) = \begin{cases} 0 & if \quad -\varepsilon \geq \varphi(x) \\ \frac{1}{2} + \frac{\varphi}{2\varepsilon} + \frac{1}{2\pi}\ sin\ \frac{\pi\varphi}{\varepsilon} & if\ -\varepsilon < \varphi(x) < \varepsilon \\ 1 & if \quad \varphi(x) \geq \varepsilon \end{cases} \qquad (2-23)$$

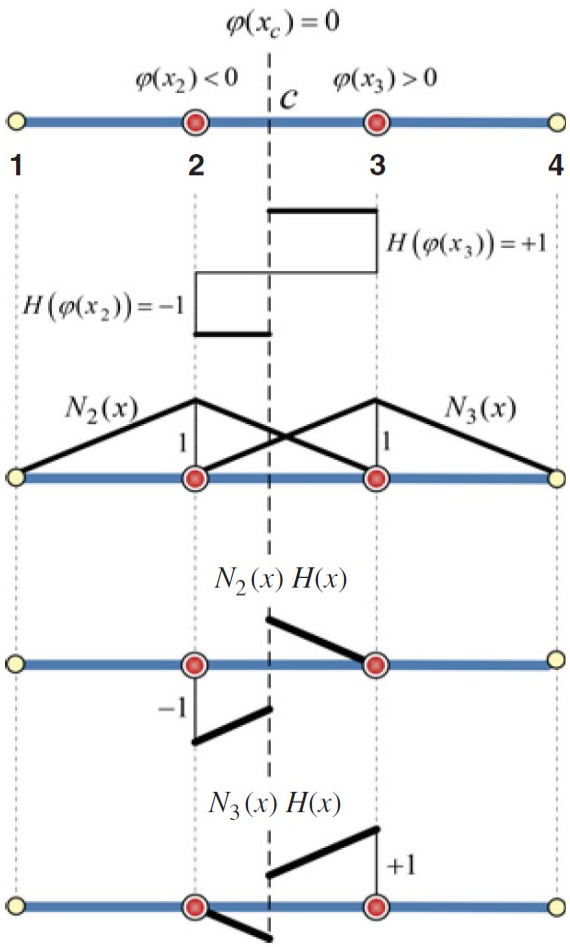

Figure 2-10 The principle of X-FEM with a strong discontinuity for an axial bar using the Heaviside function Nj(x)H(x) [42]

References

[1] CSA Z662-11 (2011). Oil and gas pipeline systems. Canadian Standards Association (CSA).

[2] API Specification 5L (2012). Specification for line pipe (45th ed.). Washington, DC: American Petroleum Institute (API).

[3] ISO 3183 (2012). Petroleum and natural gas industries-Steel pipe for pipeline transportation systems (3rd ed.). International Organization for Standardization (ISO).

[4] Lin, M., 2015, "Characterization of Tensile and Fracture Properties of X52 Steel Pipes and their Girth Welds," M.Sc. thesis, University of Alberta, Edmonton, AB.

[5] Wang, Y.-Y., Horsley, D and Rapp, S., (2016), "Evolution of Linepipe Manufacturing and its Implications on Weld Properties and Pipeline Service" Proceedings of the International Pipeline Conference 2016, Calgary, Alberta, Canada, September 26-30, 2016.

[6] H. Gao et al., The Concepts for Pipeline Strain-Based Design. Proceedings of the Seventeenth International Offshore and Polar Engineering Conference, Lisbon, Portugal, 476-482, 2010.

[7] S. T. Barbas and M. S. Weir, Strain-based Design Methodology for Seismic and Artic Regions, Proceedings of the Seventeenth International Offshore and Polar Engineering Conference, Lisbon, Portugal, July 1-6, 2007, 3073-3080, 2007.

[8] Drive, R. G. (2013). Steel: Production, properties, and shapes. Class lecture for Behaviour and Design of Steel Members course, University of Alberta.

[9] SteelConstruction.info. Retrieved from http://www.steelconstruction.info/Welding.

[10] Sen M., Cheng J.J.R., Zhou, J. (2011): "Behaviour of Cold Bend Pipes under Bending Loads," Journal of Structural Engineering, Volume 137, Issue 5, DOI:10.1061/(ASCE)ST.1943541X.0000219.

[11] Sen M. (2006); "Behaviour of Cold Bend Pipes Under Combined Loads" Ph.D. dissertation, University of Alberta.

[12] Ahmed, A. U. (2010). Failure criteria for tearing of telescoping wrinkles (Ph.D. Dissertation). Structural Engineering, University of Alberta, Edmonton, AB, Canada.

[13] Ndubuaku, O. (2019). A new material characterization approach for evaluating the deformational capacity of onshore pipelines (Ph.D. Dissertation). Structural Engineering, University of Alberta, Edmonton, AB, Canada.

[14] Wang Y.Y., Rudland D., Denys R., Horsley D. (2002), "A Preliminary Strain Based Design Criterion for Pipeline Girth Welds," Proceedings of 4th International Pipeline Conference, Calgary, IPC2002-27169.

[15] Wang Y.Y., Cheng W., Horsley D. (2004)," Tensile Strain Limits of Buried Defects in Pipeline Girth Welds," Proceedings of IPC2004, International Pipeline Conference, IPC2004524.

[16] Wang Y.Y. et al. (2004), "Tensile Strain Limits of Girth Welds with Surface-Breaking Defects Part I – An Analytical Framework," Proceedings of the 4th International Conference on Pipeline Technology, 235-249.

[17] Wang Y.Y. et al. (2004), "Tensile Strain Limits of Girth Welds with Surface-Breaking Defects Part II – Experimental Correlation and Validation," Proceedings of the 4th International Conference on Pipeline Technology, 251-266.

[18] Østby, E., and Hellesvik, A., 2007, "Fracture Control–Offshore Pipelines JIP Results From Large Scale Testing of the Effect of Biaxial Loading On the Strain Capacity of Pipes with Defects," 17th International Offshore and Polar Engineering Conference (ISOPE), Lisbon, Portugal, Jul. 1–6, Vol. 4, Paper No. ISOPE-I-07-516.

[19] Ostby, E., and Hellesvik, A. O., 2008, "Large-Scale Experimental Investigation of the Effect of Biaxial Loading on the Deformation Capacity of Pipes with Defects," International Journal of Pressure Vessels and Piping, 85, pp. 814-824.

[20] Igi, S., Sakimoto, T., and Endo, S., 2011, "Effect of Internal Pressure on Tensile Strain Capacity of X80 Pipeline," Proc. Eng., 10, pp. 1451–1456.

[21] Verstraete, M., (2013) Experimental-Numerical Evaluation of Ductile Tearing Resistance and Tensile Strain Capacity of Biaxially Loaded Pipelines (Ph.D. Dissertation). Department of Mechanical Construction and Production, Ghent University.

[22] Abdulhameed, D., Cakiroglu, C., Lin, M., Cheng, R., Nychka, J., Sen, M., and Adeeb, S., 2016, "The effect of internal pressure on the tensile strain capacity of X52 pipelines with circumferential Abaqus," Journal of Pressure Vessel Technology, 138(6).

[23] Yong-Yi W, Ming L, and Yaxin S., 2011, "Second Generation Models for Strain-Based Design." PRCI Final Approved Report, 2011.

[24] Fairchild, D. P., Kibey, S. A., Tang, H., Krishnan, V. R., Wang, X., Macia, M. L., and Cheng, W., 2012, "Continued Advancements Regarding Capacity Prediction of Strain-Based Pipelines," ASME Paper No. IPC 2012-90471.

[25] Kibey, S., Wang, X., Minnaar, K., Macia, M. L., Kan, W. C., Ford, S. J., and Newbury, B., 2010, "Tensile Strain Capacity Equations for Strain-based Design of Welded Pipelines," Paper No. IPC10-31661, Proc. of the 8th Int'l Pipeline Conf., Calgary, Canada.

[26] Macia, M.L., Kibey, S., Arslan, H., Bardi, F., Ford, S.J., Kan, W.C., Cook, M.C., Newbury, B., 2010, "Approaches to Qualify Strain-based Designed Pipelines," Proc. 8th Int'l Pipeline Conf., Calgary, Canada.

[27] Cheng, W., Gioielli, P.C., Tang, H., Minnaar, K., and Macia, M.L., 2009, "Effect of Misalignment on the Tensile Strain Capacity of Welded Pipelines," Proc. of the 5th Pipeline Technology Conf., Ostend, Belgium.

[28] Wang, X., Barbas, S.T., Kibey, S., Gioielli, P.C., and Minnaar, K., 2009, "Validation of Strain Capacity Prediction Method – Comparison of Full-Scale Test Results to Predictions from Tearing Analysis Based on FEA," Proc. of the 5th Pipeline Technology Conf., Ostend, Belgium.

[29] Fairchild, D.P., Macia, M.L., Kibey, S., Wang, X., Krishnan, V.R., Bardi, F., Tang, H., Cheng, 2011, "A Multi-Tiered Procedure for Engineering Critical Assessment of Strain-Based Pipelines," Proc. of 21st Int'l Offshore and Polar Eng. Conf., Maui, Hawaii, USA, pp. 698-705.

[30] Tang, H., Fairchild, D. P., Noecker, F. F., Panico, M., Crapps, J., and Cheng, W., 2014, "Strain Capacity Prediction of Strain-based Pipelines," ASME Paper No. IPC2014- 33749.

[31] Bhushan, B. (2013). *Principles and applications of tribology* (2nd ed.). New York, NY: Wiley.

[32] Kailas, S.V. (n.d.). *Failure*. Class lecture for course Material Science. Indian Institute of Science, Bangalore, India. Retrieved from http://nptel.ac.in/courses/112108150/8.

[33] Askeland, D. R. & Phule, P. P. (2006). The science and engineering of materials. (5th ed). Toronto, ON: Nelson.

[34] Davis, J. R. (Eds.) (2004). *Tensile testing* (2nd ed). Materials Park, OH: American Society for Metals (ASM International).

[35] M. Kuna, (2013) Finite Elements in Fracture Mechanics, Solid Mechanics and Its Applications 201, DOI: 10.1007/978-94-007-6680-8_3, Springer Science+Business Media Dordrecht.

[36] Anderson, T. L. (2005). Fracture mechanics: fundamentals and applications (3rd ed). Boca Raton, FL: Taylor & Francis Group.

[37] Czicho, H., Saito, T., & Smith, L. (Eds.) (2006). Springer handbook of materials measurement methods. German: Springer.

[38] Zhu, X. K., & Joyce, J. A. (2012). Review of fracture toughness (G, K, J, CTOD, CTOA) testing and standardization, Engineering Fracture Mechanics, 85, 1-46. doi:10.1016/j.engfracmech.2012.02.001.

[39] Kocak, M., Webster, S., Janosch, J. J., Anisworth, R. A., & Koers, R. (Eds.). (2006). FINET Fitness-for service procedure final draft MK7. European fitness for service thematic network – FITNET, Germany.

[40] API 579-1/ASME FFS-1 (2007). *Fitness-for-service* (2nd ed). Washington, DC: American Petroleum Institute (API)/American Society of Mechanical Engineers (ASME).

[41] Adeeb, S. (2011). *Introduction to solid mechanics and finite element analysis using Mathematica*. Dubuque, IA: Kendall Hunt Publishing Company.

[42] Amir R. K. (2015). Extended finite element method, theory and applications. John Wiley and Sons Ltd, United Kingdom.

3. PREDICTION OF BURST LOAD IN PRESSURIZED PIPELINES USING EXTENDED FINITE ELEMENT METHOD (XFEM)

This chapter is derived from the published conference proceedings:

Agbo, Sylvester, Lin, Meng, Ahmed, Arman, Cheng, J.J. Roger, and Adeeb, Samer, Prediction of Burst Load in Pressurized Pipelines using Extended Finite Element Method (XFEM) in The 6th International Conference of Engineering Mechanics and Material, CSCE, May 31 - June 3, Vancouver, B.C., Canada, 2017.

3.1 Abstract

Application of principles of fracture mechanics to the response of pipelines with circumferential flaws subjected to varying internal pressure and tensile load is a relatively new field. Many researchers have studied the integrity of pipelines using many methods, but no well-established methodology exists to address the biaxial loading state introduced by a combination of internal pressure and eccentric tensile loading on pipelines. Fracture mechanics principles were applied to pipe specimens with a circumferential flaw, subjected to varying internal pressure and eccentric tensile load. Eight full-scale pressurized tests were previously carried out in our laboratory on X52 grade NPS (nominal pipe size) 12 inches steel pipe subjected to eccentric tensile load with pre-machined flaw close to the girth weld. This paper discusses the development of finite element models using the extended finite element method (XFEM) to predict burst load in pipes due to crack growth under the loading conditions of full-scale tests. The model results were validated using the load history obtained during the full-scale tests. The crack mouth opening displacement (CMOD) - load history of each model was analyzed to produce compliance measurements at increasing levels of internal pressure. This paper compares the numerical results, including burst load predicted by XFEM models with the results of the full-scale tests. This paper illustrates the potential advantage of the XFEM technique, a tool easy to implement, to predict burst load in steel pipelines due to crack growth.

Keywords: burst load, crack growth, extended finite element method, fracture mechanics, full-scale test, and remote strain.

3.2 Introduction

Oil and gas pipelines that transverse the remote seismically active regions with harsh environments may be subjected to large plastic strains. This could be as a result of increased ground movement caused by continuous freezing and thawing of the ground in addition to a continuous variation of internal pressure in the pipes. Moreover, seismic activities, frost heave,

and slope instabilities can introduce high plastic deformations to onshore and offshore pipelines. There has been an increasing demand to design pipelines that can withstand these large plastic strains [1]. The presence of fabrication flaws in girth weld is one of the major factors leading to failure in pipelines due to the associated stress concentrations and hence, excessive tensile strain within the region [2]. The ability of girth weld with defects (flaw) to resist fracture, limits the tensile strain capacity of pipelines [1]. The presence of a flaw in pipe welds coupled with the changes in internal pressure in pipelines subjected to complex environmental and working load could lead to crack initiation and propagation which eventually could lead to burst (failure). The extended finite element method [3-6], which can timely simulate and record the damage evolution history, has been widely used to model ductile fracture procedure including crack initiation and propagation. Today, the XFEM is one of the most useful methods in modelling cracks [7].

Previously, Abdulhameed et al. [8] conducted full-scale tests on X52 grade NPS 12 steel pipeline in our laboratory to investigate the effect of internal pressure on the tensile strain capacity of the pipeline with different sizes of circumferential flaws. They concluded that the internal pressure effect was responsible for the reduction in the tensile strain capacity (TSC) of the pipeline up to 50% and that the level of internal pressure has no effect on the final CMOD at failure for tests with the same flaw size. This paper is focused on the use of XFEM to model full- scale pressurized tests of X52 pipeline with different levels of internal pressure subjected to eccentric tensile loading to predict the burst load of pressurized pipelines and to validate the usefulness of XFEM as a veritable tool for modelling crack growth. Since the strain capacity is defined as the strain corresponding to maximum load (combined internal pressure and tensile load), the measured TSC will correspond to the failure load which is referred to as burst load in this paper.

3.3 Methodology

3.3.1 Full-scale test experiment.

Eight full-scale tests were carried out previously in our laboratory by Abdulhameed et al. [8].

Table 3-1 shows the parameters used in tests 7 and 8 of the eight full-scale tests previously conducted and their models 7 and 8, respectively. The pipe length was 1219.2 mm (4 OD) with girth weld in the mid-length of the pipe. A flaw was introduced close to the girth weld using a machined saw cut. The flaw dimensions for tests 7 and 8, which were modelled in this paper, were; length of 150 mm with a depth of 50% of the nominal wall thickness (3.4mm), as shown in Table 3-1. The pipes were tested in a material testing system (MTS) machine under eccentric tensile displacement in the presence of internal pressure. The eccentricity was to ensure that the circumferential flaw was subjected to the highest tensile strain throughout the test. A cap plate was welded to the pipe ends and connected to an endplate using 14 bolts. A tongue piece was positioned on the endplates with an eccentricity of 50 mm to provide the eccentric loading. This tongue plate was fitted into a pin–yoke assembly that connects the pipe to the MTS machine, as shown in Figure 3-1. The internal pressures causing 30% and 80% specified minimum yield stress (SMYS) of hoop stress were 4.389 MPa and 11.704 MPa respectively, these were obtained using the Barlow's formula [8]. The loading was applied in two steps. In the first step, the internal pressure was applied by filling the pipe with water through an opening located in the bottom endplate. In the second step, while the internal pressure was kept constant, an eccentric tensile displacement was applied to the top tongue through the MTS in increments until the instance of failure. Failure (burst) is defined as the point in time when crack penetrated through the wall thickness of the pipe and water seeps out from the pipe. The strains were evaluated using a Digital Image Correlation (DIC) technique, to obtain the variation of the strain field on the tension side of the pipe during the experiment along the pipe length. Strain gauges were positioned at a quarter of the pipe length (0.25L) away from the cap plate at 90-degrees intervals around the pipe circumference to record the remote strain. Clinometers were attached to the top and bottom endplates to measure the rotation of the pipe ends caused by the loading eccentricity, throughout the test. The MTS measured and recorded the reaction force and displacement during the test.

Table 3-1 Tests and XFEM model parameters [8]

Test / Model	Outer diameter (mm)	Pipe length (mm)	Internal pressure (% SMYS)	Internal pressure (MPa)	Flaw depth (mm)	Flaw length (mm)
Test 7	304.8	1219.2	80	11.704	3.4	150
Model 7	304.8	1219.2	80	11.704	3.4	150
Test 8	304.8	1219.2	30	4.389	3.4	150
Model 8	304.8	1219.2	30	4.389	3.4	150

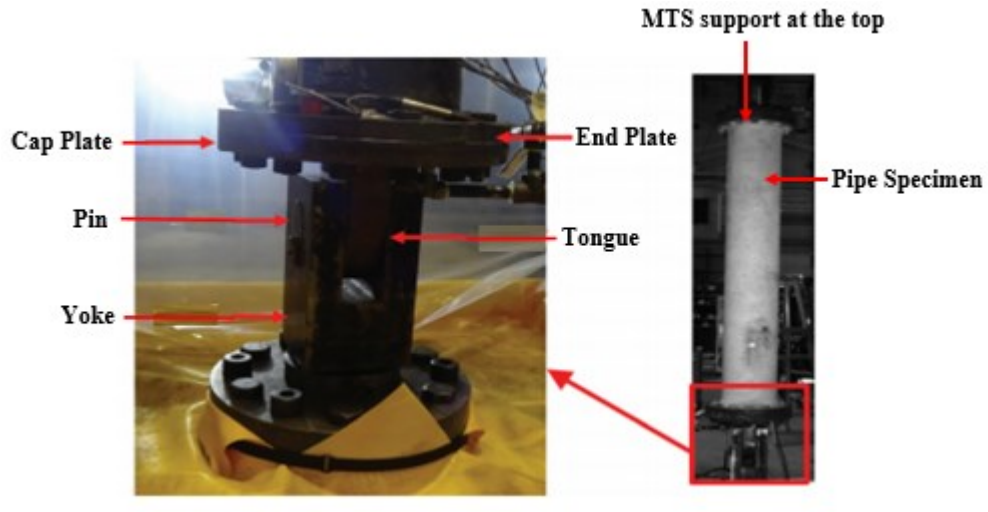

Figure 3-1 Full-scale test set-up and the details of the loading support. Abdulhameed et al. [8]

3.3.2 XFEM Model

The improvement of XFEM compared to the traditional FEA was due to the introduction of additional functions that made it suitable for modelling stationary discontinuities like crack. These newly introduced functions made the modelling of growing cracks much easier since, unlike the traditional FEA, there is no need for re-meshing the crack surface as the crack progresses [9, 10]. Shown in Equations (3-1) and (3-2) are the nodal enrichment functions that consist of the near-tip

asymptotic functions which capture the singularity around the crack tip and the discontinuous function that represents the displacement jump across the crack surfaces. An approximation for a displacement vector function u is given as:

$$u = \sum_{I=1}^{N} N_I(x) \left[u_I + H(x) a_I + \sum_{\propto=1}^{4} F_{\propto}(x) b_I^{\propto} \right] \qquad (3-1)$$

Where, $N_I(x)$, are the nodal shape functions, the first term u_I, is the nodal displacement vector; the second terms are the enriched nodal degree of freedom vector a_I, and the associated discontinuous jump function $H(x)$ across the crack surfaces. The third term is the product of the enriched nodal degree of freedom vector $b_I^{\propto}$, and the associated elastic asymptotic crack-tip functions, $F_{\propto}(x)$. From the right-hand side, the first term applies to all the nodes in the model, the second term is only valid for nodes whose shape function support is cut by the crack interior, while the third term is valid only for nodes whose shape function support is cut by the crack tip [11, 12].

The asymptotic crack tip functions in an isotropic elastic material, $F_{\propto}(x)$, is given as:

$$F_{\propto}(x) = \left[\sqrt{r} \sin\frac{\theta}{2}, \sqrt{r} \cos\frac{\theta}{2}, \sqrt{r} \sin\theta \sin\frac{\theta}{2}, \sqrt{r} \sin\theta \cos\frac{\theta}{2} \right] \qquad (3-2)$$

where(r, θ), is a polar coordinate system with its origin at the crack tip, and $\theta = 0$ is tangent to the crack at the tip [11].

Two 3D XFEM models of full-scale tests were conducted using ABAQUS software to investigate the behaviour of the tested pipes under the effect of internal pressure and eccentric tensile loading. Symmetry was considered in modelling; thus, one longitudinal half of the pipe was simulated as shown in Figure 3-2. The modelling involved creating parts in accordance with the dimension of the pipe test specimen. The model has an outer diameter (OD) of 12 in (304.8 mm), length of 4

OD (1219.2 mm), a nominal wall thickness of 0.268 in (6.8 mm), flaw depth of 3.4 mm and flaw length of 150mm. Figure 3-2 is a schematic representation of the assembled pipe model.

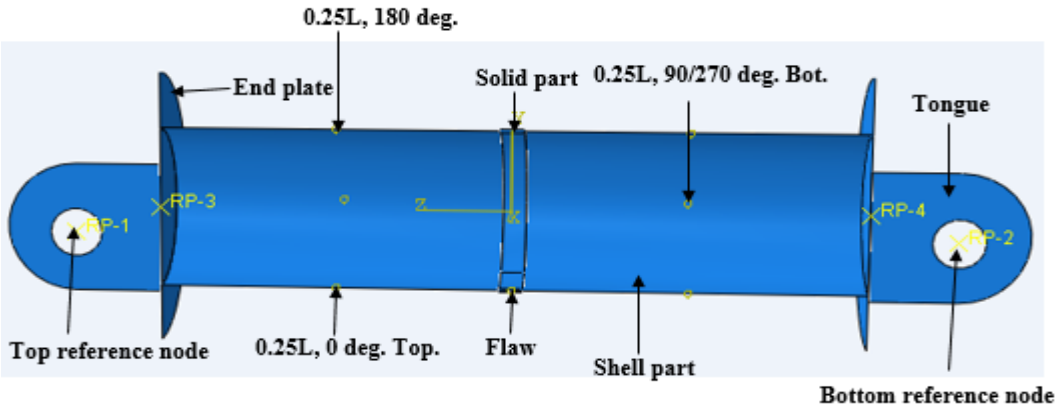

Figure 3-2 Assembled components of the model showing the geometry and reference points.

A total of eight instances were created which comprised of "solid part", which is a 3D solid part of the pipe model located at the mid-length, it was chosen to be 3D solid to allow for visualization of the crack growth and to create the solid domain for insertion of the flaw. The entire pipe length was not modelled as solid to reduce the number of element mesh created in the model for the easy running of the model. Two "shell part" instances were created which were shell extrusion elements that form the rest of the pipe length. Both were connected to the solid part using shell-solid coupling constraint, this created an interaction that made both to function as a single part. Two end plates were modelled as shell planer rigid body elements that represented a combination of the endplate and the cap plate as used in the full-scale test and were connected to shell part using a tie constraint, which simulated the welded joint. Two loading tongues were also modelled as shell planer rigid bodies and connected to the endplates at an eccentricity of 50 mm to introduce the eccentric loading in the model using tie constraint. The tongues at both ends of the model formed the top and bottom loading reference nodes and were modelled as rigid bodies. The flaw was modelled as a shell planer element and inserted into the solid part of the model and subsequently created an interaction with the solid domain as XFEM crack. These instances were assembled to form the model geometry shown in Figure 3-2. An 8-node linear brick element mesh with reduced integration, hourglass control (AC3D8R) was used in the solid part. The mesh size was controlled

by the flaw size to ensure good interaction between the flaw and the solid part to simulate crack growth. Meshes within the flaw vicinity were smaller in size compared to other parts, as shown in Figure 3-3. The shell part meshed with a 4-node doubly curved thin shell with reduced integration, hourglass control, and finite membrane strains. The crack propagation associated with the pipe specimen was assumed to be in Mode-I fracture. The maximum principal stress (σ_{maxps}) and fracture energy (Gc) were selected as the key damage parameters in the XFEM model. There were non-existing values for σ_{maxps} and Gc recommended for X52 grade steel material, but Nonn et al. and Scheider et al. [13-15] proposed recommended values to be used for three higher-grade steel: σ_{maxps} =1375 MPa and Gc = 900 N/mm for X65 grade steel, σ_{maxps} =1600 MPa and Gc = 900 N/mm for X80 grade steel and σ_{maxps} =1700 MPa and Gc =700 N/mm for X100 grade streel.

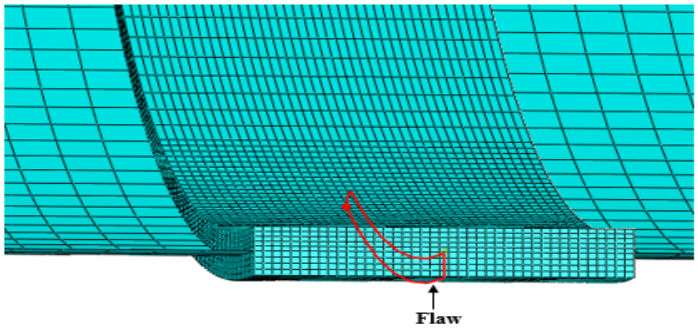

Figure 3-3 A section of the model showing the mesh sizes and the position of the flaw.

3.3.3 Materials

The pipes were modelled as a mechanical, elastoplastic isotropic material with Young's Modulus of 199 GPa and Poisson ratio 0.3. The yield stress and plastic strain parameters were obtained from the true stress-plastic strain curve obtained from small scale tension test and Charpy V-notch impact tests carried out on X52 grade pipe material in our laboratory by Lin [16]. The parameters were used as material inputs in the XFEM models. Isotropic strain-hardening plasticity was used to describe plastic behaviour. The maximum principal stress was the damage initiation criterion used in the XFEM model. Energy was selected as the type of damage evolution, while a linear softening with maximum degradation was applied.

A numerical investigation was carried out to identify the most suitable damage parameters σ_{maxps} and *Gc* to use in the XFEM modelling to produce results that agree with the full-scale test experimental result. After a series of investigations, σ_{maxps} =700 MPa and *Gc* =900 N/mm were selected and used in both models.

3.3.4 Loading and boundary conditions.

An initial condition of symmetry was applied since the pipe was modelled as a longitudinal half due to symmetry. The bottom tongue was fixed initially while the top was allowed to move in the longitudinal direction only. The pipe was loaded in the XFEM model in two steps. In the first step, the specified internal pressure was applied to the inner surfaces of pipe and end plates while the bottom reference node remained fixed. In the second step, the pipe was subjected to a longitudinal displacement at the top reference node which introduced an eccentric tensile force, and both reference nodes were allowed to rotate about the x-axis. Two models were created; model 7, with 80% SMYS and model 8 with 30% SMYS, which represented the full-scale tests 7 and 8, respectively. The model and tests parameters were as shown in Table 1. The remote strain (ε0.25L) is defined as the strain reading at a quarter of the pipe length (L) from the endplates. The position of 0.25L at angles 0, 90,180 and 270 degrees relative to the center of the flaw was shown in Figure 3-2. This location was chosen to be the remote strain measurements as it represented the flat part in a strain profile along the pipe length as described by Abdulhameed et al. [8].

3.4 Results

The reaction force obtained from the model was taken as the applied tensile force. Remote strain values (ε0.25L) were obtained from a quarter length of the pipe measured from the endplate at an angle of 90 degrees from the center of the flaw for top and bottom sides. The remote strain ε0.25L, CMOD, and rotation results obtained from the XFEM models were plotted against the applied tensile force. The result obtained from each model was compared with the corresponding full-scale test result to validate the model.

A comparison of the burst load, i.e. the applied tensile force at which the crack penetrated fully the pipe wall thickness, the remote strain, CMOD and rotation obtained from the full-scale test and that obtained from the models showed good agreement.

Figure 3-4 shows a plot of applied tensile force versus remote strain up to failure for both tests and models.

The burst load and the corresponding remote strain values of the full-scale tests and XFEM models plotted in Figure 3-4 were compared in Table 3-2.

CMOD results obtained from both tests and XFEM models were plotted against the applied tensile force up to failure, as shown in Figure 3-5. CMOD-failure is the CMOD corresponding to the burst load, i.e. when the crack fully penetrated the pipe wall thickness, as shown in Figure 3-6.

Critical CMOD is defined as the crack mouth opening at 97% of the burst load [8]. This represents the crack mouth opening at a point of time when the applied load is almost constant while the crack progressed. CMOD-failure obtained from Figure 3-5, and the critical CMOD for tests and XFEM models were compared in Table 3-2.

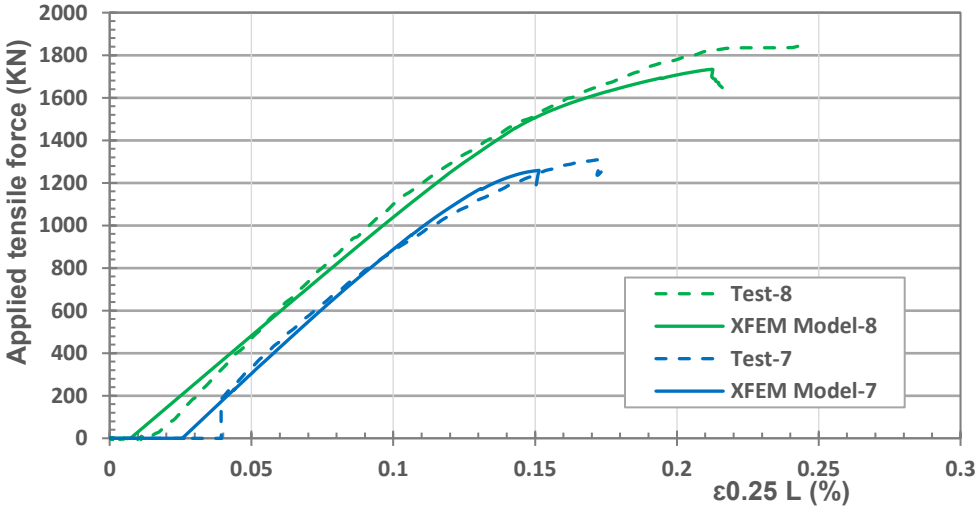

Figure 3-4 Applied tensile force versus ε0.25L up to failure.

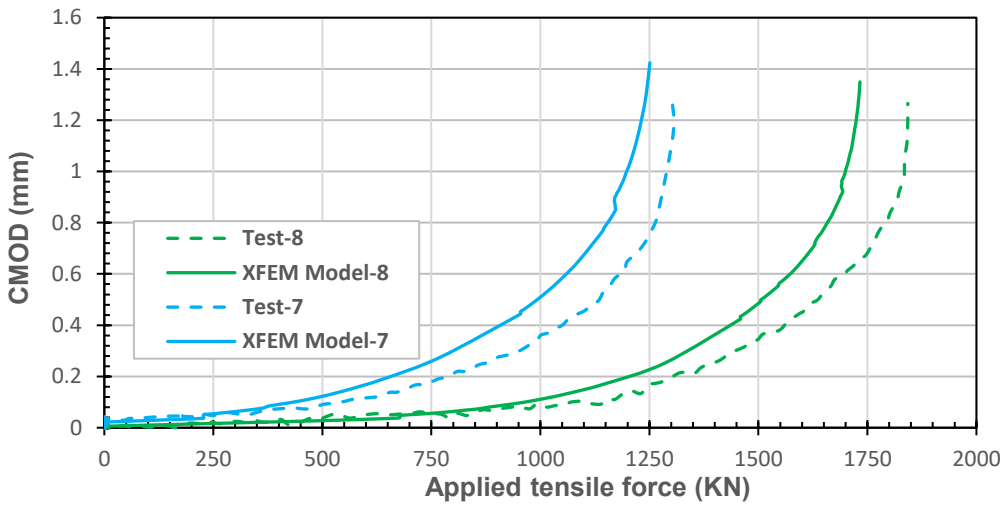

Figure 3-5 CMOD versus applied tensile force up to failure

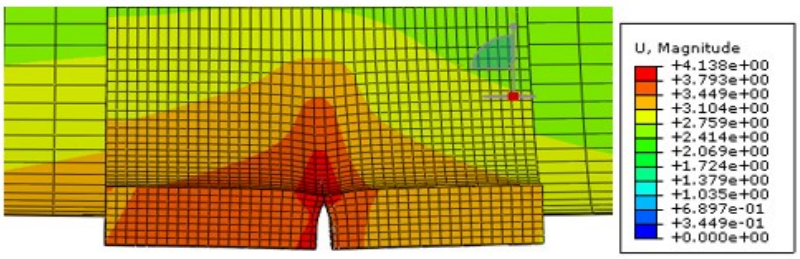

Figure 3-6 Shows the CMOD of the model at failure

Similarly, the rotation (degree) of the tests and models due to the eccentric loading was plotted against the applied tensile force up to failure, as shown in Figure 3-7. Rotations at failure from Figure 3-7, for tests and models, were equally compared in Table 3-2.

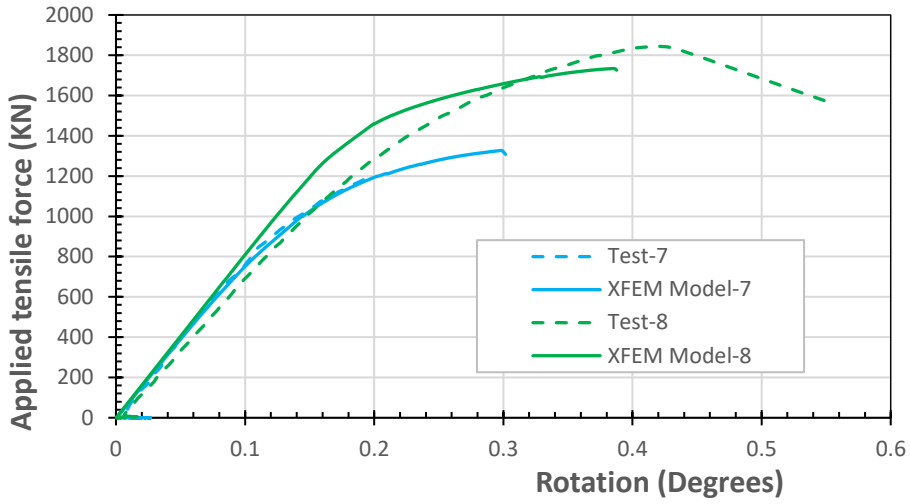

Figure 3-7 Applied tensile force versus rotation (degree) of the end plate up to failure

Table 3-2 Comparison between experimental and XFEM model results

Model/Test	Internal Pressure (%SMYS)	Burst Load (KN)	ε0.25L (%)	CMOD (mm)	Rotation (Degree)	Critical CMOD (mm)
Test 7	80.0	1302.676	0.1690	1.30	0.23	0.81
Model 7	80.0	1251.170	0.1473	1.42	0.24	0.84
%Difference	0.0	-4.0%	-12.8%	+9.2%	-4.2%	+3.6%
Test 8	30.0	1842.646	0.2428	1.27	0.45	0.81
Model 8	30.0	1734.048	0.2125	1.39	0.40	0.84
%Difference	0.0	-6.0%	-12.5%	+9.4%	-12.5%	+3.6%

Note: "-" / "+" means that data in Model is lower / higher than data obtained from the full-scale tests.

From Table 3-2, a comparison of the experimental burst-load and that of the XFEM models showed good agreement, with a percentage difference of -4.0% for XFEM model 7, while XFEM model 8 gave -6.0% difference. The negative sign indicated that the XFEM model gave lower values

compared to the experimental test result. When the remote strain was compared, XFEM model 7 gave -12.8% difference while XFEM model 8 gave -12.5%.

Also, when the CMOD of the models was compared to that of experiments, XFEM model 7 gave +9.2%, while XFEM model 8 gave a 9.4% difference. When the rotation was compared, XFEM model 7 gave -4.2% while XFEM model 8 gave -12.5% difference, as shown in Table 3-2. The non-zero rotation at zero tensile force noticed in test 7 was as a result of the high initial internal pressure applied prior to application eccentric tensile force.

3.4.1 Effect of internal pressure

The burst load, remote strain($\varepsilon 0.25L$) and CMOD obtained from the models with the same flaw size but different internal pressure levels plotted in Figure 3-4 and Figure 3-5 were compared in Table 3-3.

Table 3-3 Comparison of tests, and the XFEM models due to different internal pressure level

Model / Test	Internal pressure (%SMYS)	Burst load (KN)	Remote strain (ε0.25L) %	CMOD (mm)	Critical CMOD (mm)
Test 7	80.0	1302.676	0.1690	1.30	0.81
Test 8	30.0	1842.646	0.2428	1.27	0.81
%Difference	-62.5%	+41.5%	+43.7%	-2.3%	0.0%
Model 7	80.0	1251.170	0.1473	1.42	0.84
Model 8	30.0	1734.048	0.2125	1.39	0.84
%Difference	-62.5%	+39.0%	+44.0%	-2.1%	0.0%

Note: “-” / ”+” means that data in Test/Model 8 is lower / higher than data in the Test/Model 7

When the internal pressure was decreased from 80% SMYS to 30% SMYS, the remote strain at failure increased by 44% while the burst load at failure increased by 39% as shown in Table 3-3. When the internal pressure increased from 30% SMYS to 80% SMYS, the burst load and remote strain at failure decreased. As the internal pressure increased, there was an increase in both the longitudinal and axial tensile stresses which stimulated early crack growth thus, the pipe failed at a lower applied load.

CMOD results of each model were plotted against the applied load to observe the crack growth during the load increments in the model up to failure, as shown in Figure 3-5. Change in internal pressure did not significantly affect the CMOD-failure since only a difference of -2.1% was obtained. But XFEM models 7 and 8 gave the same critical CMOD value of 0.84mm, as shown in Table 3-3. For the two tests with the same crack dimensions but with different level of internal pressures, the resulting CMOD was found to be very close, with a percentage difference of -2.3%, but both have the same critical CMOD value of 0.81mm as shown in Table 3-3. This shows that the internal pressure has no effect on the critical CMOD at failure, but model 7 with 80% SMYS internal pressure reached the critical CMOD at lower burst load compared to XFEM model 8 with 30% SMYS internal pressure. It was observed from the curves that lower internal pressure required more load to reach the burst load. Thus, higher internal pressure pipes possess a lower burst load and are more susceptible to failure.

3.5 Discussion

Numerical investigation to identify the most suitable set of damage parameters was carried out on model 8. Table 3-4 compared the experimental data with the numerical results for burst load and remote strain at failure.

Table 3-4 Numerical investigations of damage parameters for X52 steel using XFEM model 8

Test/ Model	σ_{maxps} (MPa)	*Gc* N/mm	Burst load (KN)	% Diff. from test	ε0.25L%	% Diff. from test
Test 8	-	-	1842.6	-	0.2428	-
Model 8	700	500	1647.0	-10.6%	0.1927	-20%
Model 8	**700**	**900**	**1734.0**	**-6%**	**0.2125**	**-12.5%**
Model 8	700	1200	1771.0	-4%	0.2253	-7.2%
Model 8	700	1600	1799.0	-2.4%	0.2456	+1.2%
Model 8	650	900	1673.0	-9.2%	0.1768	-27.2%
Model 8	**700**	**900**	**1734.0**	**-6%**	**0.2125**	**-12.5%**
Model 8	750	900	1771.0	-4%	0.2253	-7.2%
Model 8	800	900	1824.0	-1%	0.2304	-5.1%

From Table 3-4, it was observed that the set with σ_{maxps} =700 MPa and *Gc*=900 N/mm gave a better result compared to the experimental data. The set with σ_{maxps} =700 MPa, *Gc*=1200 N/mm and σ_{maxps} =750 MPa, *Gc*=900 N/mm gave slightly closer values to the experimental result, but the pipe did not fail in these cases instead it leads to high-stress concentrations. It was observed that the values of burst load and remote strain obtained from both models were slightly lower than those obtained from the full-scale test experiments. This could be due to the modelled flaw being sharper than the machined flaw used during the full-scale test. This might have caused the crack in the model to progress faster than that of the experiment and thereby to reach the burst load earlier and generating lower strain value at failure.

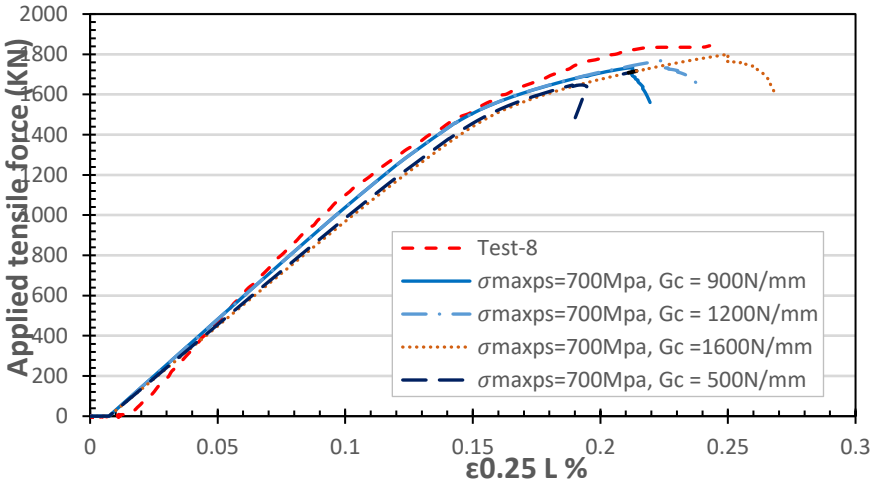

Figure 3-8 Applied Tensile force versus ε0.25L at constant σ_{maxps} =700 MPa and varying (*Gc*) in model 8.

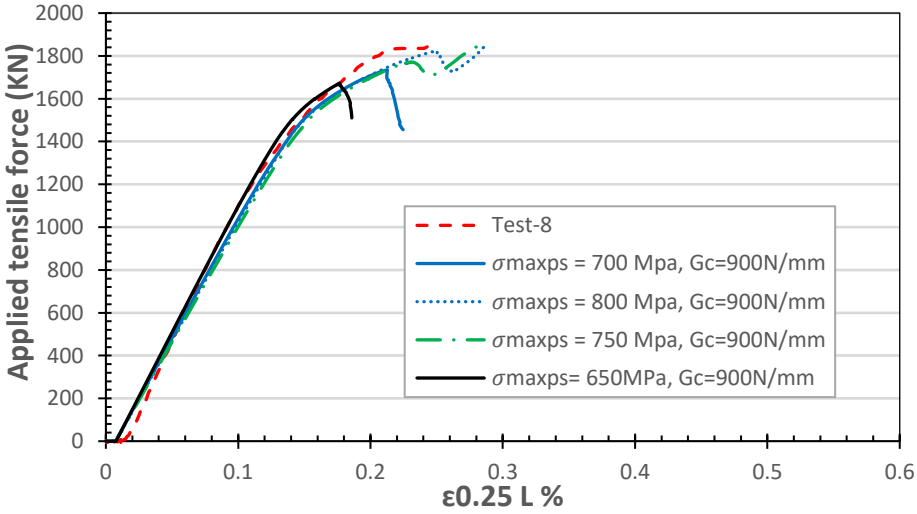

Figure 3-9 Applied tensile force versus ε0.25L at constant Gc = 900 N/mm and varying σ_{maxps} in model 8.

3.6 Conclusion

This paper utilized the XFEM modelling technique in the prediction of burst load in pressurized NPS 12 grade X52 steel pipe. Two numerical XFEM models with the same circumferential flaw dimensions but with different levels of internal pressure were subjected to eccentric tensile loading. After some numerical investigations, σ_{maxps} of 700 MPa and Gc of 900 N/mm were identified as an adequate set of damage parameters that allowed the numerical models to reproduce the experimental data with good agreement. The result of the models showed our estimated burst load to be 1251.17 KN (1302.7 KN obtained from the test) and remote strain as 0.15% (0.17% obtained from the test) for XFEM model 7, subjected to high internal pressure of 80% SMYS. For XFEM model 8, with a lower internal pressure of 30% SMYS, the burst load and remote strain increased to 1734.05 KN (1843.65 KN obtained from the test) and 0.21% (0.24% obtained from the test). The burst load and the axial remote strain of pipeline with a flaw are influenced strongly by the internal pressure and that reducing the internal pressure level from 80% SMYS to 30% SMYS could increase the burst load by up to 39% and could increase the axial remote strain by about 44%.

3.7 References

[1] Minnaar, K, Gioielli, P.C, Macia, M.L, Bardi, F, Biery, N.E and Kan, W.C. 2007. Predictive FEA Modelling of Pressurized Full-Scale Tests. International Society of Offshore and Polar Engineering, ISOPE

[2] Wang, M. L., Horsley, D., and Zhou, J., 2006. A Quantitative Approach to Tensile Strain Capacity of Pipelines, ASME Paper No. IPC2006-10474.

[3] Belytschko, T and Black T. 1999. Elastic Crack Growth in Finite Elements with Minimal Remeshing. International Journal for Numerical Methods in Engineering, IJNME, 45(5): 602-620.

[4] Moes, N, Dolbow, J. and Belytschko, T .1999. A Finite Element Method for Crack Growth Without Remeshing. International Journal for Numerical Methods in Engineering, IJNME, 46(1): 131-150.

[5] Sukumar, N, Moes, N, Moran, N and Belytschko, T. 2000. Extended Finite Element Method for Three-Dimensional Crack Modelling. International Journal for Numerical Methods in Engineering, IJNME, 48(11): 1549- 1570.

[6] Nagashima, T, and Suemasu, H. 2010. XFEM Analyses of a Thin-Walled Composite Shell Structure with a Delamination. Computer and Structure, CS, 88(9-10): 549-557.

[7] Zhang, B, Ye, C, Liang, B, Zang, Z, and Zhi, Y. 2014. Ductile Failure Analysis and Crack behaviour of X65 Buried pipes using the Extended Finite Element Method. Engineering Failure Analysis, EFA, 45: 26-40.

[8] Abdulhameed, D, Cetal, C, Lin, M, Cheng, R, Nychka, J, Sen, M and Adeeb, S. 2016. The Effect of Internal Pressure on the Tensile Strain Capacity of X52 Pipelines with Circumferential Flaws. Journal of Pressure Vessel Technology, ASME,138/06170-1.

[9] Sukumar, N, Chopp, D. L, Moës, N and Belytschko, T. 2001. Modelling Holes and Inclusions by Level sets in the Extended Finite Element Method, Computer Methods in Applied Mechanics and Engineering, CMAM, 190(46-47): 6183-2000.

[10] Stolarska, M, Chopp, D. L, Moës, N. and Belytschko, T. 2001. Modelling Crack Growth by Level Sets in the Extended Finite Element Method. International Journal for Numerical Methods in Engineering, IJNME, 51 (8):943-960.

[11] Abaqus 6.14, Analysis User's Manual Volume Number 2: Analysis, Dassault Simulia.

[12] Zhang C, Cao, P, Cao, Y and Li, J .2013. Using Finite Element Software to Simulation Fracture Behaviour of Three-point Bending Beam with Initial Crack, Journal of Software, JS, 8(5):1145-1150.

[13] Nonn, A., and Kalwa, C., 2012. Simulation of ductile crack propagation in high-strength pipeline steel using damage models. Proceedings of the 9thInternational Pipeline Conference, Calgary, Canada, IPC 90653.

[14] Nonn, A., and Kalwa, C. 2013. Analysis of dynamic ductile fracture propagation in pipeline steels: A damage mechanics approach. Proceedings of the 6th International Pipeline Technology Conference, Ostend, Belgium, IPC S34-01.

[15] Scheider, I., Nonn, A., Völling, A., Mondry, A., and Kalwa, C. 2014. A damage mechanics-based evaluation of dynamic fracture resistance in gas pipelines. Procedia Materials Science. PMS. (19) 1956.
[16] Lin, M, 2015, Characterization of Tensile and Fracture Properties of X52 Steel Pipes and Their Girth Welds, M.Sc. thesis, University of Alberta, Edmonton, AB.

4. EXPERIMENTAL EVALUATION OF THE EFFECT OF THE INTERNAL PRESSURE AND FLAW SIZE ON THE TENSILE STRAIN CAPACITY OF WELDED X42 VINTAGE PIPELINES

This chapter is derived from the research article published in the Elsevier International Journal of Pressure Vessels and Piping: Agbo, S., Lin, M., Ameli, I., Imanpour, A., Duan, D., Cheng, J. J. R, Adeeb, S., Experimental Evaluation of the Effect of Internal Pressure and Flaw Size on the Tensile Strain Capacity of Welded X42 Vintage Pipelines, International Journal of Pressure Vessels and Piping (2019), 10.1016/j.ijpvp.2019.04.010.

4.1 Abstract

Pipelines exposed to geo-hazards such as moving slopes, discontinuous permafrost, and other ground movements may be subjected to displacement-controlled loading, which may lead to significant plastic strains. This can potentially impact pipeline structural capacity and their leak-tight integrity. Traditional stress-based design methods may become uneconomical in the design of pipelines subjected to large plastic strain. Given the extensive use of such pipelines, reliable calibration of the tensile strain capacity (TSC) plays a critical role in strain-based design (SBD) methodology. Recent studies were focused mostly on high toughness modern pipelines with limited research performed on lower-grade vintage pipelines. However, the effects of biaxial loading due to internal pressure and bending stresses imposed on pipelines as a result of interactions with geo-hazards were not properly addressed in previous studies. This paper investigates the effect of internal pressure and flaw size on the TSC of X42 welded vintage pipelines using experimental testing. Eight full-scale pressurized four-point bending tests were conducted on 22 inches (558.8 mm) diameter X42 grade welded vintage pipes with a D/t ratio of 44 to examine the effect of the influential parameters on the TSC. Biaxial strain gauges and a digital image correlation (DIC) system were major instrumentations used for measuring strain. The results were used to examine the crack growth rate by estimating the crack mouth opening displacement (CMOD) at failure and the effects of internal pressure and flaw size on the TSC. The TSC obtained from the tests were compared with those predicted using TSC predictive models proposed by ExxonMobil and Pipeline research council International (PRCI).

Keywords: Geo-hazards, Strain-based design, Vintage pipelines, Tensile strain capacity, CMOD, Crack propagation, Flaw size, Internal pressure, and DIC.

Nomenclature

CMOD	Crack mouth opening displacement
CTOD	Crack tip opening displacement
DIC	Digital image correlation
ECA	Engineering critical assessment
FEA	Finite element analysis
FCAW	Flux-cored arc welding
FST	Full-scale test
HAZ	Heat affected zone
MTS	Mechanical testing system
NPS	Nominal pipe size
PRCI	Pipeline Research Council International
δ	R-curve CTOD
SMAW	Shielded metal arc welding
SENT	Single-edge notch tension
SMYS	Specified minimum yield strength
SG	Strain gauge
SBD	Strain-based design
SBECA	Strain-based engineering critical assessment
TSC	Tensile strain capacity
UEL	Uniform elongation
WCL	Weld center line
Y/T	Yield to tensile ratio

4.2 Introduction

As the global energy demand continues to grow, energy industries have pushed all the limits through increasing exploration and extraction activities of energy resources even in the remote

arctic and sub-arctic regions of Northern Canada. The majority of onshore pipelines are buried in different cold regions with remarkably harsh geo-hazards such as moving slopes, discontinuous permafrost zones, and other ground movements [1]. Such hazards may impose displacement-controlled loads on pipelines, which in turn may produce large plastic strains. Traditional stress-based design methodologies may become uneconomical in the design of pipelines subjected to such a harsh environment. In view of the extensive use of such pipelines, strain-based design (SBD) guidelines for characterization of the tensile strain capacity (TSC) of welded pipelines subjected to large plastic strains are urgently needed to improve current design practice and develop practical design tools [2]. The majority of studies conducted in recent years were focused on modern pipelines with steel grades of X60 and above with limited research performed on lower-grade vintage pipelines. Vintage pipes are characterized by old; pipe material, pipe-making, and construction practices that place more emphasis on the strength at the cost of innovation in chemical composition and steel making process [3]. Vintage pipes occasionally have lower toughness with good strain hardenability. Their stress versus strain curves does not have a well-defined yield plateau [4].

Research conducted by Wang et al. [5-7] led to the development of closed-form equations for predicting the TSC of high strength pipelines using the pipe and flaw geometries, girth weld and pipe material properties as the major influential parameters. These equations, previously included in the design standard for oil and gas pipeline systems CSA Z662-11 [8] did not consider the effect of internal pressure and were not applicable to vintage pipelines [9]. The equations were removed from the recent edition of the standard. ExxonMobil (EM) conducted an extensive experimental and numerical program, leveraging damage mechanics modelling to develop TSC predictive models capable of evaluating the TSC of welded modern pipelines ranging from X60 to X100 [10-12]. Pipeline Research Council International (PRCI) used a multidisciplinary approach involving fundamental fracture mechanics, small-scale material characterization and full-scale pipe tests to develop TSC predictive models for welded pipelines ranging from X56 to X100 [13]. Given that a significant percentage of vintage pipelines are currently in service, transporting a considerable quantity of energy resources, it is felt that research is needed to understand the effect of internal pressure and flaw size on the behaviour of vintage pipelines.

Abdulhameed et al. [14] recently carried out a full-scale experimental test program that included eight X52 NPS 12 vintage pipe specimens with 6.91mm wall thickness subjected to combined eccentric tensile force and internal pressure. The effect of internal pressure and circumferential flaws close to a girth weld on the TSC was examined in this test program. The results showed that the level of internal pressure could reduce the TSC by at least 50% depending on the flaw size. The crack mouth opening displacement (CMOD) was also measured in this test program and it was found that COMD is not affected by the level of internal pressure and is a function of flaw dimensions. The test results confirmed that the flaw depth had a greater effect on the TSC than the flaw length. Increasing the flaw depth from 25% to 50% of the wall thickness t, resulted in a decrease of 94% of the TSC of the 25%t, wall thickness test. However, increasing the flaw length from 5t to 10t resulted in a decrease of 86% of the TSC of the 5t flaw length test [14].

The major limitations of the study by Abdulhameed et al. were that the machined flaws were mostly concentrated in the pipe material rather than in the girth welds or HAZ. As well, a combination of tension and bending (eccentric tensile force) was applied on the cracked pipes, which resulted in subjecting the cracked portion of the pipe to neither pure bending nor pure tensile stress [14]. In addition, the fracture toughness (CTOD) values of the pipes were obtained by converting the Charpy test results into CTOD toughness using the available conversion equations in the literature which are known to provide inaccurate results. This resulted in a lack of confidence in the application of EM and PRCI equations.

This study, thus, aims to experimentally address most of the limitations pointed out in [14] and concerns described here as well as to produce experimental data for future research. The combination of internal pressure and four-point bending was applied to X42 pipes, ensuring that the cracked portion of the pipe is subjected to pure bending. The flaws were machined at the weld centerline (WCL) (weakest location according to the small-scale test results). The test program consists of eight full-scale X42 vintage pipes. The pipe specimens were subjected to the combined internal pressure and four-point bending to evaluate the influence of various internal pressure, flaw depth and flaw length on the tensile and compressive capacities of the vintage pipes. Specifically, the strain at the point of tensile fracture or compressive buckling is examined to evaluate the tensile and compressive capacity of the pipe. The reason for selecting the four-point bending method is because it allows for uniform distribution of maximum stress over a significant area between the loading cradles, that is, four-point bending produces a pure bending state over a significant volume

of the specimen, approximately 1/3 of the pipe length. The results obtained from the full-scale tests were then evaluated and compared to those predicted by the currently available TSC predictive models, utilizing the results of Single Edge Notch Tension (SENT) tests conducted on the pipe material reported in [15].

4.3 Current predictive models for TSC

Based on a large set of experimental and numerical results, EM proposed the set of Equations (1) to (8), considered as level 3 of the strain-based engineering critical assessment (SBECA) technique, for TSC prediction [12]:

$$\mathrm{TSC}_{0.8} = \frac{\left[\Phi\left(N, \frac{\mathrm{K}}{\sigma_Y}, \lambda, \frac{\mathrm{e}}{t}\right).\frac{\delta}{t} + C7\right].\left(C1\frac{\mathrm{D}}{t} + C2\right)}{C6 + C8\left(\frac{\frac{a}{t}}{1-\frac{a}{t}}\right)^{C3}.\tanh\left(\mathrm{C}\,4\left(\frac{2\mathrm{C}}{t}\right)^{C5}\right)} \quad (1)$$

$$\mathrm{TSC} = \begin{cases} \mathrm{PF}.\,\mathrm{TSC}_{0.8}, & TSC < 2/3UEL \\ \dfrac{2}{3UEL}, & TSC \geq \dfrac{2}{3UEL} \end{cases} \quad (2)$$

$$\mathrm{PF} = \begin{cases} (3\mathrm{X}10-4).(\sigma_h)^2 - (3.3X10-2)\sigma_h + 1.85, & \sigma_h < 40 \\ 1, & \sigma_h \geq 40 \end{cases} \quad (3)$$

$$\phi = \left[\mathrm{W}_1\left(\mathrm{N}, \frac{\mathrm{K}}{\sigma_Y}\right)\lambda + \mathrm{W}_2\left(\mathrm{N}, \frac{\mathrm{K}}{\sigma_Y}\right)\right]\frac{\mathrm{e}}{t} + \mathrm{W}_3\left(\mathrm{N}, \frac{\mathrm{K}}{\sigma_Y}\right)\lambda + \mathrm{W}_4\left(\mathrm{N}, \frac{\mathrm{K}}{\sigma_Y}\right)\lambda \quad (4)$$

$$N = \frac{(1+UEL)ln\,\frac{1+UEL}{1+eL}}{(1+UEL)-(1+eL)Y/T} \quad (5)$$

$$\frac{\mathrm{K}}{\sigma_Y} = \frac{\frac{1+UEL}{(1+eL)Y/T} - 1}{(ln\frac{1+UEL}{1+eL})^N} \tag{6}$$

$$\mathrm{W}_n = \mathrm{h}_{3n-2}\left(\frac{\mathrm{K}}{\sigma_Y}\right).N^2 + \mathrm{h}_{3n-1}\left(\frac{\mathrm{K}}{\sigma_Y}\right).N + \mathrm{h}_{3n}\left(\frac{\mathrm{K}}{\sigma_Y}\right) \tag{7}$$

where n = 1, 2, 3 and 4

$$\mathrm{h}_m = \mathrm{C}_{6+3m}\left(\frac{\mathrm{K}}{\sigma_Y}\right)^2 + \mathrm{C}_{7+3m}\frac{\mathrm{K}}{\sigma_Y} + \mathrm{C}_{8+3m} \tag{8}$$

where m = 3n-2, 3n-1, and 3n, C_1 to C_8 are part of the coefficients (C_1 to C_{44}) ranging from -29.99 to 41.77, Φ is a material property parameter, K is a strength coefficient, N is the strain hardening coefficient, σ_Y is the true yield strength, λ is the weld strength overmatch, e is the weld misalignment, δ is the weld toughness parameter (CTOD), UEL denotes the uniform elongation, PF is the pressure factor, σ_h is the hoop stress, eL is the Luder strain, Y is the yield strength at 0.5% strain, T is the ultimate tensile strength (UTS), PF. $\mathrm{TSC}_{0.8}$ is the TSC at 80% pressure factor, a is the flaw depth, t is the wall thickness, and $2C$ is the flaw length [10- 12]. Simulation results associated with ductile tearing instability were used in the nonlinear regression analysis used in fitting the TSC equation [12].

Similarly, eleven equations were developed by PRCI as level 4, tensile strain design models to evaluate the TSC of pipelines beyond the yield strain [13]. The models, which allows the use of FEA calculation to develop crack driving force relations, use two limit states based on either initiation control or ductile instability. The models for standard groove weld bevel geometry, typical of flux-cored arc welding (FCAW) and shielded metal arc welding (SMAW) are presented in Equations (9) to (19). The model was validated against 24 full-scale tests. The tested pipelines had material grades varying from X65 to X100. The proposed equation evaluates the TSC for pipes with a pressure factor of 0.72 and a wall thickness of 15.9 mm. Two correction factors were presented to account for the different internal pressure levels and pipe wall thicknesses.

$$\mathrm{TSC}_P = \mathrm{A}\frac{f(\delta_A)}{1 + f\ (\delta_A)} \tag{9}$$

$$f(\delta_A) = (C\delta_A)^{B\delta_A{}^D} \tag{10}$$

$$TSC_p(t) = TSC_p.sf(t) \tag{11}$$

$$sf(t) = (\frac{t_0}{t})^{\ 0.8096(11.503\Psi^{1.229})} \tag{12}$$

$$\mathrm{TSC} = \begin{cases} \mathrm{TSC}_p & if \quad 0.6 \le PF \le 0.8 \\ \mathrm{TSC}_0 + \dfrac{5PF}{3}\left(\mathrm{TSC}_p - \mathrm{TSC}_0\right) & if\ PF < 0.6 \end{cases} \tag{13}$$

$$\mathrm{TSC}_0 = 1.5\mathrm{TSC}_p \tag{14}$$

The pressure effect factor C_p is defined as:

$$\mathrm{C}_p = \frac{\mathrm{TSC}_0}{\substack{min\,\{TSC\} \\ 0 \le PF \le 0.8}} \tag{15}$$

where $t_0 = 15.9\,mm$, $sf(t)$ is the thickness correlation function, $0.5'' \le t \le 1.0''$, and TSC_0 is the TSC of non-pressurized pipes.

The fitted functions A, B, C, and D for SMAW TSC_p are obtained as follows:

$$\mathrm{A} = \mathrm{a}_1 \mathrm{e}^{\frac{\mathrm{a}_2}{\beta}} \mathrm{e}^{\mathrm{a}_3\eta\beta} \mathrm{e}^{\frac{\mathrm{a}_4}{\beta}} [1 + \mathrm{a}_5\Psi^{\mathrm{a}_6} + \mathrm{a}_7\Psi^{\mathrm{a}_8}(\eta\beta)^{\mathrm{a}_9}](1 + \mathrm{a}_{10}\xi^{\mathrm{a}_{11}}\phi^{\mathrm{a}_{12}}) \tag{16}$$

$$B = \beta^{b_1}\eta^{b_2\beta^{b_3/\eta}}\left[b_4\phi^{b_5}\left(b_6\phi^{b_7}\right)^{\xi} + b_8\Psi^{b_9}\right] \quad (17)$$

$$C = e^{\frac{c_1}{\beta}}e^{\frac{c_2\beta}{(1+c_3\beta)\eta}}\left(1 + c_4\Psi^{c_5} + c_6\Psi e^{-\eta} + c_7\Psi e^{-\beta}\right)\left(c_8 + c_9\phi^{c_{10}} + c_{11}\xi^{c_{12}}\phi\right) \quad (18)$$

$$D = d_1\beta^{d_2}\eta^{d_3}\left(1 + d_4\Psi^{d_5} + d_6\eta\beta\Psi\right)\left(1 + d_7\xi^{d_8} + d_9\phi^{d_{10}}\right) \quad (19)$$

where a is the flaw depth, 2C is the flaw length, η is the normalized flaw depth, β is the normalized flaw length, Ψ is the normalized girth weld high-low misalignment, ϕ the is weld strength mismatch at the ultimate tensile strength (UTS), h is the girth weld high-low misalignment, t is the wall thickness, ξ is the base metal Y/T ratio, T is the UTS, TSC_p is the TSC for pressure factor of 0.72, and δ_A is the girth weld apparent CTOD toughness [13].

In the PRCI model, four categories of failure strains were defined as; failure in the pipe body, overall maximum load reached at limited flaw growth, flaw failure with finite flaw growth (local or global instability depending on the loading method) and local instability (flaw failure in the elastic strain range) [13].

4.4 Experimental test program

4.4.1 Test matrix

Nine NPS 22, X42 girth welded vintage pipes, which were originally used for transporting oil and gas in the last decades by Enbridge Pipelines Inc., were provided for the test program developed in this study (Figure 4-1). The X42 vintage pipes used in these experiments were manufactured in the late 1960s, and the construction was in the 1970s. Eight of the pipes were used in fabricating eight full-scale test specimens, while the ninth pipe was used to perform small-scale tension tests. The pipes have an outer diameter (D) 558.8 mm, nominal wall thickness (t) 12.7 mm and length (L) of approximately ($7D$) 3962.4 mm with an SMAW girth weld at the mid-length. The SMAW

girth weld was produced using a stick electrode equivalent of E6010 G, with the design UTS of 60 ksi.

As shown in the test matrix of Table 4-1, various parameters were used to examine the X42 vintage pipelines with defected girth weld subjected to internal pressure and bending. The levels of internal pressure causing hoop stress equivalent to 30% and 80% specified minimum yield strength (SMYS) were considered and four specimens were subjected to each of the internal pressure levels (i.e. a total of 8 specimens were considered). Similarly, flaw depth to wall thickness ratios (a/t) of 25% and 50% were chosen as shown in Table 4-1. Also, the effect of flaw length to wall thickness ratio was examined by selecting two values for $2C/t$: 5 and 10.

Table 4-1 Test matrix.

Test	Internal pressure P (MPa)	Flaw depth a (mm)	a/t (%)	Flaw length $2C$ (mm)	$2C/t$
1	10.5	3.23	25	64.37	5
2	4	3.12	25	64.08	5
3	10.5	6.34	50	63.34	5
4	4	6.34	50	64.34	5
5	10.5	3.18	25	127.24	10
6	4	3.30	26	127.83	10
7	10.5	6.46	51	127.07	10
8	4	6.42	51	127.35	10

The girth weld of the pipes was covered with girth weld sleeves, which were typically used to reinforce or repair girth weld defects (Figure 4-1). The girth weld sleeves were removed mechanically by gouging, which was carried out by cutting and grinding off the girth weld sleeve without applying any heat treatment that could affect the pipe material property. At each end of the pipe, a 1.5-inch-thick steel endplate was welded and a 1inch threaded hole was drilled on each endplate to provide water containment for pressurizing the pipe.

Figure 4-1 Photographs of: (a) Pipe specimens, (b) Sleeved girth weld and (c) Pipe cradle.

4.4.2 Test setup and procedure

The test specimen was mounted on two support cradles, which were mounted on knife-edges, and roller plates system supported on pedestals. The pedestals were fixed on the strong floor in the laboratory (Figure 4-2 and Figure 4-3). Two loading cradles similar to the support cradles were connected to a knife-edge and roller plate assembly attached to a load-distributing beam. The load-distributing beam was used to transfer the point load applied by the testing machine to the specimen. The loading beam was designed as a stiff member to minimize deformations. As shown in Figure 4-3, longitudinal and lateral bracing was provided to prevent lateral instability and excessive lateral movement of the specimen and the distributing beam during testing. The loading was carried out in three steps: 1) the internal pressure was applied; 2) the head of the loading machine was lowered to make contact with the pipe specimen (Figure 4-3), and 3) a displacement-controlled loading at the rate of 1.2 mm per minute was applied on the top flange of the distributing beam using a uniaxial testing machine to produce a four-point bending scenario in the pipe. The load was then transmitted through the load-distributing beam (F/2) to the pipe specimen, which resulted in a flexural bending moment on the specimen (Figure 4-2). The four-point bending technique ensured that the portion of the pipe containing flaw was subjected to maximum tensile stress throughout the test process. The displacement was incrementally increased until the stiffness of the specimen was significantly degraded as a result of crack initiation and gradual propagation to a critical point when water leaked from the flaw. This was deemed the beginning of failure and the test was halted.

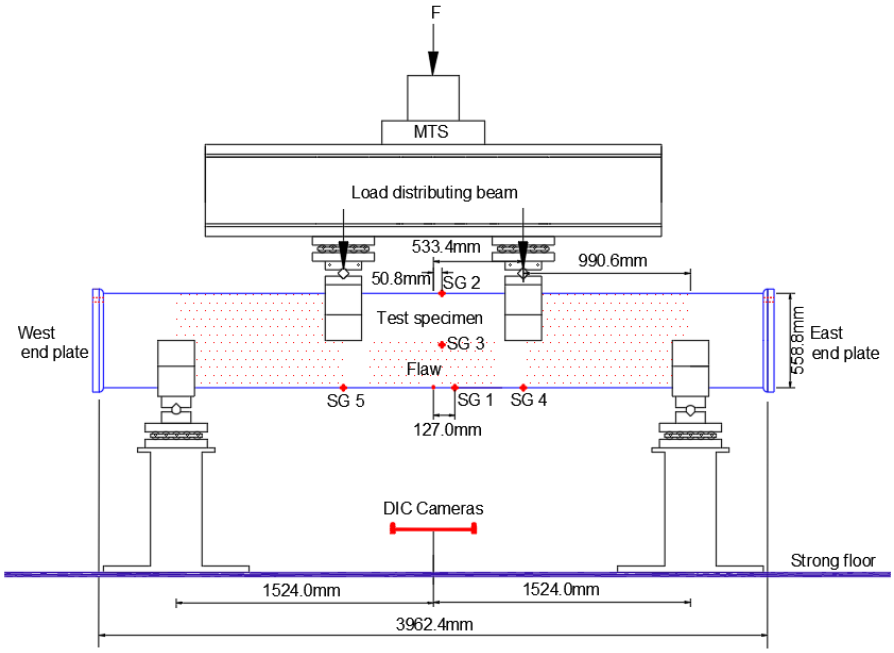

Figure 4-2 Schematic of the test set up showing the instrumentation and boundary conditions

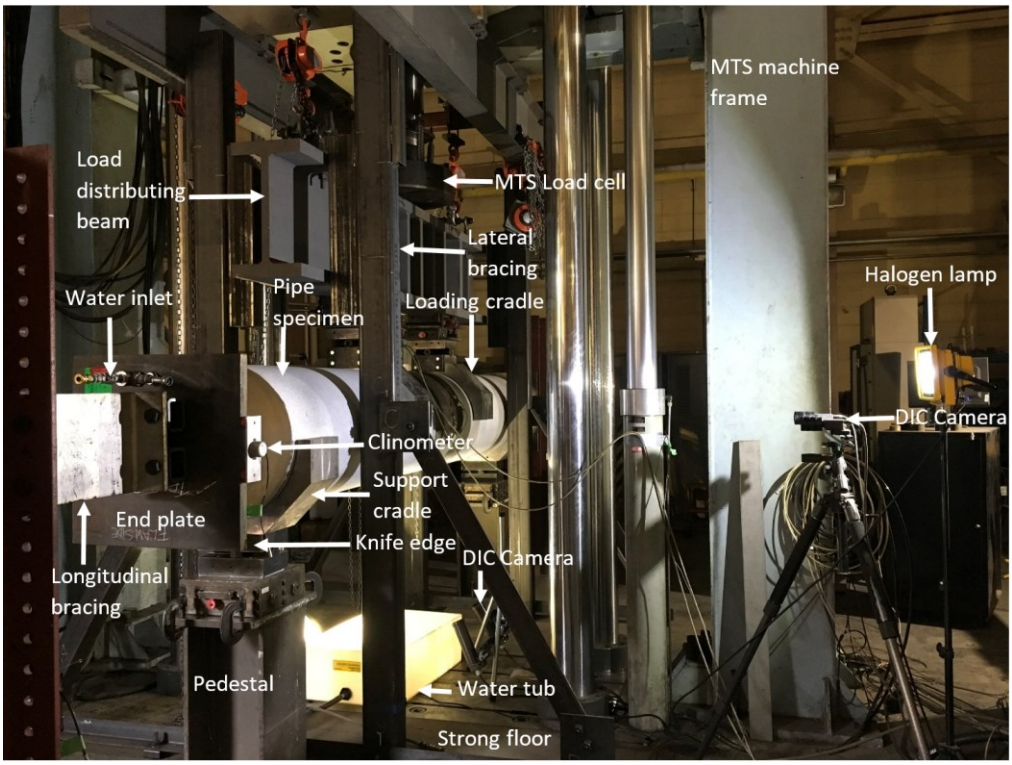

Figure 4-3 Photograph of the test set up showing the bracing, instrumentation and boundary conditions

4.4.3 Design of test setup

The design of the experimental test setup, including loading cradles, end plates, roller plates, and lateral bracing system was performed using the numerical model of the test procedure. The finite element analysis (FEA) of the test specimen was first developed by subjecting a symmetric X42 pipe model discretized using 8 node brick elements to internal pressure and four-point bending using the ABAQUS program [16]. The FEA predicted local buckling near the loading cradles as a possible failure mode; this can potentially affect the design, as the pipe will buckle at the compression side instead of the expected tensile rupture at the flaw location. Attention was paid to this possible failure mode when designing and machining cradles. The reaction forces imposed on the cradles by the pipe specimen, during the critical load of the test was used in designing the cradles. Four pipe cradles were fabricated to serve as loading and support collars as shown in (Figure 4-1 c). The cradles distribute the loads applied on the pipe specimen and minimize the risk of local buckling at the load application and support points.

4.4.4 Machining of the flaw on girth weld

A circumferential flaw was machined at the WCL of each specimen. The was cut initially using a 0.3048 mm thick blade followed by a thinner blade of thickness 0.1524 mm used for cutting the flaw tip. A typical flaw cut is shown in Figure 4-4 with section X-X showing the depth of flaw a and wall thickness t.

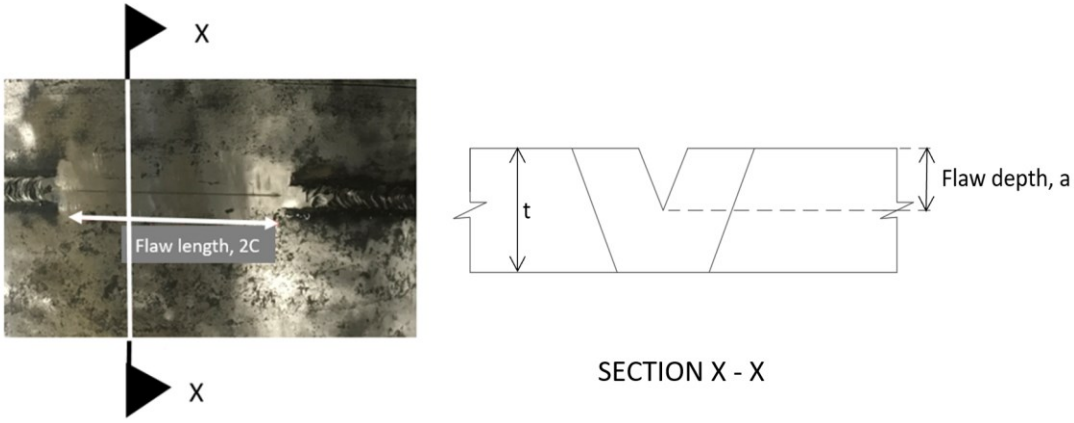

Figure 4-4 Photograph of the circumferential flaw machined at the WCL

4.4.5 Instrumentation

The main instrumentations consisted of biaxial strain gauges, digital image correlation (DIC) technique, which typically involved the use of a set of digital cameras to capture images, which track the displacement of black speckle pattern sprayed on the pipe surface according to the deformation under load. The DIC was capable of measuring strain distribution on the pipe surface as well as tracking the CMOD. The locations of the strain gauges (SGs) and DIC on the specimen are shown in Figure 4-2. The CMOD was evaluated by tracking the displacements of two points lying on each side of the flaw. Three sets of cameras were calibrated and used to capture images every 2 *s* during the test for the DIC analysis. The strain readings obtained from the DIC on the tension side were to be compared to those obtained from SG1, SG4 & SG5 on the tension surface. Internal pressure was measured using a pressure transducer while pressure relief valves regulated it. Reaction force exerted on the loading beam and applied displacement by the MTS machine were measured using the controller of the loading machine. Clinometers attached to the end plates measured the rotation of end plates (Figure 4-3). All the experimental tests were conducted at room temperature.

4.4.6 Small scale tests

The X42 pipe and weld material properties were measured in a companion research [15] where small-scale tension coupons were tested in accordance with ASTM E8/E8M - 11 [17]. The average result of 3 longitudinal test specimens machined from the pipe base and weld metal were used to define the engineering stress versus engineering strain relationship of the X42 pipe and weld materials. The stress-strain curves of the pipe and weld materials are shown in Figure 4-5. Furthermore, SENT tests were conducted [15] in accordance with DNV [18] and BS8571 [19] to determine the fracture toughness of the X42 pipe weld material. All the tension coupons and SENT tests were carried out at room temperature. The results of the SENT tests are presented in section 4.

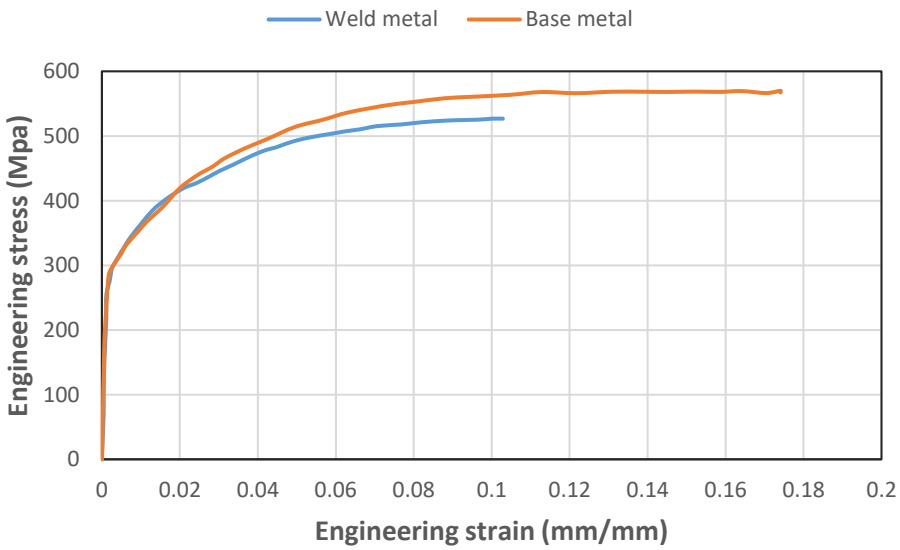

Figure 4-5 Average engineering stress versus engineering strain curves of the X42 pipe and weld materials obtained from three longitudinal test specimens

4.5 Test results and discussion

4.5.1 Small scale test results

The average value of the Young's modulus (E) is 200 GPa, the Poison's ratio is 0.3, the average true yield strength (Y) defined according to 0.5% of total strain, for the longitudinal base and weld metal specimens are 314 MPa and 324 MPa, respectively while the average UTS (T) are 640 MPa and 525 MPa, respectively.

For the circumferential round bar; base metal, weld metal and HAZ specimens, the average true Ys defined according to 0.5% of total strain, are 306 MPa, 444 MPa, and 340 MPa, respectively, while the Ts are 622 MPa, 647 MPa, and 656 MPa, respectively [15].

The SENT tests resulted in the R-curve for the weld and pipe metal as $CTOD = 0.64(\Delta a)^{0.20}$ and $CTOD = 0.69(\Delta a)^{0.59}$, respectively. Additional information on the SENT test procedure and results can be found in [15].

4.5.2 Full-scale test results

4.5.2.1 Global response

Moment-rotation responses of test specimens 1 to 4 and 5 to 8 obtained from the pipe moment and end plate rotation are given in Figure 4-6 a and b, respectively. A linear response was observed at the beginning of the tests; a nonlinear response followed this in tests 1 to 6. However, tests 7 and 8 failed at the linear elastic range before the inelastic response occurs.

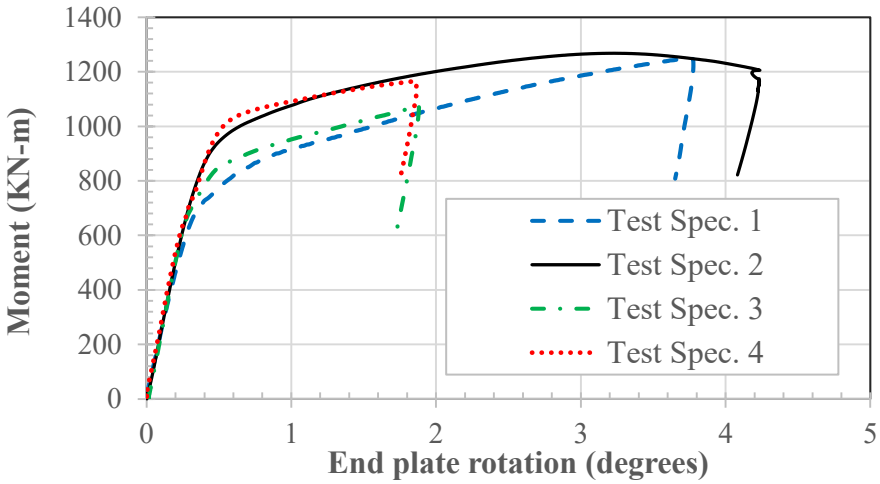

(a)

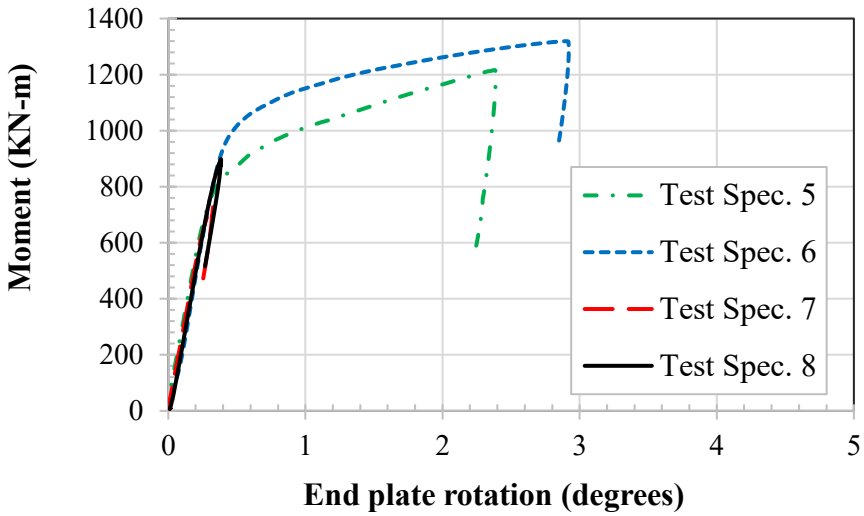

(b)

Figure 4-6 Moment–end plate rotation response: (a) Tests 1 to 4; and (b) Tests 5 to 8.

The global behaviours of Tests 1 to 8 were compared in Figure 4-6 a and b. Test specimens 1 and 2 (with flaw length of 5*t* and flaw depth of 0.25*t* subjected to different levels of internal pressure) at the critical moment experienced an end plate rotation of approximately 3.8 degrees (°) and 4.2° respectively. The flaw size when subjected to 4 MPa internal pressure (Test 2), was not adequate to influence crack initiation and growth on the tension side of the pipe, significant buckle was developed with an outward bugle-shape, which corresponds to the peak load during testing and after a long period of inelasticity (Figure 4-6 a and Figure 4-7) [20]. However, test specimens 3

and 4 (with flaw length of 5*t* and flaw depth of 0.5*t* subjected to different levels of internal pressure) failed after a maximum rotation of approximately 1.9°. The failure in test specimens 5 and 6 (with flaw length of 10*t* and flaw depth of 0.25*t* subjected to different levels of internal pressure) was observed after rotations of 2.4° and 2.9°, respectively. For test specimens 7 and 8, though they both failed at the linear elastic stage, the same trend was observed as the specimen subjected to a lower level of internal pressure rotated noticeably prior to failure, i.e. higher level of internal pressure tends to decrease specimen rotation at failure and the associated TSC. These results indicated that the flaw size and internal pressure level significantly affect the rotation level of the specimen before failure.

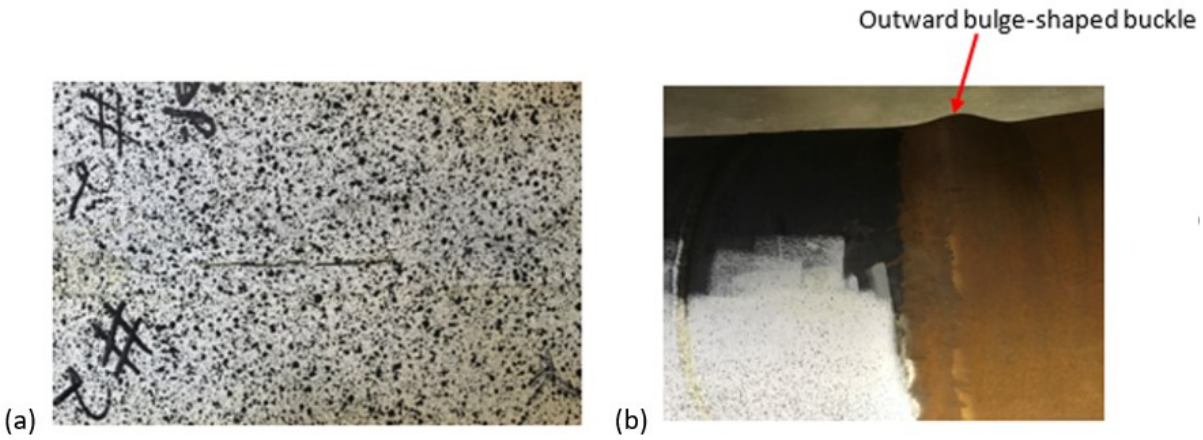

Figure 4-7 Photograph of specimen 2 samples at the end of the test: (a) Tension side flaw with no significant crack growth; and (b) Compression side showing buckle.

4.5.2.2 Local response

All the tests failed by tensile rupture as crack initiation and gradual propagation to a point when water leaked from the flaw was observed, except for Test 2, which buckled at the compression side. Crack propagation path through the weld metal dominated in the crack extension during tests as observed in Tests 1, 3, 6, 7 and 8, while Tests 4 and 5 deviated direction and ended in the HAZ. This deviation could be attributed to the presence of defects in the vintage girth welds.

TSC of specimens was defined using three strain values: 1) The average strain (ε_{Avg}) measured on the tension side using the DIC when the critical load is achieved, starting from a point 50 mm away

from the circumferential flaw to a point 180 mm from the flaw; 2) The tensile strain recorded by strain gauges at the critical load, and 3) The global tensile strain due to bending at the critical load as given in Eq. (20) knowing the curvature of the pipe:

$$\varepsilon_x = \frac{-y}{\rho}, \ \rho = \frac{L_0}{\theta} \text{ and } \theta = 2\phi \tag{20}$$

where ε_x is the global longitudinal strain, ρ is the radius of curvature at the critical load, y is the distance from the neutral axes to the pipe outer diameter surface, L_0 is the distance between the loading cradles, ϕ is the estimated pipe rotation at the loading cradle location (at the critical load). The pipe rotation at the loading cradle location was calculated using beam theory, assuming a circular cross-section of the pipe and utilizing the measured rotation at the pipe support. In this equation, it is assumed that the middle-third section of the pipe in the four-point bending arrangement is under pure bending. To verify the tensile strain response in the third step of loading, the longitudinal tensile strains measured by SG1, SG4, SG5 and DIC for Test 3 were plotted (Figure 4-8) against distance along the pipe starting from the circumferential flaw.

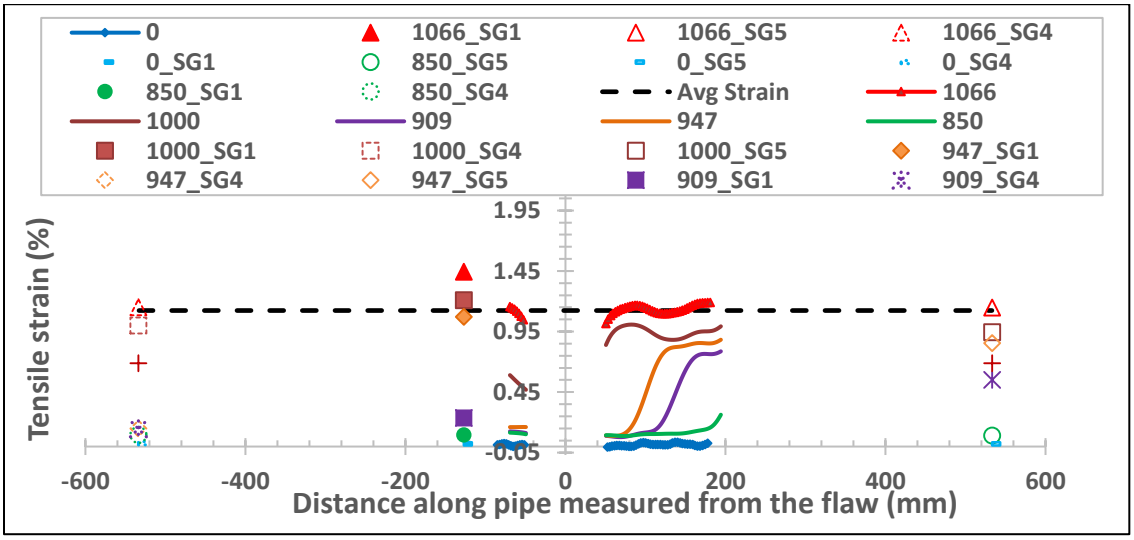

Figure 4-8 Longitudinal tensile strain distribution for Test 3.

In Figure 4-8, the red line with a triangular marker indicates the strain measurement recorded at the critical load prior to failure. The dashed black line represents the average strain. The marker points without lines indicate strain gauge readings and global strain. The series labelled 0 represented the strain distribution at the end of the internal pressure step (Step 1). The legends were labelled based on the moment level in KN-m. Test 3 failed at a critical moment of 1066 KN-m. It was observed that the DIC strain results agreed well with those obtained from strain gauges in the linear elastic stage and the early stages of nonlinear response. Note that some of the strain gauges failed before the critical load was reached (Table 4-2).

Table 4-2 presents the strain responses recorded at the critical moment when the specimen fails and the global strain due to bending. Additionally, the ratio (difference) between the average strain and that of the SG1 as well as the ratio between the average strain and the global strain are presented.

Table 4-2 TSC measured using different techniques at the critical moment.

Test	Critical moment	SG1	Test Avg strain	Global strain	Test Avg vs. SG1	Test Avg vs. Global strain
	(KN-m)	(%)	(%)	(%)	(%)	(%)
1	1244	-	1.79	1.40	-	0.39
2*	1270	-	2.50	1.55	-	0.95
3	1066	1.45	1.13	0.69	-0.32	0.44
4	1166	1.30	1.05	0.68	-0.25	0.37
5	1209	1.46	1.41	0.87	-0.05	0.54
6	1313	-	1.54	1.07	-	0.47
7	729	0.12	0.11	0.12	-0.01	-0.01
8	891	0.12	0.14	0.14	0.02	0.00

*Test 2 did not fail by tensile rupture at the flaw location as no leakage was observed.

As shown in Table 4-2, SG results were slightly higher than DIC average strain values except in Test 8; a maximum difference of 0.32% was obtained in Test 3.

The SG1 in Tests 1, 2 and 6 failed before the critical moment (Table 4-2). The computed global strain due to bending gave slightly lower strain values compared to the test average strain results except in Test 7, which resulted in higher global strain while Test 8 was approximately equal to the average strain. The maximum difference of 0.95% was recorded in Test 2. Note that Test 2 did not fail by tensile rupture at the flaw location, rather it buckled at the compression side, and the test was halted. It is essential to note that Test 2 had a higher strain than Test 1 even though Test 2 did not fail by tensile rupture, indicating that for small flaw depth (i.e. 0.25*t*), the internal pressure has an important effect on the TSC.

Similarly, the results obtained from Tests 5 and 6 showed the effect of internal pressure on the TSC by recording a difference of 0.13% strain. However, for flaws with higher depths (i.e. 0.5*t*), Tests 3 vs. 4, and Tests 7 vs. 8, the internal pressure does not significantly influence the TSC as the differences were significantly low. This finding was also confirmed by Abdulhameed et al. (2016) as the specimen with a deeper flaw (i.e. 0.5t) showed little effect of the internal pressure on the TSC [14].

4.5.3 Tensile Strain Capacity

Effect of internal pressure on TSC: as shown in Table 4-3, when the internal pressure increased, the pipe failed at a lower applied load and lower TSC. This was expected, as the increased internal pressure caused an increase in the longitudinal and circumferential tensile stresses on the pipe, which led to the failure of the pipe at a lower applied moment and lower longitudinal tensile strain (TSC). It was observed that the decrease in internal pressure level from 80% to 30% SMYS in Tests 1 and 2 caused a significant increase of 0.71% in TSC. Similarly, an increase of 0.13% in TSC was observed after reducing the internal pressure from 80% to 30% SMYS between Tests 5 and 6. For Tests 7 and 8, decreasing the internal pressure led to only a 0.03% increase in TSC. However, the opposite trend was observed in Tests 3 and 4, and the lower internal pressure was associated with a lower TSC. This opposite trend could be attributed to inhomogeneity in pipe body and random error in the measurement of flaw size.

Table 4-3 Effect of the internal pressure on the TSC.

Test	ε_{Avg} (%) (80% SMYS)	ε_{Avg} (%) (30% SMYS)	Increase in ε_{Avg} (%)
1 & 2[1]	1.79	2.50	0.71
3 & 4	1.14	1.05	-0.09
5 & 6	1.41	1.54	0.13
7 & 8	0.11	0.14	0.03

[1]Test 2 did not fail by leakage due to tensile rupture but buckled at the compression side.

Effect of flaw depth on TSC: Table 4-4 presents the comparison between two flaw depths: shallow, 25% of the wall thickness, and deep, 50% of the wall thickness. For each set, the internal pressure and flaw length are the same. It was observed for all four sets considered, the deeper flaw resulted in lower TSCs and lower critical moments. It is worth mentioning that Tests 7 and 8, which had the largest crack sizes, failed very early when the load-deformation response was still linear in comparison to tests 5 and 6 that failed after complete yielding (Figure 4-6 b).

Table 4-4 Effect of the flaw depth on the TSC.

Test	ε_{Avg} (%) (a=0.25t)	ε_{Avg} (%) (a=0.5t)	Decrease in ε_{Avg} (%)
1 & 3	1.79	1.14	0.65
2[1] & 4	2.50	1.05	1.45
5 & 7	1.41	0.11	1.30
6 & 8	1.54	0.14	1.40

[1]Test 2 did not fail by leakage due to tensile rupture but buckled at the compression side.

Effect of flaw length: Table 4-5compares the TSC and critical moments of test specimens subjected to the same internal pressure and having the same flaw depth but with different flaw length (long versus short). It was observed that the long flaw in Test 1 compared to the short flaw in Test 5

reduces the TSC. All the pairs compared followed the same reduction pattern as the length of the flaw increases. The results presented in Table 4-4 and Table 4-5 showed that the effect of flaw depth on the TSC is more pronounced than the effect of the flaw length.

Table 4-5 Effect of flaw length on the TSC.

Test	ε_{Avg} (%) (2C=5t)	ε_{Avg} (%) (2C=10t)	Decrease in (ε_{Avg}) %
1 & 5	1.79	1.41	0.38
2[1] & 6	2.50	1.54	0.96
3 & 7	1.14	0.11	1.03
4 & 8	1.05	0.14	0.91

[1]Test 2 did not fail by leakage due to tensile rupture but buckled at the compression side.

4.5.4 Experimental CMOD

Effect of the internal pressure on CMOD: each pipe specimen was pressurized through water containment provided by the end cap plates. The internal pressure caused an initial longitudinal strain, which in turn caused a noticeable crack mouth opening prior to the application of the bending moment. An equivalent bending moment (M_{eq}) was defined as the moment that would produce a longitudinal strain similar to that caused by the action of internal pressure on the end cap plates, which was estimated using the bending equation shown in Eq. (21):

$$M_{eq} = \frac{2\mathrm{EI}\varepsilon_l}{\mathrm{D}} \qquad (21)$$

where ε_l is the longitudinal strain measured at the end of the pressurization, D is the pipe outer diameter, M_{eq} is the equivalent applied bending moment and I is the moment of inertia of the pipe. The equivalent moments for 10.5 MPa and 4.0 MPa internal pressures were found to be 134 KN-m and 51 KN-m, respectively.

The values of the bending moment in the CMOD-applied moment curves were shifted by the corresponding M_{eq} to account for the noticeable effect of internal pressure on CMOD. The term "with M_{eq}" as used in Figure 4-9 is the CMOD-moment curve obtained using the sum of M_{eq}, and the bending moment obtained from the test while "without M_{eq}" is the CMOD-moment curve obtained using only the bending moment from the test. It is important to note that these shifts would decrease the observed difference between the CMOD, and the applied moment obtained for the same crack geometry with different internal pressure levels. However, as shown in Figure 4-9, this shift was relatively small and did not affect the results. This noticeable effect of internal pressure on the CMOD referred to the non-zero CMOD observed at the of the internal pressure step was more pronounced in tests with large flaw size subjected to higher internal pressure level such as Test 7 (Figure 4-9). This exercise was conducted to ensure that the high internal pressure and the end cap configuration did not contribute to the difference between the results of the lower pressure and the higher-pressure specimens. The two curves almost coincided with the majority of cases considered. What is interesting is that for tests 3, 4, 5, and 6, the internal pressure did not affect the value of CMOD at failure, as will be described below. This is similar to the trends observed by Abdulhameed et al., who concluded that internal pressure has a minimal effect on the CMOD [14].

The CMOD calculated using data obtained from the DIC was plotted against the applied bending moment to demonstrate the crack growth during the test, up to failure. As shown in Figure 4-9, the response is linear with a shallow slope then increased gradually when crack initiated and propagated until it became almost vertical (infinite) towards the failure moment. The infinite slope portion of the CMOD curve represented rapid crack growth when the crack became unstable at constant applied load, which means, a significant increase in CMOD without a commensurate increase in the applied load. CMOD-failure was defined as the CMOD value at which water leaked from the pipe, which was characterized by a significant pressure drop and almost constant applied moment. However, CMOD-critical was defined as the onset of unstable crack growth when the CMOD increased at constant applied load. The CMOD value represented CMOD-critical at 98% of the critical moment. CMOD results obtained for all specimens are presented in Table 4-6.

Table 4-6 CMOD response obtained from the test.

Test	1	2*	3	4	5	6	7	8
CMOD- failure (mm)	1.50	N/A	1.39	1.38	1.35	1.36	1.10	0.56
CMOD-critical (mm)	1.10	N/A	0.82	0.82	0.75	0.73	0.70	0.56

*Test 2 did not fail by leakage due to tensile rupture but buckled at the compression side.

A significant difference in the CMOD behaviour was observed between Tests 1 and 2, as shown in Figure 4-9, the flaw geometries of the two specimens were similar, but the internal pressure was different, which led to different failure modes. Test 1, with a 10.5 MPa internal pressure, failed by tensile rupture, causing a significant CMOD-failure of 1.5 mm with CMOD-critical of 1.1mm. Whereas, Test 2 with a 4 MPa internal pressure buckled as significant wrinkle developed on the compression side of the pipe (Figure 4-7 b) and water did not leak during the test. However, the CMOD-failure recorded for Tests 3 and 4 both having CMOD-critical of 0.82 mm were 1.39 mm and 1.38 mm, respectively. The CMOD-failure for Tests 5 was 1.35 mm, with CMOD-critical of 0.75 mm, while for test 6, CMOD-failure was 1.36 mm with CMOD-critical of 0.73 mm as shown in Table 4-6.

The closeness of the values is remarkable and shows that the CMOD-critical can be used as a measure of TSC as a function of the crack dimensions and is independent of the internal pressure. However, the value of CMOD-failure for Test 7, with CMOD-critical of 0.7 mm, was 1.1 mm, which was quite different from Test 8. Test 8 failed by water leaking from the crack location, but no significant crack growth was observed during the test (Figure 4-9 d, Figure 4-10 a and c). Upon inspection after the test, girth weld defects were observed at the inner surface of the specimen 8 sample (Figure 4-10 b). It should be noted that if the CMOD-moment curve of Test 8 is extrapolated, CMOD-failure of Test 8 will approach that of Test 7. The results of CMOD-failure showed that the CMOD decreases when the flaw length and flaw depth increase except for Test 2, which buckled instead of tensile rupture.

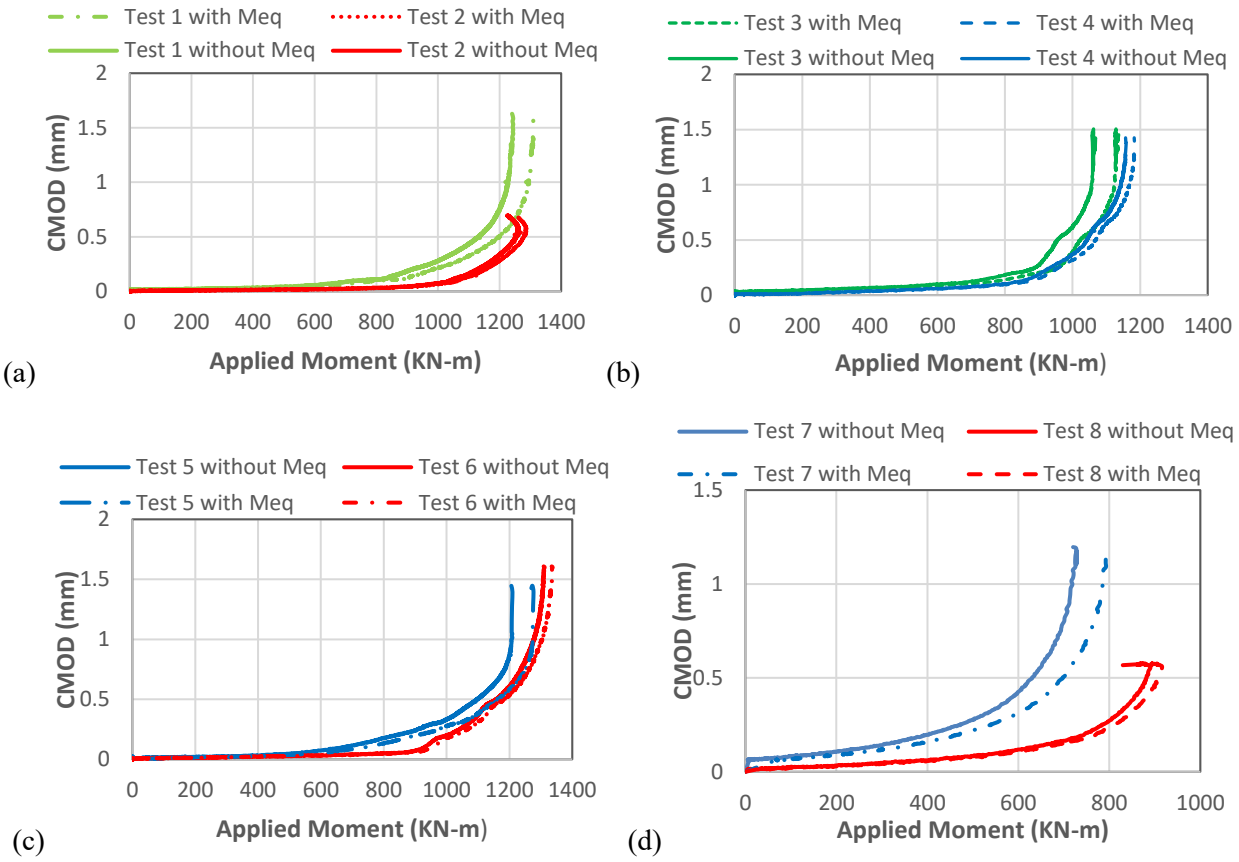

Figure 4-9 Variation of CMOD with applied moment: (a) Tests 1 and 2 (b) Tests 3 and 4 (c) Tests 5 and 6 (d) Tests 7 and 8.

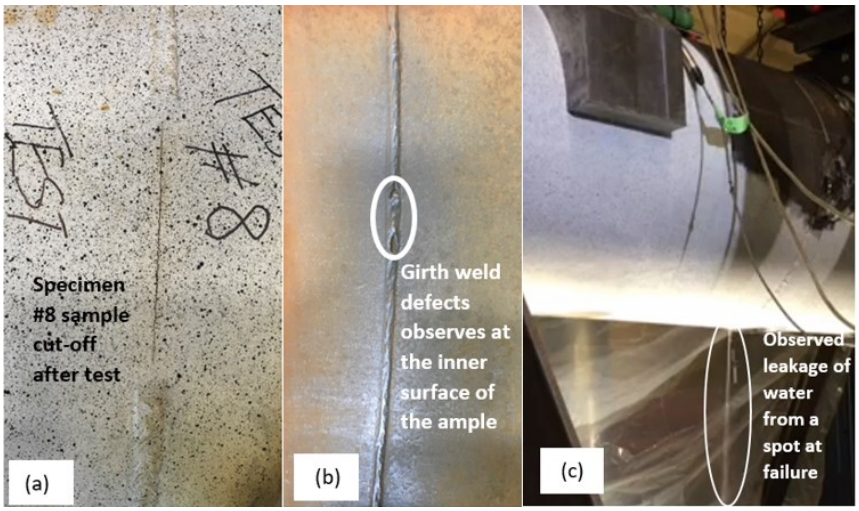

Figure 4-10 Photograph of Test Specimen 8 (a) sample cut for post-fracture analysis; (b) observed girth weld defects at the inner surface; and (c) leakage of water at failure.

4.5.5 Comparison of test results with TSC predictive models proposed by ExxonMobil and PRCI.

ExxonMobil and PRCI research programs investigating the behaviour of the pipeline girth weld subjected to strain-based loading developed SBECA models for predicting the TSC of pipelines [10- 13]. The average strain obtained from experimental testing of X42 pipes in this study were compared with the results obtained from EM and PRCI TSC predictive models. The purpose of this comparison is to investigate the applicability of the EM and PRCI models to X42 vintage pipeline material.

The input parameters used in the calculation were geometric and material properties obtained from the small scale and SENT tests conducted on X42 pipe and weld materials, as shown in Table 4-7 [15]. PRCI uses apparent toughness, δa, i.e. the CTOD in the girth weld SENT R-curve corresponding to crack growth of 0.5 mm, for the X42 pipes with a wall thickness of 12.7mm [21]. According to PRCI, toughness depends on the flaw size and strain redistribution in the vicinity of the flaw due to crack tip plasticity [13]. Whereas, toughness, δ, as used by EM is the CTOD in the girth weld SENT R-curve corresponding to 1mm crack growth based on a power-law fit [21]. Table 4-7 gives a comparison between the initial data used to evaluate the TSC using the EM and PRCI TSC predictive models.

As shown in Table 4-7, the deeper flaw depth (a≈6.35 mm) in Tests 3, 4, 7, and 8 fell outside the applicable range of EM TSC predictive model, which has an upper limit of a = 4.5 mm. In addition, the measured CTOD toughness equal to 0.64 mm fell below the lower limit (0.9 mm) of the applicable range of EM TSC equation. Finally, the measured yield-to-tensile ratio (Y/T) of the pipe material was 0.492, which is well below the applicable range for the EM TSC equation (0.76). However, the predictions of the models using these input parameters that fell outside the range were still compared with the experimental results to investigate the applicability of the models to X42 vintage pipelines. For the PRCI predictive model, most input parameter ranges were within the prescribed limit except for the pipe grade (X42) and Y/T (0.492), which fell below the lower limit (0.75).

Table 4-7 Input parameters used in evaluating the TSC for EM and PRCI models.

Parameters	EM applicable range	Parameters used for EM TSC	PRCI applicable range	Parameters used for PRCI TSC
Pipe Grade	X60 - X80	X42	X56 - X100	X42
Pipe diameter *D* (mm)	219.1 -762	558.8	304-1219	558.8
Wall thickness, *t* (mm)	13 - 22	12.7	12.7 - 25.4	12.7
Flaw depth, *a* (mm)	3 - 4.5	3.12 - 6.46	a/t = 0.05 - 0.5	a/t=0.25 - 0.51
Flaw length, 2C (mm)	25 - 200	63.5 &127	2C/t = 1 - 20	2C/t=4.99 - 10.07
Weld misalignment, *e* (mm)	0 - 3	0	e/t = 0.0 - 0.2	0
Internal pressure (% SMYS)	0 - 80	30 & 80	0 - 80	30 & 80
Weld overmatch, λ (%)	0 - 40	4	0 - 30	4
Uniform elongation, UEL (%)	6.7-– 13	11.70	-	-
CTOD toughness, δ (mm)	0.9 - 2.3	0.64	δ_a = 0.2 - 2.5	0.55
Yield-to-Tensile ratio, Y/T	0.76 - 0.87	0.492	0.75 - 0.94	0.492

Table 4-8 and Figure 4-11 presents a comparison of TSCs obtained from experimental tests and those obtained using EM and PRCI predictive models. TSC (leak strain), as defined in these tests, corresponded to the strain at leakage, which mostly coincided with the peak loads. The EM TSC defined failure at ductile tearing instability, which indicates the point of rapid crack growth without a commensurate increase in load. This point is similar to the critical CMOD defined in our tests as 98% of the critical load. PRCI TSC was defined as remote strain during; failure in pipe body, local (flaw cutting through pipe wall) and global (maximum load) instabilities, which included the failure defined in our tests.

Table 4-8 and Figure 4-11 suggests that the EM equation predicted conservative results in all tests except for Tests 7 and 8 when compared with the average test strain. In particular, the EM model predicted TSC that is 20 to 40% lower than the recorded TSC for Tests 1, 2, 5, and 6. For Tests 3 and 4, this level of conservatism increased to 66-71%. The bigger difference between Tests 3, 4, 7, 8 could be attributed to the fact that the flaw depth *a*, of these specimens fell outside the applicable range of the EM model.

As shown in Table 4-8 and Figure 4-11, the PRCI model predicted non-conservative results in all tests compared to the average test strain. This may be attributed to the use of input parameters outside the applicable range in estimating the TSC. The X42 vintage pipe gave a Y/T ratio of 0.492, which is well below the lower bound of the applicable range for EM (0.76) and PRCI (0.75). Using a lower bound Y/T ratio applicable to both EM and PRCI (0.76) to avoid extrapolation and comparing the responses with those obtained using X42 Y/T ratio, showed a significant impact on the predictions of the PRCI model (Table 4-9 and Figure 4-12). In particular, increasing the Y/T to 0.76 leads to the PRCI equation being highly conservative except for Tests 7 and 8. The level of conservatism for the EM predictive model slightly increased when the Y/T within the applicable range was used. This result is similar to findings by Robin et al. [21] who concluded that the PRCI model has a medium sensitivity to the Y/T while the EM model has a low sensitivity to Y/T. This suggests the need to develop a TSC predictive model that can accurately estimate the TSC of vintage pipelines as the findings of this study suggest EM and PRCI could not reliably predict the TSC of X42 vintage pipe material. It is important to note that the tests did not meet all the applicability requirements of the EM and PRCI equations.

Table 4-8 Comparison of test and predicted TSCs obtained using EM and PRCI models for X42 pipes.

Test	Test Avg ε (%)	EM TSC (%)	PRCI (SMAW) TSC (%)	Test Avg ε vs. EM (%)	Test Avg ε vs. PRCI (%)
1	1.79	1.38	4.11	+23	-57
2[a]	2.50	1.66	5.35	+34	-53
3	1.13	0.33	1.85	+71	-39
4	1.05	0.36	2.27	+66	-54
5	1.41	0.87	2.12	+38	-34
6	1.54	0.92	2.48	+40	-38
7	0.11	0.18	0.52	-39	-79
8	0.14	0.21	0.65	-33	-79

Note: '+' represented conservative results while '-' represented non-conservative results.

[a]Test 2 did not fail by leakage due to tensile rupture but buckled at the compression side.

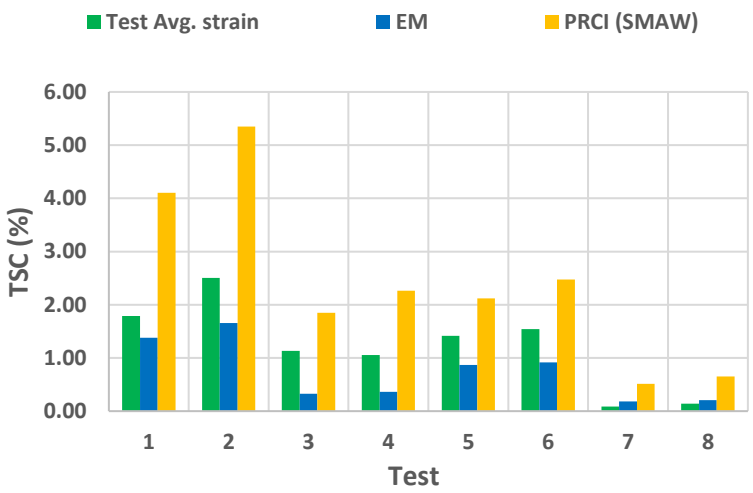

Figure 4-11 Comparison of the TSC between the obtained from the test and EM and PRCI models for X42 pipelines.

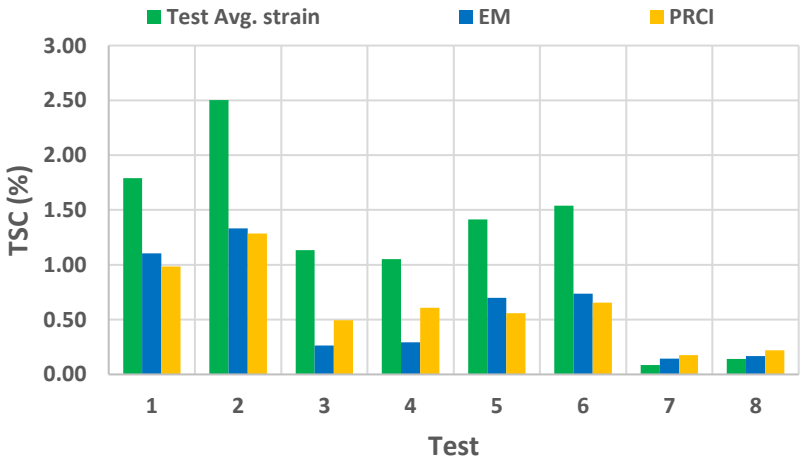

Figure 4-12 Tests and predicted TSCs obtained using X42 input parameters and Y/T = 0.76.

Table 4-9 Comparison of the test result with predicted TSC using Y/T = 0.76.

Test	Test Avg. ε (%)	EM TSC (%)	PRCI (SMAW) TSC (%)	Test Avg. ε vs. EM (%)	Test Avg. ε vs. PRCI (%)
1	1.79	1.11	0.99	+38	+45
2[a]	2.5	1.33	1.29	+47	+48
3	1.13	0.26	0.50	+77	+56
4	1.05	0.29	0.61	+72	+42
5	1.41	0.70	0.56	+50	+60
6	1.54	0.74	0.65	+52	+58
7	0.11	0.14	0.18	-21	-39
8	0.14	0.17	0.22	-18	-36

Note: '+' represented conservative results while '-' represented non-conservative results.

[a]Test 2 did not fail by leakage due to tensile rupture but buckled at the compression side.

As was stated earlier in this section, the deeper flaw depth (a≈6.35 mm) in Tests 3, 4, 7, and 8 fell outside the applicable range of EM TSC predictive model, which has an upper limit of $a = 4.5$ mm. The PRCI stated the following conditions for category No. 4 failure mode, which permits failure to occur in the elastic range; if the flaw is large, there is a gross weld strength under matching, there is a large magnitude of high-low misalignment, or the combination of those conditions, the growth of the crack-driving force may be unbounded. The remotely applied displacement is almost entirely taken up by the flawed plane; the failure strain under this scenario is near or less than the yield strain [13].

The non-conservativeness of the models could be attributed to the presence of inner diameter (ID) surface and buried weld defects in samples 7 and 8 weld microscopy (Figure 4-13-Figure 4-15). These defects can potentially reduce the TSC of test samples thereby keeping predictions from TSC models non-conservative. Vintage pipelines are associated with old girth welds, which are potentially more exposed to defects. This confirms the need for TSC predictive models for vintage pipelines that will put into consideration some of these uncertainties, which are not common in modern pipeline girth welds.

We did not analyze the test using a conventional stress-based approach because our major focus was on the strain-based approach. The major reason for comparing our results with the EM and

PRCI models was to verify the applicability of these existing TSC predictive models to X42 vintage pipes. Our results indicate the need for the development of the TSC predictive model for a robust assessment of in-service vintage pipelines.

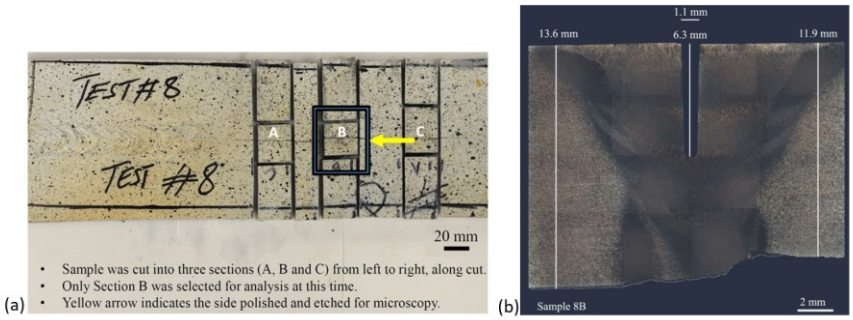

Figure 4-13 (a) Specimen 8 sample cut into three sections for analysis, (b) Details of flaw dimensions and etched weld microscopy of section B.

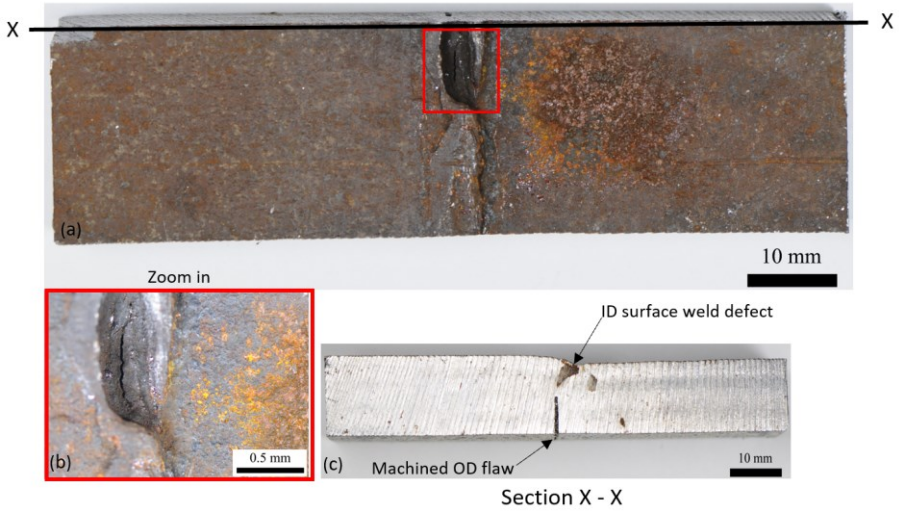

Figure 4-14 Details of pipe failure through weld defect and section through the wall thickness.

Figure 4-15 shows a sample cut of specimen 7 and the actual dimension of the machined flaw and wall thickness. Evidence of ductile crack extension and a buried weld defect found in section B of the sample 7 weld microscopy (Figure 4-15).

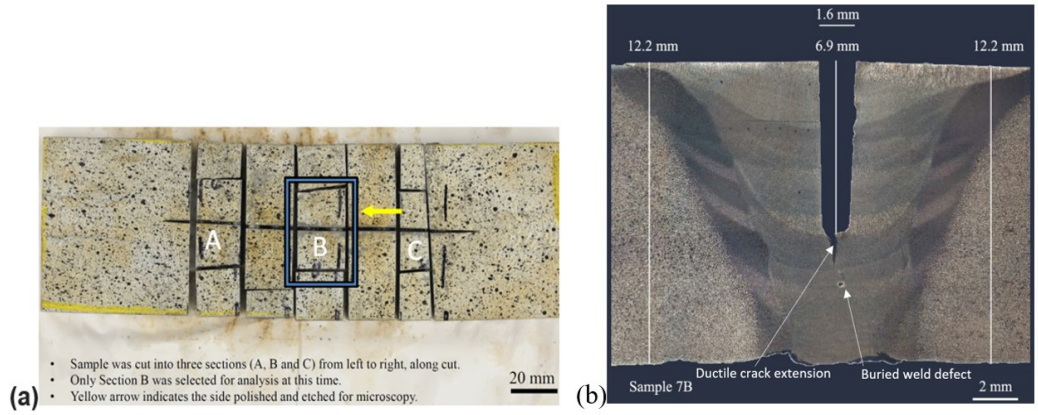

Figure 4-15 (a) Specimen 7 sample cut into three sections for analysis, (b) Details of flaw dimensions and etched weld microscopy of section B.

In Figure 4-9 d, the CMOD-moment curve shows crack propagation up to failure by tensile rupture for Tests 7 and 8. For Test 7, the ductile crack extension occurred after the blunting of the crack tip, (Figure 4-15 b), which was the expected procedure for the ductile tearing process. In Test 8, section of sample 8B did not reveal any evidence of ductile tearing (Figure 4-13), however, another section X-X was taken, which revealed that the ductile tearing occurred only through the remaining wall thickness after subtracting the machined flaw and the ID surface defect from the original wall thickness (Figure 4-14), which led to the premature failure as observed in CMOD-moment curve (Figure 4-9 d).

4.6 Conclusions

This study presents the results of experimental testing of eight full-scale pipe specimens with circumferentially oriented external surface flaw at the weld centerline under the effect of internal pressure and four-point bending. Tests served to evaluate the tensile strain capacity (TSC) of X42 vintage pipes. The results obtained from the experimental program was used to evaluate the applicability of the ExxonMobil and PRCI models for the prediction of TSC. The main findings of this study are summarized as follows:

- TSC of welded pipelines is strongly influenced by the flaw depth, flaw length and the level of internal pressure applied. The flaw depth was found to have a major effect. The flaw

length had a minor effect, and the internal pressure effect was more pronounced when the flaw depth was 0.25t.

- Strain results obtained from strain gauges and the DIC system were in a good agreement for all the tests. The computed global strain due to curvature gave slightly lower strain values compared to the average test strain.
- The level of internal pressure could reduce the TSC by 40% or more depending on the flaw size, which represents a significant impact on the TSC.
- For the specimens with the smallest flaw (0.25*t* depth and 5*t* length), the decrease in internal pressure caused a change in failure mode from tensile rupture to compressive buckling. This was highlighted by the difference in behaviour between Tests 1 and 2.
- We observed that the internal pressure has no effect on the CMOD-failure for tests 3 vs. 4 and tests 5 vs. 6. Test 8 seemed to have failed prematurely due to the presence of additional unaccounted for flaws in the girth weld.
- Comparison between the test results for X42 pipelines and those obtained using TSC predictive models developed by EM and PRCI showed that the EM model results in conservative values in all tests except Tests 7 and 8 while the TSC value is overestimated in all tests when using the PRCI method. Furthermore, when the Y/T was changed from 0.492 to 0.76, both models resulted in highly conservative values. This suggests that caution should be taken when the PRCI model is used for Y/T ratio below its applicable range because it can lead to highly non-conservative estimations of the TSC.
- The results of the experimental study suggest that EM and PRCI models cannot realistically predict the TSC for X42 vintage pipelines.
- Furthermore, a TSC predictive model for vintage pipelines will be developed in the future study to address the limitations by the EM and PCRI models based on the experimental data produced in this study.

- The main scientific contributions of the present study are; (a) Evaluation of the influential parameter including internal pressure and flaw size on the TSC of X42 vintage pipelines, (b) Critical evaluation of the available TSC predictive equations, and (c) producing experimental data for future research, namely for the development of an advanced predictive model for TSC.

4.7 Acknowledgments

The authors wish to thank Mr. Greg Miller and Mr. Cameron West of the I. F. Morrison Structural lab, the University of Alberta for their efforts and cooperation. We also wish to thank ExxonMobil Upstream Research, Enbridge Pipelines Inc., and Trans Canada Pipelines for providing funding for this research.

4.8 References

[1] Ahmed, A. U. (2010). Failure criteria for tearing of telescoping wrinkles (Ph.D. Dissertation). Structural Engineering, University of Alberta, Edmonton, AB, Canada.

[2] Mannucci, G., Lucci, A., Spinelli, C., Baldi, A., Mascia, G., (June 2011). "Full-Scale Bend Testing of Strain Based Designed High Grade Buried Gas Pipeline" Proceedings of the Twenty-first International Offshore and Polar Engineering Conference Maui, Hawaii, USA, ISSN 1098-6189.

[3] Leis, B., (2009) "PHMSA R&D Forum" Battelle Pipeline Development Center, Virginia, USA.

[4] Wang, Y.-Y., Horsley, D and Rapp, S., (2016), "Evolution of Linepipe Manufacturing and its Implications on Weld Properties and Pipeline Service" Proceedings of the International Pipeline Conference 2016, Calgary, Alberta, Canada, September 26-30, 2016.

[5] Wang Y.Y., Rudland D., Denys R., Horsley D. (2002), "A Preliminary Strain-Based Design Criterion for Pipeline Girth Welds," Proceedings of 4th International Pipeline Conference, Calgary, IPC2002-27169.

[6] Wang, Y. Y., Cheng, W., McLamb, M., Horsley, D., Zhou, J., Glover, A. G., (2004), "Tensile strain limits of girth welds with surface-breaking defects - Part 1: An analytical framework" Proceedings of the 4th International Conference on Pipeline Technology, 235-249, Ostend, Belgium.

[7] Wang, Y. Y., Cheng, W., McLamb, M., Horsley, D., Zhou, J., Glover, A. G.,(2004), "Tensile Strain Limits of Girth Welds with Surface-Breaking Defects Part II – Experimental Correlation and Validation," Proceedings of the 4th International Conference on Pipeline Technology, 251-266 Ostend, Belgium.

[8] CSA Z662 (2011, 2015). Oil and gas pipeline systems. Canadian Standards Association (CSA).
[9] Cakiroglu, C., Adeeb, S., Cheng, J. J. R., and Sen, M., 2014, “Design of the Full-Scale Experiments for the Testing of the Tensile Strain Capacity of x52 Pipes with Girth Weld Flaws Under Internal Pressure and Tensile Displacement,” ASME Paper No. IPC2014-33225.
[10] Kibey, S., Wang, X., Minnaar, K., Macia, M. L., Fairchild, D. P., Kan, W. C., Ford, S. J., and Newbury, B., 2010, “Tensile Strain Capacity Equations for Strain-Based Design of Welded Pipelines,” ASME Paper No. IPC2010-31661.
[11] Fairchild, D. P., Kibey, S. A., Tang, H., Krishnan, V. R., Wang, X., Macia, M. L., and Cheng, W., 2012, “Continued Advancements Regarding Capacity Prediction of Strain-Based Pipelines,” ASME Paper No. IPC 2012-90471.
[12] Tang, H., Fairchild, D. P., Noecker, F. F., Panico, M., Crapps, J., and Cheng, W., 2014, “Strain Capacity Prediction of Strain-based Pipelines,” ASME Paper No. IPC2014- 33749.
[13] Yong-Yi W, Ming L, and Yaxin S., 2011, "Second Generation Models for Strain-Based Design." PRCI.
[14] Abdulhameed, D., Cakiroglu, C., Lin, M., Cheng, R., Nychka, J., Sen, M., and Adeeb, S., 2016, “The effect of internal pressure on the tensile strain capacity of X52 pipelines with circumferential flaws,” J. Press. Vessel Technol. 138 (2016) 61701-0-61701-18, https://doi.org/10.1115/1.4033436.
[15] Ameli, I., Asgarian, B., Lin, M., Agbo, S., Imanpour, A., Duan, D., Cheng, J. J., Adeeb, S., (2018) “Determination of CMOD-force Curves and R-curves in Side-grooved Single Edge Notched Tensile (SENT) Specimens in Welded X42 Pipeline Steel”, International Journal of Pressure Vessels and Piping (2018), 10.1016/j.ijpvp.2018.04.003.
[16] ABAQUS 6.14, 2014, “Analysis User’s Guide,” Dassaultt Systèmes.
[17] ASTM E8/E8M-11. Standard test methods for tension testing of metallic materials. West Conshohocken, PA: American Society of Testing and Materials; 2011.
[18] Det Norske Veritas. DNV-RP-F108: Recommended practice–fracture control for pipeline installation methods introducing cyclic plastic, strain; 2006.
[19] British Standard Institution. BS 8571: Method of test for determination of fracture toughness in metallic materials using single edge notched tension (SENT) specimens; 2014.

[20] Sen, M., Cheng, J. J. R., & Zhou, J. (2011, May). Behaviour of cold bend pipes under bending loads. Journal of Structural Engineering, 137(5), 571-578. doi:10.1061/(ASCE)ST.1943-541X.0000219.

[21] Robin G., Neil G., Gregory S., Frank R., (2017), "A Comparison of Strain-Based Design ECA Models," Proceedings of the Twenty-seventh International Ocean and Polar Engineering Conference San Francisco, CA, USA, ISBN 978-1-880653-97-5.

5. EVALUATION OF THE EFFECT OF INTERNAL PRESSURE AND FLAW SIZE ON THE TENSILE STRAIN CAPACITY OF X42 VINTAGE PIPELINE USING DAMAGE PLASTICITY MODEL IN EXTENDED FINITE ELEMENT METHOD (XFEM)

This chapter is derived from the published conference proceedings:
Agbo, S., Lin, M., Ameli, I., Imanpour, A., Duan, D., Cheng, J. J., Adeeb, S., Evaluation of the Effect of Internal Pressure and Flaw Size on the Tensile Strain Capacity of X42 Vintage Pipeline using Damage Plasticity Model in Extended Finite Element Method (XFEM), Proceedings of the ASME 2019 Pressure Vessels & Piping Conference, July 14-19, 2019, San Antonio, Texas, USA PVP2019-94005

5.1 Abstract

Pipelines subjected to displacement-controlled loading such as ground movement may experience significant longitudinal strain. This can potentially impact pipeline structural capacity and their leak-tight integrity. Reliable calibration of the tensile strain capacity (TSC) of pipelines plays a critical role in strain-based design (SBD) methods. Recent studies were focused mostly on high toughness modern pipelines, while limited research was performed on lower-grade vintage pipelines. However, a significant percentage of energy resources in North America are still being transported in vintage pipelines. Eight full-scale pressurized four-point bending tests were previously conducted on X42, NPS 22 vintage pipes with 12.7 mm wall thickness to investigate the effect of internal pressure and flaw size on TSC. The pipes were subjected to 80% and 30% specified minimum yield strength (SMYS) internal pressures with different girth weld flaw sizes machined at the girth weld centerline. This paper evaluates the TSC of X42 vintage pipeline by utilizing ductile fracture mechanics models using damage plasticity models in ABAQUS extended finite element method (XFEM). The damage parameters required for simulating crack initiation and propagation in X42 vintage pipeline are calibrated numerically by comparing the numerical models with the full-scale test results. With the appropriate damage parameters, the numerical model can reasonably reproduce the full-scale experimental test results and can be used to carry out parametric analysis to characterize the effect of internal pressure and flaw size on TSC of X42 vintage pipes.

Keywords: Crack initiation and propagation, full-scale test, girth weld flaw, parametric analysis, strain-based design, tensile strain capacity, vintage pipeline, XFEM.

NOMENCLATURE

ASD	Allowable stress design
CMOD	Crack mouth opening displacement
XFEM	Extended finite element method
FEA	Finite element analysis
G_C	Fracture energy
FST	Full-scale test
ID	Internal diameter
M_{axpe}	Maximum principal strain
M_{axps}	Maximum principal stress
GI_C	Mode I energy release rate
NPS	Nominal pipe size
OD	Outer diameter
PGD	Permanent ground deformations
P_f	Pressure factor
SENT	Single-edge notch tension
SMYS	Specified minimum yield strength
SBD	Strain-based design
TSC	Tensile strain capacity

5.2 Introduction

There is generally an increased demand for energy resources such as oil and natural gas due to rapid global industrialization. Development of these resources, which often transverse remote and remarkably harsh geological terrains with potential ground movement is necessary to boost energy supply. Recently, pipelines subjected to permanent ground deformations (PGD) such as slope movement, landslide, fault movements, and seismic activities have gained more attention since pipeline limit states need to be checked under these phenomena. The effect of ground movement on buried pipelines is the imposition of high longitudinal stresses and strains in the local domain. High-stress localization can typically result in local instability at these critical locations, especially in welded pipelines, which potentially contain crack-like surface breaking flaws at the girth weld.

Traditional pipeline design procedures are usually based on the allowable stress design (ASD) concept, which aims to control the resultant longitudinal and circumferential stresses in pipelines, either due to load-controlled or displacement-controlled conditions, to a percentage of the specified minimum yield strength (SMYS) of the pipeline material. However, the ASD approach is constrained by its inability to distinguish between stable and unstable failure modes, and between loss of serviceability and loss of pressure containment integrity [1]. The strain-based design (SBD) approach is thus considered a more suitable option and has been recently more accepted by several pipeline design standards (e.g., CSA Z-662 [2], API RP 1111 [3], DNV-OS-F101 [4],) for the design of pipelines exposed to high longitudinal plastic strains due to ground movement [5, 6]. The SBD approach overcomes the characteristic conservativeness of the ASD method by sustaining a finite amount of plastic strain while addressing both the serviceability and ultimate limit states.

The majority of research conducted in recent years focused on modern pipelines with steel grades of X60 and above with limited research performed on lower-grade vintage pipelines [7]. The research study conducted by Wang et al. [8, 9, 10] led to the development of closed-form equations for predicting the TSC of pipelines using the pipe and flaw geometries, girth weld and pipe material properties as the major influential parameters. These equations, previously included in the design standard for oil and gas pipeline systems CSA Z662-11 [11], did not consider the effect of internal pressure and were not applicable to vintage pipelines. Given that a significant percentage of

vintage pipelines are currently in service, transporting a considerable quantity of energy resources, there is an urgent need to evaluate the response of such pipelines when subjected to geo-hazards. Specifically, the effect of biaxial loading due to internal pressure and bending stresses imposed on pipelines should be addressed.

Today, the extended finite element method (XFEM), cohesive zone method (CMZ) and virtual crack closure technique (VCCT) are the three most representative methods to simulate the fracture process [12]. Since XFEM can simulate discrete crack initiation and propagation along arbitrary paths (i.e. the crack can cut through the elements) without re-meshing the crack-tip domain, it becomes a very effective tool to study the ductile fracture mechanism of welded pipelines subjected to biaxial loading condition. Zhang et al. [13] used XFEM to demonstrate fracture history, including crack initiation and growth using a small scale; tensile and three-point bending specimens on X65 pipe material. Ameli et al. [14] used XFEM to characterize the fracture history, including crack initiation and growth using SENT specimens on X42 vintage pipe material. There is a need to apply this XFEM tool to simulate full-scale fracture response on X42 pipe material subjected to internal pressure and four-point bending. The numerical results will be validated against full-scale test results.

This paper evaluates the TSC of X42 vintage pipeline by applying the ductile fracture mechanics principle using the damage plasticity model in the ABAQUS XFEM program [12]. The damage parameters required for simulating crack initiation and propagation in API X42-grade vintage pipe is calibrated numerically by validating the numerical models against full-scale test results. With the appropriate damage parameters, the numerical model can reasonably reproduce the full-scale experimental test results and can be used to carry out a parametric study to characterize the effect of internal pressure and flaw size on TSC of X42 vintage pipes.

5.2.1 Extended Finite Element Method (XFEM)

The XFEM solution space was obtained by further enriching the traditional finite element (FE) method using two additional functions. One is a discontinuous function that reflects the displacement jumps across the crack surface while the other is a near-tip asymptotic function that

captures the singularity in the neighbourhood of the crack-tip field [15]. The maximum principal strain criterion is used for damage initiation of Mode-I crack due to the inherent non-linear geometrical and material behaviour that dominated the plastic regime. An energy type damage evolution with linear softening, maximum degradation and a power-law mixed mode behaviour with energy mode mix ratio is used to define the damage evolution [15].

5.3 Surface-cracked Pipe Model

Eight full-scale four-point bending tests were previously conducted on API X42-grade vintage pipes by our group. The details of the experimental procedure can be found in a future publication [7]. The test/model matrix is presented in Table 5-1. Schematic diagram of a typical four-point bending test frame with the specimen containing circumferentially oriented outer diameter (OD) crack-like defect on the tension side (bottom), is illustrated in Figure 5-1.

Table 5-1 Test/model matrix.

Test/ Model #	Internal pressure *P*(MPa)	Flaw depth *a* (mm)	*a*/*t* (%)	Flaw length *2C* (mm)	*2C*/*t*
1	10.5	3.23	25	64.37	5
2	4	3.12	25	64.08	5
3	10.5	6.34	50	63.34	5
4	4	6.34	50	64.34	5
5	10.5	3.18	25	127.24	10
6	4	3.3	26	127.83	10
7	10.5	6.46	51	127.07	10
8	4	6.42	51	127.35	10

The full-scale test was numerically simulated in this study using a three-dimensional (3D) solid XFEM model developed with ABAQUS/CAE with Standard/Explicit Scheme [15], in order to

study the TSC and ductile fracture failure mechanism of steel pipes subjected to internal pressure and bending. The pipe geometry was modelled as a 3D deformable solid structure, and for computational efficiency, symmetric boundary conditions were applied in the longitudinal direction of the pipe, so that only one half of the full pipe specimen can be modelled. The XFEM model layout and applied boundary conditions are presented in Figure 5-2.

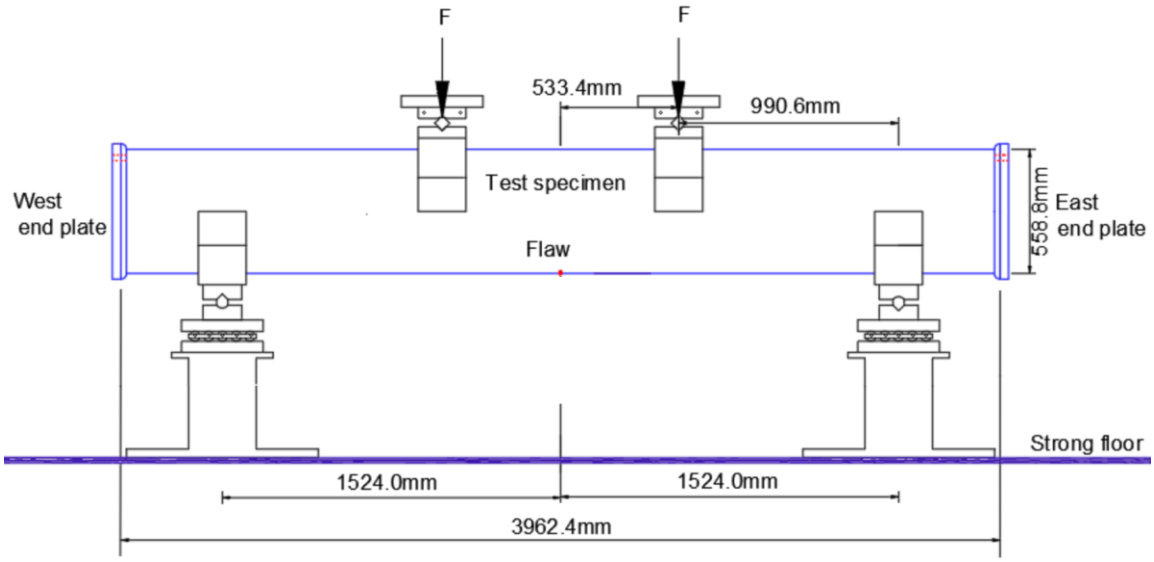

Figure 5-1 Schematic of the four-point bending test set up.

The material response assigned in the model is the true stress vs. true strain relationship (Figure 5-3) obtained from a uniaxial tensile test performed on longitudinal coupon specimens of the X42 vintage pipe materials [14]. A surface to surface contact was used to define the contact between the loading cradles and the pipe specimen. The end plates were tied to both ends of the pipe using tie constraint.

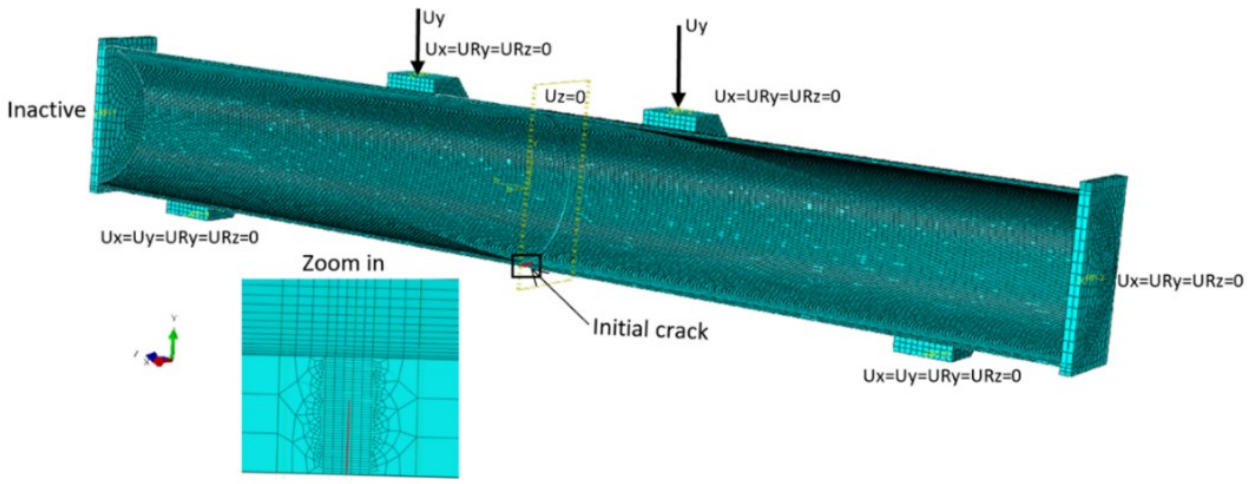

Figure 5-2 Finite element model and boundary conditions.

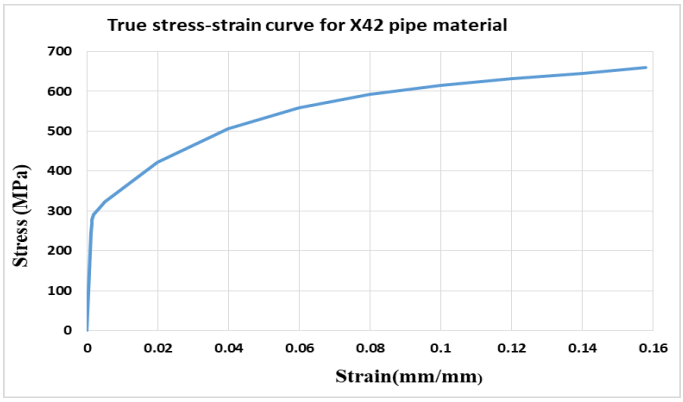

Figure 5-3 Average true stress-strain curve of the X42 pipe material.

In the XFEM technology, the pipe is independently meshed using an 8-node linear brick element (C3D8) with reduced-integration and hourglass control in the ABAQUS element library. The initial crack was inserted into the given location, with the elements aligned to the crack propagation direction (Figure 5-2) in the XFEM model. However, the loading and support cradles, as well as the end plates in the four-point bending model, were defined as analytical rigid parts. In order to ensure calculation accuracy, the element size along the through wall thickness (crack propagation

path) is about 0.45 mm, while other sections of the pipe were meshed with coarser elements, based on the result of a mesh sensitivity analysis. The model was loaded in three steps, including an initial load-controlled step followed by a contact step and finally a displacement-controlled step. In Step 1, the load-controlled internal pressure was applied; Then, the analytical rigid loading cradles were displaced monotonically to contact the pipe specimen.

Finally, a displacement-controlled loading was applied using monotonically increasing displacement through the reference points of the loading cradles. The displacements applied resulted in a flexural bending moment on the pipe specimen (Figure 5-2). The four-point bending technique ensured that the portion of the pipe containing flaw was subjected to maximum tensile stress throughout the loading process. This loading continued until crack initiated and propagated through the pipe wall. The XFEM damage stabilization cohesive was set to a viscosity coefficient of 0.0002. The maximum principal strain damage initiation tolerance was increased to 0.1. In the analyses, general solution controls were applied in the third step, by adjusting the time incrementation to allow for many small-time increments, also discontinuous general solution controls were applied by increasing the maximum number of cutbacks allowed for an increment to up to 20. The maximum number of increments allowed was increased to 10000, the initial increment size was decreased to 0.1, the minimum increment size decreased to 1E-009, and the maximum increment size decreased to 0.1. This time increment sizes were specified such that the simulated pipe failure could be achieved at a reasonably acceptable computing cost. ABAQUS static general procedure with nonlinearity in the geometry was used to solve the static equilibrium equations.

A mesh convergence analysis was conducted to establish the optimum number/size of elements required for the simulation. The XFEM model was run with three different mesh sizes, which were aligned to the crack propagation direction; 0.9 mm (14 though mesh), 0.45 (28 through mesh) and 0.3 mm (42 through mesh) near the initially defined crack area while monitoring the response to loading. The far-field elements had a coarser mesh to reduce computational time. The results are summarized in Figure 5-4 and Table 5-2. The results of the mesh sensitivity analysis indicated that mesh size of 0.9 gives a less accurate result at the best computational time while 0.45 mm results in a more accurate result at a good computational cost compared to 0.9 mm size, but 0.3 mm leads to almost the same result with 0.45 mm at a significantly more expensive computational cost.

Mesh size of 0.45 mm is selected as the optimum mesh size within the vicinity of the flaw since it gives reasonably accurate results at a good computational cost.

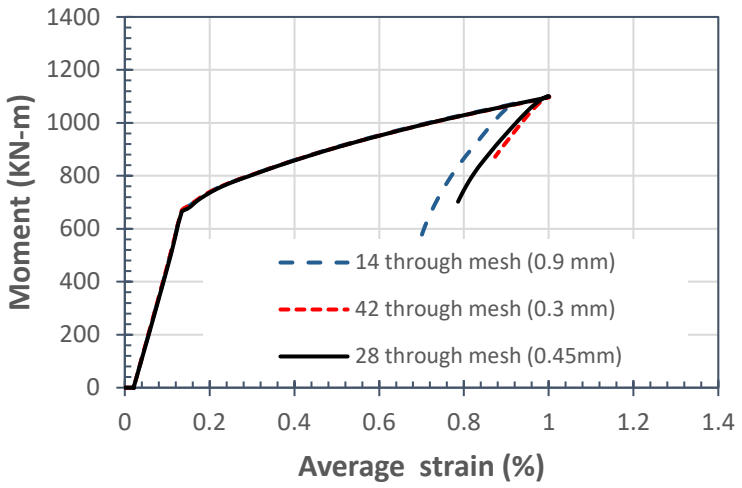

Figure 5-4 Mesh sensitivity study showing the response of Model 3.

Table 5-2 Mesh sensitivity analysis result.

Mesh size (mm)	Critical Strain (%)	% Difference
0.9	0.923838	-
0.45	1.00079	0.076952
0.3	1.00123	0.00044

5.4 Model Validation

5.4.1 Calibration of XFEM Parameters

The XFEM parameters were evaluated through a nonlinear parametric analysis to determine the best set of damage parameters for simulating crack initiation and growth in the pipe model. The key parameters used for the simulations of X42 pipes in XFEM were calibrated against the full-scale CMOD-moment curves. The maximum principal strain (M_{axpe}) and the fracture energy (G_C) are two key parameters selected in the XFEM procedure to affect the mechanical response and crack behaviour of the cracked X42 vintage pipes subjected to internal pressure and bending. M_{axpe} was selected against maximum principal stress (M_{axps}) because preliminary investigation shows that M_{axpe} was better in capturing the geometric and material non-linearity of all the full-scale tests using one set of damage parameters, unlike M_{axps}, which could capture only a few tests using one set of damage parameters. M_{axpe} controls the damage initiation of Mode-I crack and G_C dominates the resistance ability against crack propagation. Effects of M_{axpe} and G_C on the load-deformation responses of specimen 6 model during full-scale four-point bending numerical tests are presented in Figure 5-5 a and b. Figure 5-5*a* indicated that critical strain value grows rapidly as M_{axpe} increases, which means the specimen exhibits satisfactory load-bearing ability before the damage initiation. The CMOD- moment curves tend to decrease in slope as the G_C increases, (Figure 5-5 b), which suggests that the specimen keeps better residual strength and ductility to resist crack propagation after damage initiation, leading to a gradual increase in critical moment and strain. When the parameters are set as M_{axpe} = 0.013 and G_C = 450 N/mm, a better prediction is achieved. Therefore, this parameter set will be used in the subsequent analysis. The deformed shape of Model 6 captured at the onset of crack initiation, showing the distributions of M_{axpe} and M_{axps} at the crack-tip domain, when the selected set of damage parameters are applied in the model are shown in Figure 5-6. M_{axpe} = 0.0133 and a corresponding M_{axps} = 603.5 MPa were the crack-tip condition. Correlating the parameters with the mechanical properties of X42 vintage material resulted in the following values: M_{axps} of 603.5 MPa is equivalent to 1.92 yield strength and 1.06 ultimate tensile strength, and the G_C of 450 N/mm is equivalent to the critical energy release rate (G_{IC}), which is

the fracture toughness of X42 vintage material. G_C = 450 N/mm is also equivalent to the critical stress intensity factor (K_{IC}) of 314.5 MPa√m, under plane strain condition (Figure 5-6) [16].

The numerical model was calibrated by matching the CMOD-moment curve extracted from the simulation of a full-scale pipe to the experimentally measured CMOD-moment curve for Test 6. By using the numbers obtained from the calibration procedure, and applying it to the remaining tests, the experimentally measured TSC was effectively simulated. Figure 5-7 shows the critical strain profile obtained from the pipe body for different sets of damage parameters considered during the critical load. The gauge length where longitudinal strain is extracted from is approximately one outer diameter (OD) within the middle 3rd of the pipe length i.e. half OD from each side of the flaw, which is assumed to be subjected to pure bending (maximum bending moment), free from boundary effect and high strain concentration within the flaw. The strain distribution obtained from the numerical results is very close to that obtained from the experiments (Figure 5-7).

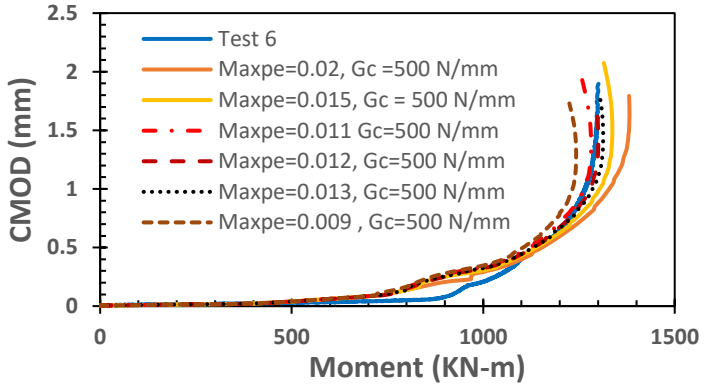

(a)

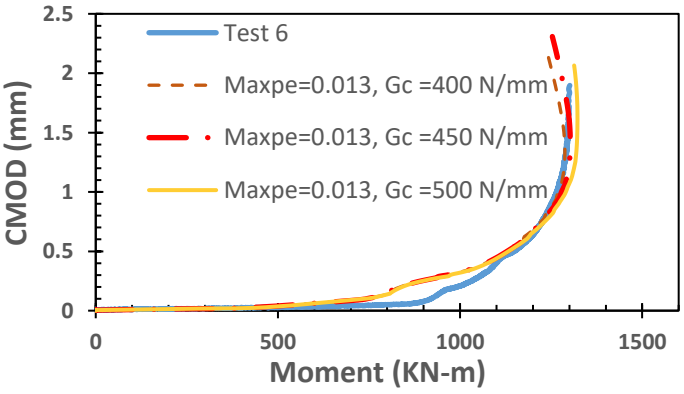

(b)

Figure 5-5 Effects of (a) Maxpe and (b) Gc on the load-deformation response of specimens 6.

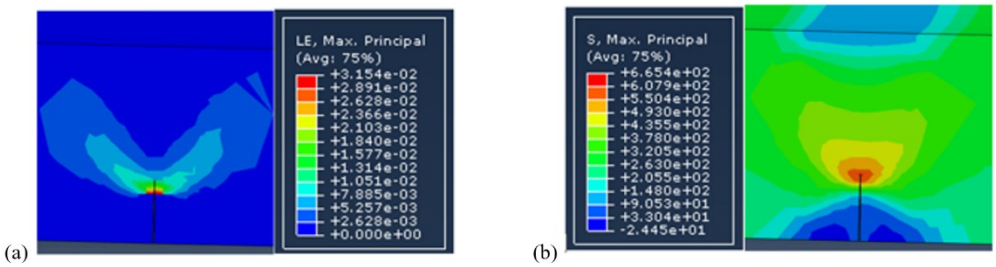

Figure 5-6 Crack-tip condition expressed in terms of maximum principal strain and stress during crack initiation (a) Maxpe at the crack-tip during crack initiation = 0.0133 and (b) Maxps at the crack-tip during crack initiation = 603.5 MPa for specimen 6

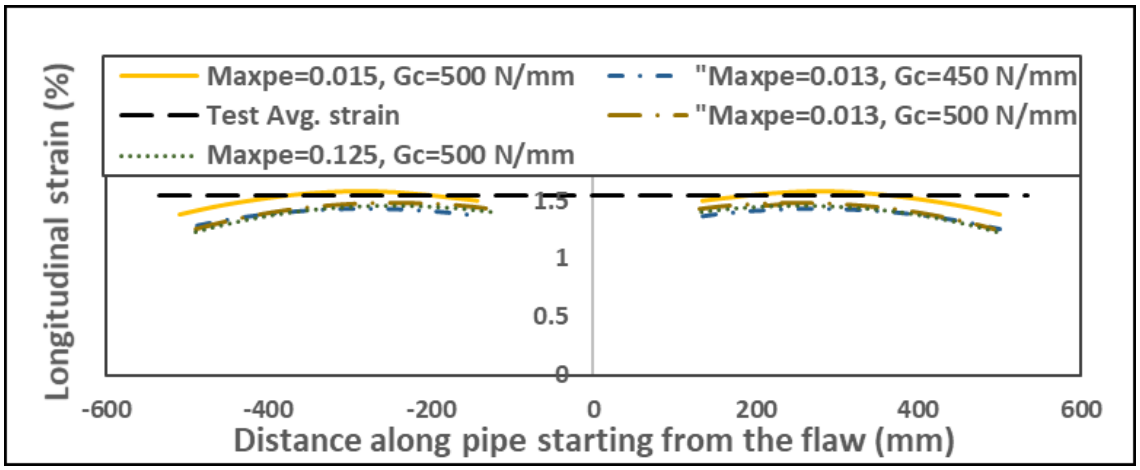

Figure 5-7 Longitudinal strain distribution along the gauge length of the pipe segment at the critical load for specimen 6.

5.4.2 The Ductile Fracture Process

The crack evolution histories during the loading can be described in three stages: Stage 1, the damage initiation on the nearest element of crack-front field occurs when first principal strain reaches its critical value, then a cohesive crack appears when the crack mouth opening

displacement (CMOD) equals to 0.22 mm (Figure 5-8a). Stage 2, the cohesive crack starts propagation with the increase of external loading, and a segment of this cohesive crack coalesces into the real crack when the energy release rate reaches the critical value. At this point, the originally real crack starts to propagate across an entire element as CMOD increased to 0.41 mm (Figure 5-8b). Stage 3, the real crack propagated until it penetrated through the pipe wall when the CMOD is 1.47 mm (Figure 5-8c).

As evidence of successful calibration, the CMOD-moment curves of four experimental tests modelled are matched with those obtained from the full-scale pipe models, as shown in Figure 5-9. The good agreement between the simulation and test results shows that the XFEM model is effective in simulating the pipeline fracture behaviour.

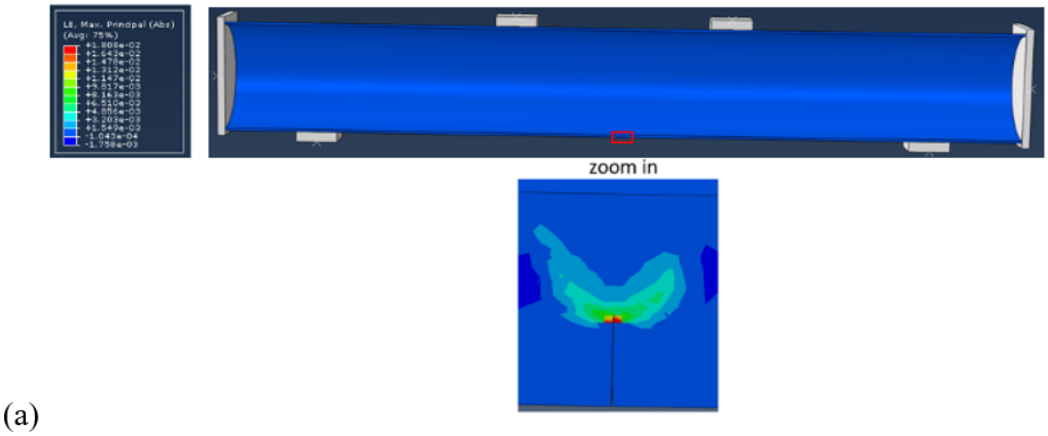

Figure 5-8 Stages of ductile fracture of cracked X42 vintage pipe subjected to four-point bending and internal pressure. (a) Formation of cohesive crack, CMOD =0.22 mm, (b) Crack propagation with CMOD=0.41 mm, (c) Crack penetrated through the pipe wall (failure), CMOD = 1.47 mm

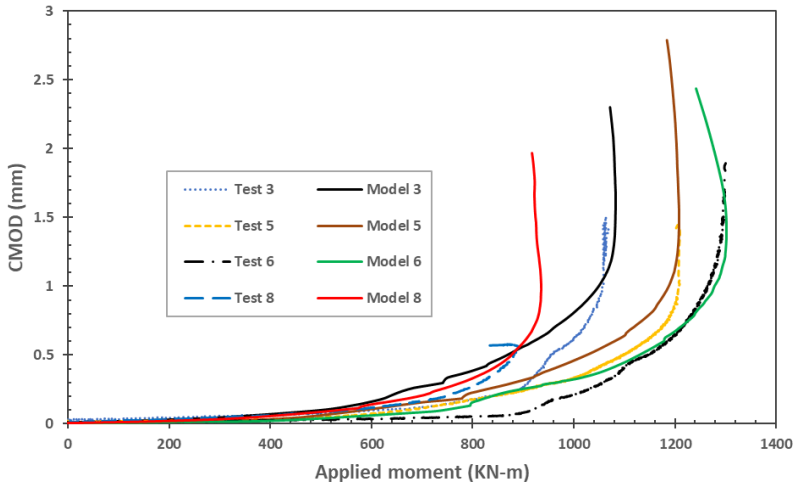

Figure 5-9 CMOD-moment curves obtained from the full-scale pipe tests and numerical models.

In Figure 5-9, it was observed that the CMOD-moment curves for experimental tests and those of the corresponding XFEM models followed nicely except for Test 8, because the pipe ruptured prematurely, and the moment decreased (Figure 5-9). This could be attributed to the presence of buried defects as well as internal diameter (ID) surface defect observed in the vintage (old) girth weld of test sample 8, which affected the crack propagation, as the pipe ruptured through the defect (Figure 5-10). It is important to note that the numerical models developed, did not consider these imperfections and thus gave smooth CMOD-moment curves.

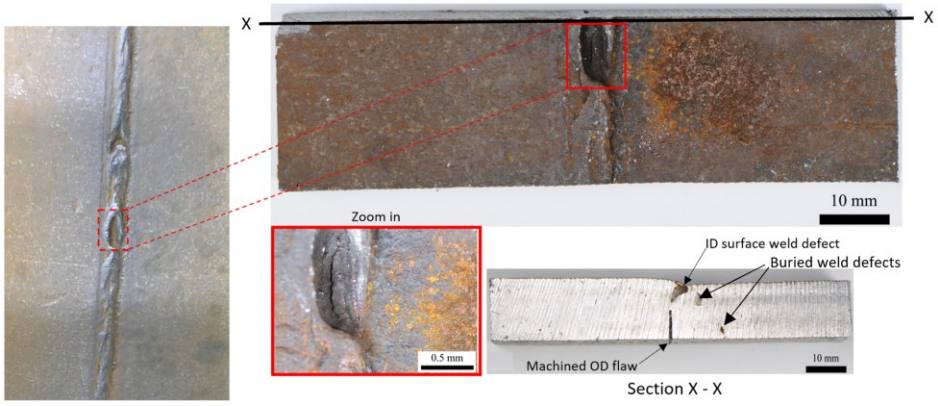

Figure 5-10 Girth weld defects observed in pipe specimen 8 sample examined after the full-scale test.

5.5 Numerical Results

The TSC obtained from XFEM numerical study and those obtained from full-scale tests are presented in Table 5-3. The ratio of the XFEM to full-scale test TSCs are also presented in Table 5-3. The average ratio is -0.01%, and the associated standard deviation is 0.06. The negative average ratio indicated that XFEM gave relatively lower TSC compared to the full-scale tests. The standard deviation of 0.06 is low, which indicated that XFEM and full-scale test results were very close.

In some cases, the numerical results predicted TSC slightly above the experimental results, while some were slightly below, as was observed in Models 2, 5, 7 and 8, and Models 1, 3, 4 and 7, respectively. This could be due to the imperfections in pipe geometry, variation of material properties and potential girth weld defects mentioned earlier. Model 2 did not fail by tensile rupture but buckled on the compression side of the pipe; the same behaviour was observed in Test 2.

The CMOD responses as a function of average tensile strain measured from 1 OD gauge length of the pipe body for models 3, 5, 6, and 8 are presented in Figure 5-11. The critical strain (TSC) for each model represented the maximum strain attained during loading, which approximately coincided with the moment the crack penetrated the pipe wall (leakage).

Model 8 failed at the elastic regime; this is similar to the response obtained from the experimental test 8. This result agrees with PRCI [17] category 4, failure mode for pipes with a large flaw or with gross weld strength undermatch, or large magnitude of high-low misalignment, or a combination of the listed conditions, subjected to tensile strain loading. The failure strain under this scenario is near or less than the yield strain.

Models 3, 5 and 6 failed at the plastic regime after a long period of stable ductile crack propagation (Figure 5-11).

TSC obtained from the XFEM numerical study are compared with those obtained from full-scale tests in Figure 5-12.

It was observed that the XFEM numerical results agreed well with the test results as all the data points (XFEM numerical results) aligned close to the 45 degrees line (full-scale test results), which suggests a good fit between the XFEM numerical results and the full-scale test results.

Table 5-3 TSCs of XFEM models and full-scale tests.

Model /Test #	XFEM TSC (%)	Test TSC (%)	Ratio (%)
1	1.786	1.791	-0.005
2[a]	2.504	2.502	0.002
3	1.001	1.135	-0.134
4	1.103	1.053	0.050
5	1.455	1.414	0.041
6	1.486	1.539	-0.053
7	0.127	0.110	0.017
8	0.142	0.140	0.002

[a]Model 2 and Test 2 did not fail by tensile rupture but buckled on the compression side.

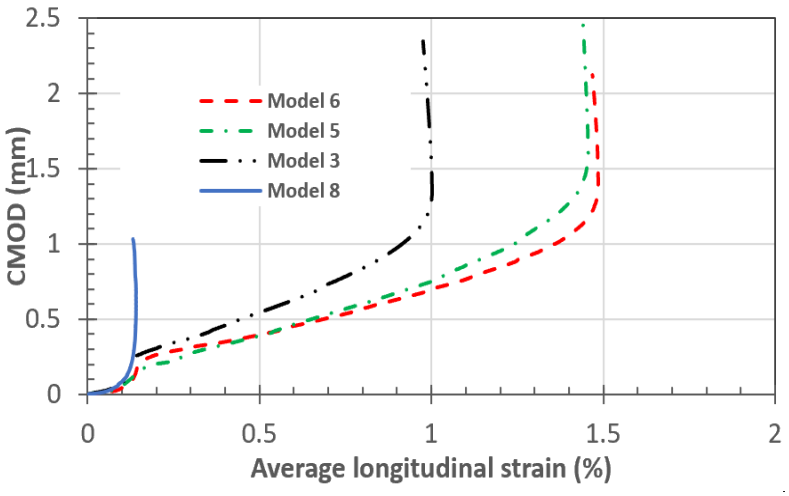

Figure 5-11 CMOD-average longitudinal strain response of XFEM numerical models.

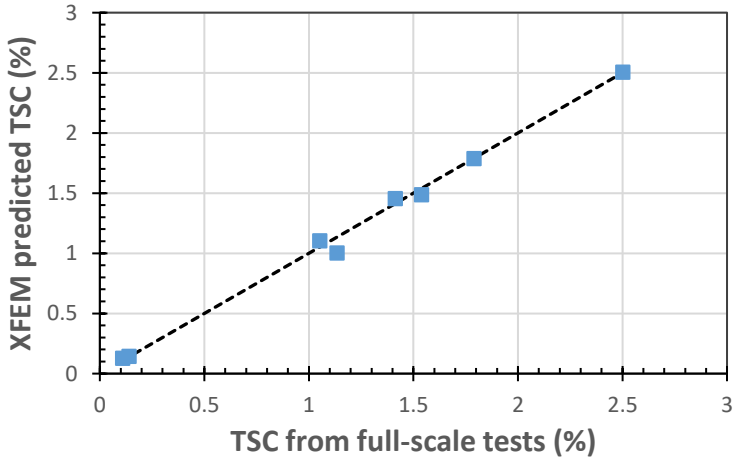

Figure 5-12 Comparison of TSCs from XFEM numerical models and full-scale tests.

5.5.1 Effect of influential parameters on the tensile strain capacity of X42 pipes.

Internal pressure: Two levels of internal pressure, i.e. 80% SMYS, pressure factor (P_f) = 0.8 and 30% SMYS (P_f = 0.3), were used to examine the global effect of the change in pressure to TSC numerically. The TSC and internal pressure are observed to be inversely correlated, with greater

influence observed in pipes with shallow flaw depth. This is evident in the change of failure mode of Model 2 as it buckled on the compression side instead of failure by tensile rupture, as observed in Model 1. In conformance with the experimental result, the internal pressure is observed to have a negligible influence on the TSC of pipes with a deeper flaw, as shown in Model 7 versus 8.

Flaw depth on TSC: For X42 pipes subjected to 25% and 50% flaw depths under the same level of internal pressure and flaw lengths. The global correlation between the TSC and flaw depth is found to be inversely proportional as an increase in flaw depth led to a reduction in TSC. This was expected since the flaw depth is directly related to the resistance of the pipe to fracture which is the common failure mode expected when structures with defects are subjected to excessive tensile stress. This relationship was obtained when TSC of Models 1 versus 3, 2 versus 4, 5 versus 7 and 6 versus 8 were compared.

Flaw length on TSC: The correlation between the TSC and flaw length followed globally the same inverse proportional trend as was observed in the case of flaw depth but with lower influence on the TSC compared to flaw depth. This relationship was observed when TSC of Models 1 versus 5, 2 versus 6, 3 versus 7 and 4 versus 8 were compared.

5.6 Conclusions

This study presents the results of the numerical study performed on full-scale X42 vintage pipes with circumferentially oriented external surface flaw under the effect of internal pressure and four-point bending using damage plasticity model developed in ABAQUS XFEM. The results obtained from the numerical program was validated using full-scale experimental test results. The main findings of this study are as follows:

- Accurate calibration of the XFEM model provides a veritable and reliable tool for simulating ductile fracture response of steel pipelines under load.

- Maximum principal strain M_{axpe} and fracture energy G_C are two major influential damage parameters of XFEM that significantly affect the ductile fracture behaviour of pipe specimens, especially when modelling full-scale pipe response that involved geometric and material non-linear behaviour in the plastic regime.
- M_{axpe} controls the damage initiation of Mode I fracture while G_C controls crack propagation, a critical value of M_{axpe} of 0.013 mm/mm and G_C of 450 N/mm, was used in simulating the ductile tearing process in X42 vintage pipe material.
- The predicted TSC using XFEM models agreed well with those obtained from full-scale tests since an average ratio of -0.01% strain, and a standard deviation of 0.06 was obtained.
- Globally, the internal pressure, flaw depth and flaw length were observed to be inversely correlated with the TSC.
- Internal pressure was observed to have a greater influence on pipes with shallow flaw depth, and flaw depth showed greater influence on TSC than flaw length.

5.7 References

[1] Kan, W.C.; Weir, M.; Zhang, M.M.; Lillig, D.B.; Barbas, S.T.; Macia, M.L.; Biery, N.E. Strain-Based Pipelines: Design Consideration Overview. In Proceedings of the Eighteenth International Offshore and Polar Engineering Conference, Vancouver, BC, USA, 6–11 July 2008; International Society of Offshore and Polar Engineers: Vancouver, BC, USA, 2008.

[2] Canadian Standards Association Oil and Gas Pipeline Systems; CSA-Z662-2007; CSA Group: Mississauga, ON, Canada, 2007.

[3] API 1111 Design, Construction, Operation, and Maintenance of Offshore Hydrocarbon Pipelines; American Petroleum Institute (API): Washington, DC, USA, 1999.

[4] Det Norske Veritas. Submarine Pipeline Systems—DNV-OS-F101; DNV: Oslo, Norway, 2010.

[5] Macia, M.L.; Kibey, S.A.; Arslan, H.; Bardi, F.; Ford, S.J.; Kan, W.C.; Cook, M.F.; Newbury, B. Approaches to Qualify Strain-Based Design Pipelines. In Proceedings of the 2010 8th

International Pipeline Conference, Calgary, AB, Canada, 27 September–1 October 2010; Volume 4, pp. 365–374.

[6] Liu, B.; Liu, X.J.; Zhang, H. Strain-based design criteria of pipelines. J. Loss Prev. Process Ind. 2009, 22, 884–888.

[7] Agbo, S., Lin, M., Ameli, I., Imanpour, A., Duan, D., Cheng, J. J., Adeeb, S., (2019) "Experimental Evaluation of the Effect of Internal Pressure and Flaw Size on the Tensile Strain Capacity of Welded X42 Vintage Pipelines", International Journal of Pressure Vessels and Piping (2019), under review.

[8] Wang Y.Y., Rudland D., Denys R., Horsley D. (2002), "A Preliminary Strain Based Design Criterion for Pipeline Girth Welds," Proceedings of 4th International Pipeline Conference, Calgary, IPC2002-27169

[9] Wang, Y. Y., Cheng, W., McLamb, M., Horsley, D., Zhou, J., Glover, A. G., (2004), "Tensile strain limits of girth welds with surface-breaking defects - Part 1: An analytical framework" Proceedings of the 4th International Conference on Pipeline Technology, 235-249, Ostend, Belgium.

[10] Wang, Y. Y., Cheng, W., McLamb, M., Horsley, D., Zhou, J., Glover, A. G.,(2004), "Tensile Strain Limits of Girth Welds with Surface-Breaking Defects Part II – Experimental Correlation and Validation", Proceedings of the 4th International Conference on Pipeline Technology, 251-266 Ostend, Belgium.

[11] CSA Z662 (2011, 2015). Oil and gas pipeline systems. Canadian Standards Association (CSA).

[12] Oh CS, Kima, NH, Kim YJ. A finite element ductile failure simulation method using a stress-modified fracture strain model. Eng Fracture Mech 2011; 78:124–37.

[13] Zhang BJ, Yi C, Liang B, Zhang Z, Zhi Y. Ductile failure analysis and crack behaviour of X65 buried pipes using the extended finite element method.

[14] Ameli, I., Asgarian, B., Lin, M., Agbo, S., Imanpour, A., Duan, D., Cheng, J. J., Adeeb, S., (2018) "Determination of CMOD-force Curves and R-curves in Side-grooved Single Edge

Notched Tensile (SENT) Specimens in Welded X42 Pipeline Steel", International Journal of Pressure Vessels and Piping (2018), 10.1016/j.ijpvp.2018.04.003.

[15] ABAQUS CAE 6.14-2 / Documentation.

[16] E.E. Gdoutos (1993) Fracture Mechanics - An Introduction, Kluwer Academic Publishers, Dordrecht, Boston, London.

[17] Yong-Yi W, Ming L, and Yaxin S., 2011, "Second Generation Models for Strain-Based Design." PRCI Final Approved Report, 2011.

6. DEVELOPMENT OF A TENSILE STRAIN CAPACITY PREDICTIVE MODEL FOR API 5L X42 WELDED VINTAGE PIPELINES

This chapter is derived from a research article submitted for publication in the ASME Pressure Vessel Technology Journal

6.1 Abstract

Pipelines can be exposed to a wide variety of loads, depending on the environments and the area of application. These loads may impose large longitudinal plastic strain on pipelines, which could constitute a significant threat to the structural capacity of the pipeline. Reliable calibration of the strain capacity of pipelines plays an important role in the strain-based design (SBD) method.

In this paper, a tensile strain capacity (TSC) predictive model (an equation) for welded X42 vintage pipes has been developed by conducting nonlinear parametric analysis followed by nonlinear regression analysis. Firstly, our previously validated XFEM model was used to demonstrate the applicability of the extended finite element method (XFEM) in simulating full-scale ductile fracture response of pipelines subjected to biaxial loading, using pressurized API 5L X42 vintage pipes subjected to four-point bending. Secondly, a parametric study investigating the effects of pipe and defect geometries, as well as loading on the pipe TSC, is presented. The nonlinear parameterization using XFEM was conducted in Abaqus/Standard. The TSC trends obtained for the various parameters considered were examined to derive appropriate individual variable functions for each parameter while taking any significant interactions between the parameters into consideration. Also, a nonlinear regression analysis is employed to develop a nonlinear semi-empirical model for predicting the TSC. The results obtained from the developed TSC predictive model ($TSC_{vin.}$) was compared with those evaluated using the validated XFEM models. The results showed good agreement. Finally, a conservative factor is proposed to account for the difference between semi-empirical model predictions and XFEM model results in addition to the non-conservative global failure TSC definition adopted in the full-scale tests and XFEM models. This safety factor is useful in practical applications because it provides a quantifiable degree of conservatism and reliability to the predicted TSCs.

Keywords: tensile strain capacity; X42 vintage pipelines; parametric analysis; predictive model; ductile fracture; conservative factor

Nomenclature

API	American Petroleum Institute
BM	Base metal
CMOD	Crack mouth opening displacement
XFEM	Extended finite element method
FEA	Finite element analysis
GC	Fracture energy
HAZ	Heat affected zone
OD	Outer diameter
M_{axpe}	Maximum principal strain
M_{axps}	Maximum principal stress
CL	Confidence limit
CDF	Cumulative distribution function
NPS	Nominal pipe size
CF	Conservative factor
PGD	Permanent ground deformations
P_f	Pressure factor
SENT	Single-edge notch tension
SMYS	Specified minimum yield strength
SBD	Strain-based design
TSC	Tensile strain capacity
TSC_{vin}	Tensile strain capacity for X42 vintage pipes
WM	Weld metal

6.2 Introduction

Pipelines can be exposed to a wide variety of environmental loads, such as slope movement, landslide, fault movements, and seismic activities. Such loads may subject pipelines to permanent ground displacements (PGDs). The displacements, if become large, can impose significant

longitudinal plastic strains on pipelines, which may cause a loss of containment failure [1]. Welded pipelines that contain defects (e.g. cracks) may stimulate crack growth capable of causing leakage or even collapse under large plastic strains. The ability to resist such longitudinal tensile strains is often determined by the longitudinal tensile strain capacity (TSC), which is defined as the amount of longitudinal strain that can be sustained before leakage occurs [1].

The common aspect of most of these PGD events is the application of deformations to pipelines rather than forces, which requires a more advanced design methodology based on the strain. This design methodology is referred to as the strain-based design (SBD) method and is commonly used by engineers in the pipeline industry and has been adopted by the current design guidelines [2]. The key objective of SBD is to maintain the safety of pipeline service and improve its integrity under high longitudinal plastic strains (i.e. > 0.5%) [3].

According to an American Petroleum Institute (API) report in 2001, about 44% of in-service pipelines in the US and Canada were constructed before 1960, while the construction of 22% of the pipelines in service begun in the 1950s [4], these pipelines were made from vintage hot-rolled and normalized steels herein known as vintage pipelines [5]. The majority of past research studies focused more on modern control-rolled microalloyed steel pipelines otherwise called modern pipelines, such as X60 and higher grades [6]. Currently, there is no robust model that can predict the TSC of lower grade vintage pipelines, such as X42 vintage pipes. The current predictive models for high-grade pipelines comprise the models developed by ExxonMobil (EM) and Pipeline Research Council International (PRCI). The former TSC predictive model is only applicable to welded pipelines ranging from X60 to X100 [7], using a wide range of full-scale experimental and numerical test results; similarly, the latter model was developed for predicting the TSC of welded pipelines made of steel grades spanning from X56 to X100. A multidisciplinary approach including fundamental fracture mechanics, small-scale material characterization and full-scale pipe tests were used to obtain the PRCI model [3]. None of these TSC predictive models applies to the vintage pipelines [6]. Given the extensive use of such low-grade pipelines in the US, Canada and across the global oil and gas communities, the development of a criterion namely, the TSC model to evaluate the capacity of such pipelines in design is urgently needed.

Abdulhameed et al. [8] and Agbo et al. [6] conducted full-scale tests on eight pressurized welded X52 vintage pipes subjected to eccentric tension, and on eight pressurized welded X42 vintage pipes subjected to four-point bending respectively at the University of Alberta to characterize the

effect of internal pressure and flaw size on their TSCs. It was shown that the flaw depth significantly influenced the TSC; additionally, the flaw length was found to have a stronger influence than the internal pressure whose influence was more noticeable in shallower and shorter flaws. The results of this study confirmed that the effect of internal pressure is insignificant on the crack mouth opening displacement (CMOD). Both studies confirmed that the available predictive models are not capable of predicting the TSC of the tested pipelines.

This paper presents a new predictive model developed using numerical simulations to estimate the tensile strain capacity of X42 vintage pipelines. A brief overview of the full-scale test program used in validating the numerical models of this study is first presented [6] followed by the development of the three-dimensional (3D) extended finite element method (XFEM) model used to conduct a parametric study [9]. The parametric study was performed to evaluate the effects of influential parameters on the TSC behaviour of the X42 vintage pipes, including the pipe geometry, defect dimension and internal pressure level. Nonlinear regression analysis was finally conducted on the TSC data obtained from the parametric study to develop a nonlinear semi-empirical predictive model.

6.3 Methods

The XFEM in Abaqus/Standard [8] was used in this study to simulate the ductile fracture response observed in full-scale pipe tests, where the pipe specimens were subjected to biaxial loading. A nonlinear parametric study investigating the effects of pipe and defect geometries, as well as loading conditions on the TSC of X42 vintage pipes, was carried out. Afterward, a nonlinear regression analysis was conducted to develop a nonlinear semi-empirical model (an equation) for predicting the TSC of X42 welded vintage pipes as a function of the various flaw and pipes diameters. Finally, a safety factor was proposed based on a statistical analysis of the TSC data obtained from the parametric study to improve the reliability of the predicted TSC.

6.3.1 Experimental data

This section summarizes the full-scale experimental program that was used to develop the XFEM model [6]. A schematic of the four-point bending test setup is shown in Figure 6-1. The eight test specimens were all NPS 22 girth welded pipes (X42 pipeline steel) with an outer diameter (OD) = 558.8 mm and wall thickness, t of approximately 12.7 mm. Outer surface flawed pipes were tested under four-point bending with varying levels of internal pressure. Table 6-1 gives the flaw geometry, including the flaw depth (a) and the circumferential length ($2C$) as well as applied internal pressure (Pi). As shown, the influence of two normalized flaw depths, 0.25 and 0.5, two normalized flaw lengths, 5 and 10 and two levels of internal pressure (Pi), 4 MPa (30% SMYS) and 10.5 MPa (80% SMYS) were experimentally examined. Further details regarding the specimen properties, defect geometries, test procedures and results can be found in [6].

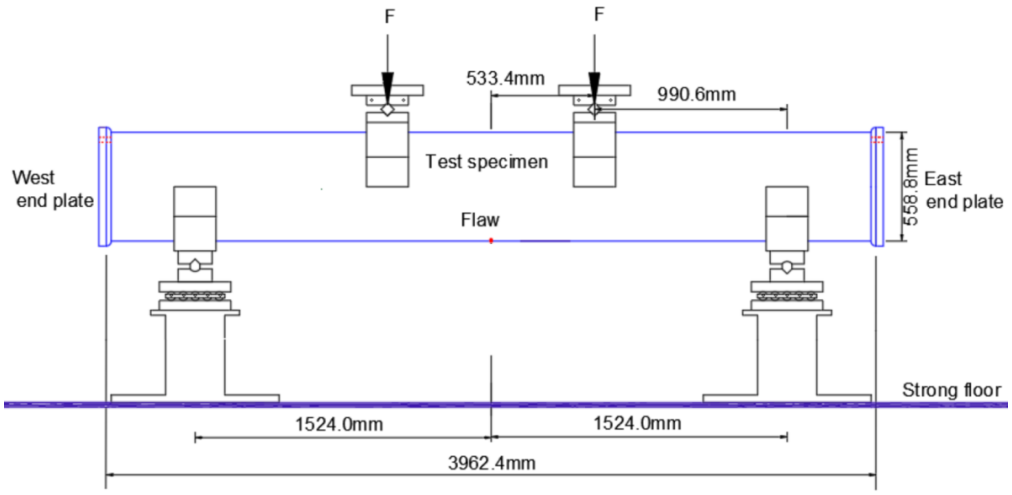

Figure 6-1 Schematic of a four-point bending test set up [9]

Table 6-1 Experimental testing parameters

Test / Model	*Pi* (MPa)	*a*/*t*	*2C/t*
1	10.5	0.25	5
2	4	0.25	5
3	10.5	0.50	5
4	4	0.50	5
5	10.5	0.25	10
6	4	0.26	10
7	10.5	0.51	10
8	4	0.51	10

6.4 XFEM Model development

The major techniques applied in the development of the XFEM numerical models simulating the full-scale tests are presented in this section. A preliminary study was performed to evaluate the TSC of X42 pipe specimens using 3D XFEM models of the X42 pipes in the ABAQUS/CAE program [10] based on the parameters presented in Table 6-1. The XFEM model of the pipe, discretization type and major boundary conditions applied are shown in Figure 6-2. An initial circumferentially oriented flaw (crack) located at the OD side was inserted into the mid-length of the tension side of the pipe specimen shown in Figure 6-2. The loading was applied in three steps: the pipe specimen was first pressurized, followed by a contact made with both the loading and support cradles to ensure stable numerical convergence in the XFEM model analysis and finally, a monotonically increasing displacement applied to the loading cradles using the displacement-controlled loading mode in order to impose a four-point bending loading condition. The boundary conditions given on the XFEM pipe model shown in Figure 6-2 are those applied during the bending step. The term “inactive” on the left-hand-side endplate reference point refers to a deactivated boundary condition during the bending step. The longitudinal displacement at the top-middle location of the model was restricted (uz = 0). The loading cradle was allowed translation in the y and z-directions and rotation about the x-direction while the support cradles were allowed

translation only in the z-direction and rotation about the x-direction. During the bending step, right-hand-side endplate was allowed to translate in both the y and z-directions, rotation about the x-direction was also allowed. No restriction was imposed on the left-hand-side endplate. The welded pipe is subjected to a combination of internal pressure and bending. A static general nonlinear incremental solution algorithm was adopted in the analysis with a time increment size that allows the simulated pipe failure to be achieved with acceptable computational efficiency. Additional details on the numerical model development can be found in [9].

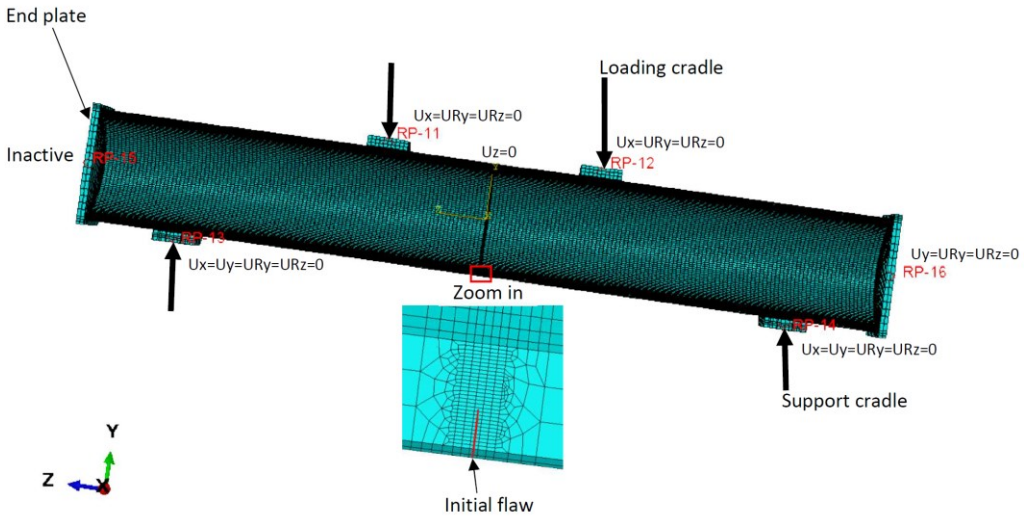

Figure 6-2 XFEM model of the pipe

The stress-strain response of the pipe material used in the XFEM model was obtained from an average value of the small-scale coupon tests conducted on the pipe material [11]. The material response for the pipe is shown in Figure 6-3. The elastic region was assumed to be linearly elastic and represented by Young's modulus, E = 200 GPa, and Poisson's ratio, ν = 0.3.

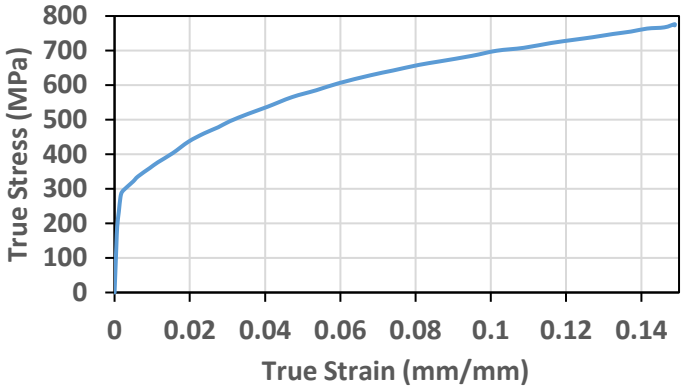

Figure 6-3 Average true stress-strain curve for X42 vintage pipe material

6.4.1 Calibration of XFEM damage parameters

The XFEM damage parameters were calibrated using a series of nonlinear numerical analyses to determine the best set that can better simulate the ductile crack initiation and growth process as obtained in the full-scale tests as described in our previous work [9] and repeated here to make this work comprehensive. The maximum principal strain, M_{axpe}, which controls the initiation of ductile crack, and fracture energy, G_C, which influences the crack growth rate, were the parameters used to define the damage in the simulation of the mechanical response and fracture behaviour of the pipe. The comparison between the results obtained from an XFEM model of test specimen 6 and the full-scale test result was used to calibrate the XFEM model. Figure 6-4 a and b show the crack mouth opening displacement (CMOD) against bending moments at the middle span and the average critical longitudinal tensile strain versus the pipe gauge length of 1 OD, respectively. The CMOD was estimated in the XFEM model by tracking the displacement of the nearest nodes on each side of the middle of the flaw throughout the loading period. The XFEM critical longitudinal tensile strain was, however, defined as the strain corresponding to the maximum applied load and extracted from 1 OD gauge length half OD away from the flaw. Reasonably accurate prediction of the fracture response and TSC was obtained using M_{axpe} = 0.013 mm/mm and G_C = 450 N/mm as the damage parameters for all the eight full-scale tests.

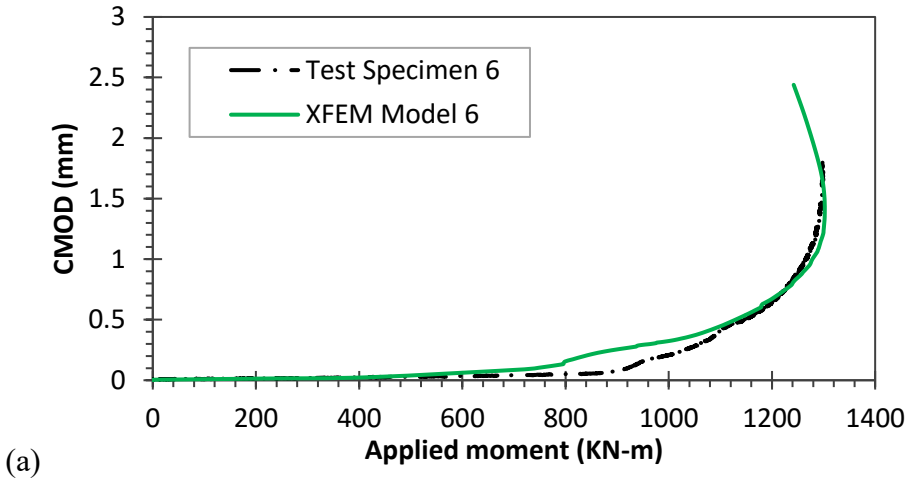

(a)

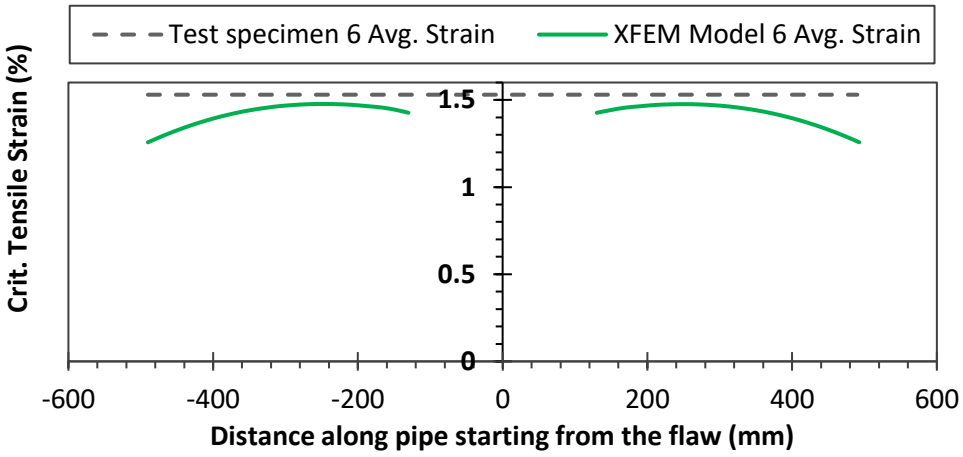

(b)

Figure 6-4 Comparison between the XFEM and full-scale experimental testing for Test Specimen 6: (a) CMOD versus moment response; and (b) Longitudinal tensile strain distribution along the pipe segment at the critical load

6.4.2 Comparison of XFEM evaluated TSC with experimentally measured TSC

This section serves as a global validation of the XFEM modelling approach, which is comparing the simulated full-scale test results with the experimental results, as was published in [9]. The comparison between the numerical simulation results and those obtained from the full-scale tests

are presented in Figure 6-5. Note that since Test 2 failed due to local buckling on the compression side of the pipe, the associated results were not included in this comparison. As shown in Figure 6-5, the data points were aligned closely along the 45° line meaning a very good agreement between the XFEM evaluated TSCs and those measured from the experimental test program, which suggests the capability of the XFEM model developed in this study to estimate the failure response of X42 vintage pipes.

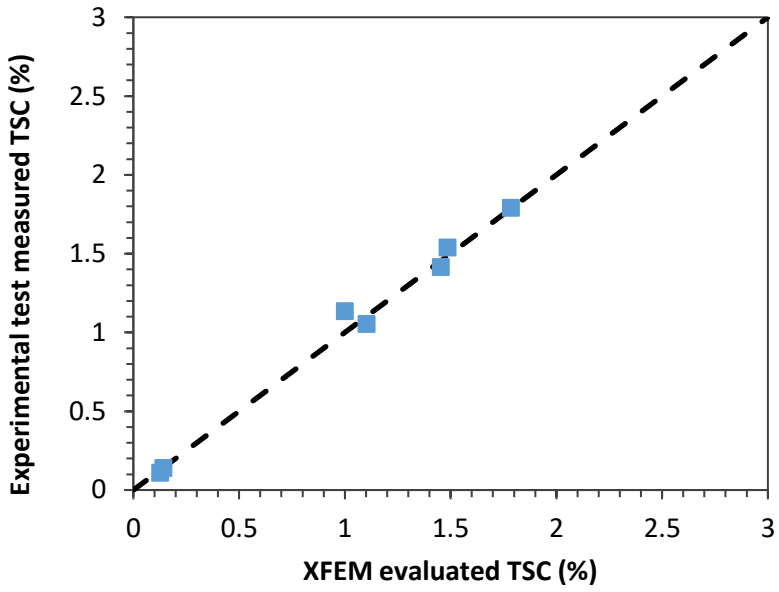

Figure 6-5 Comparison of TSCs from XFEM numerical simulations and full-scale tests

.

6.5 Parametric study

A nonlinear parametric study was performed using the validated XFEM model. Several influential parameters including pipe geometry, defect dimensions, and internal pressure levels were varied under biaxial loading to characterize the TSC of X42 pipelines and propose a predictive model capable of estimating the design capacity of the pipe while evaluating the interaction of several parameters on the TSC prediction. In the parametric study, an identical pipe grade of API 5L X42 vintage material model [12] together with a constant pipe outer diameter of 558.8 mm was

considered. Two wall thicknesses of 12.7 mm and 6.91 mm were selected. The varying parameters are shown in Table 6-2. As shown, two diameter-to-wall thickness ratios (*D/t)*, four flaw depts, four flaw lengths, and four internal pressure levels were considered to cover a wide range of practical geometry, loading and defect properties. To maintain correspondence with the non-dimensionality of the critical tensile strain, the parameters were all normalized. The same pipe length of approximately seven times the pipe diameter (= 3962.4 mm), as was the case in the experiment, was chosen to avoid boundary effects. The element size and discretization were kept identical, as described in Section 3. The parametric numerical simulations consisted of 128 numerical models. Both compressive buckling (plastic collapse) and ductile tearing instability were predicted in the simulations. It is worth noting that only the results associated with ductile tearing were used in the predictive model development.

Table 6-2 Parametric study matrix

D/t	Normalized Flaw depth (a/t)	Normalized Flaw length (*2C/t*)	Normalized Internal Pressure (P_f)
44, 81	0.25, 0.3, 0.4, 0.5	5, 6, 8, 10	0.3, 0.4, 0.6, 0.8

Note that $P_f = Pi/P_y$, where *Pi,* is the internal pressure level and P_y, is the pipe yield pressure i.e. the internal pressure equivalent to the hoop stress corresponding to the SMYS.

The parameter variations adopted in this study included those used in the full-scale test program such as short flaw length (5*t*) and shallow flaw depth (0.25*t*) combined with a lower level of internal pressure (30% SMYS). This permitted the calibration of the XFEM model against the experimental data. Furthermore, the parameter range considered was truncated at this lower bound to reduce cases of compressive buckling (plastic collapse) failure mode. The effect of the influential parameters studied here on the TSC of X42 pipes is discussed as follows.

6.5.1 Effect of the flaw depth

The effect of the normalized flaw depth, *a/t* on the TSC of X42 pipes for various internal pressure levels, P_f is demonstrated in Figure 6-6. A major TSC reduction was observed as the flaw depth

increases from 25% of the wall thickness to 50% of the wall thickness. The response is approximately linear, with some degree of nonlinearity noticed as the flaw depth decreased.

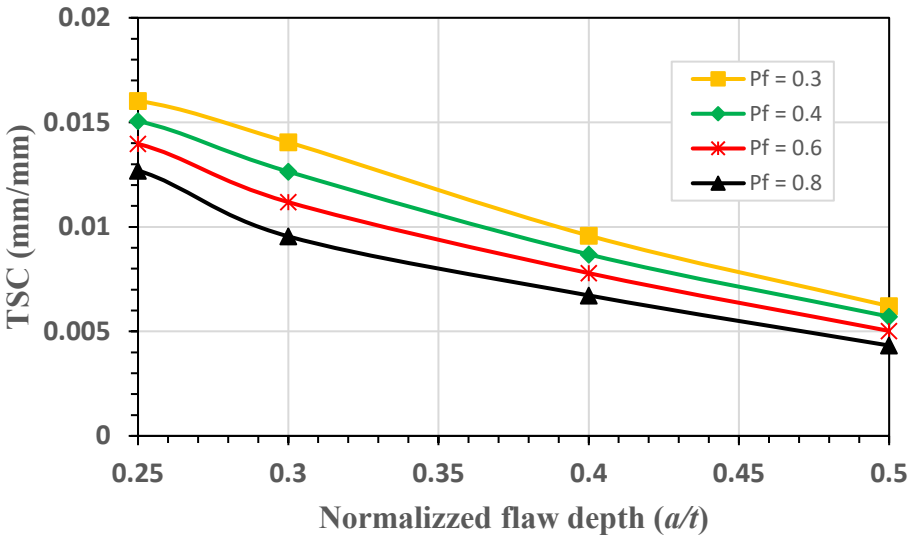

Figure 6-6 TSC vs. normalized flaw depth and internal pressure

6.5.2 Effect of the flaw length

Figure 6-7 shows the influence of the normalized flaw length, *2C/t* on the TSC of the selected pipes for various normalized flaw depths, *a/t*. When the flaw length is increased from 5 to 10 wall thicknesses, a significant reduction in the TSC is observed. A nonlinear response was observed, nonlinearity increases as both the flaw depth and length decrease.

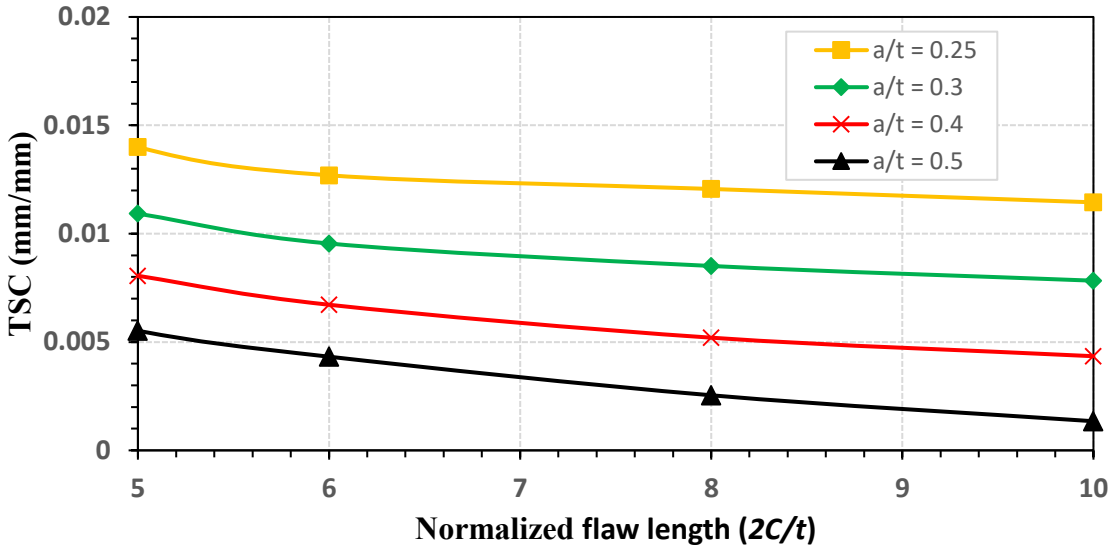

Figure 6-7 TSC vs. the normalized flaw length and flaw depth

6.5.3 Effect of the internal pressure

Internal pressure, in combination with bending, led to a biaxial loading case in the pipe, which had a significant influence on the TSC. Increasing the internal pressure level from 30% to 80% SMYS (i.e., from pressure factor, P_f of 0.3 to 0.8) for different normalized flaw lengths, $2C/t$ resulted in the gradual reduction of the TSC as shown in Figure 6-8. Additionally, the results obtained from the analyses as expected, show that the TSC reduces when the internal pressure increases, and the flaw length increases. It is important to emphasize that the internal pressure effect is more noticeable in pipes with smaller flaw sizes. For example, combining a flaw depth of $0.25t$ and flaw length of $5t$ resulted in a change of failure mode for internal pressure levels less than or equal to 30% SMYS while higher pressure levels caused pipe having the same flaw size to fail by tensile rupture.

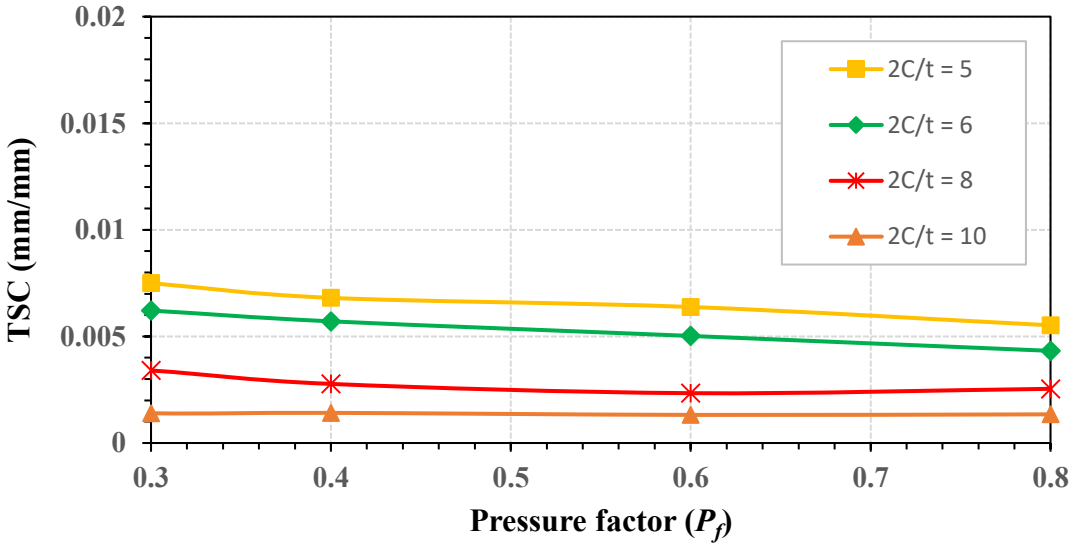

Figure 6-8 TSC vs. the pressure factor and flaw length

6.5.4 Effect of the diameter-to-wall thickness ratio

Varying the diameter-to-wall thickness ratio, D/t in combination with various internal pressure levels, P_f resulted in a minimal influence on the TSC compared to other parameters considered in this study (see Figure 6-9). Increasing D/t from 44 to 81 resulted in a slight decrease in the TSC as depicted in Figure 6-9. A similar trend was observed when varying the internal pressure.

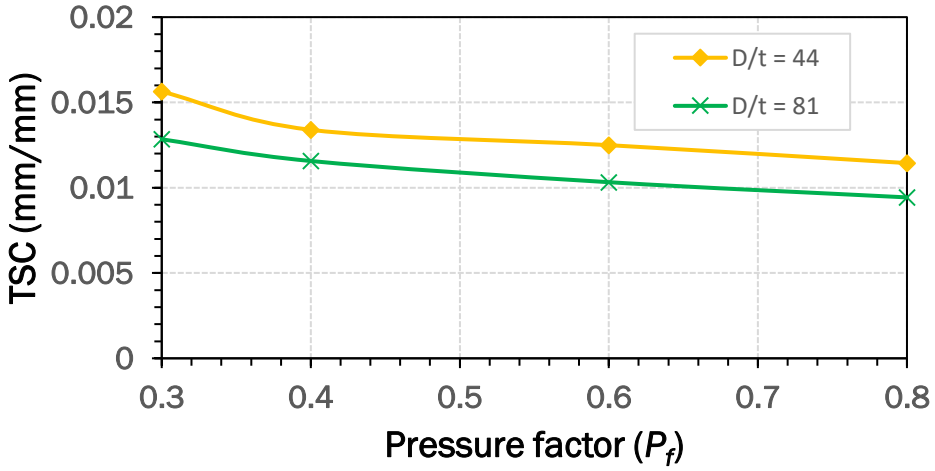

Figure 6-9 TSC vs. the pressure factor and D/t

6.5.5 Parameter range beyond which buckling governs

As mentioned earlier, the truncation of parameters such as internal pressure, flaw depth and flaw length to the lower bound (Table 6-2) was to minimize the cases of compressive buckling failure mode observed in both the full-scale test and XFEM models. This failure mode was observed as a result of the nature of external load imposed (bending) on the pipe specimen, in addition to the size of the flaw anomaly and the internal pressure level. Buckling governed when the maximum moment applied coincided with the development of buckles on the compression side of the pipe (Figure 6-10) while the crack did not propagate through the wall thickness.

The maximum longitudinal strain extracted from the tensile and compressive sides is plotted against the applied bending moment, showing a higher compressive strain compared to the remote tensile strain measured 1 OD away from the flaw (Figure 6-11).

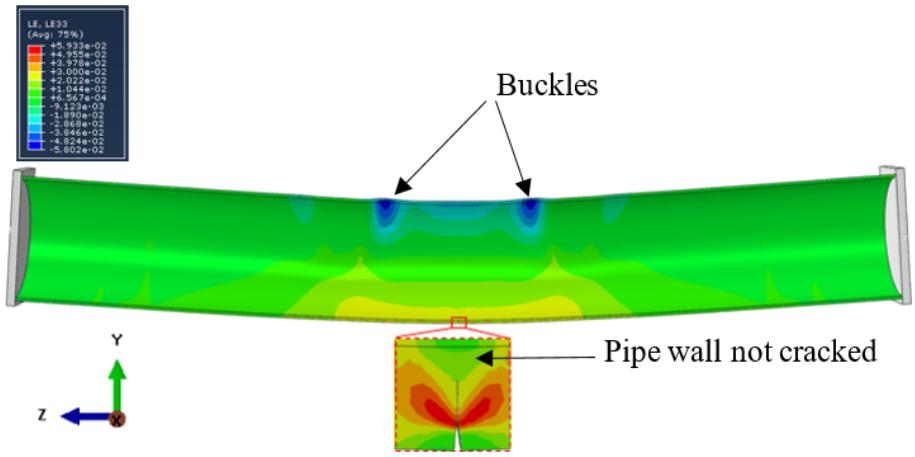

Figure 6-10 Deformed shape of the pipe showing buckles on the compression side without tensile crack cutting through the pipe wall, for pipe having a/t = 0.25, $2C/t$ = 10 subjected to Pi = 30% SMYS

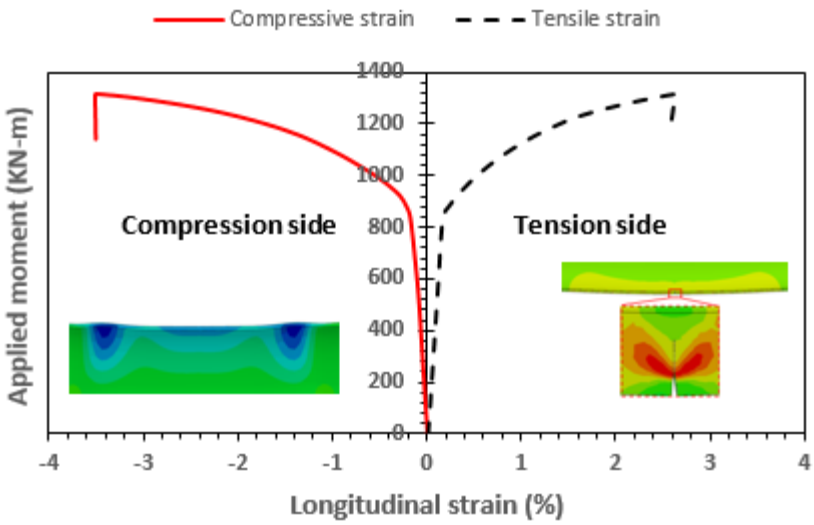

Figure 6-11 Bending moment as a function of the longitudinal tensile and compressive strain

Based on the result of the parametric study, the combination of parameters that resulted in a change of failure mode to buckling is $a/t \leq 0.25$, $2C/t \leq 5$ and $P_f \leq 0.3$. It is important to note that the following conditions need to be satisfied for a likelihood of buckling failure mode to govern; $a/t \leq 0.25$, $2C/t \leq 5$ and $P_f \leq 0.3$. It is worth mentioning that this observed change of failure mode is applicable only to X42 pipe with similar material response as used in this research, precisely assuming an equally matched weld and base; metals in the longitudinal stress versus strain response.

6.6 Proposed TSC equations

The XFEM modelling technique developed here is computationally intensive, time-consuming and requires extensive expertise. Thus, the application of the procedure becomes prohibitive for the routine engineering assessment. To provide pipeline engineers with a practical tool to evaluate the adequacy of the capacity of X42 vintage pipelines, a nonlinear semi-empirical model was developed here. Such a model can be used in practice to evaluate the TSC response and enhance the performance of X42 vintage pipes in service.

The results of the sensitivity examination of the four influential parameters (see Section 4) obtained from the XFEM simulations were used first to develop an appropriate variable function of a representative trend of the TSC with respect to each parameter, taking into account the interaction between the individual parameters. Mathematical expressions for the individual variable functions were then assigned to respective parameters, accordingly, as given in Eqs. (1 – 4):

$$f_1 = a_1 \frac{a}{t} + b_1 P_f \quad (1)$$

$$f_2 = a_2 \left(\frac{2C}{t}\right)^{\left(b_2 \frac{a}{t}\right)} \quad (2)$$

$$f_3 = d_3 \frac{2C}{t} + c_3 P_f + a_3 (P_f)^{(b_3)} \quad (3)$$

$$f_4 = a_4 (P_f)^{\left(b_4 \frac{D}{t}\right)} \quad (4)$$

where $f_1, f_2, f_3,$ and f_4 are functions of (*a/t, P_f*), (*a/t*, *2C/t*), (*2C/t, P_f*) and (*P_f*, *D/t*), respectively. a_1 to a_4, b_1 to b_4, and c_3 are the regression coefficients.

A multiplicative approach, which has proven to be effective for the formulation of semi-empirical models for pipelines [2, 13-15], was employed by multiplying the different variable functions (f_i, *I = 1, 2, 3, 4*) to form a nonlinear expression having the following basic form as given in Eq. (5):

$$TSC_{vin.} = \mathrm{F}(f_1, f_2, f_3, f_4) = \mathrm{F}\left(\frac{a}{t}, \frac{2C}{t}, P_f, \frac{D}{t}\right) \quad (5)$$

A fully implemented iterative process was required to achieve a good correlation between the proposed TSC predictive equation and the results of the XFEM parametric study. The coefficient of multiple determination (R-squared) of the data set was evaluated by repeatedly changing the functional forms of the individual variable functions. The equation with the highest possible R-square value in a considerably simplified form (i.e. closest to one and not less than 0.95) was selected [2]. A nonlinear regression analysis was then performed using the highly versatile, general-purpose computational software program, Wolfram Mathematica [16], to obtain the

predictive model and the associated regression coefficients. The final form of the equation that describes the proposed TSC predictive model is given in Eq. (6). The corresponding coefficients and the final R-squared values are presented in Table 6-3.

$$TSC_{vin} = \left(a_2\, a_4 \left(\left(\frac{2C}{t}\right)^{\left(b_2 \frac{a}{t}\right)} \right) . \left(P_f^{\left(b_4 \frac{D}{t}\right)} \right) . \left(a_1 \frac{a}{t} + b_1 P_f \right) . \left(d_3 \frac{2C}{t} + c_3 P_f + a_3 \left(P_f \right)^{\left(b_3 \right)} \right) \right) \qquad (6)$$

Table 6-3 Regression coefficients and R-squared values for the proposed predictive model's equation

Coefficients	Values
a_1	-0.03568
b_1	1.48768
a_2	0.106754
b_2	-2.23463
a_3	2.33798
b_3	-1.51737
c_3	-0.59511
d_3	0.054418
a_4	0.089697
b_4	0.004049
R^2 =	**0.977401**

Eq. (6) was used to predict the TSC values for the cases studied in Section 4. The 126 predicted TSCs were compared with the XFEM-evaluated TSCs in Figure 6-12. As shown, the majority of the data points lie closely along the 45° line, which suggests that the proposed equation can appropriately estimate the TSC of the selected cases. It should be noted that two XFEM models that failed by plastic collapse were removed from the data set before nonlinear regression analysis.

However, due to the significant scatter observed in the figure, additional statistical quantification is required to ensure the model predicts unbiased and conservative TSCs that can be adopted in design [17].

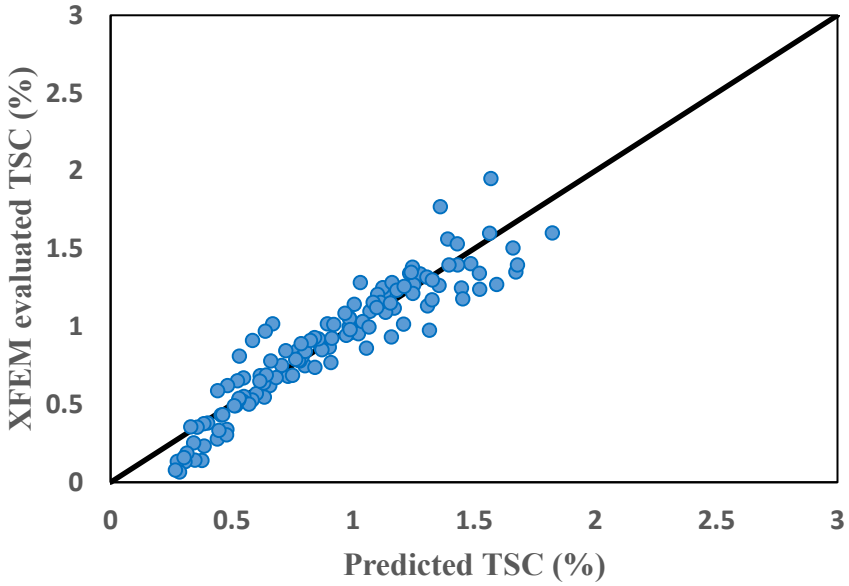

Figure 6-12 Validation of the TSC predictive model ($TSC_{vin.}$)

6.7 Statistical analysis

Model accuracy was further verified by using a probabilistic approach involving the analysis of error distribution (data scatter) around the 45° line. The error (i.e. the differences between predicted TSC and XFEM evaluated TSC) was fitted to a normal distribution shown in Figure 6-13. The mean (μ) of the normal distribution of the error is -0.01066%, with a standard deviation (σ) of 0.14197%, which is a measure of how the error spread out from the mean to the right (positive) and left (negative) directions. This indicates that the proposed predictive model can reasonably reproduce the XFEM simulation results and, by extension, the results obtained from the full-scale experimental program.

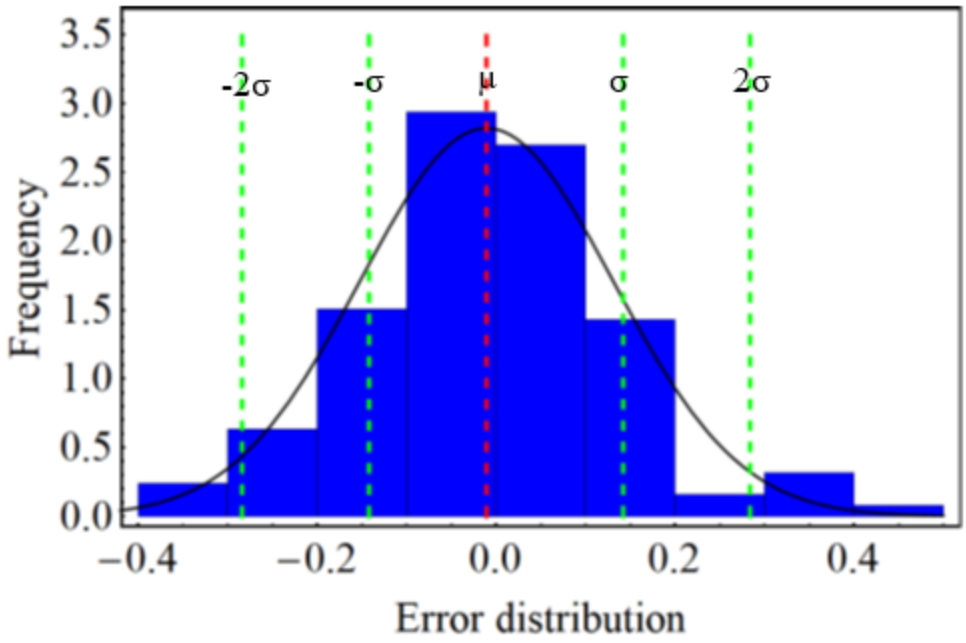

Figure 6-13 Normal distribution of error

Figure 6-13 provides a statistical quantification and visualization of the error in the TSCs predicted using the proposed model. The red dashed line represented the μ of the normal distribution, while the green dashed lines represent error of $c\sigma$ values from the mean on both sides of the mean. The coefficient c represented the number of standard deviations from the mean.

The mean of the distribution is close to zero, which is an indication of even distribution of error on both sides of the 45° line, with a slight bias to the left. A good way of controlling the bias and conservativeness of the proposed model is by adding c multiples of σ to the analytical predictive model. Adding $c\sigma$ from the left side of the error distribution to the model TSC_{vin} (Eq.7), increases the conservativeness of the model, whereas adding from the right side reduces the

conservativeness of the model.

$$\text{TSCmodif.} = \text{TSC}_{\text{vin.}} \pm c\sigma \qquad (7)$$

Applying Eq.7, using $c = 2$, resulted in the development of two error bands of 2σ on each side of the 45° line representing a quantified data spread around the accurate TSC, shown by the dashed green lines in Figure 6-14, this is useful in the modification of the predictive model.

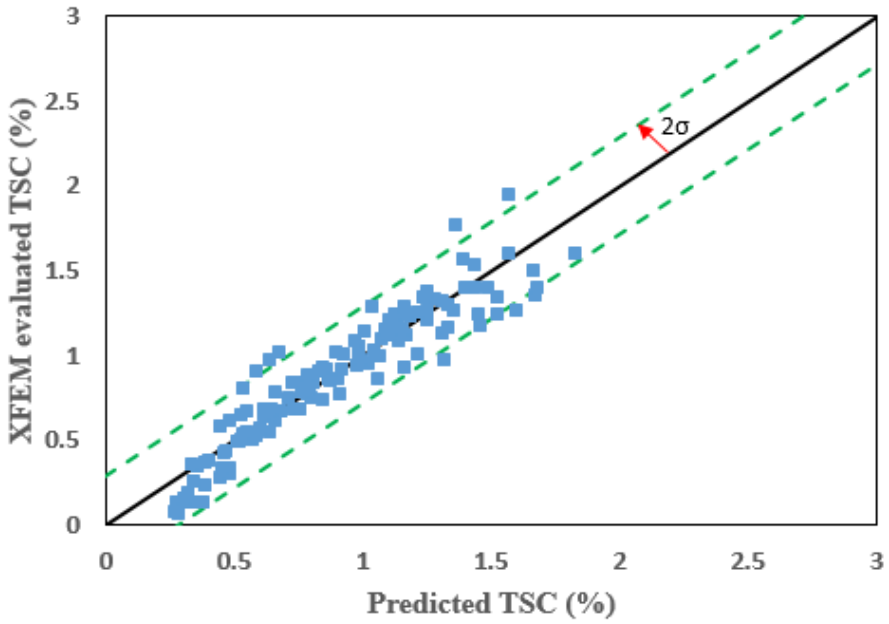

Figure 6-14 Error bands around the accurate TSC

Using Eq. 7 with c of -2, predicts conservative TSCs with 97% confidence, as shown in Figure 6-15.

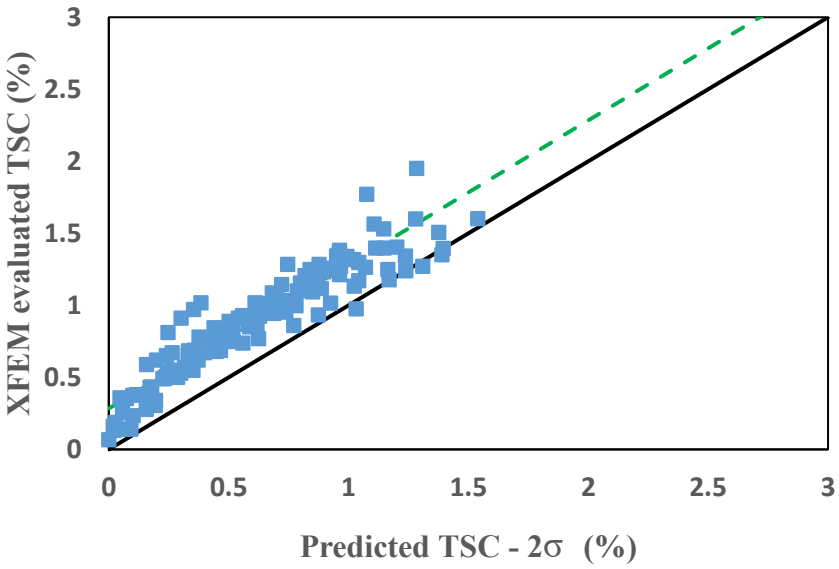

Figure 6-15 Conservative TSC prediction with 97% confidence using the modified model

The 97% upper confidence limit was measured using a cumulative distribution function (CDF) of the error distribution [17, 18].

According to the TSC results obtained from XFEM simulations, Eq. (7) is used to predict the TSC of X42 vintage pipes. The probability of predicting a conservative TSC using the model is 97%, and the probability of predicting a non-conservative TSC is only 3%. It is important to note that the decision of the *c,* to be used in Eq. 7 is to the discretion of the designer, depending on the level of conservativeness required in the design. However, c = -2 is suggested as a reasonably conservative option and will be applied in the hypothetical example implemented in this thesis.

6.8 Application of TSC predictive model

The proposed TSC predictive model provides a useful tool to facilitate the evaluation of the TSC of welded X42 vintage pipelines, which will be useful in the industry for managing such pipelines in service. In particular, the TSC equation in Eq. (6) can be used to conduct deterministic predictions when used with the proposed modification presented in Eq. (7); similarly, Eq. (6) can

also be used with Eq. (7) to generate probabilistic distributions of TSC through Monte-Carlo simulations by expressing each input variable and the modification in the form of distribution [19].

Twelve case studies given in Table 6-4 were selected to demonstrate the application of the TSC prediction using Eq. (6) and the proposed modification of the TSC presented in Eq. (7) was used in predicting the TSC of the design case studies. Weld strength was assumed to be equally matched with the base metal, and girth weld misalignment was assumed to be zero [6]. The predicted TSCs in Table 6-4 were achieved by applying Eq. (6) deterministically, while the modified TSCs were calculated using Eq. (7) deterministically as well.

Table 6-4 Design cases for twelve hypothetical SBD pipelines

Case Study	Pipe diameter	Wall thickness	Pipe material	Input Parameters				TSC	
	(inches)	(mm)		a/t	2C/t	Pf	D/t	Predicted TSC (%)	Modified TSC (%)
1	20	10.31	X42 vintage	0.3	6	0.8	49	1.02	0.73
2	20	10.31	X42 vintage	0.4	6	0.8	49	0.68	0.40
3	20	10.31	X42 vintage	0.5	6	0.8	49	0.45	0.17
4	20	10.31	X42 vintage	0.3	6	0.6	49	1.16	0.87
5	20	10.31	X42 vintage	0.4	6	0.6	49	0.77	0.49
6	20	10.31	X42 vintage	0.5	6	0.6	49	0.52	0.23
7	22	12.7	X42 vintage	0.3	6	0.8	44	1.02	0.74
8	22	12.7	X42 vintage	0.3	8	0.8	44	0.87	0.59
9	22	12.7	X42 vintage	0.3	10	0.8	44	0.78	0.49
10	30	11.91	X42 vintage	0.3	6	0.8	64	1.00	0.72
11	30	11.91	X42 vintage	0.3	8	0.8	64	0.86	0.57
12	30	11.91	X42 vintage	0.3	10	0.8	64	0.76	0.48

The modified TSCs for the selected case studies are plotted against the flaw depth and flaw length, respectively (Figure 6-16 a and b). It was shown that flaw depth has the most significant effect on the TSCs compared to the flaw length and the internal pressure levels; however, the *D/t* has the least effect on the TSC. This response agrees with those observed in both the experimental program and the XFEM parametric study.

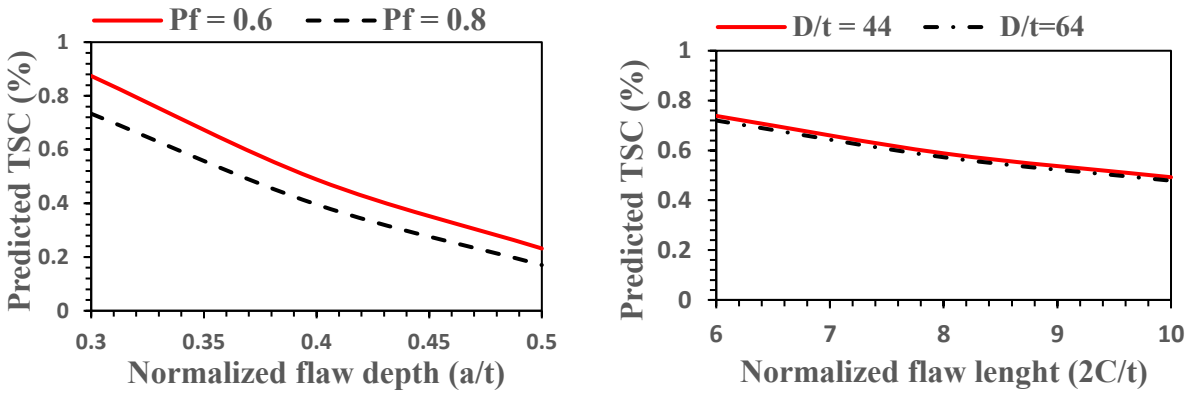

(a) Factored TSC vs. flaw depth and P_f (b) Factored TSC vs. flaw length and D/t

Figure 6-16 Trends of factored TSC due to variation of the influential parameters

6.9 Assumptions and limitations of the proposed TSC model

Assumptions made in the development of the TSC predictive model are discussed in this section.

In the XFEM simulations of the welded X42 vintage pipelines, the weld stress-strain curve is assumed to be equally matched with the base metal (BM) material stress-strain curve. The slight undermatch noticed in the weld metal (WM) stress-strain curve compared to the BM stress-strain curves shown in Figure *4-5* was ignored. It is important to mention that the material properties for the WM and heat affected zone (HAZ) are taken to be the same as BM material for the X42 vintage pipe material. Additionally, the pipes were assumed to be geometrically perfect, i.e. the outer diameter and wall thicknesses were assumed uniform throughout the pipe length. By implication, the effect of geometrical imperfection was not considered during the development of the model.

Moreover, the girth weld was assumed to be perfectly aligned with the base metals, thus the effect of weld misalignment was not considered. Also, the effect of additional flaws noticed in the girth welds of some of the full-scale test samples were not accounted for in the XFEM models used for the parametric analysis. It is important to note that the pipes were assumed to fail by mode I (opening mode) fracture.

Limitations of the model

It is prudent to limit model use to the ranges of parameters, considering some assumptions made and recognizing critical boundaries over which the model has been experimentally validated. Extrapolation beyond such limits may produce unreliable TSC predictions with non-conservative or overly conservative results. The model is pipe grade and weld specific, i.e. it should only apply to welded X42 vintage pipes with approximately equal matching pipe and weld metal material response. It should be applicable to welded X42 vintage pipes with no significant weld misalignment since the effect of weld misalignment was not investigated in the parametric study. It is important to note that applying the model to weld defect shallower or equal to 25% of wall thickness and shorter or equal to 5 times the wall thickness under internal pressure level lower or equal to 30% SMYS is likely to predict compressive buckling failure mode. It is worth clarifying that there is no established linear correlation between the yield-to-tensile ratio (Y/T) and the TSC since the effect of Y/T was not investigated in the parametric study.

The model only considered the effect of four major parameters affecting the TSC, such as; defect depth, defect length, internal pressure level, and diameter to wall thickness ratio. However, it does not capture the effect of significant variation in any parameter outside this range and should be limited to the prediction of the TSC of welded X42 vintage pipes based on the variation of the investigated parameters only.

6.10 Summary

The influence of the key factors affecting the TSC of X42 vintage pipes was first characterized using the XFEM models of pressurized surface-flawed pipes validated against the full-scale experimental tests, which confirmed the capability of the XFEM technique in simulating the ductile tearing failure mode of the pipeline. Once the XFEM model is validated, a parametric study of surface cracked pipes subjected to bending was performed. The results showed that the effect of increasing the crack depth was the most significant on TSC compared to flaw length, internal pressure, and D/t. The deformation capacity was reduced when the magnitude of internal pressure was increased. This trend increased as the flaw depth increased.

Nonlinear regression analysis was conducted to fit the TSC predictive model (semi-empirical equation) for X42 vintage pipes. Statistical analysis is conducted to ensure the model is unbiased and predicts conservative TSCs by modifying the model using probabilistic error analysis. The proposed model provides an efficient yet reliably accurate method of estimating the TSC of the X42 vintage pipeline, which can be used by engineers in their day-to-day practice.

The modified TSC model was applied to 12 hypothetical X42 pipeline cases. It was found that the flaw depth has the most significant effect on the TSC while the *D/t* has the least effect on TSC, which is identical to the observation made in both the experimental testing and XFEM numerical simulations.

6.11 Conclusions

Practical tools for the prediction of the TSC of welded pipelines are an important element of the SBD in the pipeline industry. Advancements in the computational fracture modelling technique offer engineers an increased ability to physically represent the complete ductile tearing process that is a key aspect of TSC. In turn, these new capabilities provide engineers a means to further increase their physical insight and produce practical engineering tools, both of which are critical to efficient design and managing the integrity of pipelines using a strain-based approach. The results of this study are summarized as follows:

- An XFEM model was developed using the advanced computational fracture technique to evaluate the TSC of welded X42 vintage pipes. The XFEM model was validated against eight full-scale tests.
- A novel TSC predictive model was proposed using an extensive XFEM model-based parametric simulations.
- A nonlinear regression analysis was performed to formulate the predictive model and obtain the corresponding regression coefficients.
- Statistical analysis was conducted to ensure the model is unbiased and predicts conservative TSCs by modifying the model using probabilistic error analysis to increases the confidence level of the proposed predictive model to be used as a practical tool for

reliable prediction of TSC of X42 vintage pipes needed for conducting pipeline integrity assessment.

- The proposed predictive model can appropriately estimate the TSC of X42 vintage pipes as compared with the results obtained from full-scale testing and XFEM simulations.
- The proposed TSC predictive model was used to evaluate the TSC of 12 hypothetical X42 pipeline design cases to demonstrate the applicability of the new model.

6.12 References

[1] Sandvik, A., Østby, E., Thaulow, C., "Fracture Control - Offshore Pipelines JIP. Use of Abaqus Explicit simulations of ductile tearing in pipes with defects loaded beyond yielding" Proceedings of ISOPE2008, Eighteenth International Offshore, and Polar Engineering Conference, July 6-11, Vancouver, BC, Canada, 2008. ISBN 978-1-880653-70-8 (Set); ISBN 1-880653-68-0 (Set).

[2] Ndubuaku, O. (2019). A new material characterization approach for evaluating the deformational capacity of onshore pipelines (Ph.D. Dissertation). Structural Engineering, University of Alberta, Edmonton, AB, Canada.

[3] Yong-Yi W, Ming L, and Yaxin S., 2011, "Second Generation Models for Strain-Based Design." PRCI Final Approved Report, 2011.

[4] Kiefner, J. F., and Trench, C. J., (2001) Oil Pipeline Characteristics and Risk Factor; Illustrations from the Decade of Construction" Kiefner & Associates Inc. and Allegro Energy Group for American Petroleum Institute Pipeline Committee.

[5] Wang, Y.-Y., Horsley, D and Rapp, S., (2016), "Evolution of Linepipe Manufacturing and its Implications on Weld Properties and Pipeline Service" Proceedings of the International Pipeline Conference 2016, Calgary, Alberta, Canada, September 26-30, 2016.

[6] Agbo, S., Lin, M., Ameli, I., Imanpour, A., Duan, D., Cheng, J. J., Adeeb, S., (2019) "Experimental Evaluation of the Effect of Internal Pressure and Flaw Size on the Tensile Strain Capacity of Welded X42 Vintage Pipelines", International Journal of Pressure Vessels and Piping (2019), 10.1016/j.ijpvp.2019.04.010.

[7] Tang, H., Fairchild, D. P., Noecker, F. F., Panico, M., Crapps, J., and Cheng, W., 2014, "Strain Capacity Prediction of Strain-based Pipelines," ASME Paper No. IPC2014- 33749.

[8] Abdulhameed, D., Cakiroglu, C., Lin, M., Cheng, R., Nychka, J., Sen, M., and Adeeb, S., 2016, "The effect of internal pressure on the tensile strain capacity of X52 pipelines with circumferential flaws," J. Press. Vessel Technol. 138 (2016) 61701-0-61701-18, https://doi.org/10.1115/1.4033436.

[9] Agbo, S., Lin, M., Ameli, I., Imanpour, A., Duan, D., Cheng, J. J., Adeeb, S., (2019) "Evaluation of the Effect of Internal Pressure and Flaw Size on the Tensile Strain Capacity of X42 Vintage Pipeline using Damage Plasticity Model in Extended Finite Element Method (XFEM)", Proceedings of the ASME 2019 Pressure Vessels & Piping Conference, July 14-19, 2019, San Antonio, Texas, USA PVP2019-94005.

[10] Ameli, I., Asgarian, B., Lin, M., Agbo, S., Imanpour, A., Duan, D., Cheng, J. J., Adeeb, S., (2018) "Determination of CMOD-force Curves and R-curves in Side-grooved Single Edge Notched Tensile (SENT) Specimens in Welded X42 Pipeline Steel", International Journal of Pressure Vessels and Piping (2018), 10.1016/j.ijpvp.2018.04.003.

[11] ABAQUS CAE 6.14-2 / Documentation.

[12] API Specification 5L (2012). *Specification for line pipe (45th ed.)*. Washington, DC: American Petroleum Institute (API).

[13] M. Liu, Y.-Y. Wang, F. Zhang, K. Kotian, Realistic strain capacity models for pipeline construction and maintenance. Prepared for the US Department of Transportation. Pipeline and Hazardous Materials Safety Administration, Office of Pipeline Safety. Contract No. DTPH5610-T-000016, Dublin, OH, USA, 2013.

[14] A.B. Dorey, D.W. Murray, J.J.R. Cheng, Critical Buckling Strain Equations for Energy Pipelines-A Parametric Study, J. Offshore Mech. Arct. Eng. 128 (2006) 248. doi:10.1115/1.2199561.

[15] X. Liu, H. Zhang, Y. Han, M. Xia, W. Zheng, A semi-empirical model for peak strain prediction of buried X80 steel pipelines under compression and bending at strike-slip fault crossings, J. Nat. Gas Sci. Eng. 32 (2016) 465–475. doi:10.1016/J.JNGSE.2016.04.054.

[16] Wolfram Research Inc., Mathematica, Version 11.3, Champaign, IL, 2018.

[17] Fairchild, D. P., Crapps, J. M., Cheng, W., Tang, H., and Shafrova, S., 2014, "Full-scale Pipe Strain Test Quality and Safety Factor determination for Strain-based Engineering critical Assessment," ASME Paper No. IPC2016- 64191.

[18] Liu, M., Zhou, H., Wang, B., Wang Y.-Y., 2017 “Guidelines fir Strain-Based Design and Assessment (SBDA) of Pipeline Segments” Draft report to US DOT PHMSA, US DOT Contract No. DTPH56-14-H-00003.

[19] Fairchild, D. P., Panico, M., Crapps, J. M., Cheng, W., Tang, H., and Cook, M. F., 2017, “Benchmark Examples of Tensile Strain Capacity Prediction and Strain-Based Engineering Critical Assessment Calculations ” Proceedings of the Twenty-seventh (2017) International Ocean and Polar Engineering Conference ISOPE2017, San Francisco, CA, USA, June 25-30, 2017. ISBN 978-1-880653-97-5; ISSN 1098-6189.

7. SUMMARY, SCIENTIFIC CONTRIBUTIONS, CONCLUSIONS, ASSUMPTIONS AND LIMITATIONS OF THE MODEL, AND RECOMMENDATIONS FOR FUTURE WORK

This chapter summarizes the research and findings, enumerates the scientific contributions, draw suitable conclusions on the work that has been done under the scope of this thesis, listed the assumptions made and the limitations of the model developed, and recommends further work that is necessary to complete the research.

7.1 Summary

This research was designed to study extensively the effects of flaw and pipe geometries, in addition to the effect of internal pressure on the tensile strain response of welded onshore vintage steel pipelines subjected to biaxial loading. The overall objective is to evaluate the tensile strain capacity (TSC) of welded X42 vintage pipelines and to develop a novel tool for predicting the TSC of such pipelines.

A detailed review of the literature reveals that virtually all the existing TSC predictive models are not applicable to lower grade welded vintage pipelines, such as X42 pipe grade, which is the pipe under consideration in this work.

Field observations of onshore pipelines, especially those buried in discontinuous permafrost or seismically active regions, have indicated that large ground movement can result in high longitudinal plastic strain distribution along the pipe length with more concentration around the girth weld, which can potentially lead to the violation of the pipe's integrity by causing the release of product (leakage) to the environment.

However, majority of pipelines constructed in the 50s and earlier which are still in service are more likely exposed to major threat due to; the pipe material used in the construction are mostly vintage (with relatively lower yield strength compared to modern pipelines) and are more prone to defect as a result of old welding practice used in construction. Additionally, increasing cases of pipeline failure due to ground movement has underscored the necessity of a comprehensive research program by the pipeline research group at the University of Alberta to understand the strain capacities of vintage pipelines currently in service to enhance its safe management and operability.

For the cracked pipe under the biaxial load condition, there are two possible limit states: ' tensile tearing' and 'compressive buckling (plastic collapse)'.

This research program was set with the intention to understand the strain capacity of vintage pipelines which constitute a significant percentage of in-service pipelines in Canada and the US. Focusing specifically on the tensile strain capacity of welded X42 vintage pipelines.

The first phase of this research program was focused on understanding and simulating the effect of major parameters affecting the TSC of vintage pipelines with specific emphasis on pipes of X42 steel grade by designing and conducting eight full-scale pressurized pipe tests.

Eight full-scale tests using the same pipe geometry in two different flaw depths, two different flaw lengths, and two different levels of internal pressure were undertaken in this experimental program to investigate the effect of the parameters on the pipe TSC. The result obtained from the tests were compared with those predicted using existing TSC predictive models; EM and PRCI. In two peculiar cases in the tests, the pipes failed at the linear elastic stage, these were the specimen with the deepest and longest flaw, a post-fracture investigation revealed that in each of these cases, the girth weld contained extra defect which was unaccounted for, therefore making the total flaw depth far greater than the expected; consequently, the TSC was significantly reduced causing failure at the linear elastic regime. In one instance, the pipe specimen buckled on the compression side instead of the expected local ductile tearing failure mechanism at the flaw location, this happened to the specimen with the shallowest and shortest flaw subjected to the lowest level of internal pressure, the phenomenon highlighted that the effect of internal pressure is more significant when the flaw size is small. A Comparison between the test results and those estimated using EM and PRCI predictive models suggest that both models cannot realistically predict the TSC of welded X42 vintage pipelines. As a result, the development of the TSC predictive model for vintage pipelines was recommended to address the limitations.

Additionally, the eight full-scale tests were numerically simulated using 3D ABAQUS XFEM models to study the TSC and ductile fracture failure mechanism of X42 vintage steel pipes subjected to internal pressure and bending. XFEM damage parameters required for the simulation were calibrated using; full-scale local fracture response and a global longitudinal tensile strain response of the full-scale test. The XFEM results were validated using full-scale test results. The predicted TSC using XFEM models agreed well with those obtained from full-scale tests. The internal pressure, flaw depth and flaw length were observed to be inversely correlated with the TSC. Additionally, the internal pressure was observed to have a greater influence on pipes with shallower flaw depths in combination with shorter flaw lengths, also flaw depth showed greater influence on TSC than the flaw length.

After validating the XFEM model, a nonlinear parametric study was designed and carried out to investigate extensively the effects of different parameters including pipe geometry, defect dimensions, and internal pressure on the TSC of X42 pipes under biaxial loading condition. Both compressive buckling and ductile tearing instability were predicted in the simulations, but only the results associated with ductile tearing failure were used in the predictive model development. The results showed that the effect of increasing the crack depth was the most significant on TSC compared to flaw length, internal pressure, and D/t.

As the last component of this research project, due to the computationally intensive, time-consuming and expertise demanding nature of the XFEM technique, which makes it prohibitive for routine engineering assessment, a nonlinear regression analysis was carried out using a fully implemented iterative process in a highly versatile, general-purpose computational software program, Wolfram Mathematica to develop a new predictive model and the associated regression coefficients for estimating the TSC of X42 vintage pipes. The new model predicted the TSC response of cracked X42 vintage pipes with reasonable accuracy. Therefore, it seemed rational to use this predictive model to predict TSC response of welded X42 vintage pipes using pipe geometry, internal pressure level and flaw dimensions as the basic input parameters.

Finally, a statistical analysis was conducted to ensure that the developed model predicts unbiased, more reliable and conservative TSCs of X42 vintage pipes.

7.2 Scientific Contributions

The main scientific contributions of this Ph.D. study are

- to evaluate the TSC of pressurized welded X42 vintage pipes using four-point bending approach
- to develop a new approach for simulating the ductile tearing process in pressurized pipelines subjected to bending using ABAQUS XFEM
- to develop a novel TSC predictive tool for evaluating the TSC of welded X42 vintage pipelines
- to produce full-scale experimental data that can be used in future research work.

7.3 Conclusions

Significant progress has been made in understanding the ultimate/fracture limit state, specifically the TSC of welded X42 vintage pipe subjected to biaxial loading condition and the potential pipeline safety risk associated with this failure mode. Practical tools for predicting the TSC of pipeline are crucial elements of the strain-based design approach in the pipeline industry, which are typically developed due to advancements in the computational fracture modelling technique [3]. In turn, these new capabilities provide a means to further increase the physical insight of engineers to produce practical engineering tools, which are critical to efficient design, safety and the management of pipeline integrity using a strain-based approach.

The main conclusions of this study are summarized as follows:

- TSC of welded pipelines is strongly influenced by the flaw depth, flaw length and the level of internal pressure applied. However, while the flaw depth was found to have a major effect, the flaw length had a minor effect, and the internal pressure effect was more pronounced when the flaw depth was 0.25t.
- The welded X42 vintage pipe specimens exhibited ductile tearing fracture failure mode globally, under biaxial loading. However, while few cases of relatively brittle fracture failure mode was noticed when the flaw depth was greater than 50% of the pipe wall thickness, buckling failure mode at the compressive side was observed in pipes having very shallow and short flaws, such as; $a \leq 0.25t$ and $2C \leq 5t$ respectively, subjected to a lower level of internal pressure, $Pi \leq 40\%$ SMYS.
- The estimated global strain due to curvature gave slightly lower strain values compared to the average strain obtained using the strain gauges and the DIC system. Meanwhile, the strain results obtained from strain gauges and the DIC system during full-scale tests were in a good agreement.
- The level of internal pressure could reduce the TSC of the X42 vintage pipes by 40% or more depending on the flaw size, which has a significant impact on the TSC.
- The internal pressure level globally has no significant effect on the critical CMOD for pressurized X42 vintage pipes subjected to bending.

- The TSCs obtained from the full-scale experimental study compared with predictions made using the EM and PRCI models suggest that both models cannot realistically predict the TSC of welded X42 vintage pipelines.
- XFEM model developed using ABAQUS CAE, which is accurately calibrated and validated using full-scale test results provides a veritable and reliable tool for simulating the ductile fracture response of pressurized steel pipelines under biaxial loading condition.
- Maximum principal strain M_{axpe} and fracture energy G_C are two major influential damage parameters of the XFEM technique that significantly affect the ductile fracture behaviour of pipe specimens, especially when modelling full-scale pipe response that involved geometric and material non-linear behaviour in the plastic regime.
- M_{axpe} controls the damage initiation of Mode I fracture while G_C controls crack propagation, a critical value of M_{axpe} of 0.013 mm/mm and G_C of 450 N/mm, was used in simulating the ductile tearing process in the X42 vintage pipe material.
- The evaluated TSCs using XFEM simulations of the full-scale tests agreed well with those obtained from full-scale.
- Globally, the internal pressure, flaw depth, flaw length and diameter-to-wall thickness ratio (D/t) were found to be inversely correlated with the TSC, while the flaw depth has the greatest influence, followed by the flaw length, then the internal pressure, and finally the D/t influence the TSC in that decreasing order.
- Internal pressure was observed to have a greater influence on pipes with shallow flaw depth; consequently, it influenced a change of failure mode for such pipes.
- A novel TSC predictive model, *TSCvin* was proposed using an extensive XFEM model-based parametric simulations and nonlinear regression analysis.
- Statistical analysis is conducted to ensure the model is unbiased and predicts conservative TSCs using probabilistic error analysis to increases the confidence level of the model to be used as a practical tool for reliable prediction of TSC of X42 vintage pipes.
- The proposed predictive model can appropriately estimate the TSC of X42 vintage pipes as compared with the results obtained from full-scale testing and XFEM simulations.
- The proposed TSC predictive model was used to evaluate the TSC of 12 hypothetical X42 pipeline design cases to demonstrate the applicability of the new model.

7.4 Recommendations for Future Research

This research has provided a number of significant enhancements to the objectives of the project. Based on this research program, the following recommendations can be made in order to expand the applicable range of the model and make it more robust in estimating the TSC of onshore steel pipelines:

1. Additional experimental works including full-scale pressurized and non-pressurized pipe tests in addition to an expanded SENT tests to estimate the CTODs of pipes and weld metals that include X46 and X56 vintage pipe grades to widen the full-scale test data range, which will enhance the validation of both numerical models and semi-empirical models.
2. The effect of additional parameters that affect the TSC of the welded pipeline such as high-low misalignment, weld strength overmatch, CTOD parameter (fracture toughness) and the HAZ softening, etc. should be investigated and incorporated into the predictive model to have an all-inclusive and an expanded range of application.
3. A hybrid XFEM model capable of reducing drastically the computational cost of the model while maintaining the accuracy should be developed to enhance the efficiency of the parametric analysis while investigating the effect of the enumerated parameters above.
4. This predictive model is limited to vintage pipelines. There is a need to extend the research to bridge the gap between vintage and modern pipelines and come up with a unified model capable of predicting the TSC of both vintage and modern pipelines.
5. An extended numerical program should be carried out using different loading conditions such as a combination of internal pressure and axial tension, a combination of tension and bending, and non-pressurized bending and tensile cases should be considered too.
6. Field monitoring should be planned to investigate the actual loading spectra generated from operational, environmental, and geotechnical effects on buried pipelines using instrumented sites.

7.5 Assumptions and limitations of the model

Assumptions made in the model development:

1. The girth weld and base metal material were assumed equally matching in the stress-strain response.
2. The pipes were assumed to be geometrically perfect throughout the pipe length.
3. The girth weld was assumed to be perfectly aligned with the pipe base metals.
4. The effect of additional unaccounted-for defects noticed in the girth welds of the full-scale test samples were not accounted for in the XFEM models used for parametric analysis.

Major limitations of the predictive model:

1. The model should only apply to welded X42 vintage pipes with equal matching pipe and weld metal material response.
2. It should apply to welded X42 vintage pipes with no significant weld misalignment.
3. Applying the model to pipes with small weld defect subjected to lower internal pressure level is likely to predict compressive buckling failure mode.
4. There is no proven linear correlation between the yield-to-tensile ratio and the TSC.
5. The model can only apply to pipes with significant variations in the defect depth, defect length, internal pressure level, and diameter to wall thickness ratio.

REFERENCES

A.B. Dorey, D.W. Murray, J.J.R. Cheng, Critical Buckling Strain Equations for Energy Pipelines-A Parametric Study, J. Offshore Mech. Arct. Eng. 128 (2006) 248. doi:10.1115/1.2199561.

ABAQUS 6.14, 2014, "Analysis User's Guide," Dassaultt Systems.

ABAQUS CAE 6.14-2 / Documentation.

Abdulhameed, D., Cakiroglu, C., Lin, M., Cheng, R., Nychka, J., Sen, M., and Adeeb, S., 2016, "The effect of internal pressure on the tensile strain capacity of X52 pipelines with circumferential flaws," J. Press. Vessel Technol. 138 (2016) 61701-0-61701-18, https://doi.org/10.1115/1.4033436.

Adeeb, S. (2011). Introduction to solid mechanics and finite element analysis using Mathematica. Dubuque, IA: Kendall Hunt Publishing Company.

Agbo, S., Imanpour, A., Li, Y., Kainat M., Yoosef-Ghodsi, Cheng, J. J. R, Adeeb, S., (2019) "Development of a Tensile Strain Capacity Predictive Model for API 5L X42 Welded Vintage Pipelines", ASME Pressure Vessel Technology Journal (under review).

Agbo, S., Lin, M., Ameli, I., Imanpour, A., Duan, D., Cheng, J. J., Adeeb, S., (2019) "Experimental Evaluation of the Effect of Internal Pressure and Flaw Size on the Tensile Strain Capacity of Welded X42 Vintage Pipelines", International Journal of Pressure Vessels and Piping (2019), 10.1016/j.ijpvp.2019.04.010.

Agbo, S., Lin, M., Ameli, I., Imanpour, A., Duan, D., Cheng, J. J., Adeeb, S., (2019) "Evaluation of the Effect of Internal Pressure and Flaw Size on the Tensile Strain Capacity of X42 Vintage pipeline using Damage Plasticity Model in Extended Finite Element Method (XFEM)", Proceedings of the ASME 2019 Pressure Vessels & Piping Conference, July 14-19, 2019, San Antonio, Texas, USA PVP2019-94005.

Ahmed, A. U. (2010). Failure criteria for tearing of telescoping wrinkles (Ph.D. Dissertation). Structural Engineering, University of Alberta, Edmonton, AB, Canada.

Ahmed, H., Abbas, M. I., and Shahen, M. A. K., 2013, "Girth Weld Fitness after Multiple SMAW Repairs," Pipeline and Gas Journal, 240, pp. 1-4.

Alberta Energy Regulator (2013, August). Report 2013-B: Pipeline Performance in Alberta, 1990-2012. Retrieved from: http://www.aer.ca/documents/reports/R2013-B.pdf.

Ameli, I., Asgarian, B., Lin, M., Agbo, S., Imanpour, A., Duan, D., Cheng, J. J., Adeeb, S., (2018) "Determination of CMOD-force Curves and R-curves in Side-grooved Single Edge Notched Tensile (SENT) Specimens in Welded X42 Pipeline Steel", International Journal of Pressure Vessels and Piping (2018), 10.1016/j.ijpvp.2018.04.003.

Amir R. K. (2015). Extended finite element method, theory and applications. John Wiley and Sons Ltd, United Kingdom.

Anderson, T. L. (2005). Fracture mechanics: fundamentals and applications (3rd ed). Boca Raton, FL: Taylor & Francis Group.

API 1104: Welding of Pipelines and Related Facilities.

API 1111 Design, Construction, Operation, and Maintenance of Offshore Hydrocarbon Pipelines; American Petroleum Institute (API): Washington, DC, USA, 1999.

API 579-1/ASME FFS-1 (2007). *Fitness-for-service* (2nd ed.). Washington, DC: American Petroleum Institute (API)/American Society of Mechanical Engineers (ASME).

API Specification 5L (2012). *Specification for line pipe (45th ed.)*. Washington, DC: American Petroleum Institute (API).

Arslan, H., Hamilton, J., Lele, S., Minnaar, K., Albrecht, B., Cook, M. F., and Wong, P., 2010, "Strain Demand Estimation for Pipelines in Challenging Arctic and Seismically Active Regions," International Pipeline Conference, Calgary, Alberta, Canada, paper n° IPC2010-31505.

Askeland, D. R. & Phule, P. P. (2006). The science and engineering of materials. (5th ed). Toronto, ON: Nelson.

ASTM E8/E8M-11. Standard test methods for tension testing of metallic materials. West Conshohocken, PA: American Society of Testing and Materials; 2011.

Belytschko, T and Black T. 1999. Elastic Crack Growth in Finite Elements with Minimal Remeshing. International Journal for Numerical Methods in Engineering, IJNME, 45(5): 602-620.

Bhushan, B. (2013). *Principles and applications of tribology* (2nd ed.). New York, NY: Wiley.

British Standard Institution. BS 8571: Method of test for determination of fracture toughness in metallic materials using single edge notched tension (SENT) specimens; 2014.

Cakiroglu, C., Adeeb, S., Cheng, J. J. R., and Sen, M., 2014, "Design of the Full-Scale Experiments for the Testing of the Tensile Strain Capacity of x52 Pipes with Girth Weld Flaws Under Internal Pressure and Tensile Displacement," ASME Paper No. IPC2014-33225.

Canadian Standards Association Oil and Gas Pipeline Systems; CSA-Z662-2007; CSA Group: Mississauga, ON, Canada, 2007.

Cheng, W., Gioielli, P.C., Tang, H., Minnaar, K., and Macia, M.L., 2009, "Effect of Misalignment on the Tensile Strain Capacity of Welded Pipelines", Proc. of the 5th Pipeline Technology Conf., Ostend, Belgium.

CSA Z662-11 (2011). Oil and gas pipeline systems. Canadian Standards Association (CSA).

CSA Z662 (2011, 2015). Oil and gas pipeline systems. Canadian Standards Association (CSA).

CSA Z662-11. Oil and gas pipeline systems. Sixth Edition; Update No 1; January 2012.

Czicho, H., Saito, T., & Smith, L. (Eds.) (2006). Springer handbook of materials measurement methods. German: Springer.

Davis, J. R. (Eds.) (2004). *Tensile testing* (2nd ed). Materials Park, OH: American Society for Metals (ASM International).

Det Norske Veritas. DNV-RP-F108: Recommended practice–fracture control for pipeline installation methods introducing cyclic plastic, strain; 2006.

Det Norske Veritas. Submarine Pipeline Systems—DNV-OS-F101; DNV: Oslo, Norway, 2010.

DNV, Major New Oil Discovery in the Barents Sea, via www.dnv.com accessed on: 02-02-2012.

Lillig, D. B., 2008, "The First (2007) ISOPE Strain Based Design Symposium - a Review", International Offshore and Polar Engineering Conference, Vancouver, Canada, pp. 1-12.

Drive, R. G. (2013). Steel: Production, properties, and shapes. Class lecture for Behaviour and Design of Steel Members course, University of Alberta.

E.E. Gdoutos (1993) Fracture Mechanics - An Introduction, Kluwer Academic Publishers, Dordrecht, Boston, London.

Fairchild, D. P., Crapps, J. M., Cheng, W., Tang, H., and Shafrova, S., 2014, "Full-scale Pipe Strain Test Quality and Safety Factor determination for Strain-based Engineering critical Assessment," ASME Paper No. IPC2016- 64191.

Fairchild, D. P., Kibey, S. A., Tang, H., Krishnan, V. R., Wang, X., Macia, M. L., and Cheng, W., 2012, "Continued Advancements Regarding Capacity Prediction of Strain-Based Pipelines," ASME Paper No. IPC 2012-90471.

Fairchild, D.P., Macia, M.L., Kibey, S., Wang, X., Krishnan, V.R., Bardi, F., Tang, H., Cheng, 2011, "A Multi-Tiered Procedure for Engineering Critical Assessment of Strain-Based Pipelines," Proc. of 21st Int'l Offshore and Polar Eng. Conf., Maui, Hawaii, USA, pp. 698-705.

Fairchild, D. P., Panico, M., Crapps, J. M., Cheng, W., Tang, H., and Cook, M. F., 2017, "Benchmark Examples of Tensile Strain Capacity Prediction and Strain-Based Engineering Critical Assessment Calculations " Proceedings of the Twenty-seventh (2017) International Ocean and Polar Engineering Conference ISOPE2017, San Francisco, CA, USA, June 25-30, 2017. ISBN 978-1-880653-97-5; ISSN 1098-6189.

Fyrileiv, O. and Collberg, L. (2005). Influence of pressure in pipeline design: effective axial force. In ASME 2005 24th International Conference on Offshore Mechanics and Arctic Engineering (pp. 629-636). American Society of Mechanical Engineers.

Glover, A. G., and Coote, R. I., 1984, "Full-Scale Fracture Tests of Pipeline Girth Welds," Circumferential Cracks in Pressure Vessels and Piping, Vol. II, PVP Vol. 95, G. M. Wilkowski, ed., American Society of Mechanical Engineers, New York, pp. 107–121.

Glover, A. G., Coote, R. I., and Pick, R. J., 1981, "Engineering Critical Assessment of Pipeline Girth Welds," Conference on Fitness for Purpose Validation of Welded Construction, The Welding Institute, London.

H. Gao et al., The Concepts for Pipeline Strain-Based Design. Proceedings of the Seventeenth International Offshore and Polar Engineering Conference, Lisbon, Portugal, 476-482, 2010.

Igi, S., Sakimoto, T., and Endo, S., 2011, "Effect of Internal Pressure on Tensile Strain Capacity of X80 Pipeline," Proc. Eng., 10, pp. 1451–1456.

Kailas, S.V. (n.d.). *Failure*. Class lecture for course Material Science. Indian Institute of Science, Bangalore, India. Retrieved from http://nptel.ac.in/courses/112108150/8.

Kan, W.C.; Weir, M.; Zhang, M.M.; Lillig, D.B.; Barbas, S.T.; Macia, M.L.; Biery, N.E. Strain-Based Pipelines: Design Consideration Overview. In Proceedings of the Eighteenth International

Offshore and Polar Engineering Conference, Vancouver, BC, USA, 6–11 July 2008; International Society of Offshore and Polar Engineers: Vancouver, BC, USA, 2008.

Kibey, S., Wang, X., Minnaar, K., Macia, M. L., Fairchild, D. P., Kan, W. C., Ford, S. J., and Newbury, B., 2010, "Tensile Strain Capacity Equations for Strain-Based Design of Welded Pipelines," ASME Paper No. IPC2010-31661.

Kiefner, J. F., and Trench, C. J., (2001) Oil Pipeline Characteristics and Risk Factor; Illustrations from the Decade of Construction" Kiefner & Associates Inc. and Allegro Energy Group for American Petroleum Institute Pipeline Committee.

Knauf, G., and Hopkins, P., 1996, "The EPRG Guidelines on the Assessment of Defects in Transmission Pipeline Girth Welds," 3R International, 35, pp. 620-624.

Kocak, M., Webster, S., Janosch, J. J., Anisworth, R. A., & Koers, R. (Eds.). (2006). FINET Fitness-for service procedure final draft MK7. European fitness for thematic service network – FITNET, Germany.

Lee, J.P. and Bohinsky, J.A. (1996). Design of buried pipeline subjected to large fault movement. In Proceedings of the 11th World Conference on Earthquake Engineering, Acapulco, Mexico (pp. 23-28).

Lee, K. Y., 2008, "Reducing Pipeline Construction Costs with Girth Weld ECA," Pipeline and Gas Journal, 235, pp. 16-17.

Leis, B., (2009) "PHMSA R&D Forum" Battelle Pipeline Development Center, Virginia, USA

Lillig, D. B., Newbury, B. D., and Altstadt, S. A., 2009, "The Second (2008) ISOPE Strain-based Design Symposium - a Review", International Offshore and Polar Engineering Conference, Osaka, Japan, pp. 1-10.

Lin, M, 2015, Characterization of Tensile and Fracture Properties of X52 Steel Pipes and Their Girth Welds, M.Sc. thesis, University of Alberta, Edmonton, AB.

Liu, B.; Liu, X.J.; Zhang, H. Strain-based design criteria of pipelines. J. Loss Prev. Process Ind. 2009, 22, 884–888.

Liu, M., Zhou, H., Wang, B., Wang Y.-Y., 2017 “Guidelines fir Strain-Based Design and Assessment (SBDA) of Pipeline Segments” Draft report to US DOT PHMSA, US DOT Contract No. DTPH56-14-H-00003.

Lower, M., 2014. (Strain based) Oak Ridge National Laboratory. ORNL/TM-2014/106 Design Methodology of Large Diameter grade X80 Line pipe, Spring field VA, USA.

M. Kuna, (2013) Finite Elements in Fracture Mechanics, Solid Mechanics and Its Applications 201, DOI: 10.1007/978-94-007-6680-8_3, Springer Science+Business Media Dordrecht.

M. Liu, Y.-Y. Wang, F. Zhang, K. Kotian, Realistic strain capacity models for pipeline construction and maintenance. Prepared for the US Department of Transportation. Pipeline and Hazardous Materials Safety Administration, Office of Pipeline Safety. Contract No. DTPH5610-T-000016, Dublin, OH, USA, 2013.

Macia, M.L.; Kibey, S.A.; Arslan, H.; Bardi, F.; Ford, S.J.; Kan, W.C.; Cook, M.F.; Newbury, B. Approaches to Qualify Strain-Based Design Pipelines. In Proceedings of the 2010 8th International Pipeline Conference, Calgary, AB, Canada, 27 September–1 October 2010; Volume 4, pp. 365–374.

Mannucci, G., Lucci, A., Spinelli, C., Baldi, A., Mascia, G., (June 2011). “Full-Scale Bend Testing of Strain Based Designed High Grade Buried Gas Pipeline” Proceedings of the Twenty-first International Offshore and Polar Engineering Conference Maui, Hawaii, USA, ISSN 1098-6189

McLamb, M., Hopkins, P., Marley, M., and Nessim, M., 2002, "A Justification for Designing and Operating Pipelines up to Stresses of 80% SMYS", International Pipeline Conference, Calgary, Alberta, Canada, paper number IPC02-27007.

Minnaar, K, Gioielli, P.C, Macia, M.L, Bardi, F, Biery, N.E and Kan, W.C. 2007. Predictive FEA Modelling of Pressurized Full-Scale Tests. International Society of Offshore and Polar Engineering, ISOPE.

Moes, N, Dolbow, J. and Belytschko, T .1999. A Finite Element Method for Crack Growth Without Remeshing. International Journal for Numerical Methods in Engineering, IJNME, 46(1): 131-150.

Nagashima, T, and Suemasu, H., 2010. XFEM Analyses of a Thin-Walled Composite Shell Structure with a Delamination. Computer and Structure, CS, 88(9-10): 549-557.

National Energy Board, (2014) Mackenzie Gas Project

Natural Resources Canada (NRCan) Energy fact book 2016-2017.

Ndubuaku, O. (2019). A new material characterization approach for evaluating the deformational capacity of onshore pipelines (Ph.D. Dissertation). Structural Engineering, University of Alberta, Edmonton, AB, Canada.

Nobahar, A., Kenny, S., Phillips, R., 2007, "Buried Pipelines Subject to Subgouge Deformations," International Journal of Geomechanics 7, pp. 206-216.

Nonn, A., and Kalwa, C., 2013. Analysis of dynamic ductile fracture propagation in pipeline steels: A damage mechanics approach. Proceedings of the 6th International Pipeline Technology Conference, Ostend, Belgium, IPC S34-01.

Nonn, A., and Kalwa, C., 2012. Simulation of ductile crack propagation in high-strength pipeline steel using damage models — proceedings of the 9thInternational Pipeline Conference, Calgary, Canada, IPC 90653.

Nyhus, B., Østby, E., Zhang, Z., Olsø, E., Røstadsand, P A., Eikrem, P A., (2009). "Large Scale Tests of Strain Capacity of pipe Sections with Circumferential Defects Subjected to Installation-induced Plastic Strain History." Proceedings of the ASME 28th International Conference on Ocean, Offshore and Arctic Engineering OMAE2009 May 31 - June 5, 2009, Honolulu, Hawaii.

Oh CS, Kima NH, Kim YJ. A finite element ductile failure simulation method using a stress-modified fracture strain model. Eng Fracture Mech 2011; 78:124–37.

Olso, E., Berg, E., Holthe, K., Nyhus, B., Skallerud, B., Thaulow, C., and Ostby, E., 2008, "Effect of Embedded Defects in Pipelines Subjected to Plastic Strains During Operation," International Offshore and Polar Engineering Conference, Vancouver, Canada, pp. 143-148.

Ostby, E., and Hellesvik, A. O., 2008, "Large-Scale Experimental Investigation of the Effect of Biaxial Loading on the Deformation Capacity of Pipes with Defects," International Journal of Pressure Vessels and Piping, 85, pp. 814-824.

Østby, E., and Hellesvik, A., 2007, "Fracture Control–Offshore Pipelines JIP Results From Large Scale Testing of the Effect of Biaxial Loading On the Strain Capacity of Pipes with Defects," 17th

International Offshore and Polar Engineering Conference (ISOPE), Lisbon, Portugal, Jul. 1–6, Vol. 4, Paper No. ISOPE-I-07-516.

Pick, R. J., Glover, A. G., and Coote, R. I., 1980, "Full-Scale Testing of Large Diameter Pipelines," Proceedings of the Pipeline Energy Plant Piping Conference, The Welding Institute of Canada, Calgary, Alberta, Canada, pp. 357–366.

Robin G., Neil G., Gregory S., Frank R., (2017), "A Comparison of Strain-Based Design ECA Models", Proceedings of the Twenty-seventh International Ocean and Polar Engineering Conference San Francisco, CA, USA, ISBN 978-1-880653-97-5.

S. T. Barbas and M. S. Weir, Strain-based Design Methodology for Seismic and Artic Regions, Proceedings of the Seventeenth International Offshore and Polar Engineering Conference, Lisbon, Portugal, July 1-6, 2007, 3073-3080, 2007.

Sandvik, A., Østby, E., Thaulow, C., "Fracture Control - Offshore Pipelines JIP. Use of Abaqus Explicit simulations of ductile tearing in pipes with defects loaded beyond yielding" Proceedings of ISOPE2008, Eighteenth International Offshore, and Polar Engineering Conference, July 6-11, Vancouver, BC, Canada, 2008. ISBN 978-1-880653-70-8 (Set); ISBN 1-880653-68-0 (Set).

Scheider, I., Nonn, A., Völling, A., Mondry, A., and Kalwa, C. 2014. A damage mechanics based evaluation of dynamic fracture resistance in gas pipelines. Procedia Materials Science. PMS. (19) 1956.

Sen M. (2006); "Behaviour of Cold Bend Pipes Under Combined Loads" Ph.D. dissertation, University of Alberta.

Sen M., Cheng J.J.R., Zhou, J. (2011): "Behaviour of Cold Bend Pipes under Bending Loads," Journal of Structural Engineering, Volume 137, Issue 5, DOI:10.1061/(ASCE)ST.1943541X.0000219.

Sen, M., Cheng, J. J. R., & Zhou, J. (2011, May). Behaviour of cold bend pipes under bending loads. Journal of Structural Engineering, 137(5), 571-578. doi:10.1061/(ASCE)ST.1943-541X.0000219.

SteelConstruction.info. Retrieved from http://www.steelconstruction.info/Welding.

Stolarska, M, Chopp, D. L, Moës, N. and Belytschko, T. 2001. Modelling Crack Growth by Level Sets in the Extended Finite Element Method. International Journal for Numerical Methods in Engineering, IJNME, 51 (8):943-960.

Sukumar, N, Chopp, D. L, Moës, N and Belytschko, T. 2001. Modelling Holes and Inclusions by Level sets in the Extended Finite Element Method, Computer Methods in Applied Mechanics and Engineering, CMAM, 190(46-47): 6183-2000.

Sukumar, N, Moes, N, Moran, N and Belytschko, T. 2000. Extended Finite Element Method for Three-Dimensional Crack Modelling. International Journal for Numerical Methods in Engineering, IJNME, 48(11): 1549- 1570.

Tang, H., Fairchild, D. P., Noecker, F. F., Panico, M., Crapps, J., and Cheng, W., 2014, "Strain Capacity Prediction of Strain-based Pipelines," ASME Paper No. IPC2014- 33749.

Verma, N., Fairchild, D. P., Noecker, F. F., Macia, M. L., and Nissley, N. E., 2014, "Advanced Strain-Based Design Pipeline Welding Technologies," ASME Paper No. IPC2014-33079.

Verstraete, M., (2013) Experimental-Numerical Evaluation of Ductile Tearing Resistance and Tensile Strain Capacity of Biaxially Loaded Pipelines (Ph.D. Dissertation). Department of Mechanical Construction and Production, Ghent University.

Verstraete, M., De Waele, W., Hertelé, S. and Denys, R., 2014, "Experimental-Numerical Evaluation of Ductile Tearing Resistance and Tensile Strain Capacity of Biaxially Loaded Pipelines," (Ph.D. Dissertation). Department of Mechanical Construction and Production, Faculty of Engineering and Architecture, Ghent University, Belgium.

Vitali, L., Torselletti, E., Marchesani, F., and Bruschi, R., 1996, "Use (and Abuse) of Strain Based Criteria in Offshore Pipeline Technology," Advances in Subsea Pipeline Engineering and Technology, Aberdeen, UK, paper number ASPECT96-135.

W. Ramberg and W. R. Osgood, "Description of stress-strain curves by three parameters," Technical Note No. 902, National Advisory Committee for Aeronautics, Washington DC., 1943.

Wang, X., Barbas, S.T., Kibey, S., Gioielli, P.C., and Minnaar, K., 2009, "Validation of Strain Capacity Prediction Method – Comparison of Full-Scale Test Results to Predictions from Tearing Analysis Based on FEA", Proc. of the 5th Pipeline Technology Conf., Ostend, Belgium.

Wang Y.Y., Cheng W. (2004),” Guidelines on Tensile Strain Limits. Gas Research Institute Report 04/0030”, Des Plaines, IL.

Wang Y.Y., Cheng W., Horsley D. (2004),” Tensile Strain Limits of Buried Defects in Pipeline Girth Welds,” Proceedings of IPC2004, International Pipeline Conference, IPC2004524

Wang Y.Y., Rudland D., Denys R., Horsley D. (2002), “A Preliminary Strain Based Design Criterion for Pipeline Girth Welds,” Proceedings of 4th International Pipeline Conference, Calgary, IPC2002-27169.

Wang, M. L., Horsley, D., and Zhou, J., 2006. A Quantitative Approach to Tensile Strain Capacity of Pipelines, ASME Paper No. IPC2006-10474.

Wang, Y. Y., Cheng, W., and Horsley, D., 2004, "Tensile Strain Limits of Buried Defects in Pipeline Girth Welds," International Pipeline Conference, Calgary, Alberta, Canada, paper no IPC04-0524.

Wang, Y. Y., Cheng, W., McLamb, M., Horsley, D., Zhou, J., Glover, A. G., (2004), “Tensile strain limits of girth welds with surface-breaking defects - Part 1: An analytical framework” Proceedings of the 4th International Conference on Pipeline Technology, 235-249, Ostend, Belgium.

Wang, Y. Y., Liu, M., Horsley, D., and Zhou, J., 2006, "A Quantitative Approach to Tensile Strain Capacity of Pipelines," International Pipeline Conference, Calgary, Alberta, Canada, paper no IPC2006-10474.

Wang, Y.-Y., Horsley, D and Rapp, S., (2016), “Evolution of Linepipe Manufacturing and its Implications on Weld Properties and Pipeline Service” Proceedings of the International Pipeline Conference 2016, Calgary, Alberta, Canada, September 26-30, 2016.

Wang, Y. Y., Cheng, W., McLamb, M., Horsley, D., Zhou, J., Glover, A. G.,(2004), “Tensile Strain Limits of Girth Welds with Surface-Breaking Defects Part II – Experimental Correlation and Validation,” Proceedings of the 4th International Conference on Pipeline Technology, 251-266 Ostend, Belgium.

Wikipedia.org/wiki/TransAlaska_Pipeline_System#/media/File:TransAlaska_Pipeline_System_Luca_Galuzzi_2005.

Wolfram Research Inc., Mathematica, Version 11.3, Champaign, IL, 2018.

X. Liu, H. Zhang, Y. Han, M. Xia, W. Zheng, A semi-empirical model for peak strain prediction of buried X80 steel pipelines under compression and bending at strike-slip fault crossings, J. Nat. Gas Sci. Eng. 32 (2016) 465–475. doi:10.1016/J.JNGSE.2016.04.054.

Yong-Yi W, Ming L, and Yaxin S., 2011, "Second Generation Models for Strain-Based Design." PRCI Final Approved Report, 2011.

Zhang BJ, Yi C, Liang B, Zhang Z, Zhi Y. Ductile failure analysis and crack behaviour of X65 buried pipes using the extended finite element method.

Zhang C, Cao, P, Cao, Y and Li, J .2013. Using Finite Element Software to Simulation Fracture Behaviour of Three-point Bending Beam with Initial Crack, Journal of Software, JS, 8(5):1145-1150.

Zhang, B, Ye, C, Liang, B, Zang, Z, and Zhi, Y. 2014. Ductile Failure Analysis and Crack behaviour of X65 Buried pipes using the Extended Finite Element Method. Engineering Failure Analysis, EFA, 45: 26-40.

Zhu, X. K., & Joyce, J. A. (2012). Review of fracture toughness (G, K, J, CTOD, CTOA) testing and standardization. Engineering Fracture Mechanics, 85, 1-46. doi:10.1016/j.engfracmech.2012.02.001.

APPENDIX: POST FRACTURE ANALYSIS OF X42 VINTAGE PIPE SPECIMENS

Post fracture analysis was conducted on the samples cut-off from all the test specimens to understand the fracture characteristics and failure mode of the X42 pipe specimens.

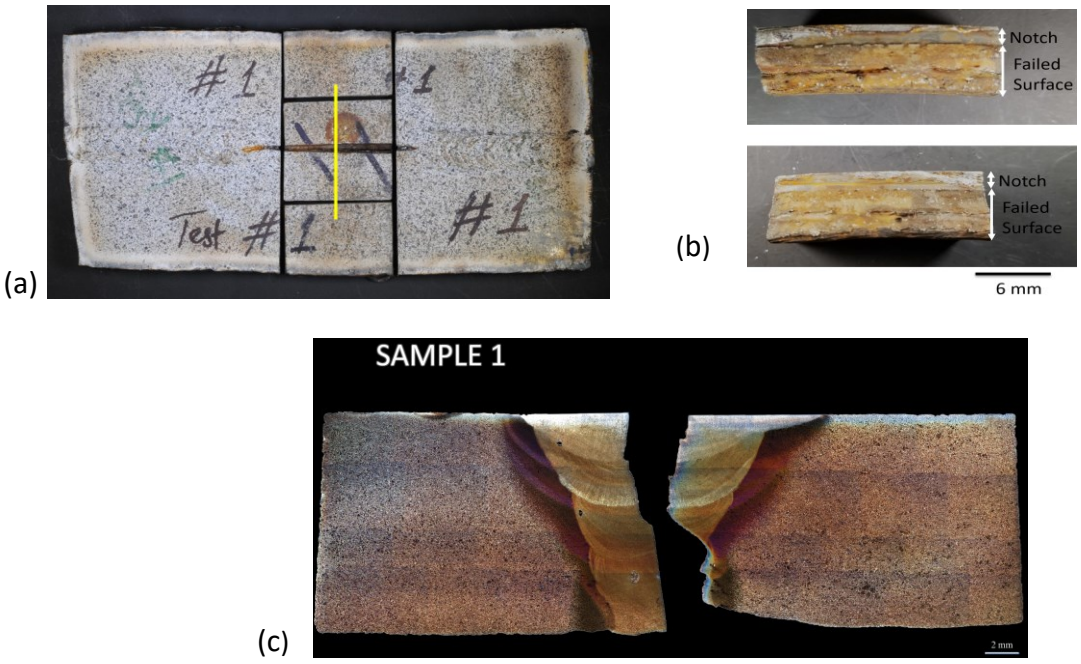

Figure 1: Sample 1 fracture analysis result (a) sectioning (b) the notch and failed surface and (c) the fracture crack path

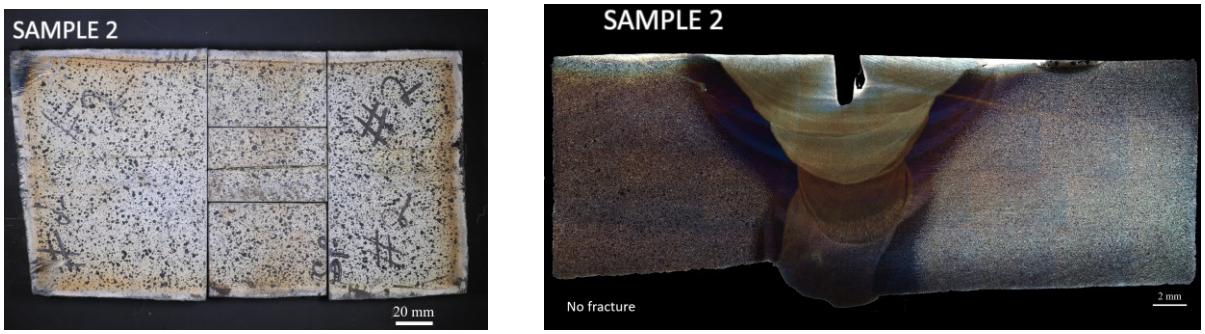

Figure 2 Sample 2 showing no fracture propagation

SAMPLE 3

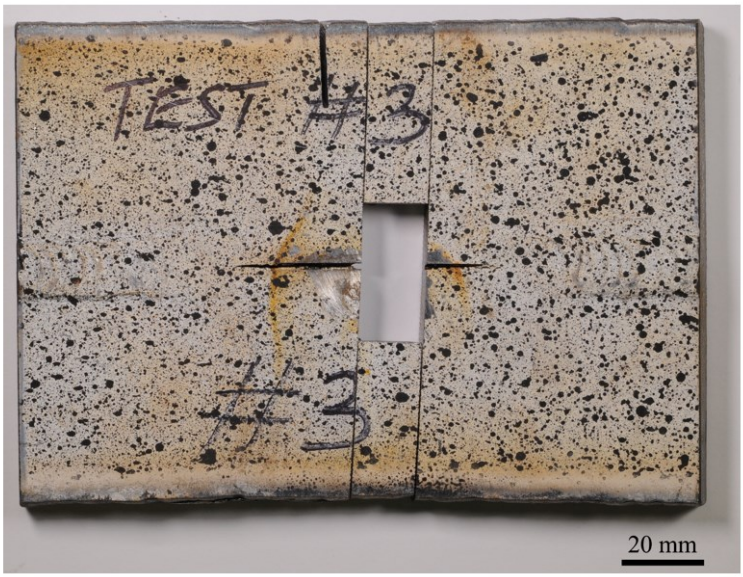

Figure 3 Photo showing sample 3 cut-off for fracture analysis.

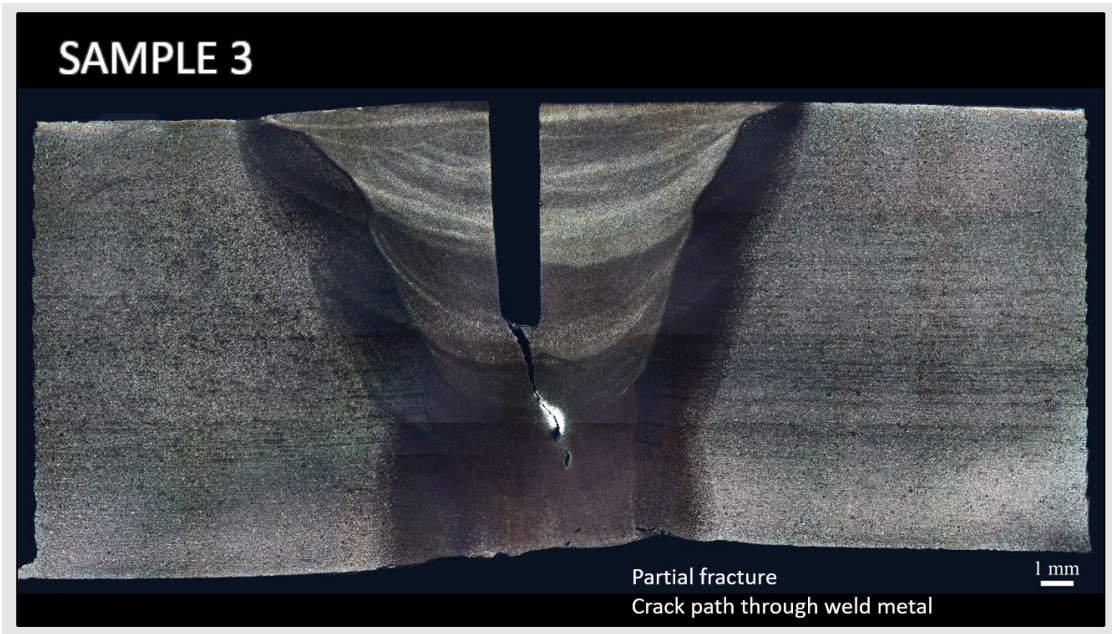

Figure 4 Photo showing the fracture analysis of sample 3, showing partial fracture crack through the weld metal.

SAMPLE 4

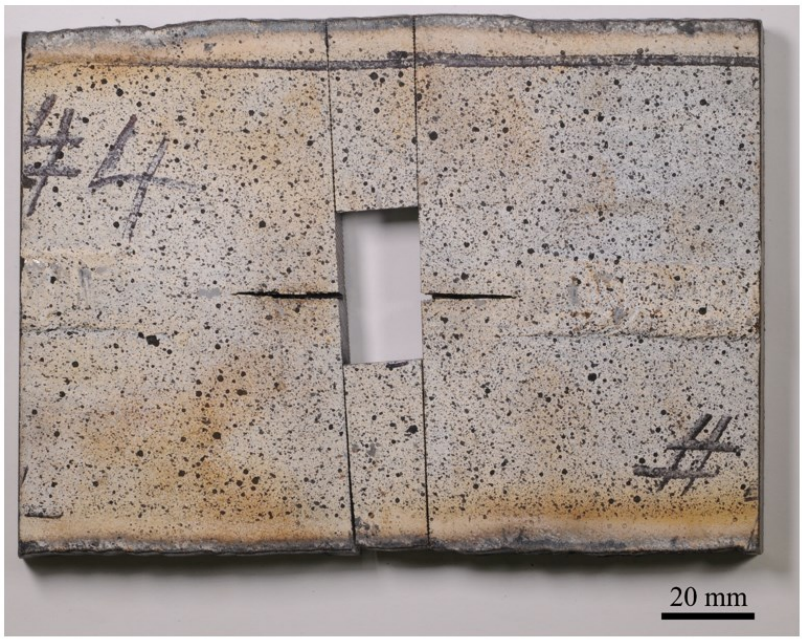

Figure 5 Photo showing sample 4 cut-off for fracture analysis.

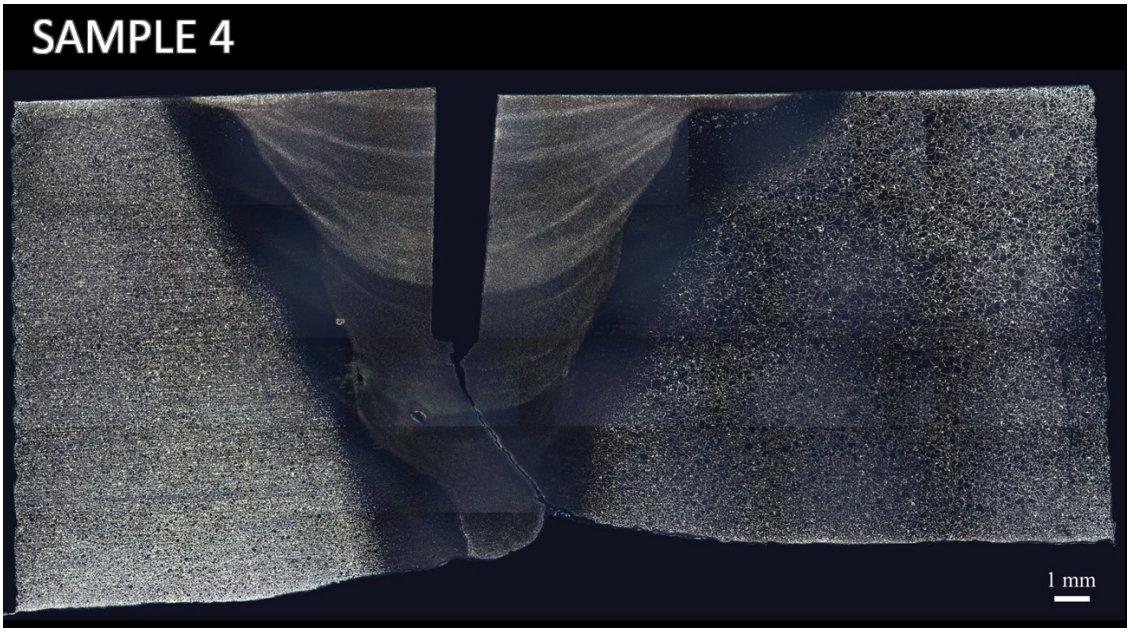

Figure 6 Photo of sample 4 showing through fracture Crack path through weld metal final fracture appears to be through HAZ.

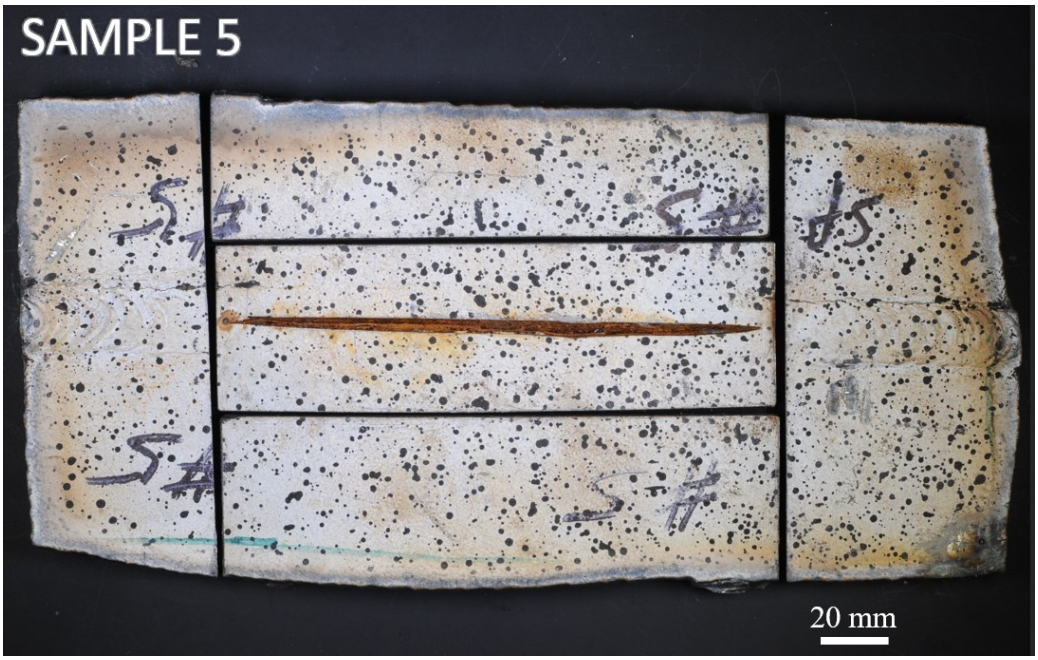

Figure 7 Photo showing sample 5 cut-off for fracture analysis.

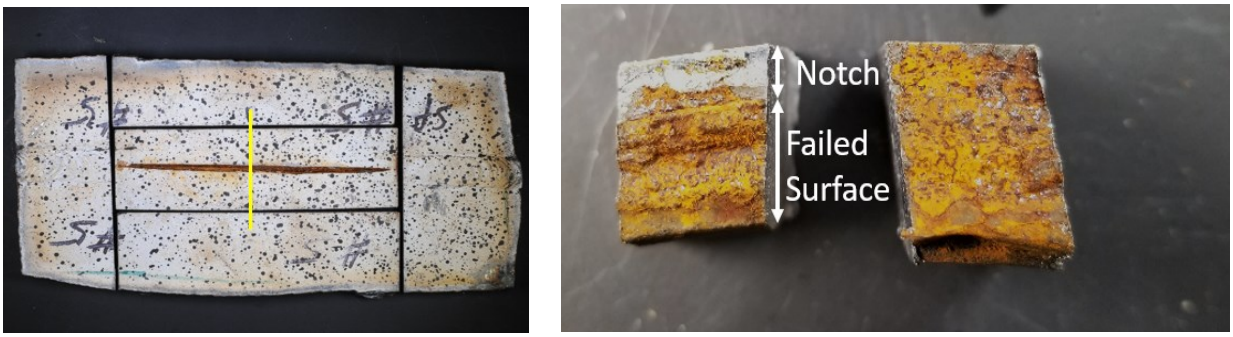

Figure 8 Photos of sample 5 showing though crack covered in corrosion products, the failed surface appears to be ductile fracture.

Due to the induced flaw from testing passing to the bottom of steel, the sectioning (yellow line) resulted in two specimens (Figure 8).

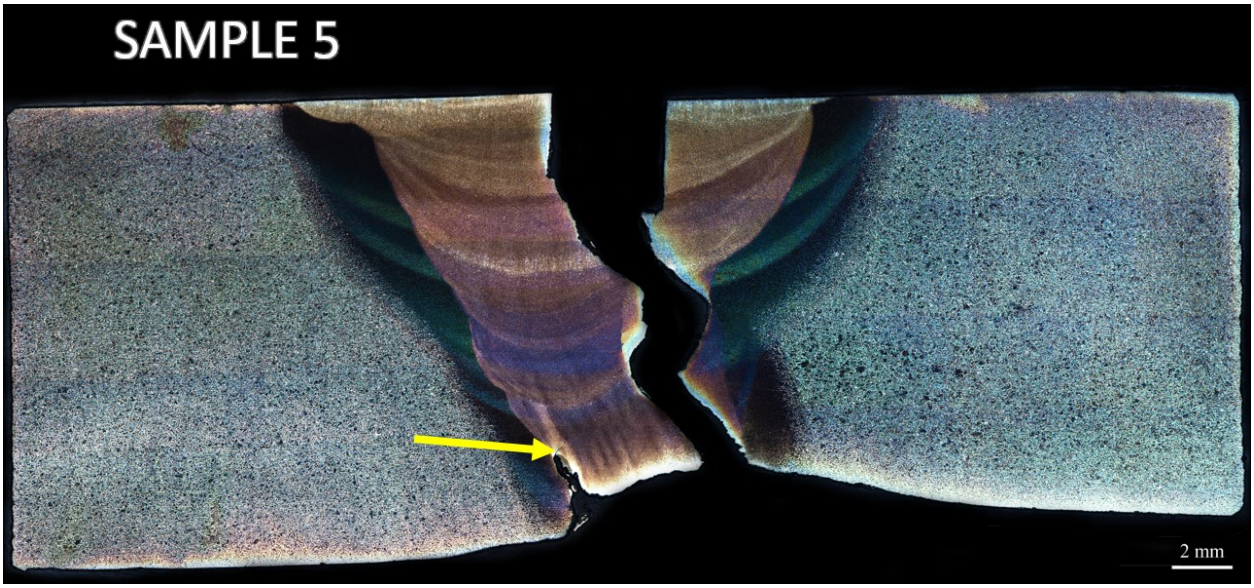

Figure 9 Photo of sample 5 showing through fracture with crack path through weld metal, with another potential crack also from root pass on the left-hand side in HAZ (yellow arrow).

The Crack path appears to deviate direction at interface of multi-pass welds

Figure 10 Photos of sample 5 showing though crack covered in corrosion products, the failed surface appears to be ductile fracture.

Due to the induced flaw from testing passing to the bottom of steel, sectioning (yellow line) resulted in two specimens, Figure 10.

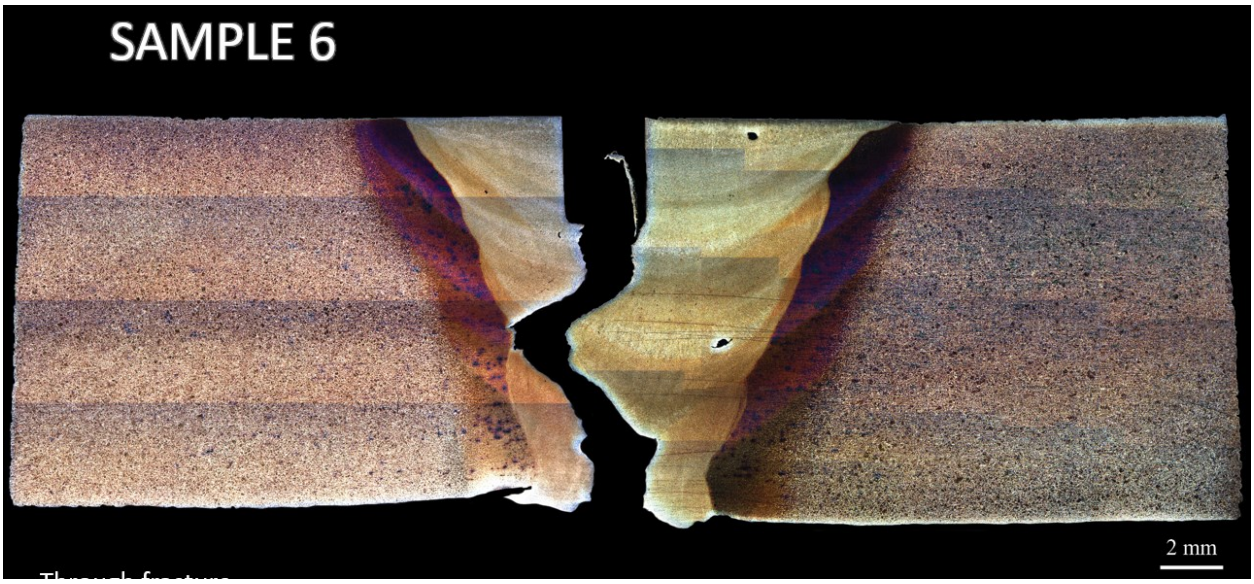

Figure 11 Photo of sample 6 microscopy showing through fracture with crack path through weld metal; crack path appears to deviate direction at the interface of multi-pass welds

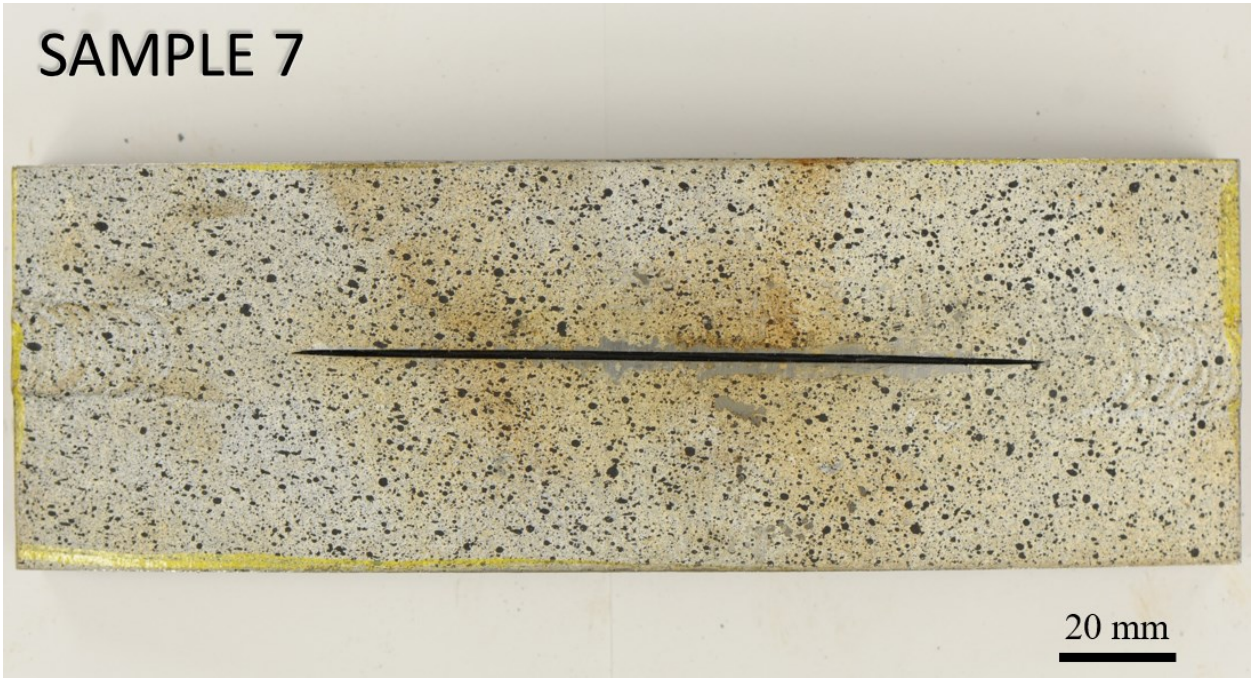

Figure 12 Photo showing sample 7 cut-off for fracture analysis.

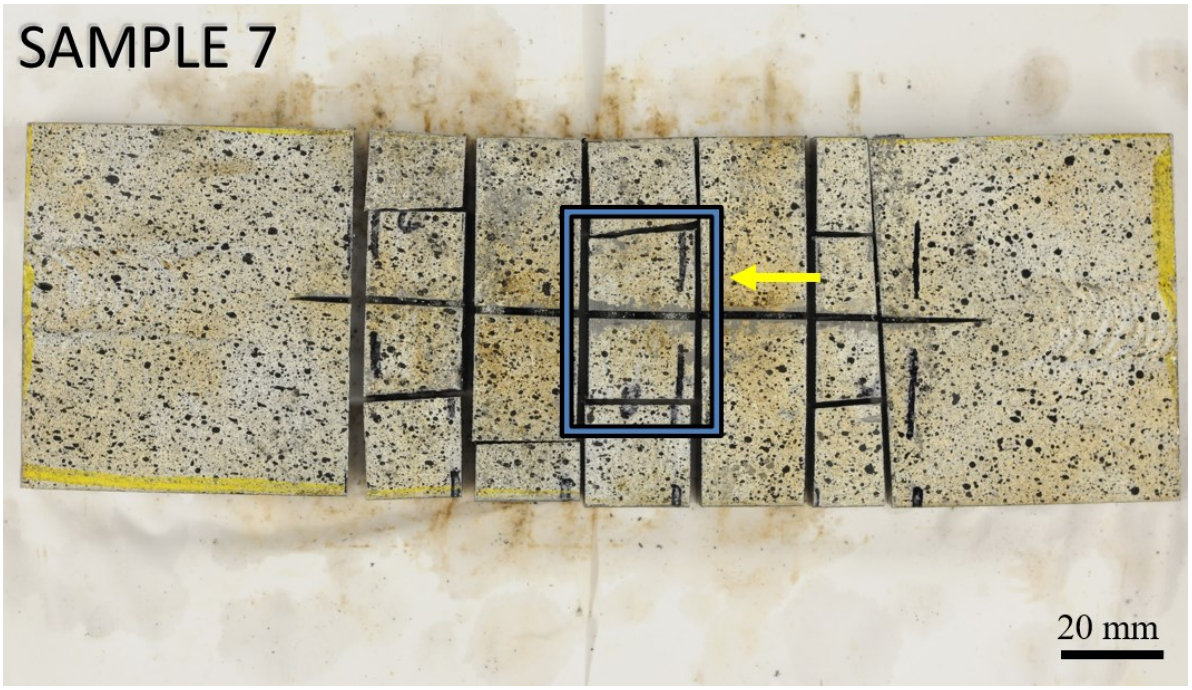

Figure 13 Sample was cut into three sections (A, B and C) from left to right, along cut, only Section B was selected for analysis at this time, the yellow arrow indicates the side polished and etched for microscopy.

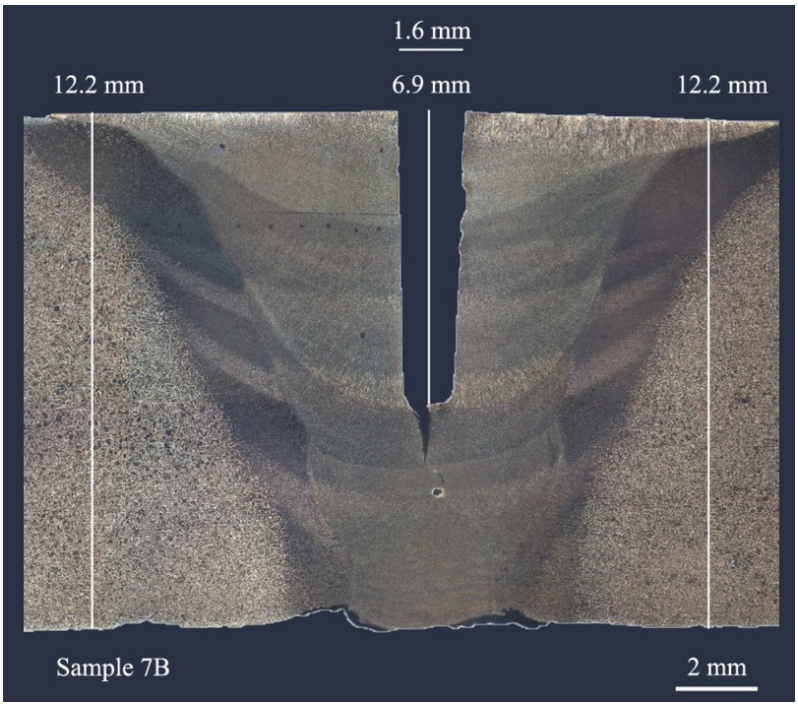

Figure 14 Partial fracture shown in the weld metal of sample 7 microscopy

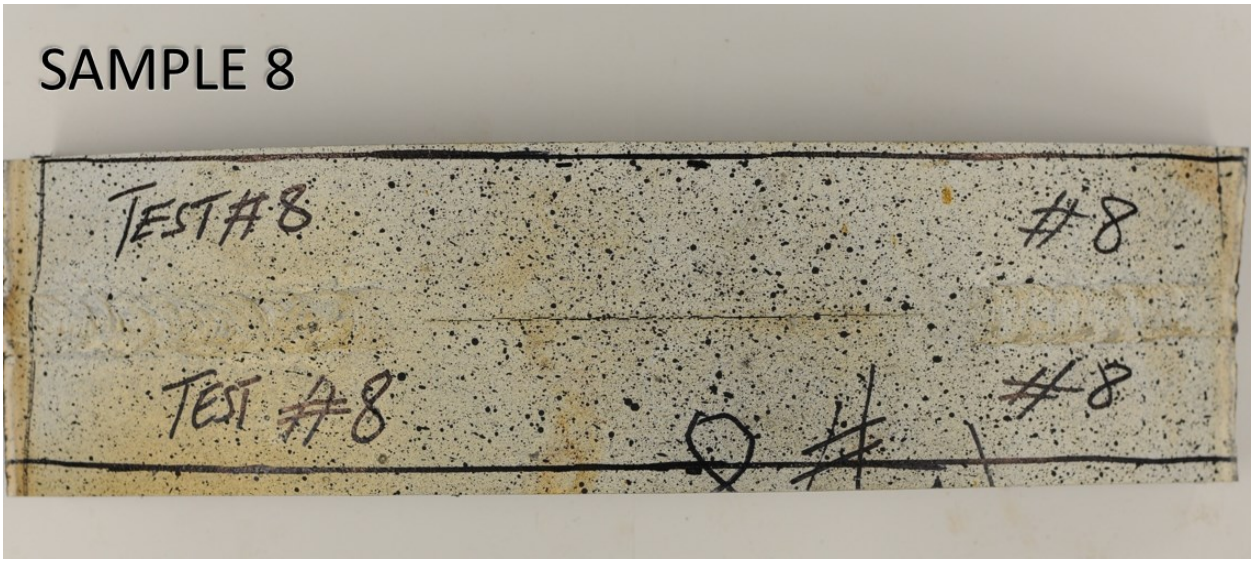

Figure 15 Photo showing sample 8 cut-off for fracture analysis.

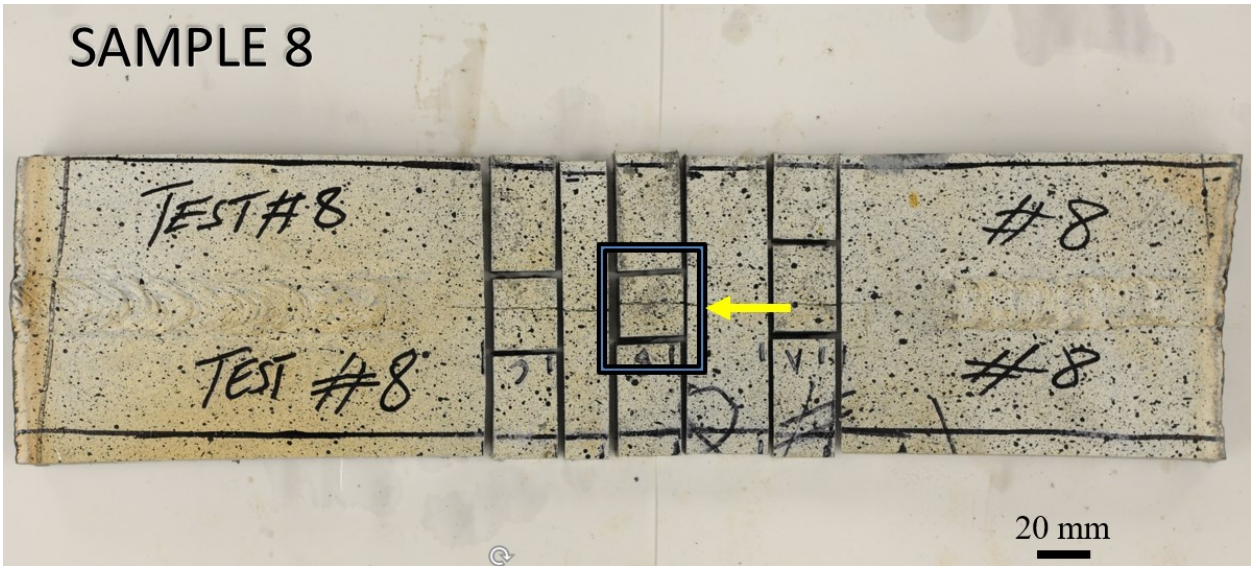

Figure 16 Sample was cut into three sections (A, B and C) from left to right, along cut, only Section B was selected for analysis at this time, the yellow arrow indicates the side polished and etched for microscopy.

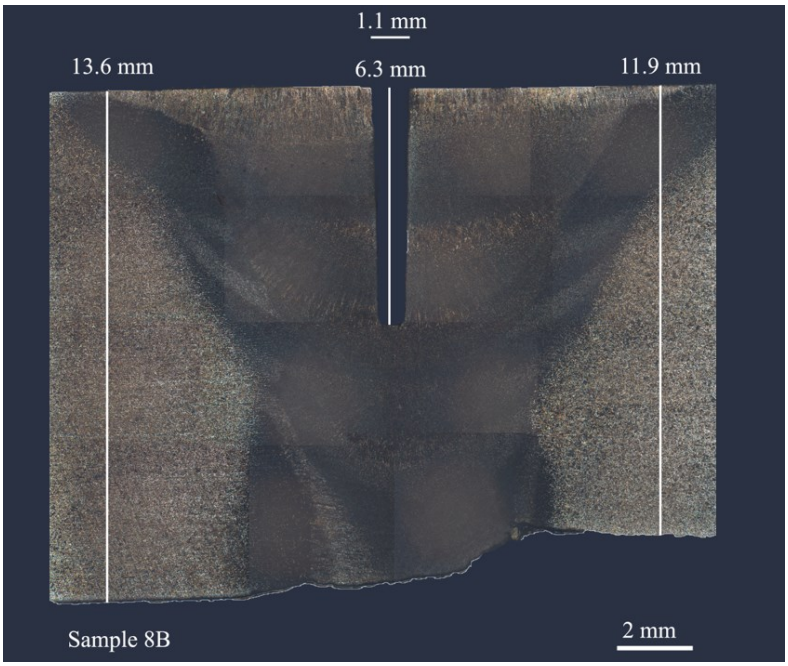

Figure 17 Microscopy of sample 8B showing no significant fracture

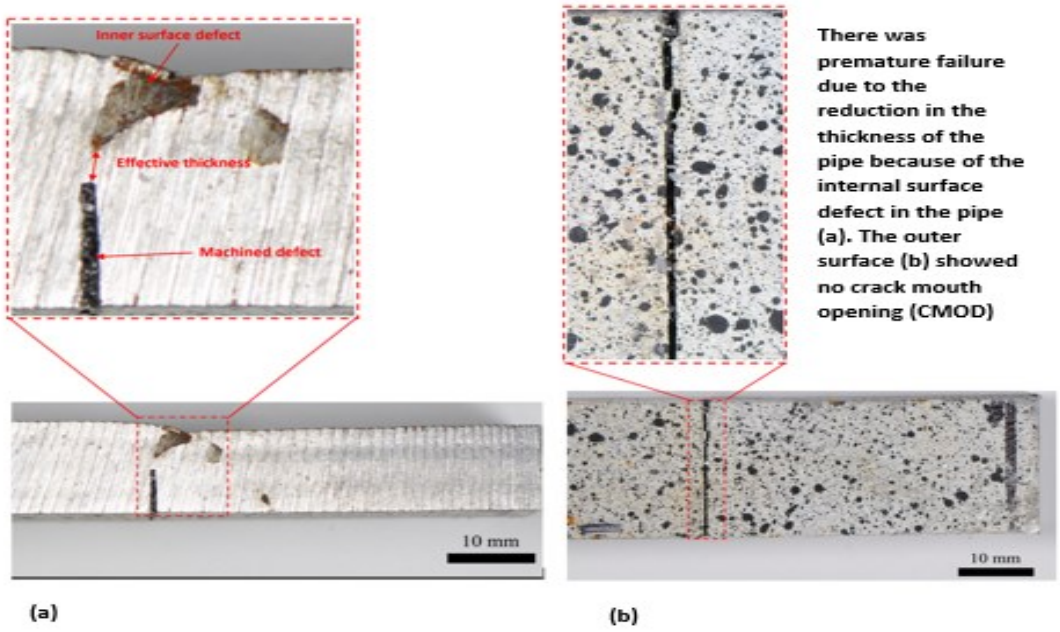

Figure 18: Sections of Sample 8 showing (a) the reduced wall thickness due to an inner surface defect; and (b) outer surface of the sample showing no sign of crack growth.

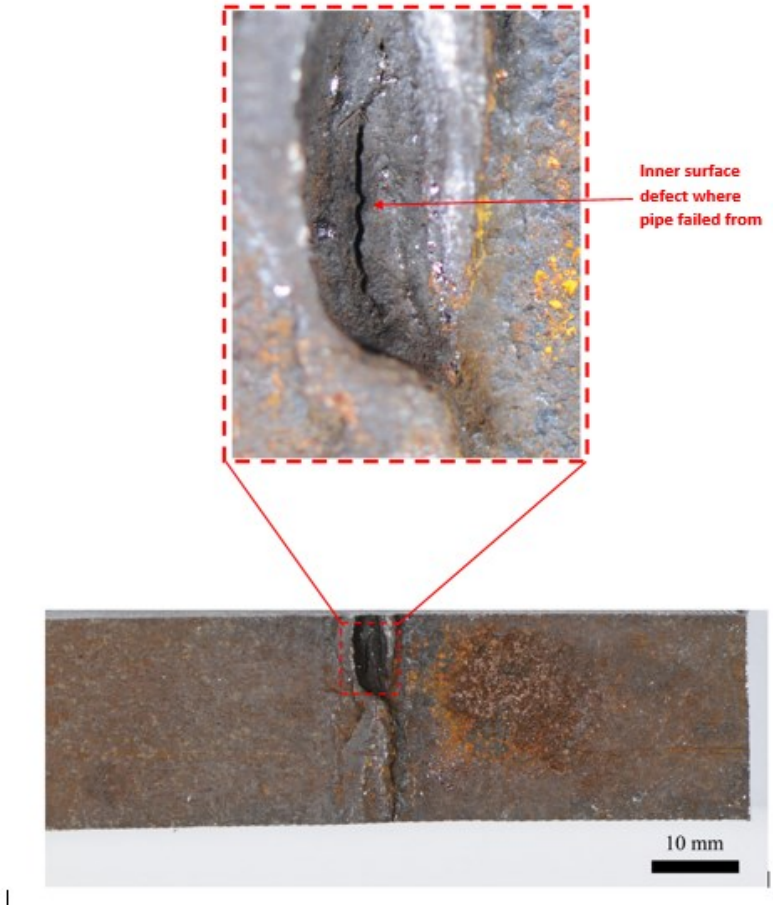

Figure 19 Inner surface defect which extended into the wall thickness and led to premature failure of test 8

Micro hardness Profile

Mitutoyo Micro Vickers hardness indenter was used in the hardness investigation. HV 500 grams force was chosen for indent size and the yellow circles (or numbers) show approximate location of indentations

Figure 20 The Mitutoyo Micro Vickers hardness indenter

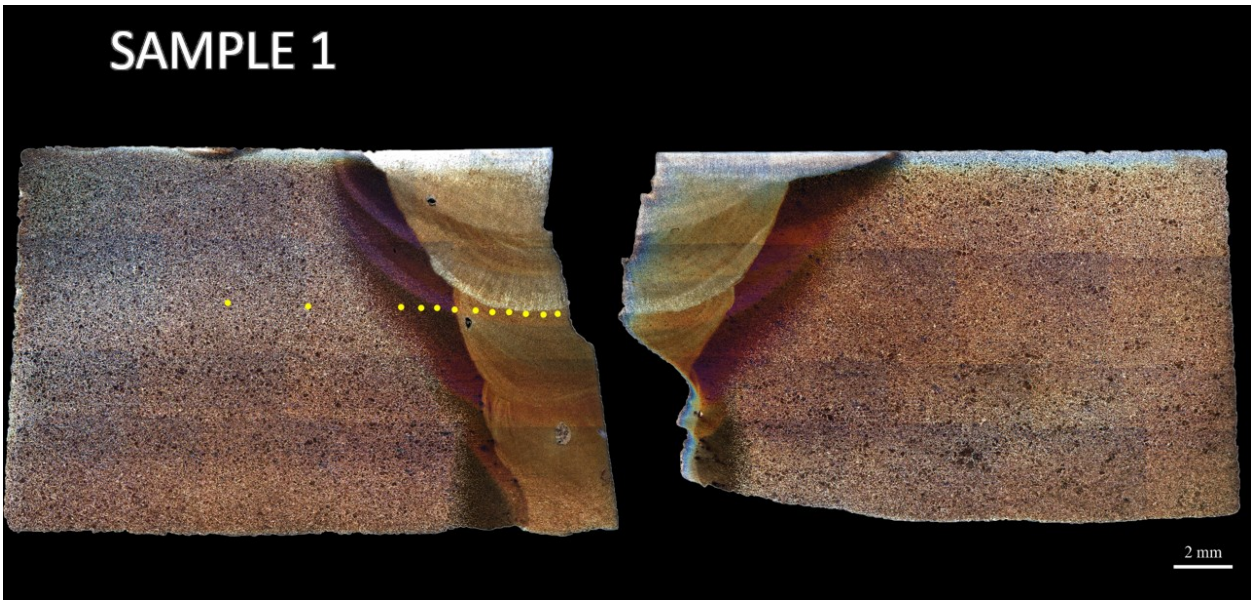

Figure 21 Sample 1 showing the approximate locations of indentations

Table 1 Result of comparison of hardness of weld metal, base metal, and the HAZ of sample 1

Indent #	Distance from Edge (mm)	HV500
1	0.5	223
2	1.0	222
3	1.5	217
4	2.0	221
5	2.5	211
6	3.0	208
7	3.5	227
8	4.0	229
9	4.5	226
10	5.0	224
11	8.0	218
12	10.0	205

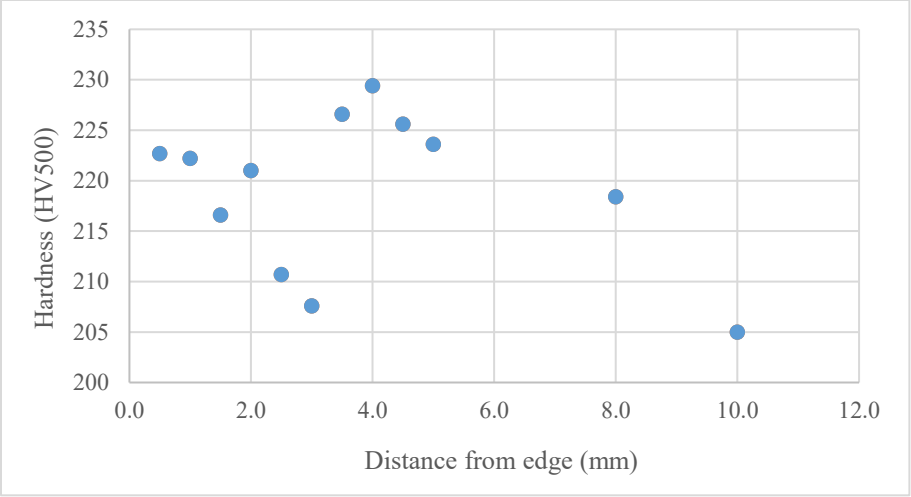

Figure 22: Distribution of hardness along the sample section in test sample 1

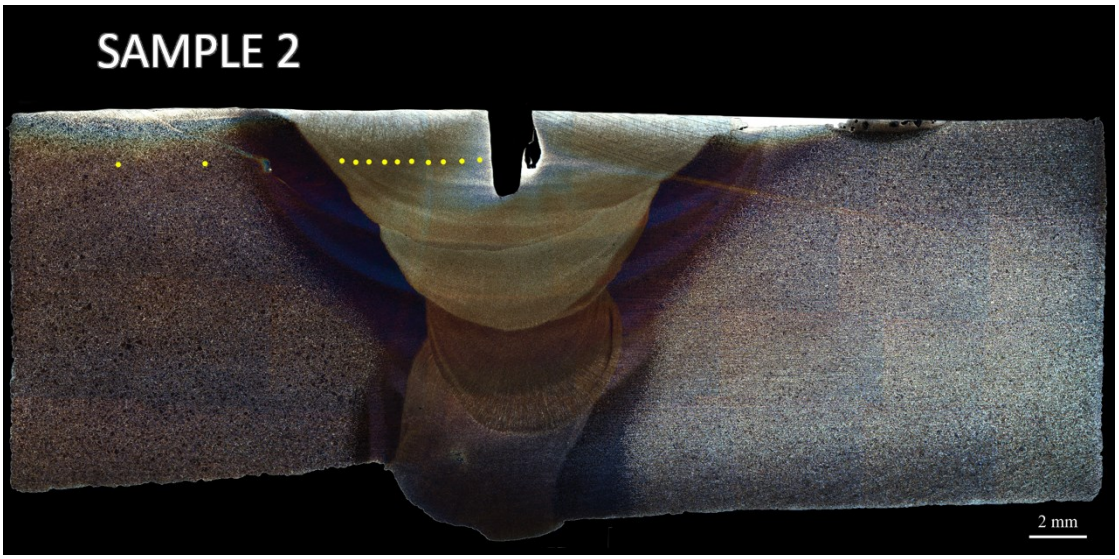

Figure 22 Sample 2 showing the approximate locations of indentations

Table 2 Result of comparison of hardness of weld metal, base metal, and the HAZ of sample 2

Indent #	Distance from Edge (mm)	HV500
1	0.5	174
2	1.0	175
3	1.5	180
4	2.0	176
5	2.5	185
6	3.0	181
7	3.5	170
8	4.0	179
9	4.5	164
10	6.7	172
11	8.8	211
12	10.0	209

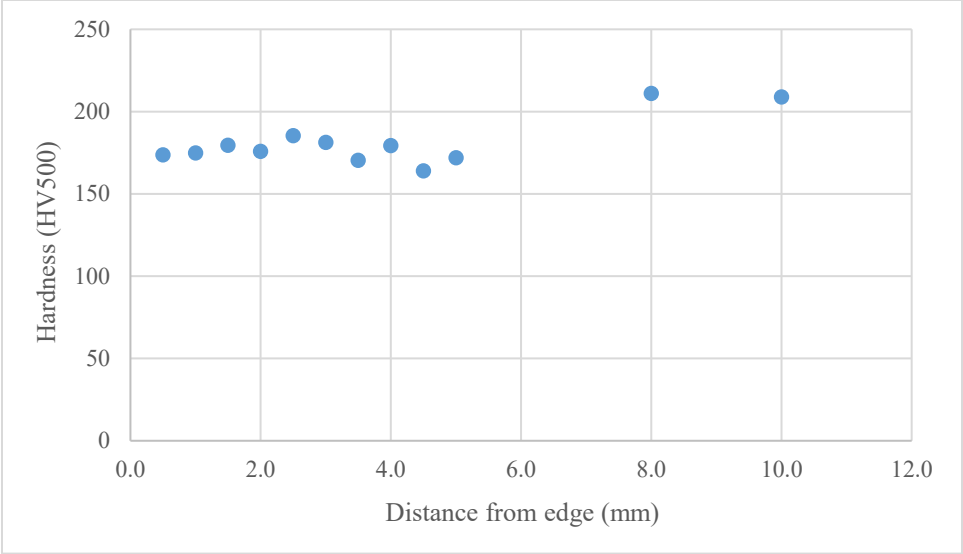

Figure 23: Distribution of hardness along the sample section in test sample 2

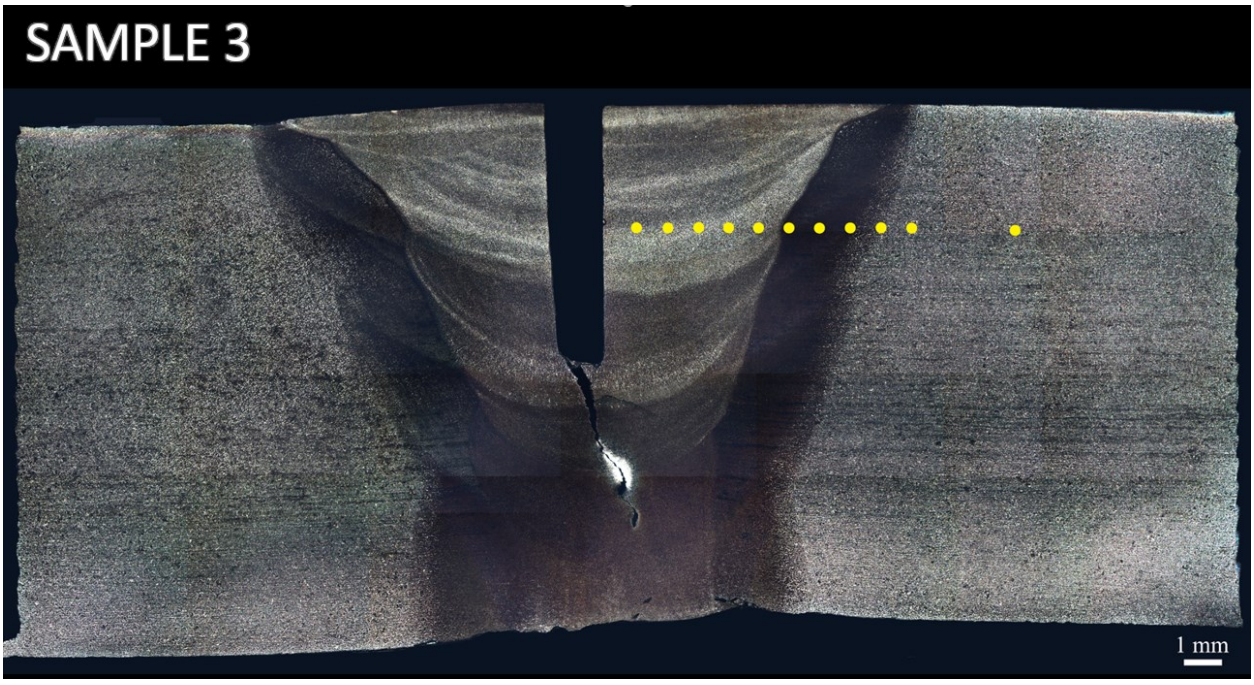

Figure 24 Sample 3 showing the approximate locations of indentations

Table 3 Result of comparison of hardness of weld metal, base metal, and the HAZ of sample 3

Indent #	Distance from Edge (mm)	HV500
1	0.7	170
2	1.4	161
3	2.1	162
4	2.8	172
5	3.5	172
6	4.2	170
7	4.9	174
8	5.6	227
9	6.3	219
10	7.0	217
11	10.0	190

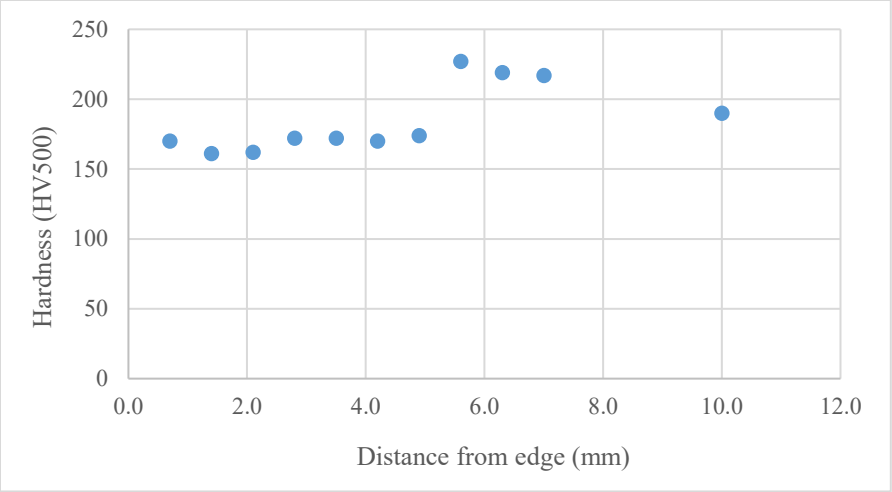

Figure 25: Distribution of hardness along the sample section in test sample 3

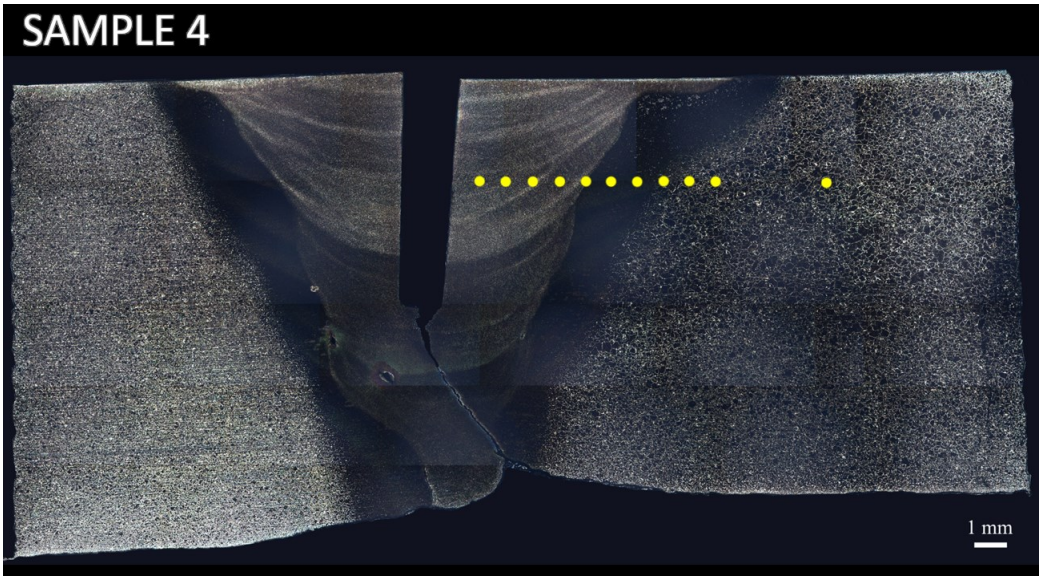

Figure 26 Sample 4 showing the approximate locations of indentations

Table 4 Result of comparison of hardness of weld metal, base metal, and the HAZ of sample 4

Indent #	Distance from Edge (mm)	HV500
1	0.7	179
2	1.4	179
3	2.1	176
4	2.8	179
5	3.5	177
6	4.2	215
7	4.9	222
8	5.6	215
9	6.3	189
10	7.0	193
11	10.0	189

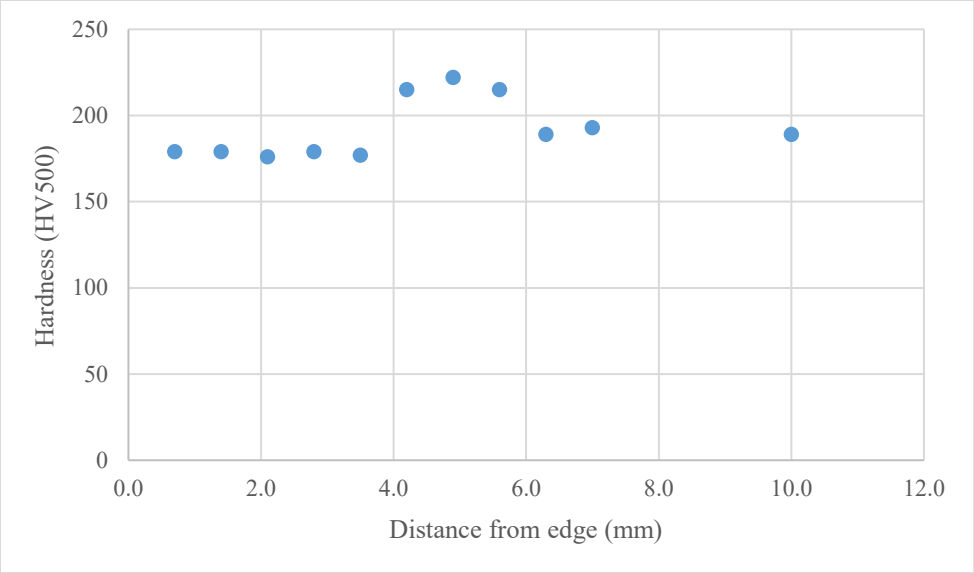

Figure 27: Distribution of hardness along the sample section in test sample 4

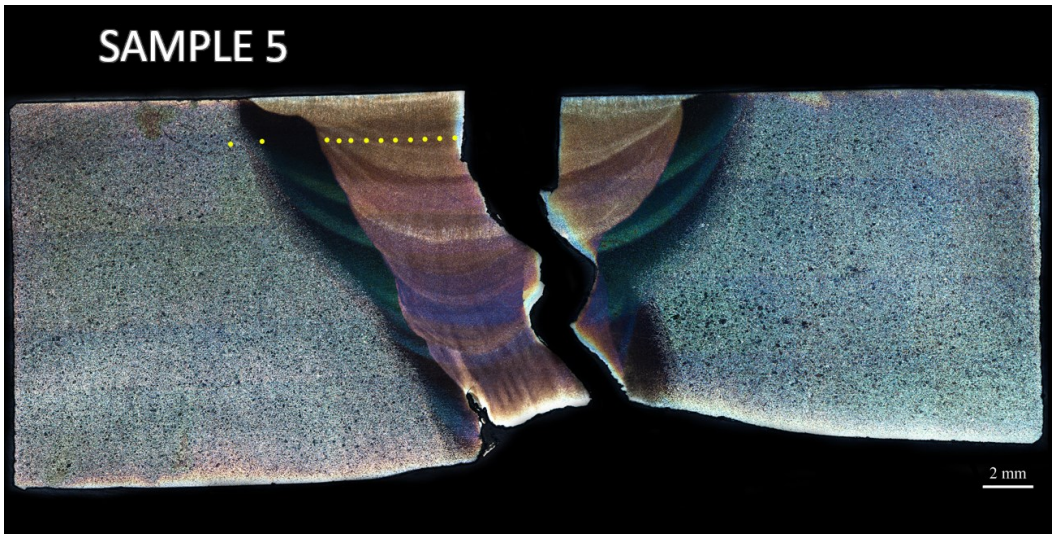

Figure 28 Sample 5 showing the approximate locations of indentations

Table 5 Result of comparison of hardness of weld metal, base metal, and the HAZ of sample 5

Indent #	Distance from Edge (mm)	HV500
1	0.5	194
2	1.0	191
3	1.5	196
4	2.0	197
5	2.5	182
6	3.0	188
7	3.5	190
8	4.0	179
9	4.5	180
10	5.0	185
11	8.0	180
12	10.0	199

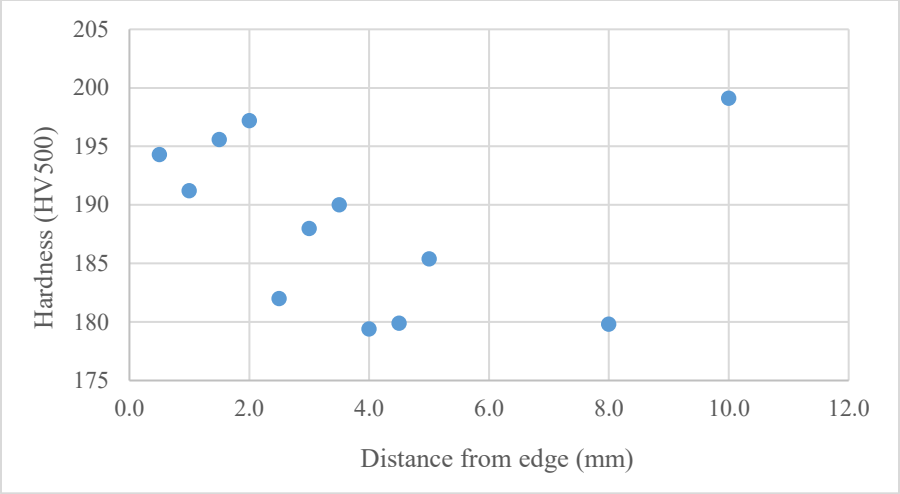

Figure 29: Distribution of hardness along the sample section in test sample 4

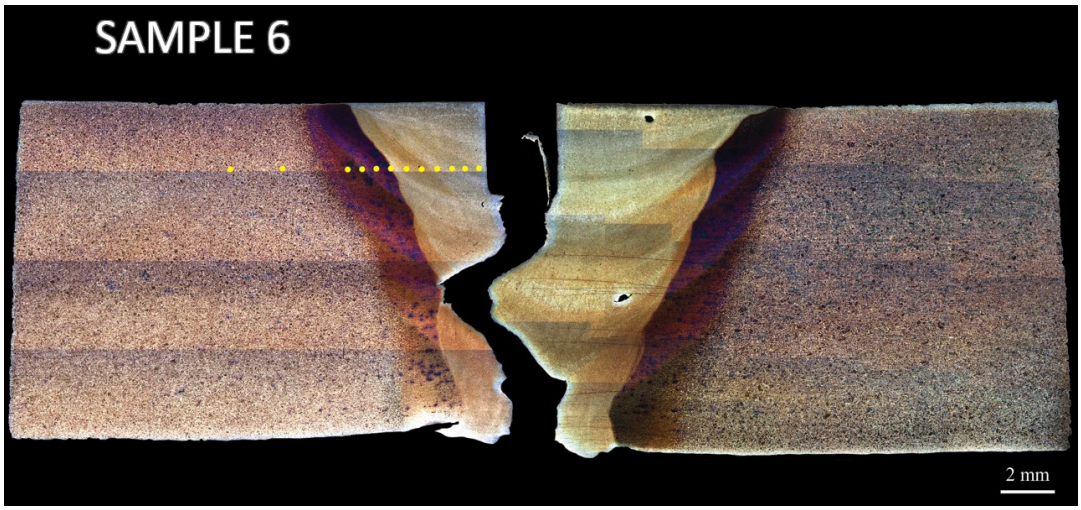

Figure 30 Sample 6 showing the approximate locations of indentations

Table 6 Result of comparison of hardness of weld metal, base metal, and the HAZ of sample 6

Indent #	Distance from Edge (mm)	HV500
1	0.5	218
2	1.0	183
3	1.5	199
4	2.0	185
5	2.5	193
6	3.0	188
7	3.5	196
8	4.0	226
9	4.5	223
10	5.0	205
11	8.0	200
12	10.0	202

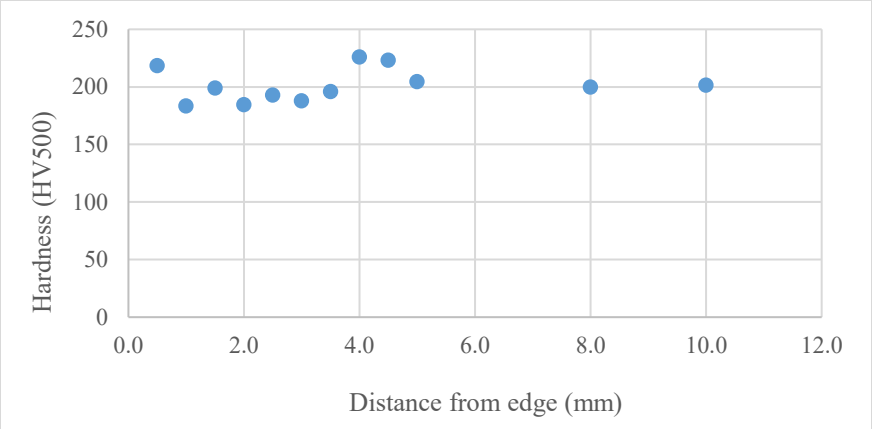

Figure 31: Distribution of hardness along the sample section in test sample 6

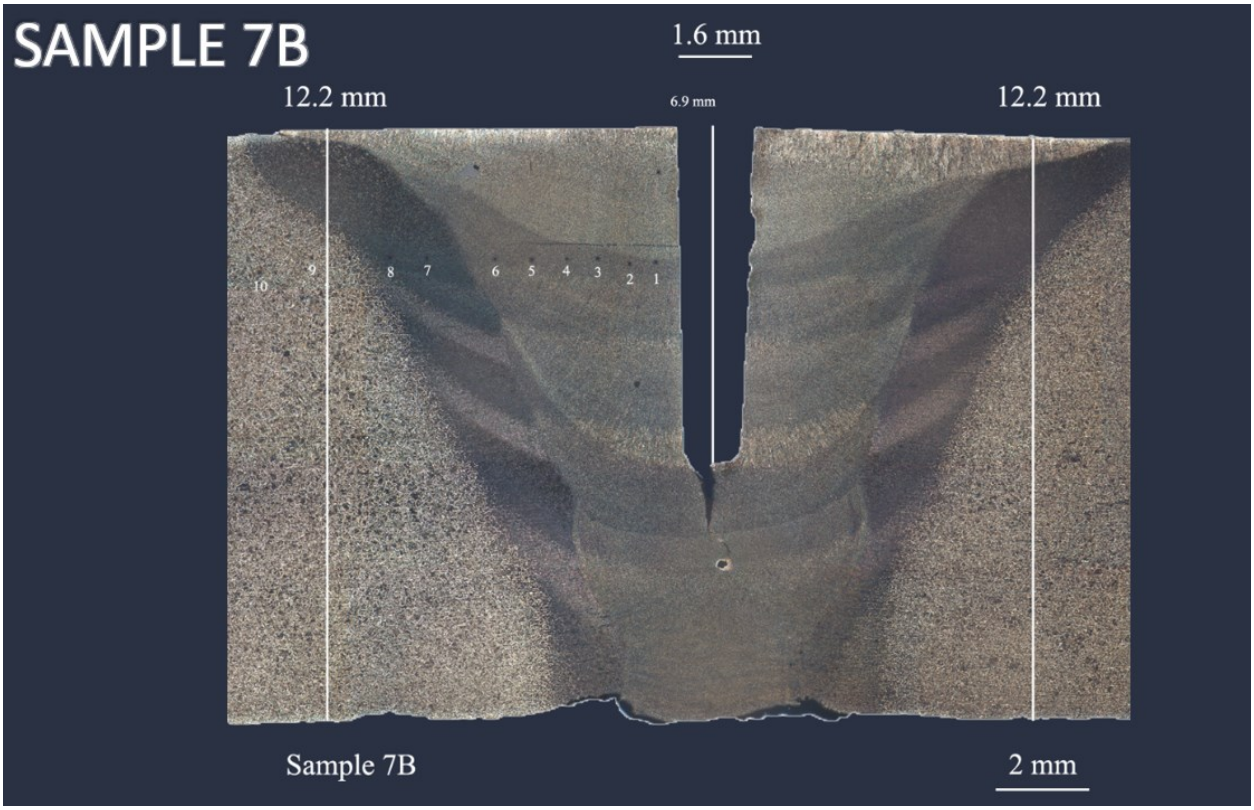

Figure 32 Sample 7 showing the approximate locations of indentations

Table 7 Result of comparison of hardness of weld metal, base metal, and the HAZ of sample 7

Indent #	Distance from Center of Cut (mm)	HV500
1	1.2	185.5
2	1.7	179.2
3	2.4	152.2
4	3.0	187.3
5	3.8	149.7
6	4.5	177.3
7	6.0	210.9
8	6.7	220.2
9	8.4	191.3
10	9.5	188.7

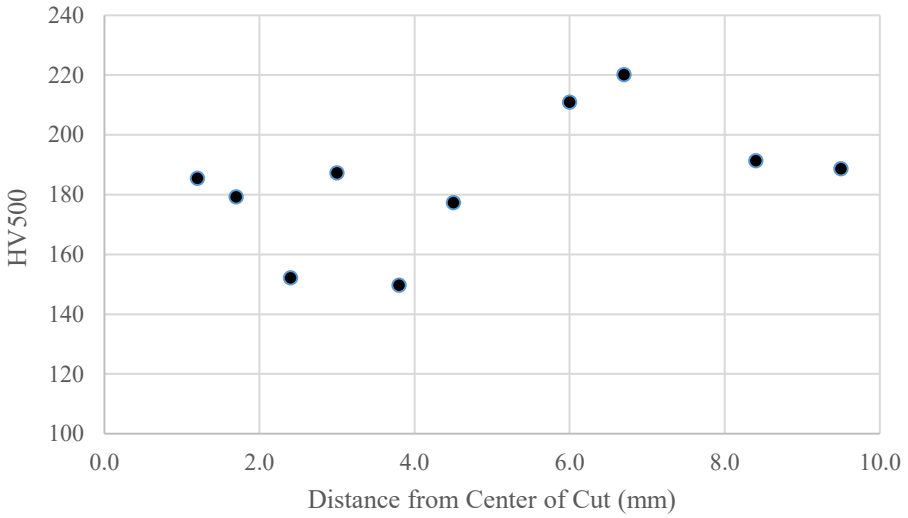

Figure 33 Distribution of hardness along the sample section in test sample 7

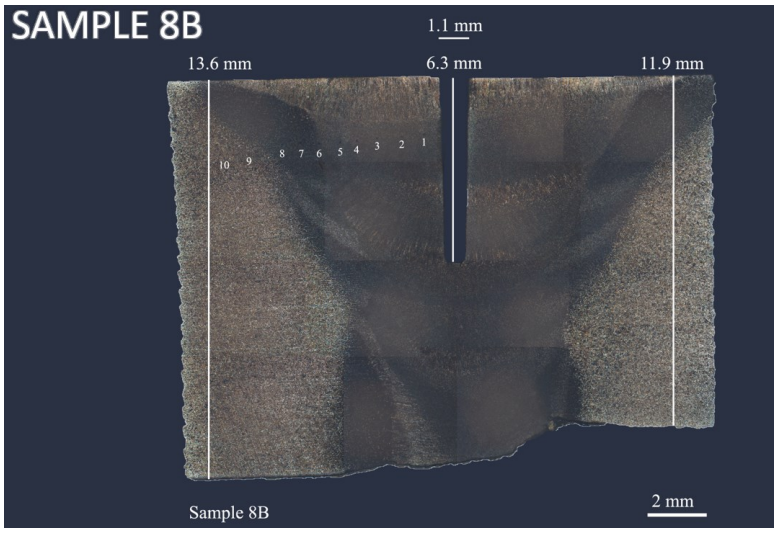

Figure 34 Sample 8 showing the approximate locations of indentations

Table 8 Result of comparison of hardness of weld metal, base metal, and the HAZ of sample 8

Indent #	Distance from Center of Cut (mm)	HV500
1	1.0	195.7
2	1.8	177.5
3	2.6	188.5
4	3.3	180.7
5	3.8	183.5
6	4.5	187.3
7	5.2	218.2
8	5.8	219.3
9	7.3	194.4
10	8.0	190.4

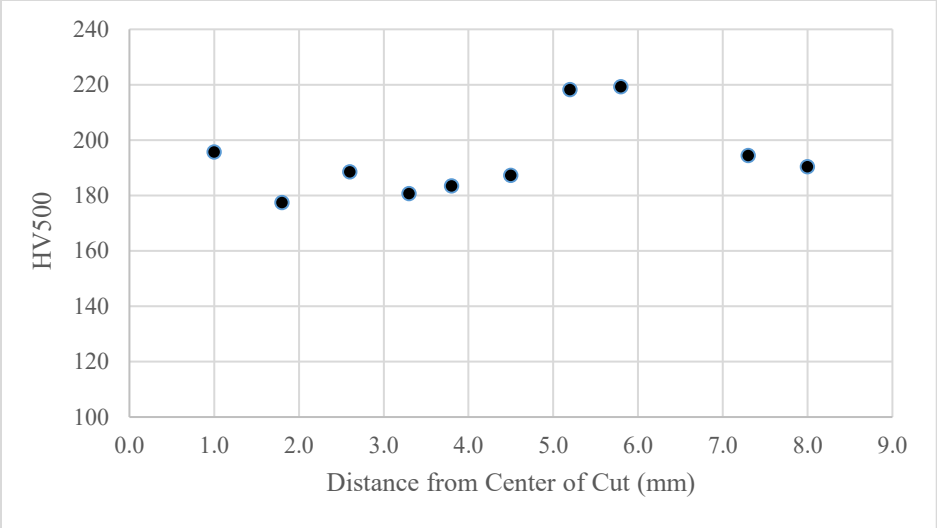

Figure 35: Distribution of hardness along the sample section in test sample 8

Measurements of pipe and flaw geometries.

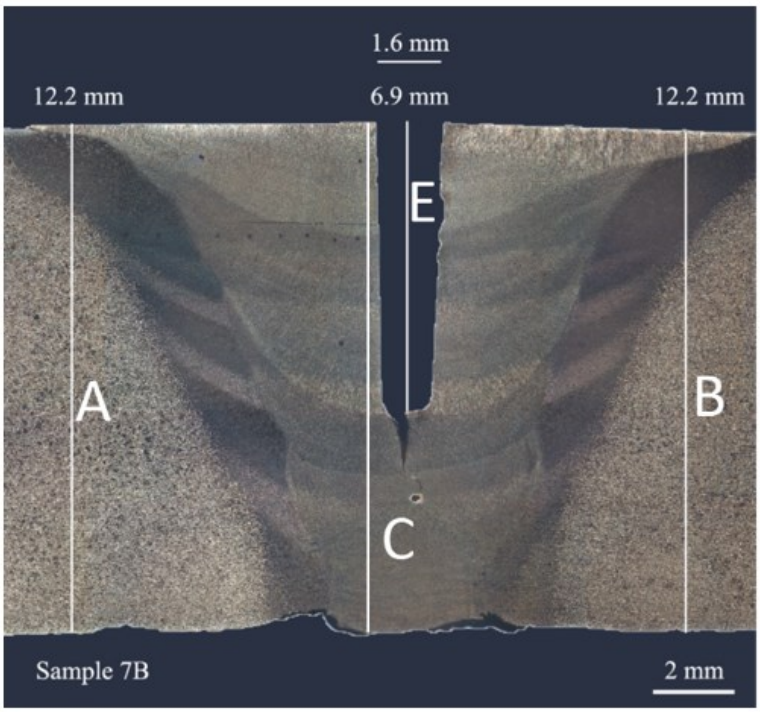

Figure 36 Sample 7B with the numbering used to study the true dimensions of the machined flaw

Table 9: Summary of the fracture analysis based on the numbering shown in Figure 36

Sample #	A (mm)	B (mm)	C (mm)	E (mm)	E' (mm)
1	12.8	12.5	11.1	2.7	4.3
2	13.1	13.3	14.9	3.0	-
3	13.8	13.4	13.7	6.8	-
4	14.2	12.6	13.0	7.0	-
5	15.1	13.8	11.9	2.8	3.8
6	12.4	12.8	12.4	3.4	-
7B	12.2	12.2	12.2	6.9	-
8B	13.6	11.9	13.0	6.3	-

Note: In some cases, there were observed multiple notches, E' = the depth of the deepest additional visible notch.

Figure 36 and Table 9 showed the numbering method, and the actual dimensions of machined flaw geometry in all test samples considered It was observed that all specimen except specimens 2 and 8, exhibited similar through-wall ductile tear fracture response, this means that the fracture cut through the wall thickness of the pipe at failure.